EFFECT OF STRESSED SKIN ACTION ON THE BEHAVIOUR OF COLD-FORMED STEEL PORTAL FRAMES WITH NON-LINEAR FLEXIBLE JOINTS AND TOP-HAT PURLINS

A thesis submitted to the University of Strathclyde

for the Degree of Doctor of Philosophy

by

Andrzej M. Wrzesien

Department of Civil and Environmental Engineering

The University of Strathclyde

2016

ABSTRACT

A conceptual design of a cold-formed steel (CFS) portal frame system proposed by the industrial partner is to be investigated and improved in light of known design challenges. Unlike previous studies which focused on the behaviour of CFS bare frame, this thesis focuses on the design and analysis methods for clad portal frames. A wide range of design problems and industry practices have been investigated by testing, as follows:

1) Resistance and stiffness of bolted moment-connections.

The bearing resistance and stiffness of the threaded bolt shank in single and double shear lapped connections were tested and compared against design recommendations. The existing methods for deriving the moment resistance and the rotational stiffness of the moment-connections were updated for tested joint configurations.

2) Shear resistance and stiffness of cladding panels.

A total of eighteen 3 x 3 m cladding panels were tested including options in which sheeting is fixed on all four sides and fixed on two sides only. The design features not yet recognized by design codes such as top-hat purlins, sheeting profiles fixed in the crest, profile thickness less than 0.5mm and composite panels were investigated in the test programme.

3) The difference in the structural behaviour of the bare and clad portal frames.

A series of six full-scale laboratory tests were conducted on cold-formed steel portal frame buildings in order to investigate the effects of joint flexibility and stressed skin diaphragm action. The frames used for the laboratory tests were of 6m span, 3 m height, 10° pitch and the frame spacing was 3 m. When the difference in loads between 2D (bare frame model) and 3D (stressed skin model) were considered, it was shown that the resistances and flexibilities of frames and cladding should be calculated or established by testing so safe and economical design is possible.

ACKNOWLEDGMENTS

TABLE OF CONTENTS

TABLE OF FIGURES

xiii

TABLE OF TABLES

1   INTRODUCTION

1.1   Background

Portal frame buildings are one of the most popular and efficient types of steel structure. They have been widely used in such sectors as: retail, leisure, transport, distribution and manufacturing. Portal frames account for 90% of all single storey buildings and 50% of all the construction steel used in the UK each year. According to a Tata Steel & BCSA joint report 'The so-called 'shed' sector is now one of the most efficient and successful in UK construction with an estimated annual value of approximately £1 billion for frames and £1.5 billion for associated envelope systems' (Target Zero (2011, p.6)).

Traditionally these types of structure were built from hot-rolled steel sections as the main structural members with rigid joints. Cold-formed steel members were only used for constructing the building envelope. Over the last three decades however, due to extensive research in the field of cold-formed steel structures and significant technical development in the field of cold-forming, cold-formed steel sections offer a viable alternative to conventional hot-rolled steel sections for frames of moderate span. A typical hot-rolled steel frame and a cold-formed steel alternative are shown in Figure 1-1.

a) Hot-rolled steel portal frame (Miracle Span Steel Buildings (n.d.))   b) Cold-formed steel portal frame (Dobosi (n.d.))

Figure 1-1 Alternatives for portal frame construction

Each year cold-formed steel construction systems are claiming a bigger share of the very lucrative 'shed' market because they can offer the following advantages:

1) Higher strength-to-weight ratio. Cold-formed steel members are usually rolled from steel of higher yield strength (S 450GD, S550GD) than this typically used for hot-rolled sections (S 355). Taking into account the fact that the price of steel is almost wholly dependent on its weight, significant savings can be obtained.

2) Reduction of erection costs. Due to its light weight, cold-formed steel frames can be quickly erected by semi-skilled workers without the need for cranes.

3) Reduction of the transportation costs. Both the primary and secondary members can be purchased from the same supplier. Most of the sections can also nest one into another, which reduces the carriage space (less load, less lorries, more environmentally friendly product).

4) Structural members can be manufactured, pre-cut and pre-punched with greater detailing accuracy.

5) Reduction of the joint manufacturing costs. Toma et al. (1993) estimated that as much as 40% of the total hot-rolled steel frame cost is due to the fabrication of the joints. As a result of extensive research effort in cold-formed steel framing, it was shown that most of the joints can be engineered inexpensively through cold-formed brackets and mechanical fasteners (see Section 2.4).

6) Unlike traditional hot-rolled sections, cold-formed steel members are protected against corrosion through zinc, aluminium or plastic coating.

7) Cold-formed steel buildings are also more sustainable. New targets in the UK aim to deliver Zero Carbon buildings in the 'operational' part of their life by 2019, thereafter, embodied carbon will account for the majority of a project's CO_2 emission (McAlinden (2015)). Designers, therefore, are encouraged to use more efficient construction materials (IStructE (2014)). The ICE Database (Hammond and Jones (2011)) shows 36% less energy used and 38% less CO_2

emitted during cold-formed steel section manufacturing process compared to traditional hot-rolled sections. Secondary processes such as cutting, welding and corrosion protection would further increase these values in the case of hot-rolled frames.

Several previous studies have demonstrated the viability of using cold-formed sections to construct portal frames with moderate spans (Baigent and Hancock (1982a), Kirk (1986), Rensburg and De Vos (1996), Mills and LaBoube (2004)). The key feature of all these studies was that eaves and apex joints were designed to function as rigid. Such joints, however, were either expensive to manufacture or difficult to erect on site. A detailed review of these systems, including details of the joints, is presented in Section 2.1 and Wrzesien et al. (2012a).

Lim and Nethercot (2004) and Chung et al. (2005) independently conducted research on determining the rotational stiffness of cold-formed portal frame joints and applying the measured rotational stiffness to frame analysis and design. The key features were the use of bolted moment-resisting connections, formed through brackets, for the eaves and apex joints. Such an arrangement for the joints was chosen to ensure that the brackets remained easy to manufacture and the joints easy to assemble on site. Interestingly, the redistribution of bending moment as a result of the semi-rigidity of the joints resulted in a semi-rigid cold-formed steel portal frame being able to carry higher load than an equivalent rigid jointed cold-formed steel portal frame.

In recent years, a number of researchers have concentrated on increasing the rotational stiffness of the eaves and apex joints (Mäkeläinen and Kankaanpää (1996), Dubina et al. (2004), Kwon et al. (2006)). Increasing the rotational stiffness of the joints will, of course, be beneficial for the overall response of the bare frame, particularly in terms of reducing frame serviceability deflections. However, research focussing entirely on joint stiffness ignores the beneficial effect of stressed skin action.

Stressed skin action is a well-established phenomenon, based on taking into account the inherent strength and stiffness of the metal cladding in overall frame

behaviour. It was demonstrated by extensive research that stressed skin action can reduce or eliminate the wind bracing, reduce sway deflections under horizontal load, and reduce the spread of the frame under vertical load. A set of design recommendations was first presented in the 'Manual of stressed skin diaphragm design' by Davies and Bryan (1982), which was then incorporated into BS 5950-9 (1994a), and the 'European recommendations for the application of metal sheeting acting as a diaphragm' ECCS (1995).

Currently a designer can choose to design portal frames using a traditional 2-dimensional design method or the stressed skin design method (see Figure1-2). The fundamental difference between these methods is that each frame in 2D design is analysed separately, and hence no interaction between frames is considered. In stressed skin design, the roof structure is considered as a deep plate girder, and forces are distributed between the internal frames through the cladding panels. This method accounts for the true load paths in a 3-dimentional structure.
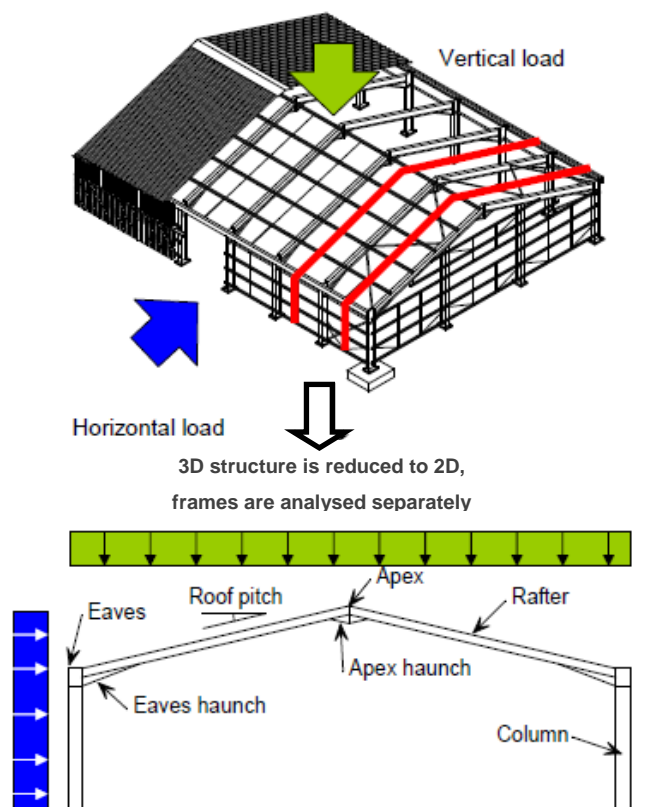
a) 2D design approach

4
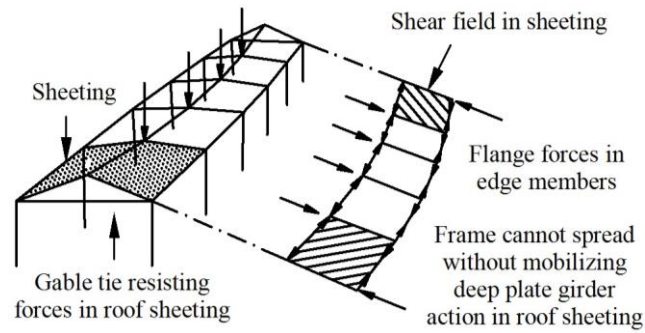
b) Stressed skin design approach

Figure1-2 Portal frame design methods

Stressed skin design was originally investigated for traditional hot-rolled steel portal frames, thus only in this area is there enough guidance to implement this design method. However, with the growing popularity of cold-formed steel portal frames in recent years, it is of great importance to investigate stressed skin effects in these types of structures. Cold-formed steel frames are often very flexible, have semi-rigid joints, and usually suffer from extensive sway deflections due high joint flexibility. In such cases, implementing the stressed skin action in their analysis can offer greater benefit than for hot-rolled steel frames Wrzesien et al. (2009a).

1.2   Typical geometry of symmetric pitched roof portal frame

According to SCI P252 (2004), a typical hot-rolled steel portal frame in the UK would have the following geometry:

1) A span between 15m and 50m

2) A height to the eaves between 5m and 10m

3) A roof pitch between 5° and 10°

4) A frame spacing between 5m and 8m

5) Rigid haunched joint at the eaves and the apex

To determine similar characteristics for cold-formed steel portal frame geometries, over 200 cold-formed steel buildings supplied to the UK market were

analysed by the author Wrzesien (2012). Based on this analysis, a typical cold-formed steel portal frame would have following geometry:

1) A span between 4m and 20m (average 7.1m)

2) A height to the eaves between 2m and 7m (average 3m)

3) A roof pitch of 10° (average 10°)

4) A frame spacing between 2m and 6m (average 4m)

5) Average length of 12 m (3 x 4m)

6) Semi-rigid bolted eaves and apex joints

Cold-formed steel portal frames currently dominate this niche in the 'shed' market. There is an opportunity to take a bigger share of this market if the average span of the frames could be increased.

1.3   Objectives of the research project

First studies in the use of cold-formed steel (CFS) members in portal frame application were reported in early 1980s (Baigent and Hancock (1982b), Kirk (1986)) and highlighted the main differences between the behaviour of tradition hot-rolled steel portal frames and their cold-formed steel equivalent. One of the key differences is joint strength and stiffness characteristic. Typical hot-rolled steel welded eaves and apex joint can be assumed as rigid and full-strength where cold-formed steel joints are often flexible (semi-rigid) and partial-strength. Joint rotation in cold-formed steel portal frames is associated with the bearing of the mechanical fasteners (generally bolts) acting in shear on relatively thin steel plates.

Although the effect of joint rotational stiffness on the structural modelling was acknowledged by BS EN 1993-1-8 (2005), the code does not present clear rules how the strength and rotational stiffness of the cold-formed steel bolted joint should be calculated. Due to the lack of dedicated worked example, designers in the UK often follow dated joint design procedures presented in SCI P125 (1993) in which the

6

moment resistance of connections between cold-formed sections is assumed to be governed by bearing resistance of fasteners. With almost 20 different researches on CFS moment-resisting joint, the conclusive design procedure has not yet been agreed but common conclusion is that bolt bearing rarely governs the design. Despite this fact, most recent CFS design manual by Dubina et al. (2012) offers no guidance on the joints resistances nor their flexibilities.

As a result, for cold-formed steel portal frames, steel designers often refer to guidance for equivalent hot-rolled steel frames SCI P397 (2012) in terms of design assumption and 2D bare frame analysis model (Dubina et al. (2012). The structural analysis is often done on the rigid joint assumption which may result in miscalculation of the bending moment and underestimation of the 'true' deflections. As deflection limits are discretionary, designers sometimes relax deflection limits even further to achieve a more economical design. This result in an underestimation of the forces in roofing due to stressed skin action and hence can lead to an under-design of the gable end-frames. In practice, however, the effects of stressed skin action are often ignored by designers of portal frames due to complexity of the calculation.

Experimental investigation on portal frames using back-to-back lipped channel sections and bolted joints had been already published (Stratan et al. (2006)) but was focused on developing full-strength connections of rotational stiffness close to rigid. The behaviour of a bare frame was investigated in the seismic design context and stressed skin action was not included in this study. The study highlighted importance of joint testing in establishing accurate strength and stiffness characteristic of joints which should be included in an analysis model.

A conceptual design of a CFS portal frame system proposed by the industrial partner is to be investigated and improved in light of some of the findings presented above. As the system includes joints more flexible than these presented by Stratan et al. (2006) and also use relatively stiffer top-hat purlins, greatest attention is given to the effect of stressed skin action in clad portal frame building. Although stressed skin design methods (BS 5950-9 (1994b), ECCS TC7 (1995)) were

developed in the past for hot-rolled steel frames, these will be re-examined in this work in the context of cold-formed steel frames with flexible joints. In comparison, for hot-rolled portal frames with rigid joints, stressed skin action is less important than in more flexible cold-formed frames and can be conservatively ignored. In case of flexible frames with high strength-to-weigh ration stressed skin action may result in large load redistribution and is expected to be crucial to economy of the design. The following objectives were set:

1. To develop an analytical method of predicting the moment-capacity of the bolted joints for cold-formed steel portal frames.

2. To produce experimental evidence showing the mode of failure of moment-resisting bolted joints.

3. To develop an analytical method of predicting the rotational stiffness of the investigated joints using joint testing and existing research. To demonstrate how the joint flexibility can affect the internal forces in both bare and clad portal frame.

4. To validate common design assumptions, structural analysis methods and design codes against the experimental data and existing research in cold-formed steel.

5. To update existing design codes on stressed skin action (BS 5950-9 (1994b), ECCS TC7 (1995)) to consider modern types of roof constructions i.e. hat-shaped purlins.

6. To demonstrate a simple analysis method suitable for design of cold-formed steel portal frames using industry standard structural analysis software.

7. To compare the traditional 2D bare frame design method against a 3D stressed skin design method.

8. To implement research on the behaviour of cold-formed steel 'sheds' into the industry so the economy, quality and robustness of the portal frame can be improved.

2   MOMENT-RESISTING JOINTS

2.1   Literature review

2.1.1   Baigent and Hancock

The earliest tests reported in the literature on cold-formed steel portal frame joints are those by Baigent and Hancock (1978). Details of this joint are given in Figure 2-1. The joints were formed through a set of brackets of significant thickness and high-strength friction grip bolts were used to avoid slip. The study focused on developing an analytical method of predicting strength and stiffness of portal frames using thin-walled asymmetric cross-sections under combined compression, major and minor bending and warping torsion. Such joints would not be practical due to high cost and were developed only to provide robust and rigid connections between single channel sections.
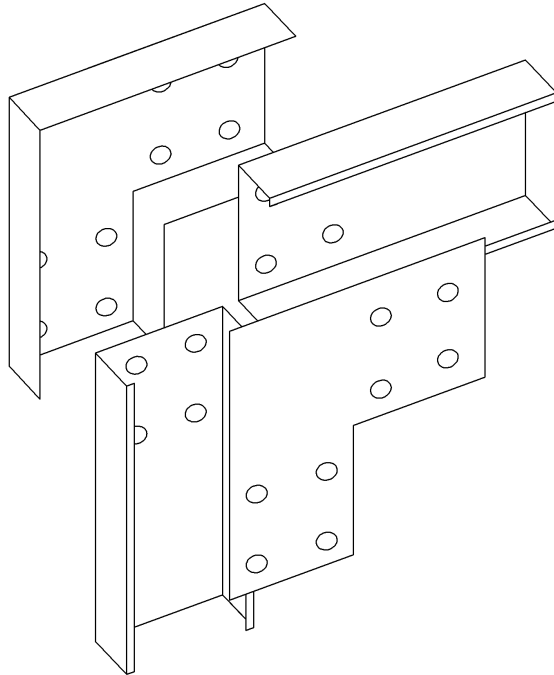
Figure 2-1 Eaves joints after Baigent and Hancock (1978)

2.1.2 Kirk

The work of Baigent and Hancock (1978) was followed by tests reported by Kirk (1986) on the award winning Swagebeam portal framing system (Design Council Award for innovative British Design). Extensive experimental investigation was undertaken including tests on eave and apex joints as well as full-scale tests on portal frames at Salford University. Figure 2-2 shows details of the joints. The primary innovation was that the joints could form through the swages rolled in the brackets which connected with matching swages in the webs of the channel sections. Such interlock system allowed reduction in the number of fixings by 50% and formed full-strength 'rigid' joint portal frame system. The extra steel used for swages in columns, rafters and brackets however, exceeded the savings from stiff and full-strength joints and this fact contributed to the little success of the system.
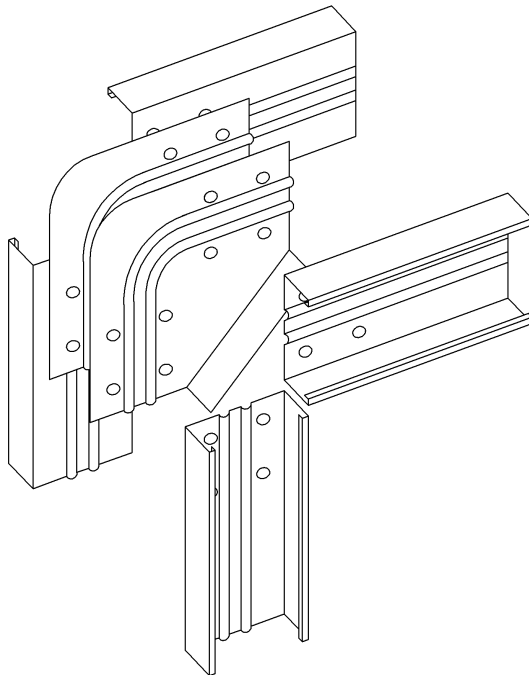
Figure 2-2 Eaves joint after Kirk (1986)

2.1.3 Zadanfarrokh and Bryan

Another early contribution to knowledge on the behavior of bolted moment connections was the work produced by Zadanfarrokh (1991) and Zadanfarrokh and

Bryan (1992). The authors focused on investigating strength and stiffness of single-fixing lapped joints. As a result of this experimental study the existing rules for calculating the strength of such joints were validated and the flexibility of the joint was described as:

$$c_{zad}=5n \ (10/t_1+10/t_2 - 2) \ 10^{-3} \ (mm/kN) \tag{2-1}$$

where:

t_1, t_2 – thicknesses of the sheet of metal (t_1 and $t_2 \leq 8mm$)

n - flexibility factor according to Table 2-1

Table 2-1 Flexibility factors after Zadanfarrokh and Bryan (1992)

Position of the shear plane on the bolts	Joint in tension	Joint under moment
Full shank diameter	3	1.8
Threaded portion	5	3

The strength and flexibility of a single lapped joint was then used to develop the analytical method for predicting strength and rotational stiffness of the bolt-group using an elastic design method. The analytical method was validated against a series of tests on moment connections comprising 2, 3 and 4 bolts located at the web of the single section as shown in Figure 2-3. These types of joints were developed mostly for semi-rigid purlins but the analytical method could also be used in portal frame design. Although the method predicted the rotational stiffness well, the strength prediction was limited to the plate bearing mode of failure and was unable to capture premature, localised section buckling at the joint. The method of predicting the joint strength was later presented in Rhodes (1991) and SCI P125 (1993), which are still used by UK cold-formed steel designers.

a) 2 bolts   b) 3 bolts   c) 4 bolts

d) staggered   e) nested
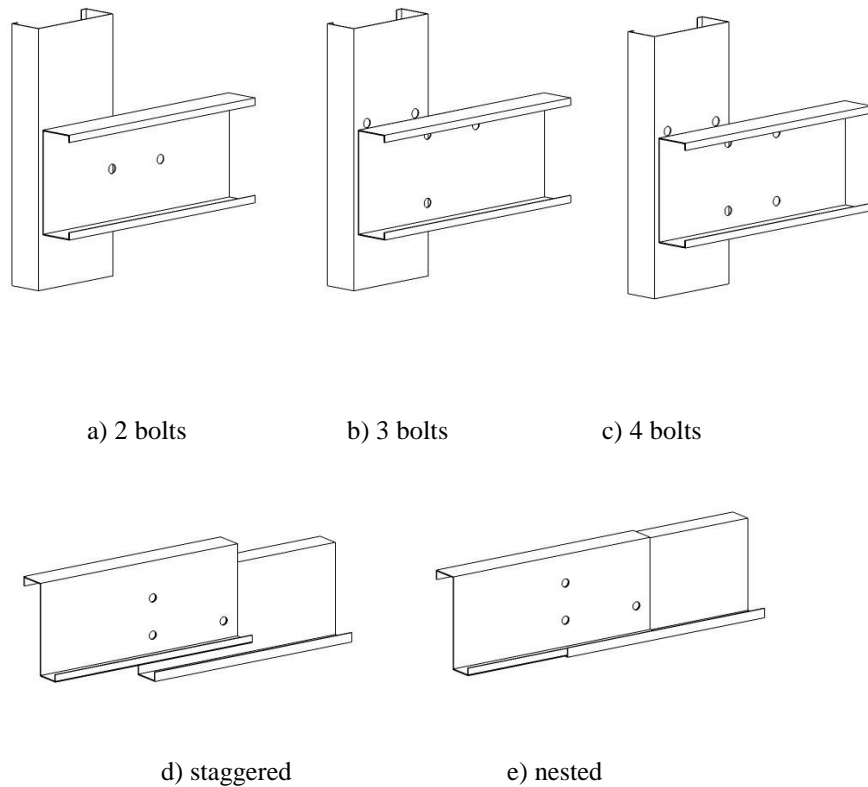
Figure 2-3 Purlin joints after Zadanfarrokh (1991)

2.1.4   Mäkeläinen and Kankaanpää

Mäkeläinen and Kankaanpää (1996) reported tests on portal frame joints constructed from back-to-back sigma sections connected though the web via brackets. To provide additional stiffness to the frame, a tie bar (double angle 50 x 50 x 2.5 mm) was bolted to both eaves brackets (Figure 2-4a). The depth of the sections used for the tests were 250 mm, 300 mm, and 400 mm; thicknesses of 2.5 mm and 3.0 mm were considered. Figure 2-4 shows details of different eaves brackets tested initially in order to choose the best performing one. These included a single plate of thicknesses of 8 mm, 10 mm and 12 mm (see Figure 2-4a), four cold-formed plates thickness of 2.5mm each (see Figure 2-4b), and four cold-formed plates with two outer plates outwardly lipped (see Figure 2-4c). In the second stage of testing only solid 12mm thick brackets were used due to little practicality of four-plate connections. The eaves tie system, proposed in a design case study, would also reduce a clear height inside the structure.

12
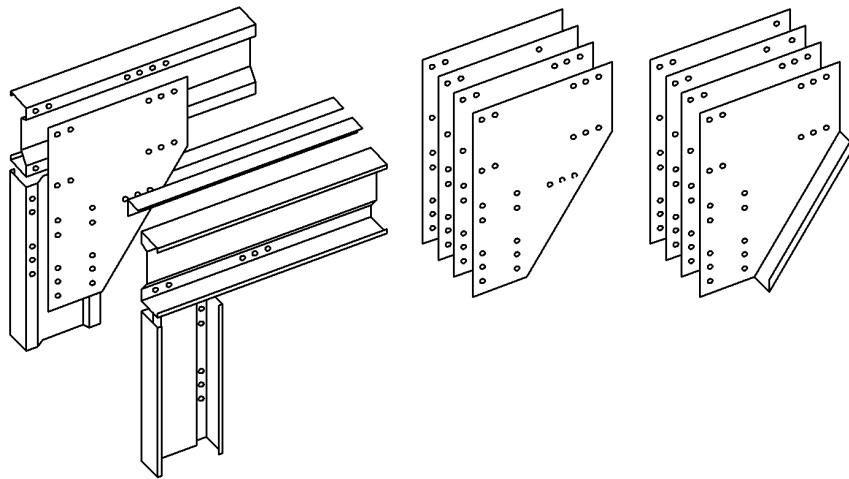
a) single hot-rolled plate   b) four cold-formed   c) four cold-formed plates
                                        plates   with

                                                                     lipped stiffener

Figure 2-4 Eaves joint having different brackets configuration after Mäkeläinen and
Kankaanpää (1996)

2.1.5   Chung et al.

Chung and Lau (1999) reported tests on an arrangement, where the joint was
formed through back-to-back brackets, bolted between the webs of the channel
sections. Figure 2-5a to d shows the different shape of the brackets studied. The study
focused on the overall economy of the joint by considering various thicknesses and
steel grades of the brackets (S350 and S450). In the initial stage of the study eaves
joints were tested through small-scale tests. Test results showed that the triangular
shape bracket formed a joint which according to BS EN 1993-1-8 (2005) should be
classified as pinned based on strength and stiffness criteria. Joints b, c and d (see
Figure 2-5) were investigated further through frame tests under horizontal load.
Similar types of joints were tested by Yu et al. (2005) (see Figure 2-6) in order to
check their ability to form beam-column sub-frame joints for multi-story frames.
Both experimental studies proposed and validated the analytical method for
preventing a premature buckling failure of the channel section in the vicinity of most
outer line of bolt. The failure of the connected member was however not separated

from the buckling failure of the hunched bracket itself as this mode of failure was observed in some tests. The torsional stiffness of the eaves brackets could also be in question as tests were conducted on frames of unrealistic dimensions (1.87m height and 1.41m span) with lateral restraints connected via web of the channel (in-line system)

a) triangular   b) rectangular

c) L-shape   d) haunch
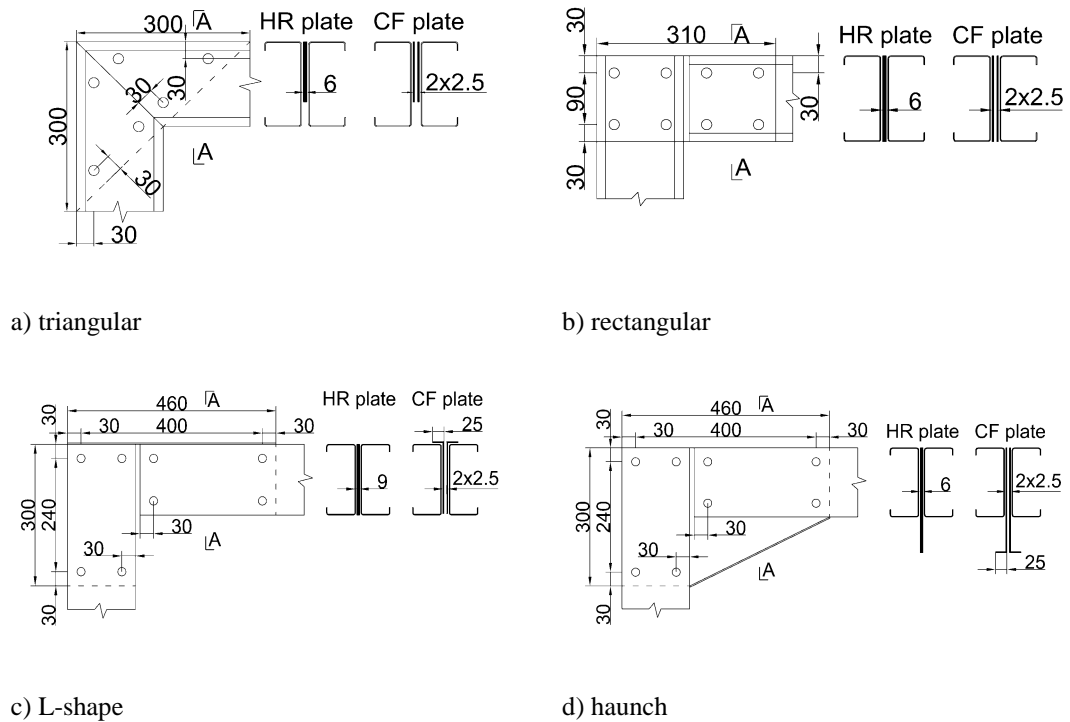
Figure 2-5 Eaves joint brackets after Chung and Lau (1999)

a) cross-shape bracket without chamfers   b) cross-shape bracket with chamfers
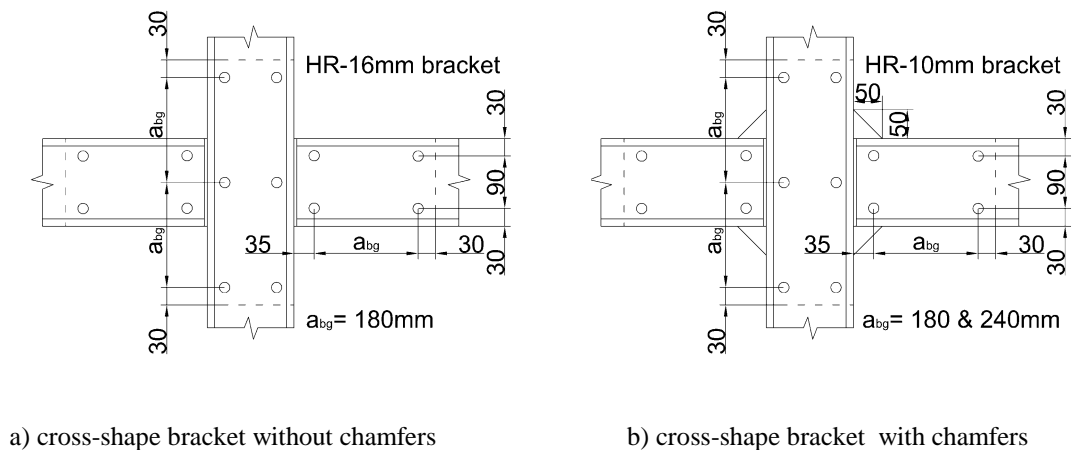
Figure 2-6 Beam-column sub-frame joint after Yu et al. (2005)

14

Summarising the research effort on cold-formed steel framing systems Chung and Ho (2005) reported tests on 26 nested Zed sections under a point load bending. The main difference between these joints (see Figure 2-7) and the joint presented in Figure 2-3 was that 4 and 6 bolts were used to form a lapped joint. The scale of the study was also far more extensive compared with that presented by Zadanfarrokh (1991). The general conclusion drawn was that in order for a joint to present full-strength the ratio of the bolt-group length to section depth must be equal or greater than 2. The investigated joint will have the stiffness similar to that of a continuous member if the bolt-group length to section depth ratio is equal or greater than 4. Although main motivation of the research was to develop design formulas suitable for designing overlapped purlins the same combined bending and shear load design equation was proposed for predicting strength of bolted joints in portal frames.
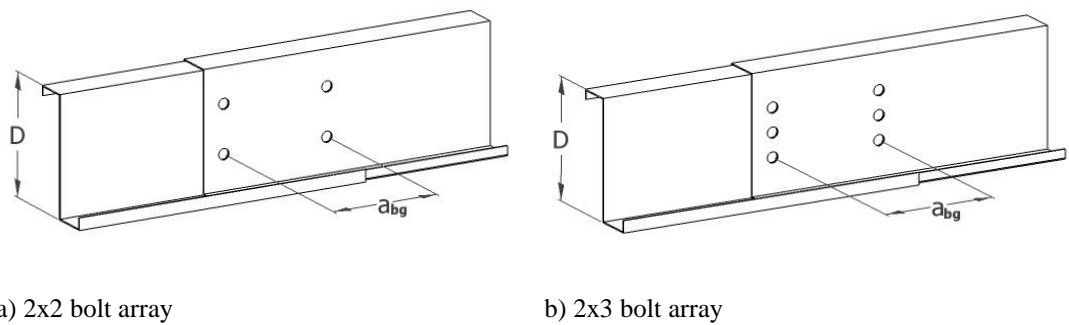
a) 2x2 bolt array   b) 2x3 bolt array

$a_{bg}/D \geq 2$ – full-strength joint , $a_{bg}/D \geq 4$ – rigid joint

Figure 2-7 Lapped Zed joints after Chung and Ho (2005)

2.1.6   Lim and Nethercot

Lim and Nethercot studied the possibility of using an inexpensive folded bracket to form joints in portal frames of moderate spans. The details of the proposed eaves and apex brackets are shown in Figure 2-8. Unlike Chung and Lau (1999), the joints tested by Lim and Nethercot isolated failure of the brackets from that of the channel sections.

Design recommendations for the stiffener depth as well as analytical methods for evaluating bracket strength were presented. The bending capacity of the back-to-back channel sections used by Lim and Nethercot (2002) was 4 times higher than that used by Chung and Lau (1999). Having ensured that the brackets themselves would not fail, research was focused on the strength of the channel sections, as influenced by the bolt-group size. An analytical method for predicting rotational stiffness of such joints was also developed where the stiffness of each component contributing to overall joint stiffness was investigated. Tests on the joints as well as a full-scale test on a 12m span portal frame were reported albeit only under gravity load. As test frame was laid flat on the laboratory floor, torsional effects were removed from the study by providing unrealistically rigid lateral and torsional restraints. The reversed load case (simulating the wind uplift) in which unstiffened bracket plate is in compression was also not considered.

c) eaves joint   d) apex joint
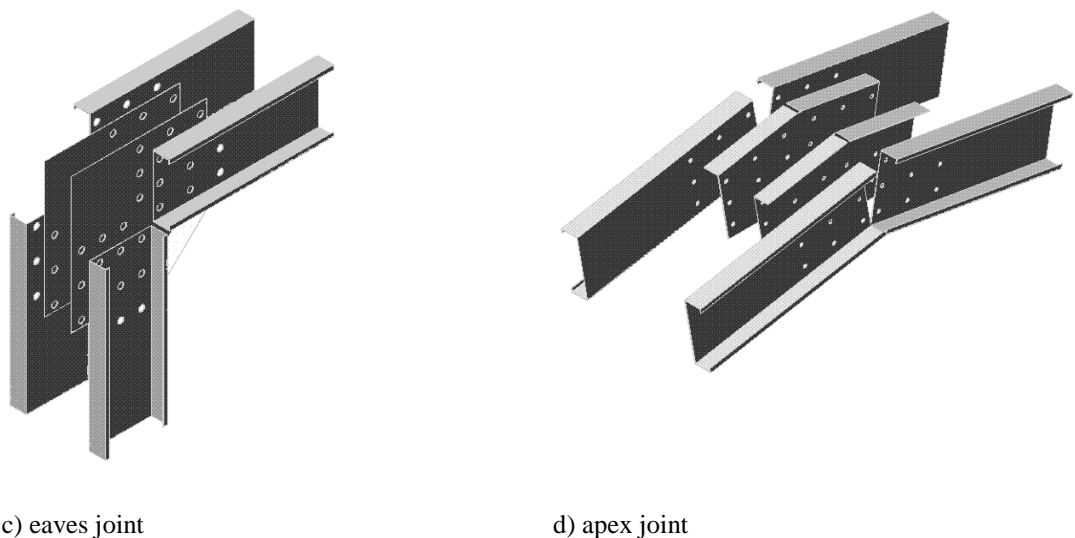
Figure 2-8 Portal frame joints after Lim and Nethercot (2002)

2.1.7   Mills and LaBoube

Mills and LaBoube (2004) conducted an experimental study on different joint arrangements which were found in the Australian cold-formed steel shed industry. Popular joints included an end plate connection bolted to the column and welded to the rafter (Figure 2-9a), and a mitred joint (Figure 2-9b). Self-drilling

16

screws were used as an alternative to conventional bolting. A similar arrangement for the apex joint was also studied, in which double lipped channel sections were used as the gusset plates and screwed back-to-back to the rafters (Figure 2-9d and Figure 2-9e). The strength and the stiffness of each proposed joint was compared against benchmark results obtained from tests on welded joints as shown in Figure 2-9f. The welded joints (see Figure 2-9 options a, b and f) are considered highly unpractical as critical structural welds on light-gauge steel would have to be done in automated process resulting in high costs. The post-welding corrosion protection would add further to the cost. The screwed connections (see Figure 2-9 options c, d and e) although inexpensive, could only offer a viable alternative for short-spanning frames.

| a) bolted end plate joint | b) mitred joint | c) self-drilling screw joint |

| d) 4 screws joint | e) 16 screws joint | f) welded joint |
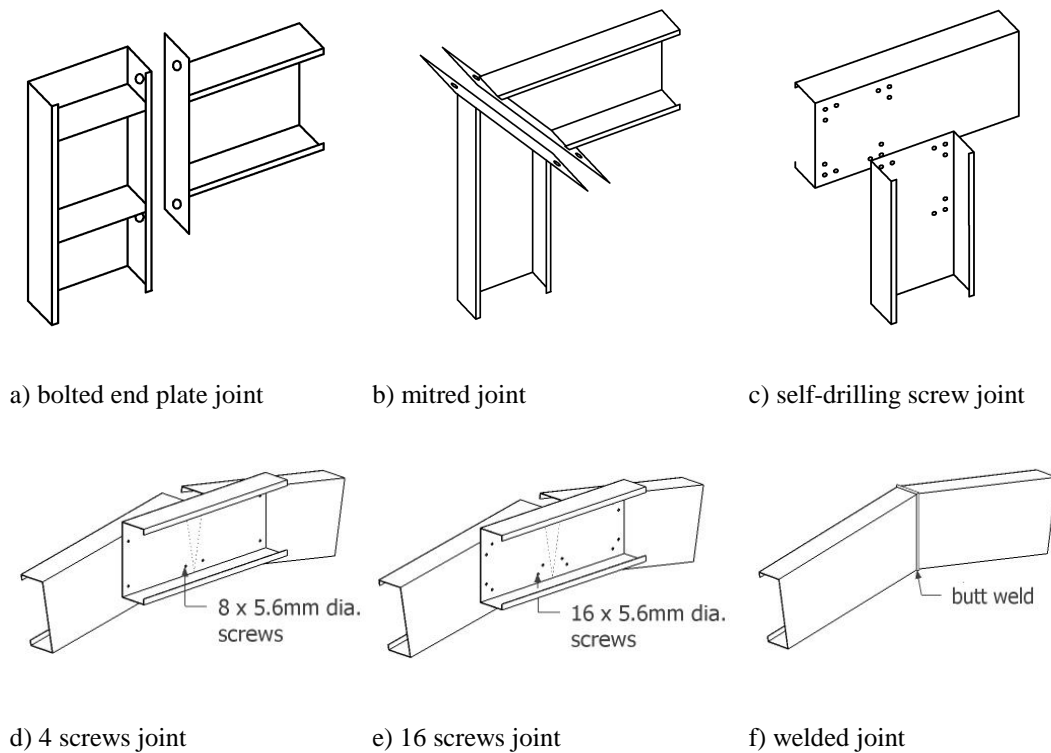
Figure 2-9 Eaves and apex joints after Mills and LaBoube (2004)

2.1.8   Dubina et al.

Dubina et al. (2004) investigated eaves and apex joints formed by three different types of welded brackets. As can be seen in Figure 2-10a and c, the channel sections were bolted only through the web of welded I-section brackets (KIS, KIP)

17

and spaced gussets bracket (KSG). In the second variant, bolts were located both on the web and on the flange (Figure 2-10b) of I-section bracket (KIS) and I-section bracket with plate bisector (KIP). The moment-capacity of the channel sections being connected was 117.8 kNm. It should be noted that unlike Chung and Lau (1999), the joint was formed through hot-rolled steel welded connection brackets.

a) I-section bracket (KIS)

b) I-section bracket with plate stiffener (KIP)

c) Spaced gusset bracket (KSG)
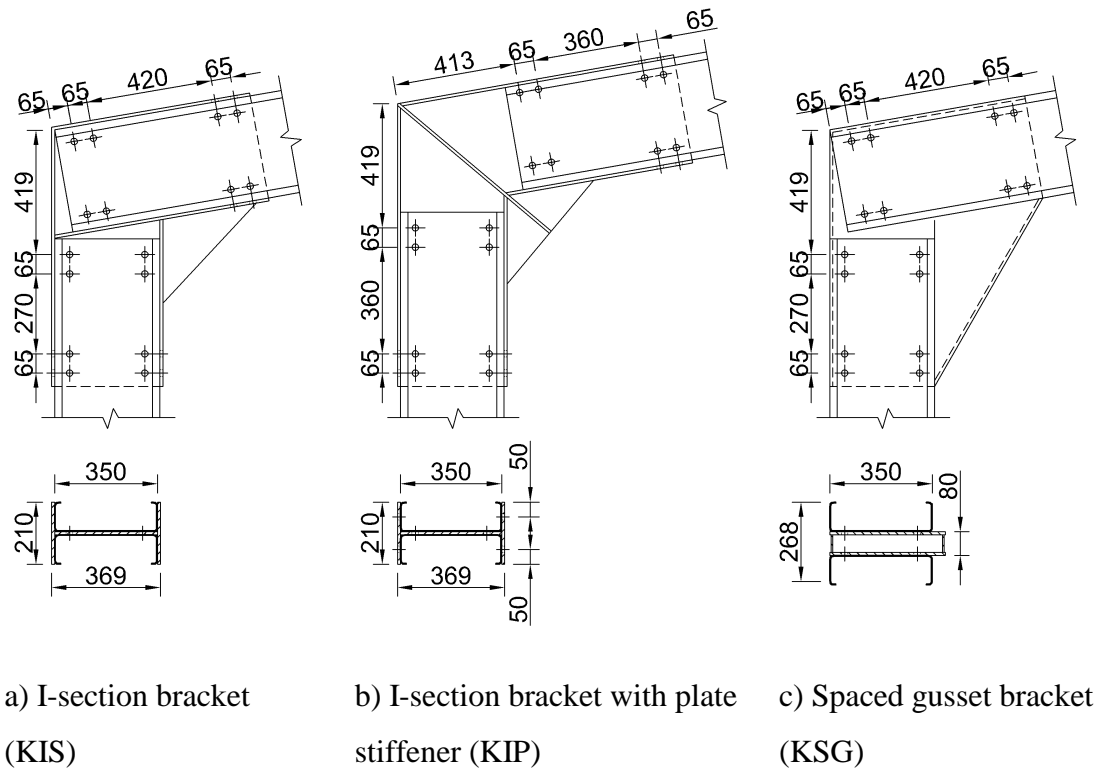
Figure 2-10 Eaves joints after Dubina et al. (2004)

Zaharia and Dubina (2006) also conducted an experimental study on the flexibility of a single fixing lap joint similar to that reported by Zadanfarrokh and Bryan (1992). The authors however introduced an additional variable into the equation previously proposed by Zadanfarrokh and Bryan (1992) in the form of he bolt diameter. Based on 27 experiments Zaharia and Dubina (2006) defined the stiffness of a single bolt lap joint as:

$$k_{Zah} = 6.8 \frac{\sqrt{D}}{\left(\dfrac{5}{t_1} + \dfrac{5}{t_2} - 1 \right)} (kN/mm) \tag{2-2}$$

where:

t_1, t_2 – thicknesses of the sheet of metal (2mm $\leq t_1$ and $t_2 \leq$ 4mm)

D – nominal diameter of the bolt (8mm $\leq D \leq$ 16mm and 1mm hole clearance).

Analytical methods for calculating joints rotational stiffness and moment-resistance were also presented and validated against full-scale 12m span portal frame tests. Despite the use of heavy brackets proposed joints still shown semi-rigid behaviour, but the full-strength requirement was achieved. The high manufacturing cost of the hot-rolled, welded brackets made this system less competitive than cold-formed bracket option. Zaharia and Dubina (2006) also conducted an experimental study on the flexibility of a single fixing lap joint similar to that reported by Zadanfarrokh and Bryan (1992). The authors however introduced an additional variable into the equation previously proposed by Zadanfarrokh and Bryan (1992) in the form of he bolt diameter. Based on 27 experiments Zaharia and Dubina (2006) defined the stiffness of a single bolt lap joint as:

$$k_{Zah} = 6.8 \frac{\sqrt{D}}{\left(\dfrac{5}{t_1} + \dfrac{5}{t_2} - 1 \right)} (kN/mm) \tag{2-3}$$

where:

t_1, t_2 – thicknesses of the sheet of metal (2mm $\leq t_1$ and $t_2 \leq$ 4mm)

D – nominal diameter of the bolt (8mm $\leq D \leq$ 16mm and 1mm hole clearance).

Analytical methods for calculating joints rotational stiffness and moment-resistance were also presented and validated against full-scale 12m span portal frame tests. Despite the use of heavy brackets proposed joints still shown semi-rigid behaviour, but the full-strength requirement was achieved. The high manufacturing cost of the hot-rolled, welded brackets made this system less competitive than cold-formed bracket option.

2.1.9 Dundu and Kemp

Dundu and Kemp (2006) conducted research on single channels connected back-to-back without a bracket (see Figure 2-11). Such an arrangement is similar to that of Mills and LaBoube (2004), the main difference being that self-drilling, self-taping screws were replaced by bolts. The bolt arrays considered in this study were 2x2 and 3x3 as shown in Figure 2-11. The authors proposed the use of the plastic hinge design method, and so concentrated on the ductility of the joints. For that reason three different grades of steel were considered with average measured yield strengths of 283N/mm^2, 345N/mm^2 and 472N/mm^2. Such bolted system although inexpensive would only offer a viable attentive for short-span portal frame as strength and stiffness of the connection is predetermined by the maximum depth of the single channel section.

a) 4-bolt joint   b) 8-bolts joint
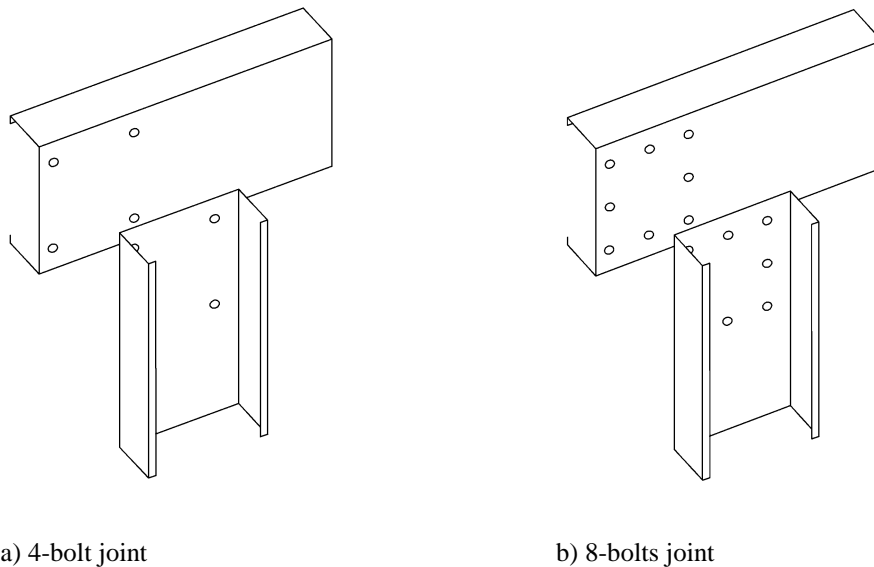
Figure 2-11 Bolted joint after Dundu and Kemp (2006)

2.1.10 Kwon et al.

Kwon et al. (2006) reported research on applications of closed sections produced by a combination of cold-rolling and clinching techniques. The sections used for the tests were 150 mm deep, 40 mm wide and 0.8 mm thick. The local buckling moment calculated from the gross section modulus was 3.55 kNm.

Connection brackets for the eaves and apex joints were constructed from mild steel plates 2.3 mm through combination of folding and welding, with four different connection types as shown in Figure 2-12. Self-drilling, self-tapping screws of 4.8mm diameter were used to form each type of joint. As highlighted previously the use of welded connection brackets will result in a high cost of the system. It was evident from tests that novel section failed at the web/flange clinched connection and better understating of flexural behaviour of the member is needed before it can be employed as a part of portal frame system.
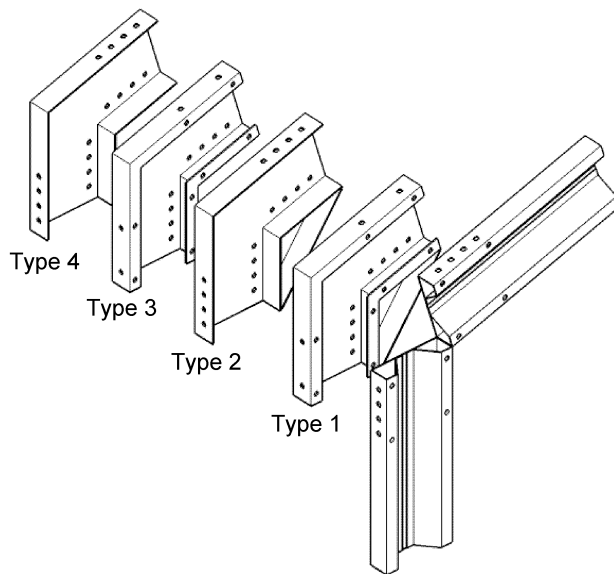
Figure 2-12 Eaves joints for PRY sections after Kwon et al. (2006)

2.1.11 Rhodes and Burns

Rhodes and Burns (2006) conducted extensive tests on joints of a cold-formed steel portal framing system. Figure 2-13 shows details of the eaves joint. The columns and rafters of the largest joint were formed from back-to-back channel sections having a moment capacity of 128.5 kNm and 76.7 kNm, respectively. The proposed eaves joint used knee-braces formed through back-to-back channel sections bolted to the flanges of the column and rafter through a welded bracket. At the eaves, the joint was formed through a pair of angle sections; to avoid the failure of the flange under concentrated load, pairs of angle stiffeners were introduced. Proposed

eaves joint offered an alternative to a haunch bracket moment-resisting connection, especially for frames of significant spans (up to 20m in the UK). In order for the knee brace joint to be effective it needs be much bigger than a haunch bracket and it creates greater obstruction to the clear height. Hot-rolled fabrication, welding costs along with complexity of the assembly will present serious cost disadvantage of this system.
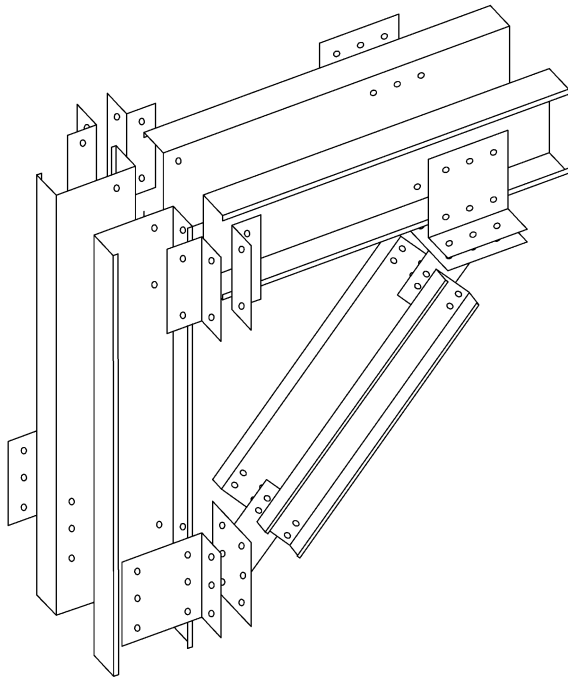
Figure 2-13 Knee brace eaves joint after Rhodes and Burns (2006)

2.1.12 Tahir and Siang

Tahir and Siang (2008) proposed bracketless joints between back-to-back double channel sections in which the beam flanges are notched and webs are bolted together as shown in Figure 2-14. Similar to joints proposed by Dundu and Kemp (2006), strength and stiffness of the joint is limited by the depth and the thickness of the channel. Potential savings in amount of steel used by decreasing channels thickness and increasing the grade of steel from 350 to 450 were also investigated. The savings in amount of steel used were consumed by the joint moment resistance reduction. Lighter gauge sections also presented significantly lower rotational

capacity, failing in premature web buckling which made such connection unsuitable for portal frame application.
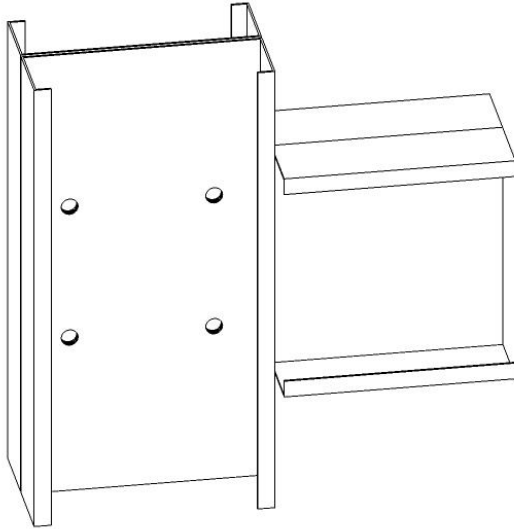
Figure 2-14 Bracketless beam-to-column joint after Tahir and Siang (2008)

2.1.13 Elkersh

Elkersh (2010) reported research on the joints formed through a flat gusset plate similar to those reported by Chung and Lau (1999) as shown in Figure 2-15. The main difference was that different bolts arrays were investigated. Extensive finite element investigation was also reported and calibrated against test results. As expected, it was demonstrated that in all the tests gusset plate of 5mm thickness (2 times thickness of the section) failed in local buckling regardless of bolt-group length. Increasing the thickness of the gusset plate to 8mm improved the strength of the joint by 17% by preventing local buckling of the gusset plate. Further increase of the gusset plate thickness to 10 mm caused failure of the channel sections at the loading points. The author focused mainly on the overall strength of the joints when the effect of different thicknesses and bolt-group configuration on the joint stiffness was not presented. The research has not offered any guidance how the work can be employed in portal frame design without using complex finite element analysis.
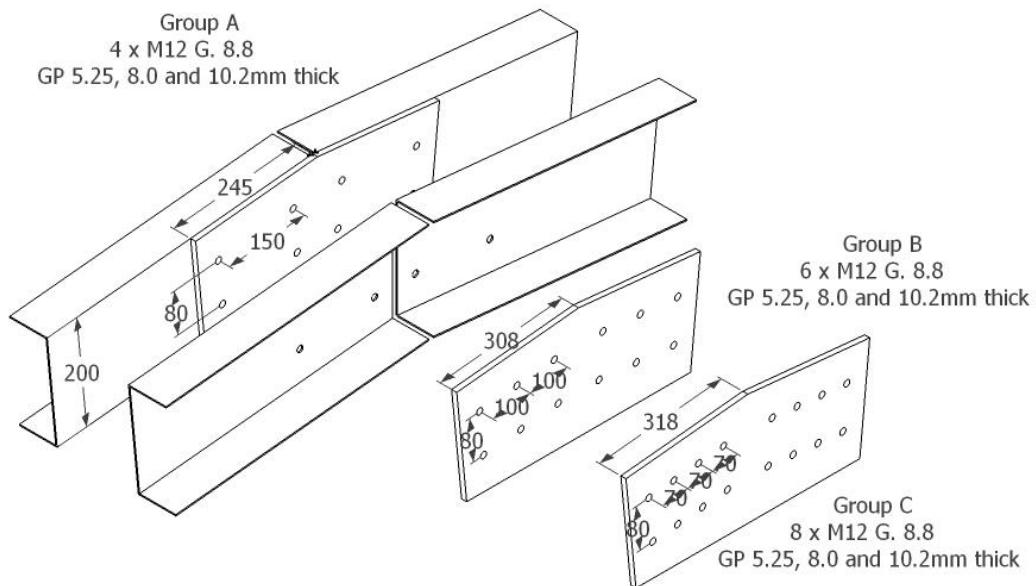
Figure 2-15 Apex joints after Elkersh (2010)

2.1.14 Hazlan et al.

Hazlan et al. (2010) reported research on four different beam-to-column joints constructed from single channel sections bolted back-to-back as shown in Figure 2-16. The main aim of the research was to improve stiffness of the joint and limit rotational capacity of the joint to 0.03rad unlike Chung and Lau (1999) who proposed the less stringent limit of 0.05rad . In order to reduce initial free body rotation a 0.5mm bolt hole clearance was used. All the joints were examined against strength, stiffness and ductility requirements according to BS EN 1993-1-8 (2005). All the joints apart from joint type 1 failed in local buckling of the web rather than connection failure (e.g. bolt tilting) and can be classified as partial-strength with moment resistance ratio ranging from 0.71 to 1.00. Only joints type 2 and 3 have presented rotational capacity, which was less than 0.03rad. Although multi-story frames application was considered, due to satisfactory strength and stiffness performance of investigated joints, the same design concept could be employed in portal frames as shown by Dundu and Kemp (2006). It can be expected that similar limitations in terms of spanning capability will apply as frame resistance would be limited to a bending capacity of a single channel.

Type 1　　　　　　Type 2　　　　　　Type 3　　　　　　Type 4
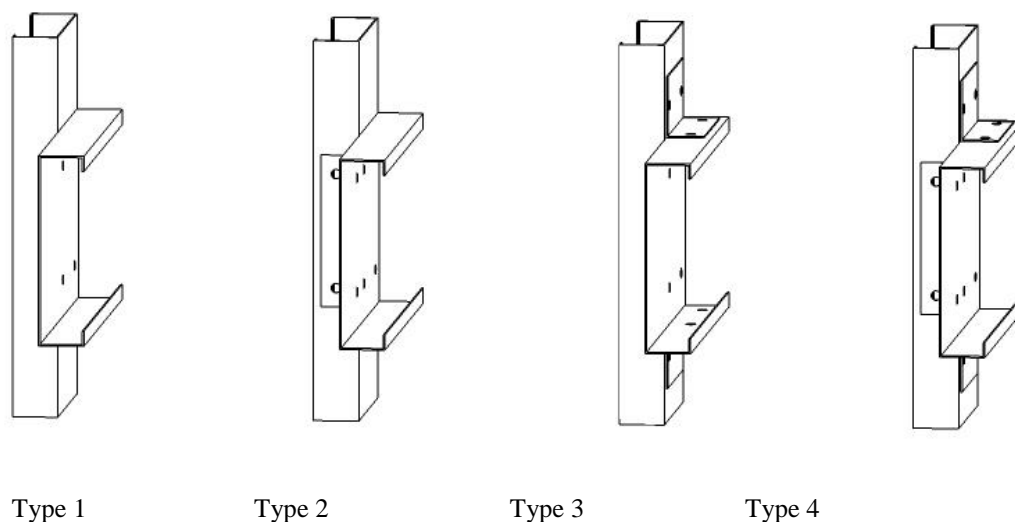
Figure 2-16 Beam-to-column joints after Hazlan et al. (2010)

2.1.15 Yang and Liu

Yang and Liu (2011) reported tests on 10 different Sigma sections connected through cold-formed sleeves of the same thickness as shown in Figure 2-17. The moment resistance of tested sections (based on Effective Width Method) varied from 8.1 to 39 kNm. Two theoretical methods (also referred to in portal frame joint design) were validated against test data: combined bending and web crippling (Dubina and Ungureanu (2008)) and combined bending and shear force (Chung and Ho (2005)). The first method produces conservative predictions with the safety margin in the range of 12%. The theoretical method of predicting the rotational stiffness of the joint, proposed by Zadanfarrokh and Bryan (1992) was also used and good correlation against test results was obtained. A tri-linear rotational stiffness model was used incorporating initial stiffness due to friction, then slip due to bolt-holes tolerance and bearing stiffness. Although the theoretical method was only calibrated for the M16 bolts, when used for joints with M12 bolts, it still represented the joint behaviour quite well. This research although originally intended for Sigma purlins systems could also be employed in the design of eaves and apex joints and presents test evidence that existing methods are suitable to design moment-resisting joints.
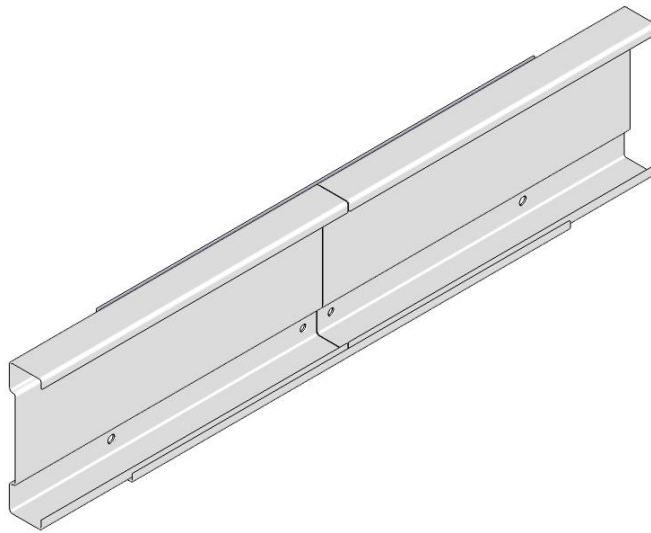
Figure 2-17 Sigma purlins sleeved joint after Yang and Liu (2011)

2.1.16 Wuwer et al.

Walentyński and Wuwer (2010), Swierczyna and Wuwer (2011) and Wuwer et al. (2012) reported research on strength and stiffness of plain channels connected back-to-back by novel mechanical fasteners called Huck BOM[®] blind bolts (see Figure 2-18). The testing methodology similar to this presented by Zadanfarrokh and Bryan (1992) was used and the authors also concentrated on the behaviour of asymmetric bolt-group. The main difference between these two studies was that Wuwer used sections of 4 and 5mm thickness instead of 2mm, and blind bolts of 13.6mm diameter with 0.7mm holes tolerance. Additionally unlike Bryan (1993) or Dubina and Zaharia (2006) who used a linear load-deflection relationship, the authors used an exponential load-displacement relationship (after Crawford and Kulak (1971)) calibrated against test results. The Instantaneous Centre of Rotation Method was also used in the analysis since the analysed joints were loaded eccentrically producing not only rotation but also translation. The mathematical model was developed in which stiffness degradation factors were introduced in order to represent linear and rotational stiffness of the joint under a complex state of loading. The effect of friction between the plates was also successfully implemented into the mathematical model. The rotational stiffness of the 3-bolt joint (see Figure

2-19a) calculated to BS EN 1993-1-8 (2005) and using the linear load-displacement relationship recommended by Dubina and Zaharia (2006) was approximately a secant of the non-linear stiffness model presented by Swierczyna and Wuwer (2011).
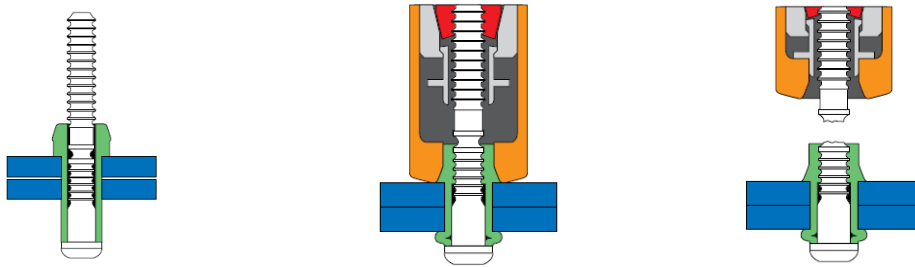
Figure 2-18 Huck BOM® blind bolts installation method
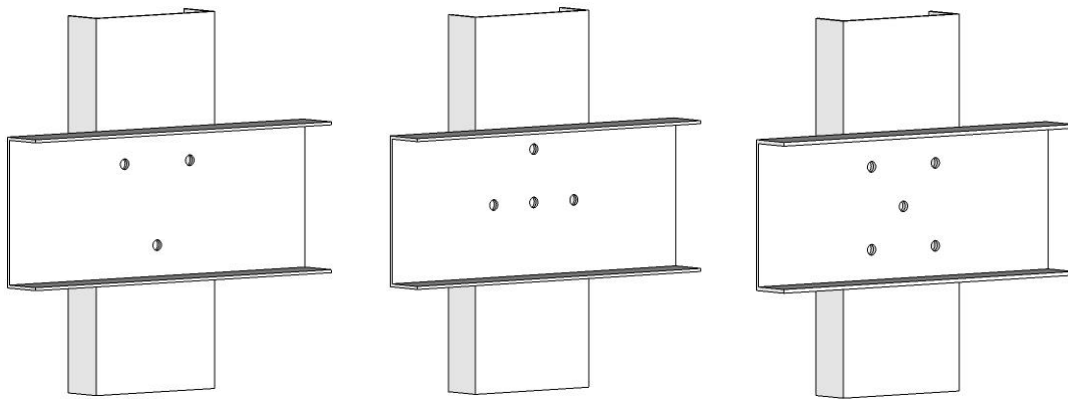
a) 3-bolts array   b) 4-bolts array   c) 5-bolts array

Figure 2-19 Plain channel bolted joints after Walentyński and Wuwer (2010) and Swierczyna and Wuwer (2011)

2.1.17 Santos and Simoes da Silva

Santos and Simoes da Silva (2011) presented a conceptual study of the potential use of back-to-back cold-formed steel members of 450mm depth and 4mm thickness in light industrial portal frames with cranes. For such buildings limiting horizontal deflection is crucial thus a knee-brace eaves joint was proposed based on the analogous joint presented by Rhodes and Burns (2006). Every joint was constructed through a welded bracket which was connected with the section through the web as well as the flanges similar to the joint investigated by Dubina et al. (2004)

(see Figure 2-10b) Each joint (base connection, eaves joint and apex joint) was tested separately in order to establish strength and stiffness characteristics. The paper does not offer enough detail to illustrate the form of the joints here. The stiffness of the apex joint was shown to be in the range of 14000kNm/rad.

2.1.18 Bolted joints proposed by the author

Only joints made entirely from cold-formed steel plates were proposed for the experimental study in order to keep the cost low. The joints contain an array of bolts in the web of the sections and additional line of bolts in each flange. Such joints had not yet been tested so their resistance and stiffness properties were unknown. The following joints of the duo-pitch portal frame were considered:

1) haunch bracket eaves joint (see Figure 2-20a)

2) haunch bracket apex joint (see Figure 2-20b)

All the brackets were manufactured by press braking from 3mm thick galvanized plates. The sections as well as the brackets were cold-formed, cut to length and pre-punched by the same manufacturer.
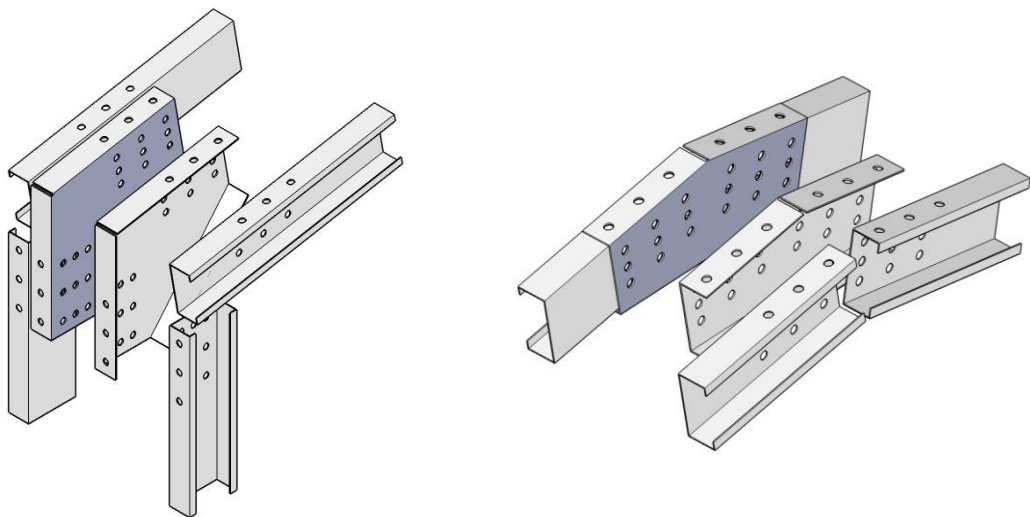
| a) Haunch eaves joint | b) Haunch apex joint |

Figure 2-20 Schematic drawings of joint assembly

2.2   Summary of the state of the art research

Over the past thirty years, researchers have undertaken tests on different arrangements for joints of cold-formed steel members. Table 2-2 summarises the joints reported in the literature by each researcher, including the moment capacity of the cold-formed steel sections being connected, rotational stiffness of the connection and the number of components and fasteners required to form the joint. When moment capacity of the cross-section was not reported in the source, it was calculated to BS 5950-5 (1998b). The ratio of the experimental moment capacity of the joint to analytical moment capacity of the cross-section was also shown to indicate if presented joint could be classified as full or partial strength according to BS EN 1993-1-8 (2005). The values of experimental rotational stiffness were expressed in the form of stiffness ratio K_j and classified according to Figure 2-21.

$$K_j=S_{j,ini}/(EI_b/L_b) \hspace{4cm} (2\text{-}4)$$

where:

$S_{j,ini}$ – rotational stiffness of the joint,

E – Modulus of Elasticity,

I_b – moment of inertia of the jointed beam member

L_b – length of the jointed beam member

The length of each beam member (L_b) was assumed as 1m for normalised stiffness ratio ($K_{j,nor}$) per meter span. The realistic stiffness ratio of each reviewed joint, in portal frame application can be calculated by multiplying ratio ($K_{j,nor}$) presented in Table 2-2 by permissible span (L_f). Additional data which was not quoted from the referred document was assumed or read from figures and is marked by asterisk in Table 2-2.

The existing codes of practice provide guidance on calculating plate critical buckling stress but neglect stresses localised around the bolts which may cause premature buckling of the plate in the vicinity of a bolt-group. Because galvanized

members cannot be welded, the use of fasteners makes joints semi-rigid. BS EN 1993-1-8 (2005) provides guidance on how to analyse structures with such joints but rotational stiffness must be established by testing. For this reason researchers have dedicated a lot of effort in testing bolted joints as summarised in Table 2-1.
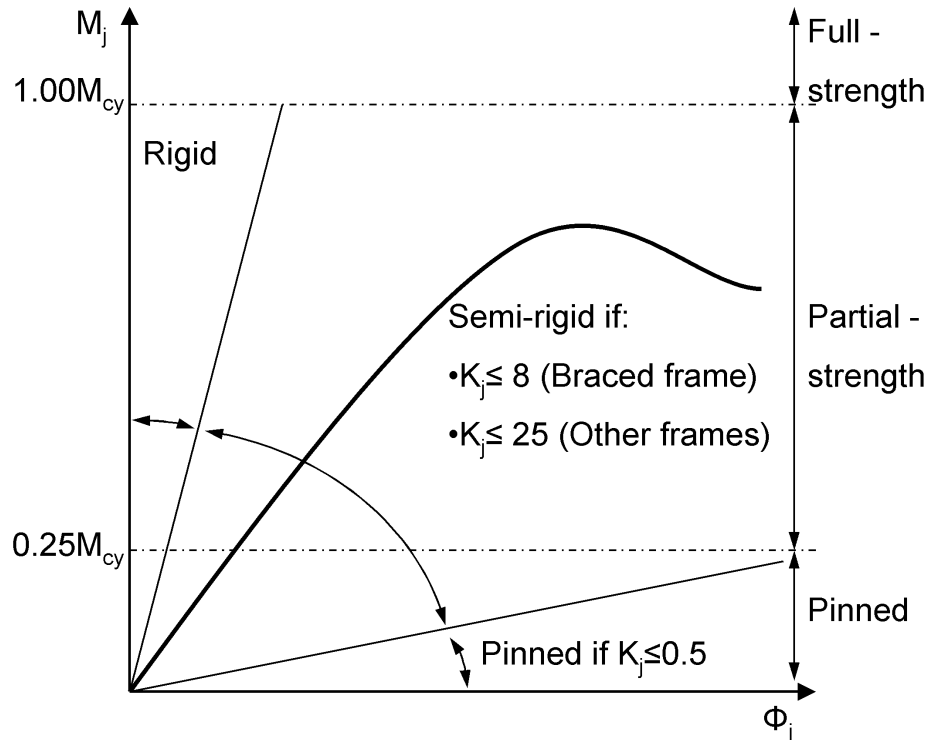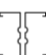
Figure 2-21 Classification of joints by strength and stiffness according to BS EN 1993-1-8 (2005)

The most popular type of joint was that with bolts in the web only (Mäkeläinen and Kankaanpää (1996), Chung and Lau (1999) and Lim and Nethercot (2003b)). Such joints, although inexpensive and easy to assemble on site, were shown to be partial-strength, since the forces could not be transferred through the flange and through the web. The other weak point of such joints is that the bending capacity of the bracket is significantly reduced when the flat portion of the bracket plate is in compression. Framing systems presented by Kirk (1986), Lim and Nethercot (2002) or Rhodes and Burns (2006), where purlins and side rails are fixed to the web of the rafter and column (in-line system), are less sensitive to torsional effects.

Table 2-2 Joints reported in the literature

Author	Sections			Connectors				Fasteners		Joint			
	$D \times B \times t$ (W_s) (kg/m)	f_{yb} N/mm^2	M_{cy} kNm	W_b kg	t_b mm	$f_{yb,b}$ N/mm^2	No. of brackets	Type	No. of fixings/ joint	a_{bg} b_{bg} mm	$S_{j,ini}$ $(K_{j,nor})$ kNm/rad	M_{exp} kNm	$M_{exp}/$ M_{cy}
Baigent (1978)	153x79x1.9 (4.69)	325.8	9.0*	13.86	12	-	1	M19 HSFG bolts	8	-	rigid	6.4*	0.78
Kirk (1986)	220x65x2.4 (14.64)	280 [n]	32.0	14.00	3	280 [n]	2	M16 G.8.8	8	300 124	rigid	41.60	1.30
Zadanfarrokh (1991)	200x70x1.5 (4.08)	317	8.2	N/A				M16 G.4.6	4	200 120	300 (0.45)	5.85	0.71
Makelainen (1996)	400x80x3.0 (28.32)	350 [n]	118.8*	45.77*	12	355 [n]	1	M16 G.8.8	22	-	-	113.2*	0.95
Chung (1999)	150x64x1.6 (7.54)	471	18.5	5.40	6	343	1	M16 G.8.8	8	240 90	1125 (1.57)	15.38	0.83

Continuation of Table 2.1

Lim (2002)		336x88x3.0 (24.50)	358	96.8	49.11	4	341	2	M16 G.8.8	18	615 230	8000 (0.77)	87.5	0.90
Mills (2004)		200x76x1.5 (4.25)	450[n]	10.8	N/A				Screws Ø 13.6	12	-	rigid	7.80	0.72
Dubina (2004)		350x100x3.0 (26.72)	452	117.8	110.79	10	355 [n]	1	M20 G.6.8	32	490 250	6957 (0.55)	116.7	0.99
Dundu (2005)		300x75x3.0 (10.81)	472	47.5*	N/A				M20 G.8.8	8	230 230	1960 (0.54)	39.4*	0.83
Rhodes (2006)		402x97x3.2 (30.23) column	352	128.5	2.74	6*	250 [n]	2	M16	32	-	-	135.8*	1.06
		342x97x2.5 (21.96) rafter	343	76.7	25.66			4				10809	84.1	1.10
		202x69x2.0 (11.12) knee brace	350 [n]	26.5	10.57 4.30 6.05			2 1 1						

Continuation of Table 2.1

Source	Section	Dimensions							Bolts					
Kwon (2006)		150x40x0.8 (2.57)	652	3.55	2.06	2.3	240 [n]	1	Screws Ø 4.8	28*	90 / 110	23 (0.13)	7.0	1.97
Tahir (2008)		250x77x2.0 (13.10)	350	37.8	-	-	-	-	M16 G.8.8	4	150 / 150	464* (0.14)	15.50	0.41
Elkersh (2010)		200x75x2.5 (14.29)	346	36.7	6.16	8.0	346	1	M12 G.8.8	4	150 / 80	1057* (0.45)	26.10	0.71
Hazlan (2010)		250x77x2.0 (6.55)	350	18.9	0.40	2.0	350	3	M12 G.8.8	16		3480 (2.15)	18.00	0.95
Yang (2011)		300x75x3.0 (11.41)	417	39.0	9.68	3.0	417	1	M16 G.8.8	4	439 / 240	481 (0.13)	39.4	1.01
Swierczyna (2011)		200x60x4.0 (9.54)	258	17.2	-	-	-	-	Blind bolts Ø 13.6	3	110 / 110	247 (0.18)	6.0*	0.35
Wrzesien (2012)		152x64x2.0 (9.34)	395	22.25	15.24	3.0	384	2	M16 G.8.8	30	280 / 80	1229 (1.36)	20.31	0.91

Unlike typical in-line systems the author has investigated a system in which hat-shaped purlins and side rails are fixed to the outside flange of the primary member (as in hot-rolled construction). In such an arrangement the torsion of the member is more likely to occur therefore out-of-plane stiffness of the brackets was increased by additional folded stiffeners. Additional bolts were also introduced which connected outside flange of the member with the bracket. The author tested both joint arrangements with and without outer stiffeners and as suspected joints without the stiffeners did not offer sufficient torsional restraint to the rafter member (shown in Figure 2-22).
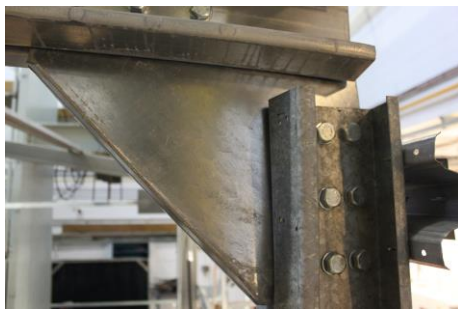
| a) Front view of the eaves bracket without outer stiffeners | b) Side view of the eaves bracket under torsion |

Figure 2-22 Mode of failure in preliminary test on brackets without outer stiffeners

The full-strength joints presented in the literature for portal frame application were by Kirk (1986), Dubina et al. (2004) and Rhodes and Burns (2006). According to the efficiency study presented in Section 2.3.4, the lightest frame was that using knee braced joints after Rhodes and Burns (2006). The high manufacturing costs of hot-rolled steel components however made this system less completive in price. The heaviest frame design was offered by the Swagebeam system (Kirk (1986)) however the same system offered the least expensive frame. The general conclusion was that frames with full-strength joints often require hot-rolled steel components which make them approximately 1.5 times more expensive than the cold-formed steel (CFS) alternative. In light of these findings the framing system manufactured entirely from CFS components for both members and

connection brackets had been selected for further investigation (see Figure 2-25) as it offered desired efficiency measures.

2.3   Structural and cost efficiency of joints

Among all of the cold-formed, moment-resisting joints reviewed only those suitable for pitched roof portal frame applications were chosen for further analysis (see Table 2-3 and Table 2-4). Two types of joints A and B proposed by the author are also considered. Both joint types contain the same 3x3 bolt-array as shown in Figure 2-20. The width of both bolt-arrays is of 80mm as it is limited by the width of the channel sections. The only difference between joint Type A and B is the length of the bolt-array which is 160mm and 280mm, respectively. Increasing the length of the bolt-array will increase joint rotational stiffness by approximately a factor of 2 (see Table 2-3) and will make the bracket larger.

These joints are used in portal frame designs according to UK loading conditions. The same cold-formed steel cross-sections as those reported in the literature are used for columns and rafters. The experimental values of ultimate bending capacity (M_{exp}) and the rotational stiffness of the joints ($S_{j,ini}$) extracted from the literature, were used for the analysis according to Table 2-3 and Table 2-4.

In order to establish the best performing joint, all the listed joints were used in the design of average dimension cold-formed steel portal frames in two spans of 6 and 12m (according to Section 1.2). The only exception from the average dimensions is the height to the eaves (H_e), which is set as 4m to accommodate 'knee brace' type of joint. The outcome of the structural analysis is the maximum permissible frame spacing (S_f) for each type of joint presented in Table 2-3 and Table 2-4. The following values were assumed as constants in the analysis:

1) Height to eaves $H_e = 4$m

2) Roof pitch of 10°

3) Frame span $L_f = 6$m or 12m depends on columns/rafters capacity

2.3.1 Beam idealisations of portal frames

Four different structural models were used to model the behaviour of reviewed joints as shown in Figure 2-23:

1) Model 1 consisting rigid joints

2) Model 2 consisting semi-rigid joints of the same rotational stiffness ($S_{j,ini}$) and finite lengths of brackets (l). Such model represents joint which are formed through connector/ bracket with bolt-group at both ends.

3) Model 3 consisting semi-rigid joints of the same rotational stiffness ($S_{j,ini}$) in which single column and rafter sections are fixed through the web. Such joint would therefore have only one rotational spring modelled.

4) Model 4 consisting semi-rigid joint at the apex and triangulated knee brace joint at the eaves. According to Rhodes and Burns (2006) recommendation the rotational stiffness of the joints at the eaves were assumed zero.

a) rigid joints

b) semi-rigid with two centres of rotation

c) semi-rigid with one centre of rotation

d) knee brace joint
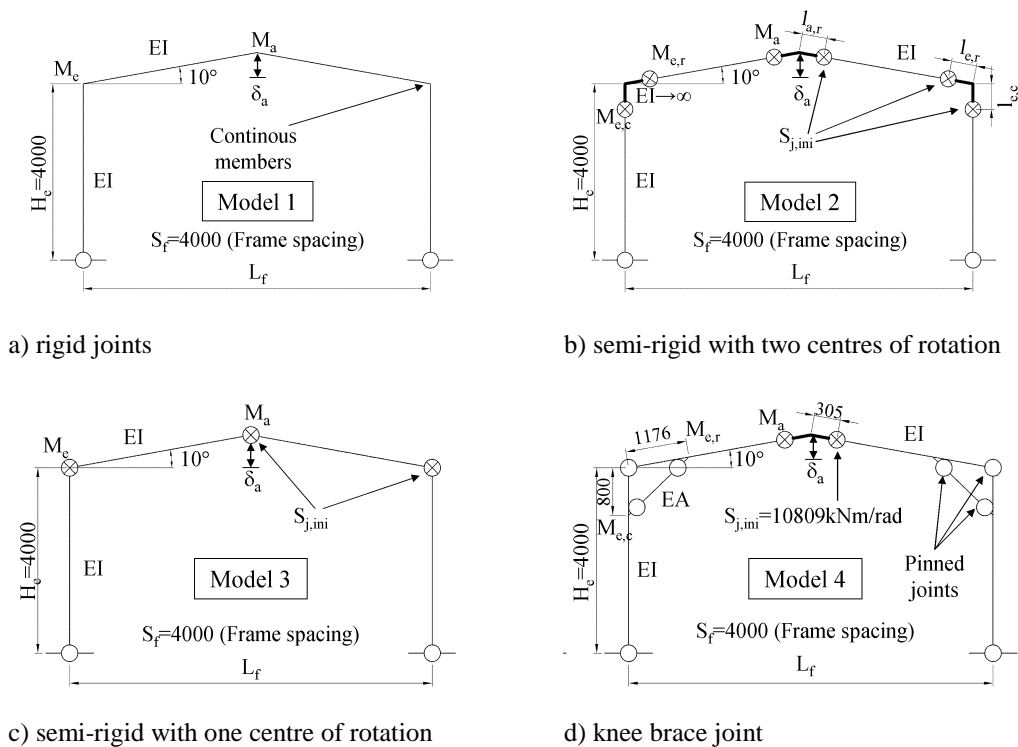
Figure 2-23 Beam idealisations of portal frames with different types of joints

36

Table 2-3 Joints reported in the literature for CFS portal frames of 6m span

Author	Sections characteristic			Joint characteristic						Permissible frame spacing		
	D x B x t	A	I_y	Model	$l_{e,c}$	$l_{e,r}$	$l_{a,r}$	$S_{j,ini}$	M_{exp}	$S_{f,max}$	f_{ULS}	f_{SLS}
	(mm)	(cm^2)	(cm^4)		(mm)	(mm)	(mm)	(kNm/rad)	(kNm)	(m)		
Baigent (1978)	153x79x1.9	5.98	221.24	1	-	-	-	rigid	6.4*	2.397	1.00	0.73
Mills (2004)	200x76x1.5	5.41	336.50	3	-	-	-	rigid	7.8	2.919	1.00	0.59
Elkersh (2010)	200x75x2.5	18.21	1107.10	2	200	200	122	1057*	26.1	5.621	0.63	1.00
Wrzesien A	152x64x2.0	11.90	429.66	2	221	221	145	596	16.2	2.753	0.48	1.00
Wrzesien B	152x64x2.0	11.90	429.66	2	266	266	205	1229	18.2	4.360	0.65	1.00

Table 2-4 Joints reported in the literature for CFS portal frames of 12m span

Author	Sections characteristic			Joint characteristic						Permissible frame spacing		
	D x B x t	A	Iy	Model	le,c	le,r	la,r	$S_{j,ini}$	M_{exp}	$S_{f,max}$	f_{ULS}	f_{SLS}
	(mm)	(cm2)	(cm4)		(mm)	(mm)	(mm)	(kNm/rad)	(kNm)	(m)		
Dundu (2006)	300x75x3.0	13.77	1713.70	3	-	-	-	1960	39.4	2.692	0.73	1.00
Kirk (1986)	220x65x2.4	18.90	1291.26	1	-	-	-	rigid	41.6	3.536	1.00	1.00
Lim (2002)	336x88x3.0	31.21	4940.10	2	550	550	447	8000	87.5	8.415	0.97	1.00
Dubina (2004)	350x100x3.0	34.02	6026.40	2	799	799	508	6957	116.7	10.399	0.89	1.00
Rhodes (2006)	402x97x3.2 column	38.58	8545.20	4	800	1176	305	10809	135.8*	11.491	1.00	0.57
	342x97x2.5 rafter	27.98	4836.40						84.1			
	202x69x2.0 knee brace	14.16	893.80									

38

2.3.2 Design loads and loads combinations

It will be shown later that in the case of horizontal loads such as wind, the stressed skin action can reduce their significance to the level at which gravity loads will govern the design. Therefore, to simplify the analysis, only the following gravity loads were considered according to SCI P252 (2004):

1) Self-weight of the frame

2) Dead Load DL=0.15+0.03 =0.18kN/m^2 (cladding + purlins)

3) Live Load LL=0.60kN/m^2

The following selected gravity load combinations were considered according to SCI P252 (2004):

1) Ultimate Limit State (ULS)

$$ULC1=1.4SW+1.4DL+1.6LL$$

(2-5)

2) Serviceability Limit State (SLS)

$$SLC1= 1.0LL$$

(2-6)

2.3.3 Serviceability and resistance requirement

The serviceability requirements in portal frame design are discretionary and are left to engineering judgement. The main reason for limiting the deflections values is to avoid damage of the cladding, ponding of water or extensive deformations which are noticeable to the naked eye. The following publications offer simple guidance on the deflection limits: Woolcock and Kitipornchai (1987), SCI Advisory Desk Notes (1991) and Lim and Nethercot (2003a). However, when the stressed skin design is introduced, the exact deflection inducing local failure of the cladding can be established. The problem of deflection limits is therefore reduced to water ponding and visual acceptance. Since stressed skin analysis is not conducted in this efficiency

study, the vertical deflection limit recommended by NA to BS EN 1993-1-1 (2005) for a general purpose beam, is used:

$$\delta_{a,max} = L_f/200 \tag{2-7}$$

Analysed frames are only examined based on bending capacity of the joint (M_{exp}) reported in a literature. The effect of axial forces on the overall capacity of the columns is neglected in the analysis. The assumption was also made that purlins provide sufficient lateral restraints so lateral torsional buckling need not to be considered.

The frame compliance with ULS and SLS design criterion is therefore described by following unity factors:

1) $f_{ULS} = \max (M_e, M_a)/ M_{exp}$ if Model 1 and Model 3,   (2-8)

2) $f_{ULS} = \max (M_{e,c}, M_{e,r}, M_a)/ M_{exp}$ if Model 2,   (2-9)

3) $f_{ULS} = \max (M_{e,c}/ M_{exp,c}, M_a/ M_{exp,r})$ if Model 4,   (2-10)

4) $f_{SLS} = \delta_a/\delta_{a,max}$ all of the models.   (2-11)

A total of ten frames with four different joint types were analysed under the structural models and loads presented in Sections 2.3.1 and 2.3.2. The frame spacing (S_f) was increased until one of the factors reached unity. The maximum permissible spacing (S_f) and the unity factors (f_{ULS}, f_{SLS}) for each frame design are presented in Table 2-3 and Table 2-4

2.3.4   Structural and cost efficiency study – results

The total weight of steel used for one portal frame was calculated and is presented in Table 2-5. The breakdown between weights of steel required for primary members and brackets is also presented in Table 2-5. The structural efficiency rating

of each frame was subsequently described as a ratio of the total weight of steel required (W_t) to the unobstructed volume under one frame (V_{ub}) (see Figure 2-24).

$$V_{ub}=A_{ub}S_f$$
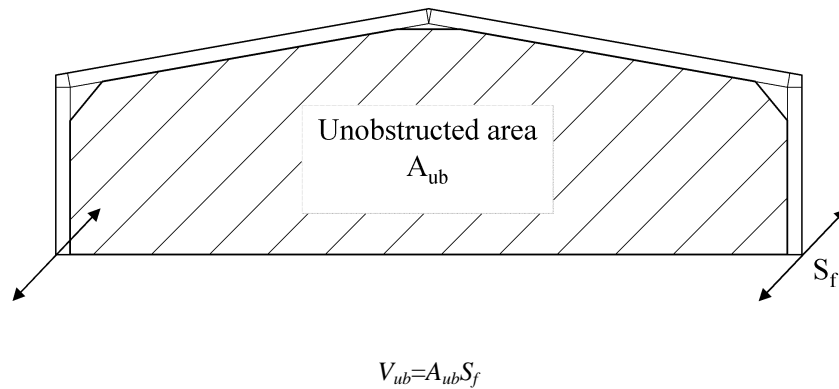
Figure 2-24 Unobstructed volume create by one portal frame

Classification based on the joint manufacturing process:

1) brackets are manufactured by the cold-formed process from galvanized plates (denoted in Table 2-6 by 'CFS')

2) brackets are manufactured from hot-rolled steel plates thus additional processes such as welding and painting are required (denoted in Table 2-6 by 'HRS')

The cost efficiency rating of each frame was subsequently expressed as a ratio of the total cost of one portal frame ($£_t$) to the unobstructed volume under one frame (V_{ub}). The breakdown in respect to the cost of the sections and the cost of the joints against total is presented in Table 2-6.The prices of each frame component were obtained from UK leading cold-formed and hot-rolled steel manufacturers in October 2011. In case of frames built entirely from cold-formed steel parts the total price includes the cost of the sections, finished brackets and fixings per one portal frame. The prices of HRS brackets include the cost of fabrication and corrosion protection so products of the same functionality are being compared. For simplicity, the transportation and the erection costs were neglected in the analysis.

From Table 2-5 and Table 2-6 it can be seen that the connection brackets can account for as much as 45% of the total weight and 76% of the total cost of one

portal frame. The joint proposed by Baigent and Hancock (1978) (see Section 2.1.1) represents the extreme case when the design criterion is maximum rigidity of the joint. Although the high cost will exclude the joint from practical solution in terms weight efficiency the joint performs reasonably well. As hot-rolled steel brackets are used, the cost is significantly increased by the additional fabrication processes such as welding and painting.

A similar trend was also observed in joints suitable for frames of 12m span. The heaviest and the most expensive joints (34% of frame weight and 59% of frame cost) are those of Dubina et al. (2004) as the author's motivation was to develop full-strength joints of high rotational stiffness (see Section 2.1.8).

Table 2-5 Weight of the steel breakdown of one portal frame

Author	Span	Weight of sections/total	Weight of connectors /total	Total weight of steel /portal	Total weight of steel/ unobstructed volume
	(m)	(%)	(%)	W_t (kg)	W_t / V_{ub} (kg/m^3)
Portal frames of 6m span					
Baigent and Hancock (1978)		55	45	119	2.03
Mills and LaBoube (2004)		97	3	62	0.88
Elkersh (2010)	6	89	11	227	1.67
Wrzesien A		83	17	160	2.38
Wrzesien B		76	24	174	1.64
Portal frames of 12m span					
Dundu and Kemp (2006)		100	0	218	1.58
Kirk (1986)		88	12	336	1.83
Lim and Nethercot (2002)	12	75	25	660	1.56
Dubina et al. (2004)		66	34	822	1.56
Rhodes and Burns (2006)		78	22	669	1.16

In the case of joint Type A proposed by the author the opposite case was considered when the joint rotational stiffness was reduced to a minimum. This was done so that the effect of rotational stiffness can be investigated. In terms of typical 2D design such a joint will produce the heaviest portal frame design. Although joints Type A and B are categorized as short-span applications; brackets of similar shape can be used in portal frames up to 18m span.

Table 2-6 Cost breakdown of one portal frame

Author	Span (m)	Bracket type	Costs of sections /total cost (%)	Cost of joints /total cost (%)	Total cost per one portal $£_t$ (£)	Total cost/ unobstructed volume $£_t / V_{ub}$ (£/m³)
Portal frames of 6m span						
Baigent and Hancock (1978)		HRS	24	76	389	6.63
Mills and LaBoube (2004)		CFS	94	6	89	1.26
Elkersh (2010)	6	HRS	80	20	354	2.61
Wrzesien A		CFS	75	25	245	3.64
Wrzesien B		CFS	71	29	262	2.47
Portal frames of 12m span						
Dundu and Kemp (2006)		-	96	4	317	2.29
Kirk (1986)		CFS	72	28	388	2.11
Lim and Nethercot (2002)	12	CFS	76	24	908	2.14
Dubina et al. (2004)		HRS	41	59	1824	3.46
Rhodes and Burns (2006)		HRS	42	58	1743	3.02

2.4   Joint efficiency – concluding remarks

It was reported in the previous section that there is not a clear correlation between frame weight (W_t / V_{ub}) and cost efficiency ($£_t / V_{ub}$) thus both efficiency ratings are summarised in Figure 2-25. The average of both ratings is also presented.

The best performing joints in terms of steel usage and cost is that presented by Mills and LaBoube (2004). The bracket is only used at the apex and the eaves joint is formed by screwing the rafter to the column back-to-back (see Section 2.1.7). The capacity of such a joint is limited by the depth of the main members and shear capacity of the screws so the joints can only be used in short-span portal frames. The least efficient joint in terms of frame weight is joint Type A investigated by the author. It has been chosen as it is similar to what can be found in practice. The most expensive frame is that using a hot-rolled joint after Baigent and Hancock (1978).

In the second category of joints suitable for portal frames of 12m span the scatter between the weight efficiency ratings is much less significant. Interestingly, the lightest frame is that using knee brace joints (Rhodes and Burns (2006) details in Section 2.1.11) but the steel savings are consumed by high manufacturing costs. The heaviest frame design is offered by the Swagebeam system (Kirk (1986) details in Section 0) however the same system offers the least expensive frame. The highest cost is expected for frames with hot-rolled steel joints (Dubina et al. (2004), Rhodes and Burns (2006). Frames with such joints are approximately 1.5 times more expensive than those built entirely from CFS components.

It is shown in Figure 2-25 that joint design largely affects the weigh and cost of a portal frame. It is shown that stiffer joint Type B, although larger, offers a more economical portal frame design. The joint Type B proposed by the author offers the second best average efficiency rating and could be successfully used for frames of larger spans.
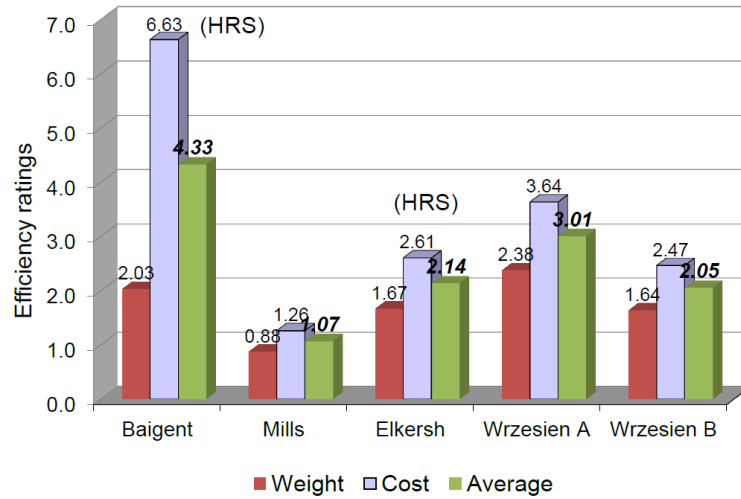
a) Portal frame of 6m span
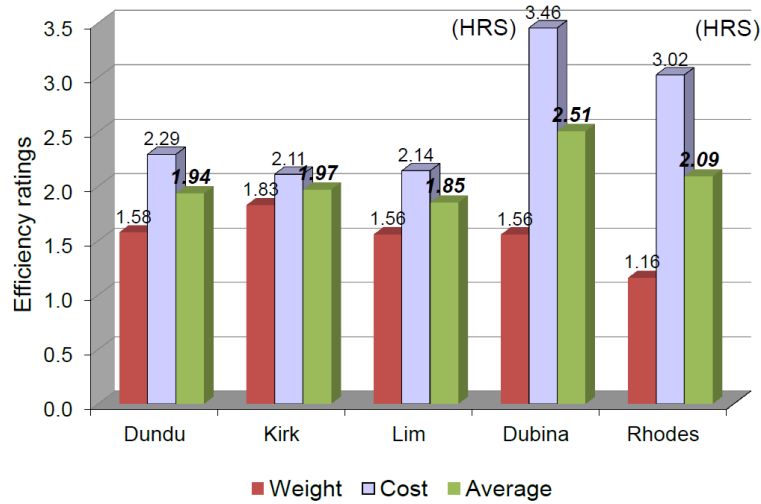
b) Portal frame of 12m span

Figure 2-25 Design efficiency ratings of reviewed joints

2.5   Investigation of the proposed joint design

2.5.1   Objectives of the joint tests

The joint was proposed with stiffeners being folded on both sides of the bracket ensuring that the bending capacity is the same regardless of the load direction

as shown in Figure 2-26. The joints type A, B and C can be manufactured in the cold-forming, automated process, in order to keep costs low. Stiffeners also allow the introduction of additional bolts at the flange of the section, which are usually required for attaching secondary members. The effect of these bolts on joint strength and stiffness is also investigated. The main motivation for the experimental study is to:

1) develop a simple analytical method for predicting strength and stiffness of the proposed type of connection,

2) validate a beam idealisation of structures that incorporate the proposed connections.

Since the experimental investigation contains not only joint test but also full-scale tests on portal frame buildings, the capacity of members under investigation had to be reduced to match the capacity of available equipment and laboratory facilities.
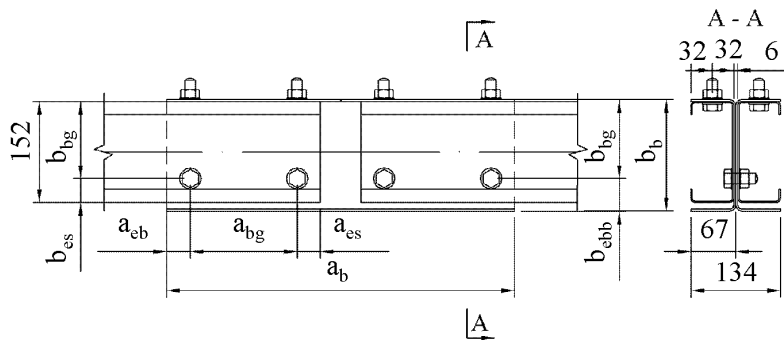
a) Type A - 2x1 web bolt array
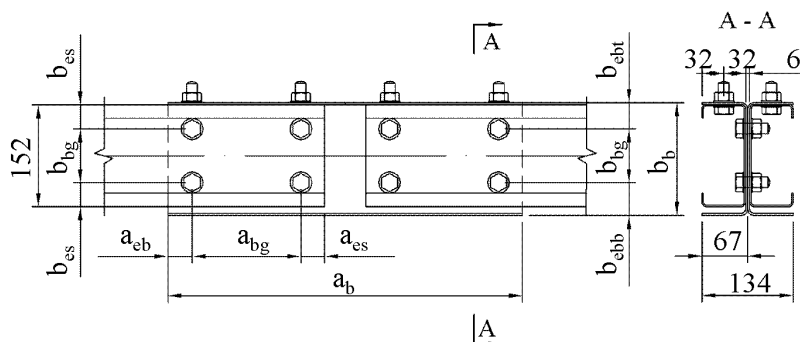
b) Type B - 2x2 web bolt array

46
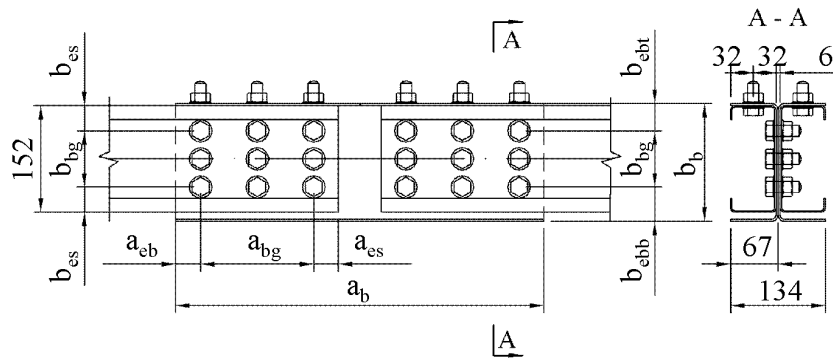
c) Type C-3x3 web bolt array

Figure 2-26 Joint types selected for testing

2.5.2   Testing methodology

In this Section, joint tests to determine the strength and stiffness of three different bolt-arrays are presented. The full-scale tests, described in Chapter 4, will use joint type C for the eaves, apex and base connections. The combinations of bolts in the web and flange are considered along with the bolt-group length.

Laboratory tests were conducted on seven joints, as well as back-to-back continuous members. Details of the laboratory test set-up are shown in Figure 2-27. As can be seen, each joint test comprises two identical bolt-group arrangements, one on either side of the vertical axis of symmetry, that are tested under four-point bending. Since the pitch of the roof should not have a significant effect on the joints behaviour, zero degree pitch was assumed so the existing test rig can be used. For all joint tests, the total length of the test specimen was 3 m and the distance from the end support to the load point was 1 m. To prevent lateral-torsional buckling, lateral restraints were provided at the supports, load points and at the mid-span.

The bolts in each test were only finger-tightened without pre-torquing. Load cycles to remove the bolt slip from the joint were not conducted as any bolt-hole elongation so caused would not be recoverable. However, before each test, the bracket was pulled as far as possible in the direction of the applied load; at this position the displacement transducers used to measure deflections were set to zero.

47

Bedding down change of angle due to slip and bolt-holes tolerance was also measured before each test by digital inclinometer.
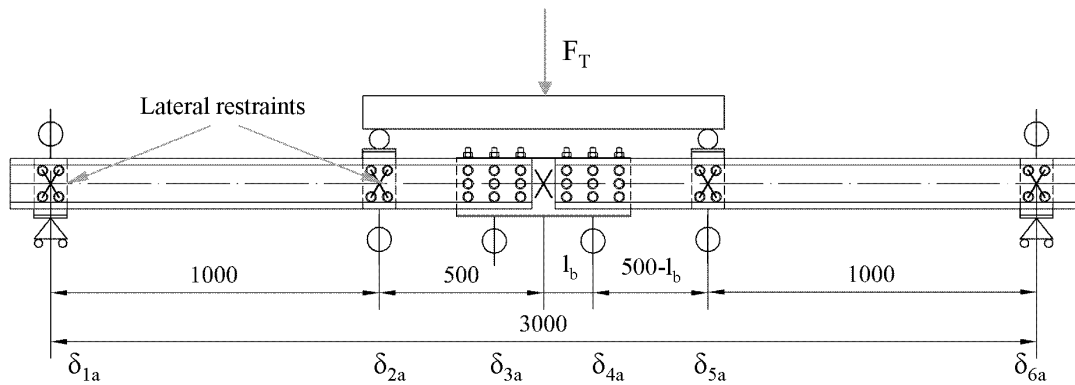
δ - displacement transducers; F_T – jacking force

Figure 2-27 Details of the joint test arrangement

2.5.3 Joints with web and flange bolts

A total of 8 joint tests were conducted on continuous member and joint configurations type A, B and C according to Figure 2-26, cross-referenced with Table 2-7. A summary of the components used for each test is presented in Table 2-8.

In order to the measure rotational stiffness of the bolt-group the flexural stiffness of the back-to-back channel beam was measured since it will contribute to the overall deflection. For this reason one test on a continuous beam was conducted.

The nominal thickness of each bracket was 3 mm, and the nominal diameters of the bolts and bolt-holes were 16 mm and 18 mm, respectively; all the bolts used were M16 Grade 8.8 and had fully threaded bolt-shanks.

In test T2/A the compression forces were carried only through the flange bolts (see Figure 2-26a). Although such a joint would not be considered in full-scale tests, it was designed purely to validate the simple physical model used to estimate strength and stiffness of joints type A. This joint used only two bolts in the web and four in the flange and the bolt-group length of 240mm. Tests T3/B and T4/B used the

48
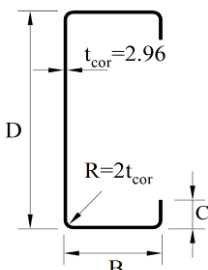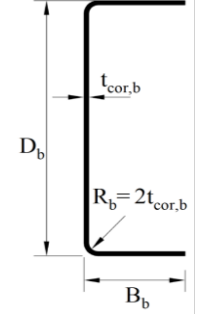
same length of the bolt-group but an additional row of bolts in the web was introduced as presented in Figure 2-26b.

Table 2-7 Joint tests - connection geometries

Test designation	Bolt array web	Bolts flange	a_{bg}	b_{bg}	a_b	a_{eb}	b_{ebb}	b_{ebt}	a_{es}	b_{es}
			(mm)	(mm)	(mm)	(mm)	(mm)	(mm)	(mm)	
T2/A/2x1/d	2x1	2	240	60	680	35	69	49	35	46
T3/B/2x2/d & T4/B/2x2/u	2x2	2	240	60	680	35	69	49	35	46
T5/C1/3x3/d & T6/C1/3x3/u	3x3	3	160	80	520	35	59	39	35	36
T7/C2/3x3/d	3x3	3	240	80	680	35	59	39	35	36
T8/C3/3x3/d	3x3	3	280	80	760	35	59	39	35	36

In portal frame applications the connection brackets require a haunch shape to increase their strength and stiffness without necessity of using very thick plates. If such brackets are to be manufactured by press break, they can only be bolted to the channel sections via the outer flanges. This introduces an asymmetry and for this reason in Test 3/B and 4/B the same joint was tested under the downward and uplift load. In case of tests T5/C1 to T8/C1 the 3x3 bolt-array in the web was used with an additional 6 bolts in the flanges (see Figure 2-26c). Due to asymmetry of the connection in test T5/C1 and T6/C1 the same joint was subjected to downward and uplift loading.

Table 2-8 Joint tests - summary of component geometries

Test designation	Average component dimensions (mm)						
	Section				Bracket type B		
Test/ Type/ Bolt array/ Downward or uplift	D	B	C	t_{cor}	D_b	B_b	$t_{cor,b}$
Nominal	152.0	64.0	20.0	1.96	178.0	67.0	2.96
T1	152.3	64.1	19.9	1.97	-	-	-
T2/A/2x1/d	152.9	65.1	19.9	2.01	179.0	64.8	2.98
T3/B/2x2/d	152.8	65.5	19.8	2.02	179.6	66.0	3.00
T4/B/2x2/u	152.6	65.0	19.9	2.01	179.5	64.4	2.99
T5/C1/3x3/d	152.2	64.6	20.3	1.98	179.4	65.4	2.98
T6/C1/3x3/u	152.6	64.4	20.2	1.98	179.9	65.8	2.98
T7/C2/3x3/d	152.2	64.7	20.1	1.98	179.5	65.7	3.01
T8/C3/3x3/d	152.7	65.2	19.9	2.01	179.6	65.4	2.98

The section diagram shows dimensions: $t_{cor}=2.96$, D, $R=2t_{cor}$, B, C. The bracket type B diagram shows: $t_{cor,b}$, D_b, $R_b=2t_{cor,b}$, B_b.

2.5.4 Continuous beam test

The nominal and average sections dimensions are shown in Table 2-8. The cold-formed steel channels were manufactured from S350GD grade of steel according to BS EN 10326:2004 (2004). Tensile coupons were collected from each member and mechanical properties of the steel were established according to BS EN 10002-1:2001 (2001). The average measured proof strength and average ultimate tensile strength are presented in Table 2-9. It should be mentioned that there was no

bedding-down load applied to the continuous beam as a bedding-down test was not conducted for joint tests to prevent bolt hole ovalisation.

Three different analytical methods were used to evaluate the bending capacity of the investigated beam:

1) Effective Width   Method ($M_{c,BS}$ - according to BS 5950-5 (1998b))

2) Effective Width and Effective Thickness Method ($M_{c,EC}$ – according to BS EN 1993-1-3 (2006))

3) Direct Strength Method ($M_{c,DSM}$ according to AS/NZS 4600:2005 (2005)

and Li and Schafer (2010))

For each method the following assumptions were made:

1) Yield strength according to Table 2-9
2) Modulus of elasticity E=210GPa
3) Effective length between lateral and torsional restraints of 500mm

The calculated capacities based on listed standard methods are summarised in Table 2-9.

Each of the listed codes also offers analytical rules for predicting the reduction in flexural stiffness by reducing the gross section second moment of inertia to the effective value I_{fic}. This stiffness reduction is described by the factor Q_b defined in Equation (2-12)

$$Q_b = I_{fic} / I_{y,gr}$$
(2-12)

Where:

I_{fic} - effective moment of area for deflection

$I_{y,gr}$ – gross second moment of area

Table 2-9 Summary of analytical versus experimental bending moment of continuous beam

Test designation	f_y	f_u	$M_{cy,BS}$	$M_{cy,EC}$	$M_{cy,DSM}$	M_{exp}	$M_{cy,BS}$ / M_{exp}	$M_{cy,EC}$ / M_{exp}	$M_{cy,DSM}$ / M_{exp}
	N/mm^2	N/mm^2	kNm	kNm	kNm	kNm			
T1	392	512	21.23	20.73	20.12	21.85	0.97	0.95	0.92

Table 2-10 Summary of analytical versus experimental flexural stiffness of continuous beam

Test designation	$Q_{b,BS}$	Reference	$Q_{b,EC}$	Reference	$Q_{b,DSM}$	Reference	$Q_{b,Exp}$
T1	0.998	Section 5.7 BS 5950-5 (1998b)	0.962	Section 7.1 BS EN 1993-1-3 (2006)	0.901	Section 7.1.4 AS/NZS 4600:2005 (2005)	0.772

The values of the flexural stiffness reduction along with the reference are presented in Table 2-10. The stiffness reduction based on the measured deflection (Q_{exp}) for test T1 is also presented in the same table. The experimental stiffness was evaluated by drawing a straight line through point (0;0) and (ϕ_t;0.6M_{exp}) according to Figure 2-28. Comparison between the analytical and the experimental deflections is presented in Figure 2-28.

2.5.5 Continuous beam – test results and concluding remarks

The comparison between experimental and analytical bending capacity is presented in Table 2-9. In Figure 2-28 the average from deflections δ_{3A} and δ_{4A} was used to plot the load-deflection relationship. The beam failed in distortional buckling of the compression flange as shown in Figure 2-28. This mode of failure is not

recognised by BS 5950-5 (1998b) which uses an Effective Width Method to consider the local buckling of the cross-section.
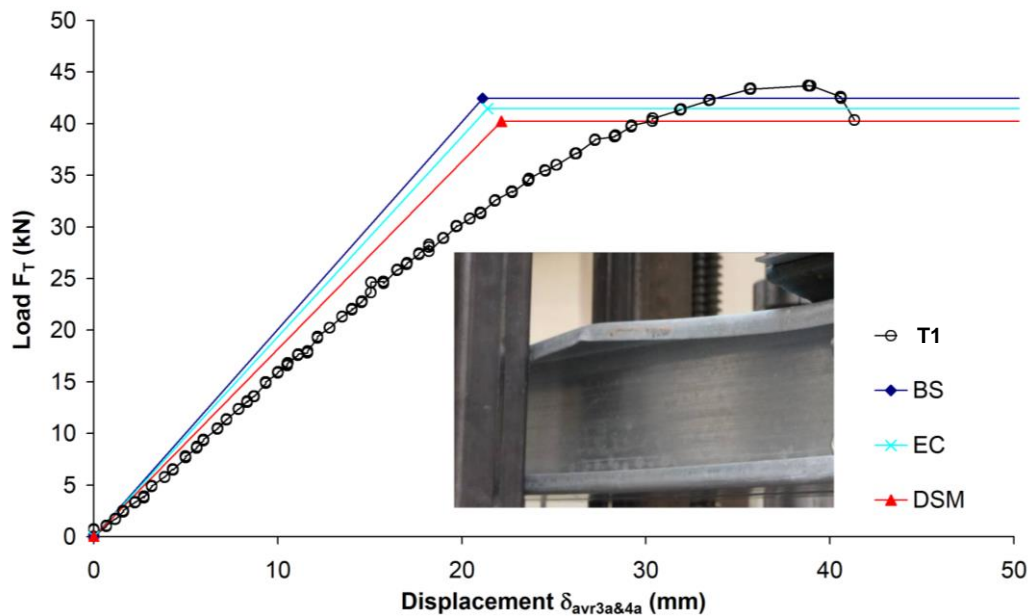
Figure 2-28 Experimental versus analytical moment-displacement relationship for continuous beam

Although the local buckling mode of failure was not observed, the estimated bending capacity was still conservative and the closest to the experimental value. The distortional buckling phenomenon is accounted for by the analytical method presented in Eurocode 3 and the Direct Strength Method (DSM) adopted by AS/NZS 4600:2005 (2005) and North American Specification for the Design of Cold-formed Steel Structural Members AISI (2004). Both these analytical methods produced conservative predictions in terms of bending capacity by 5% and 8% respectively as compared with the experimental results. The calculations were based on measured geometry thus it was confirmed that all of the analytical methods are able to account for the effect of initial imperfections with a degree of safety.

In terms of beam deflection, all of the analytical methods under-predicted the flexural stiffness reduction (see Figure 2-28). The DSM method was the closest in predicting the beam deflections as can be seen in Table 2-10 and Figure 2-28. The flexural stiffness of cold-formed steel members received little attention in the

literature since, in practical design, deflection limits are discretional. In this work however, accurate flexural stiffness is needed so that the jointed beam deflection due to rotational stiffness of the joint can be accounted for.

2.5.6   Beam idealisation of the joint tests

A simple beam model was employed to represent behaviour of a cold-formed steel beam connected through bolted joints (see Figure 2-29). The flexural stiffness of sections were modelled assuming gross cross-section properties reduced by the experimental factor of 0.772 (see Table 2-10). The flexural stiffness of the bracket sections was not reduced as no experimental data was available. The length of the bracket is also significantly smaller than the length of the channel, thus its exact stiffness is less important. The position of the centre of rotation from the centre of the bracket (l_b) was established according to Appendix B.1 and was presented in Table 2-11. The rotational stiffness of the bolt-group was modelled as a rotational spring element ($S_{j,ini}$) calculated in accordance with Table 7-5. The bracket was modelled as a beam element joining two rotational springs.
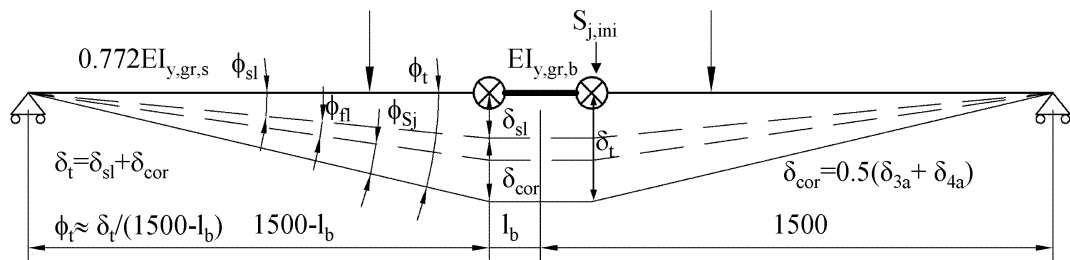
Figure 2-29 Beam idealisation of the test arrangement

In the case of bolted joints with clearance holes, the effect of slip due to the rigid body movement of bolts in clearance holes must be considered. This problem is particularly important in moment-resisting joints subject to load in opposite directions. Theoretical maximum slip (s_{sl}) between two sheets of metal is twice the hole clearances. Zadanfarrokh and Bryan (1992) suggested that in practice for multiple bolted connections it is safe to assume the slip as one times the clearance. This approach was supported by the experimental evidence presented in APPENDIX

A. The average linear displacement due to slip in double lap joints was recorded as 1.61 mm but for some tests reached nearly 2mm (sees Table 7-4 and Figure 7-4). It was assumed however that the slip displacement ($\delta_{i,th}$) can be reduced by half for joints with flange bolts according to Appendix B.1. The maximum theoretical slip rotation $\phi_{sl,anl}$ was calculated based on the length of the bolt-group according to Equation (2-13):

$$\phi_{sl,anl} = \delta_{i,th} / r_i \qquad\qquad (2\text{-}13)$$

where:

$\delta_{i,th}$ – free displacement before the furthest bolt in contact with the plate

r_i – distance from the centre of the rotation to the furthest bolt

Before the test specimen was loaded, the angle (ϕ_{sl}) was recorded so that the analytical ($\phi_{sl,anl}$) and measured values of joint rotation can be compared.

As presented in Appendix B.1, two stiffness models were considered: Model 1 considered the contribution of the flange bolts and Model 2 neglected this contribution. The distance from the centre of the rotation to the outer bolt was calculated based on data provided in Table 7-6, Table 7-7 and Figure 7-5.

The experimental data presented in Figure 7-4, shows a clear bi-linear load-displacement relationship. The initial shear stiffness recorded during the experiment was therefore classified as slip. Once the bolt started bearing onto the steel plate, the joint shear stiffness increased nearly four times (see Table 7-4 and Figure 2-30). Due to the complexity of the problem the assumption was made that the shear stiffness of the joint in slip stage ($k_{b,sl}$) is close to 0.

The initial rotational stiffness due to the slip in the joint $S_{j,ini,sl}$ was calculated from Equation (2-6)

$$S_{j,ini,sl} = M_{SW} / \phi_{sl,anl} \qquad\qquad (2\text{-}14)$$

Where:

M_{SW} – bending moment from the self-weight of the structure

$\phi_{sl,anl}$ – analytical slip rotation of the joint

The analytical rotational stiffness ($S_{j,ini.sl}$) was calculated for Model 2 as the location of the centre of the rotation is different for each model. Analogously the upper and lower bound analytical rotational stiffness ($S_{j,ini}$) due to bolt bearing were calculated according Appendix B.1 to Table 7-5.

The rotational stiffness of the joint was represented as a bi-linear moment-rotation spring (see Figure 2-30) and the values of rotational stiffness were presented in Table 2-11. All the remaining parameters were also listed in the same table.
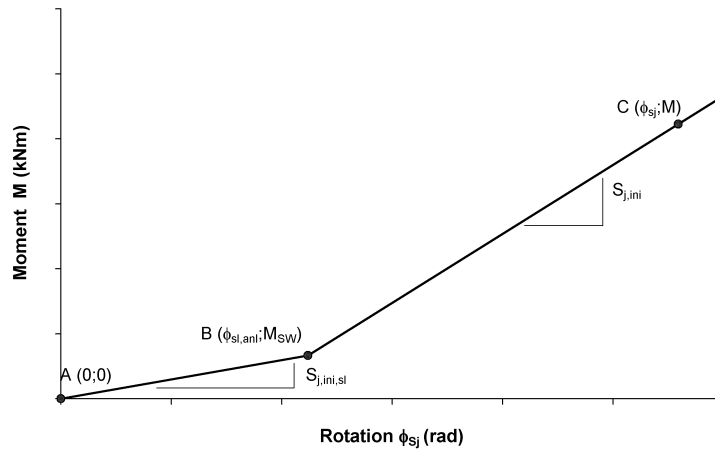
Figure 2-30 Bi-linear rotational stiffness model

2.5.7 Experimental results versus analytical models

This section presents results of seven experiments conducted on joints with different bolt arrays (Type A, B and C) and lengths of the bolt-group (a_{bg}) between 160mm and 280mm. The analytical methods for predicting rotational stiffness summarised in Appendix B.1 were compared against test results in Table 2-12.

The initial sag of the tested beam under the dead load was represented by the initial slip angle (ϕ_{sl}) measured by the digital inclinometer of 0.1° accuracy, before

the loading was initiated (see Table 2-12). The maximum initial analytical rotation ($\phi_{sl,anl,2}$) based on Model 2 is also presented in Table 2-12 along with the joint experimental rotational capacity ($\phi_{Xd,exp}$).

As can be seen in the experimental moment-rotation relationships (Figure 2-31 to Figure 2-35) some joints presented clear bi-linear stiffness behaviour with the initial stiffness stage due to slip and final stiffness stage due to bearing of the bolts into the steel plate. Only the final experimental rotational stiffness values ($S_{j,ini,exp}$) are presented in Table 2-12. The analytical over experimental rotational stiffness ratios are also summarised in Table 2-12 for upper ($S_{j,ini,1}$) and lower bound ($S_{j,ini,2}$) of stiffness.

Table 2-11 Analytical beam idealisation characteristic of joint tests

Test designation	l_b	$I_{y,gr,s}$	$I_{y,gr,b}$	a_{bg}	b_{bg}	$\phi_{sl,anl,1}$	$\phi_{sl,anl,2}$	$S_{j,ini,1}$	$S_{j,ini,2}$
		(Figure 2-29)		(Figure 2-26)		(Eq. 2-13)		(Table 7-5)	
	mm	cm^2	cm^2	mm	mm	rad	rad	kNm/rad	kNm/rad
T2/A/2x1/d	185	450.85	839.89	240	60	0.008	0.008	443	319
T3/B/2x2/d	185	453.94	858.76	240	60	0.008	0.008	762	677
T4/B/2x2/u	185	448.74	843.79	240	60	0.008	0.008	762	677
T5/C1/3x3/d	145	438.27	847.51	160	80	0.010	0.011	675	531
T6/C1/3x3/u	145	440.17	854.91	160	80	0.010	0.011	675	531
T7/C2/3x3/d	185	436.96	859.05	240	80	0.007	0.008	1205	1062
T8/C3/3x3/d	205	450.27	837.63	280	80	0.007	0.007	1551	1407

Due to the fact that analytical models presented here are not capable of considering the asymmetry of the joint, the experimental stiffness and strength of the joint can vary depending on the load direction. Under the downward load the compressed part of the section prone to buckling is restrained by the bracket stiffener which can increase the capacity. For this reason one of each joint consisting 2x2 and 3x3 bolt array was tested twice under both downward ("+" moment) and uplift load ("-" moment) as can be seen in Figure 2-32 and Figure 2-33.

Table 2-12 Experimental beam idealisation characteristic of joint tests

Test designation	a_{bg}	b_{bg}	ϕ_{sl}	$\phi_{sl,anl,2}$	$\phi_{Xd,exp}$	$S_{j,ini,exp}$	$S_{j,ini,1}$ / $S_{j,ini,exp}$	$S_{j,ini,2}$ / $S_{j,ini,exp}$
	mm	mm	rad	rad	rad	kNm/rad		
T2/A/2x1/d	240	60	0.003	0.008	0.066	534	0.83	0.60
T3/B/2x2/d	240	60	0.002	0.008	0.061	797	0.96	0.85
T4/B/2x2/u	240	60	0.005	0.008	0.052	822	0.93	0.82
						Avr	0.90	0.76
T5/C1/3x3/d	160	80	0.010	0.011	0.075	601	1.12	0.88
T6/C1/3x3/u	160	80	0.003	0.011	0.066	591	1.14	0.90
T7/C2/3x3/d	240	60	0.003	0.008	0.061	1055	1.14	1.01
T8/C3/3x3/d	280	60	0.002	0.007	0.080	1229	1.26	1.14
						Avr	1.17	0.98

The experimental moment-rotation relationships are presented in Figure 2-31 to Figure 2-35. Each graph contains:

1) Experimental moment-rotation relationship for the continuous beam test T1 as described in Section 2.5.5;

2) Idealised stiffness for the continuous beam Model (T1) base on Section 2.5.5;

3) Experimental moment-rotation relationship of the jointed beam including the offset due to measured initial slip rotation (ϕ_{sl});

4) Upper bound rotational stiffness joint model excluding slip due to hole tolerance (Model 1) according to Appendixes B.1 and B.2. The BS 5950-5 (1998b) combined bending and web crippling design criteria were chosen for establishing the ultimate moment capacity of the joints as they offered closest correlation with the experimental capacities (see Appendix B.2). The analytical rotation due to slip was not considered in the upper bound model so as to define a conservative value of rotational capacity;

5) Lower bound rotational stiffness joint model including slip due to hole tolerance (Model 2) according to Appendixes B.1, and the strength criterion as above (see Appendix B.2);

6) Experimental rotation capacity ($\phi_{Xd,exp}$) as the limiting value in terms of joint ductility.
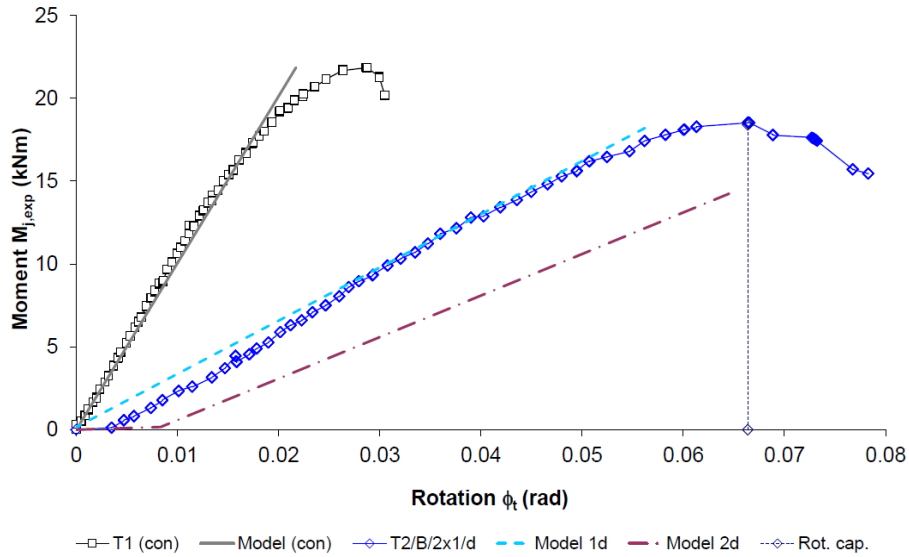
Figure 2-31 Moment-rotation relationship for experiment T2
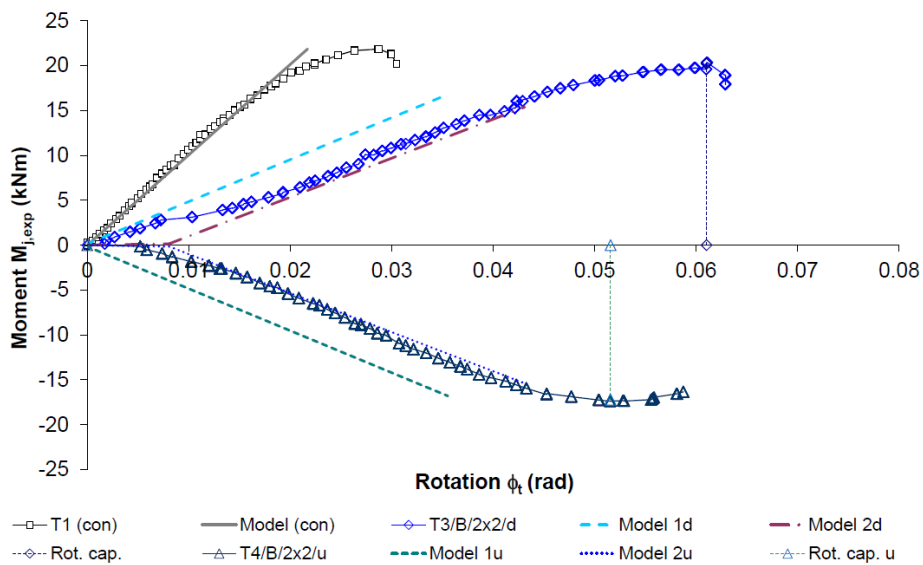
Figure 2-32 Moment-rotation relationship for experiments T3 & T4
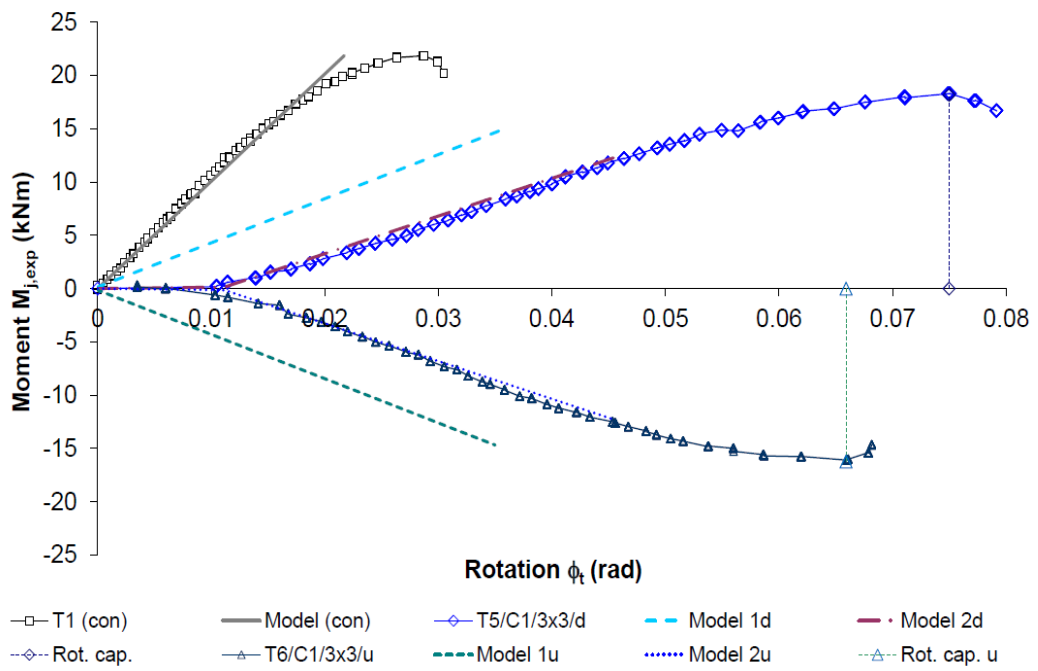
Figure 2-33 Moment-rotation relationship for experiments T5 & T6
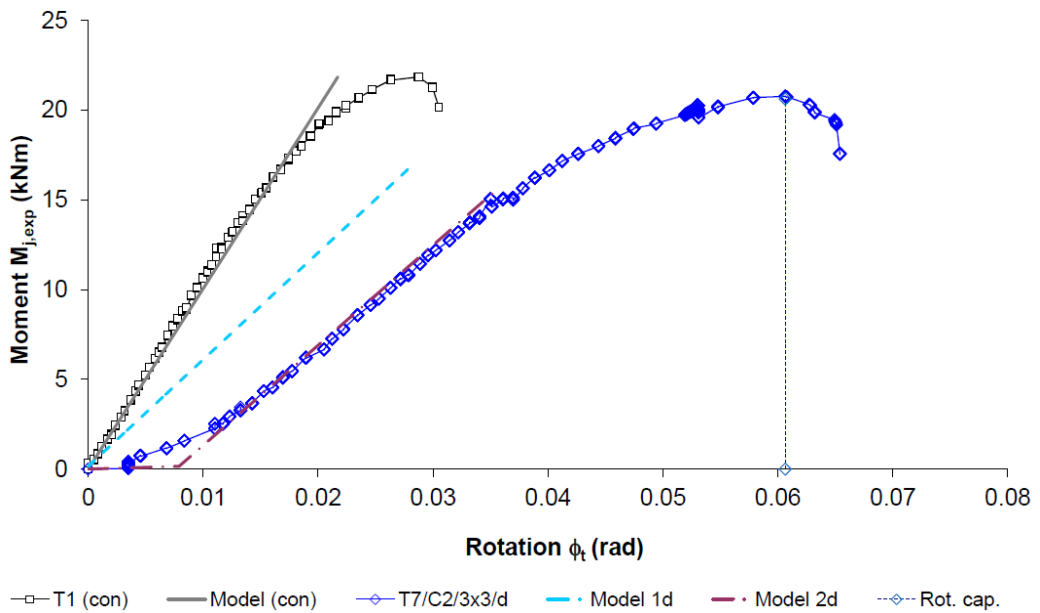
Figure 2-34 Moment-rotation relationship for experiment T7

60
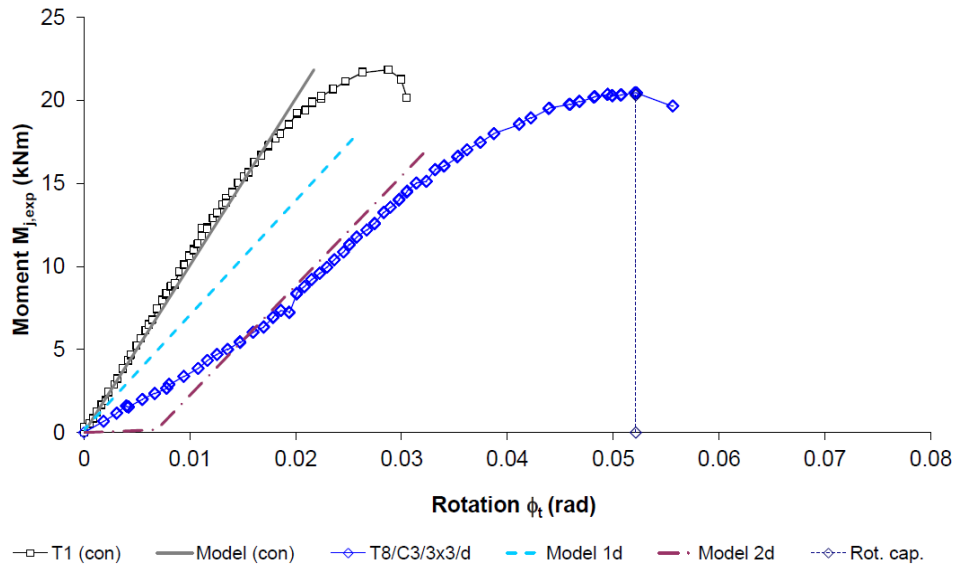
Figure 2-35 Moment-rotation relationship for experiment T8

A similar mode of failure was observed in every test where the buckling initiated in the web of the section propagated further to the flange as shown in Figure 2-36. This figure compares the mode of failure of the 2x2 bolted joint of the same bolt-group length under downward and uplift load. Generally both failure mechanisms are similar; however when the compression flange was not in contact with the bracket (see Figure 2-36b) the buckle in the flange developed closer to the first line of bolts.
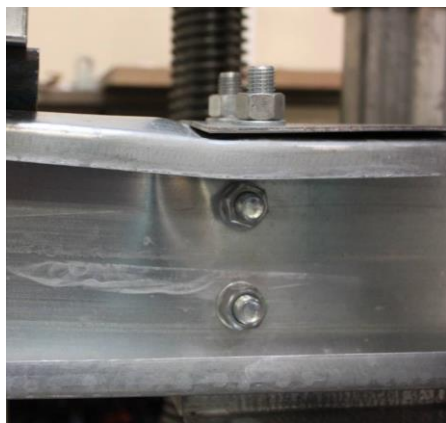
a) Downward load   b) Uplift load

Figure 2-36 Typical mode of failure of joint Type B

61

2.5.8 Joint tests – concluding remarks

It is highly recommended that the design of cold-formed steel moment resisting joints is assisted by testing as the current design codes have not yet covered such a design case. In Appendix B.1 and B.2 a simple analytical model for designing not yet investigated joints is presented. The model was carefully calibrated against seven experiments in terms of both stiffness and strength prediction.

To the author's knowledge it is common practice for engineers to design such joints based on the following assumptions:

1) full-strength assumption as long as bearing capacity check is satisfy (Rhodes (1991), SCI P125 (1993)),

2)   full rigidity assumption,

3)   disregard of initial slip due to holes tolerance.

As the moment resistance based on bearing capacity is a function of number of bolts and bolt-group length (as can be seen in Table 2-13 and Table 2-14 for test T8/B/3x3/d), Assumption 1) is extremely dangerous as it will overestimate the joints capacity by nearly 3 times. Only in one out of seven cases did the bearing check produce safe prediction of the joint capacity.

The experimental data shows that all tested joints should be classified as partial-strength as explained in Section 2.1 with the strength reduction factor ranging from 0.77 to 0.94. In order for the analytical model to estimate joint moment capacity correctly, additional design criteria for combined bending and shear and bending and web crippling should be considered (see Appendix B.2, Table 2-13 and Table 2-14). It is the combined bending and web crippling design criterion which governed the design in 6 out of 7 design cases and only this design criterion produced conservative results. As shown in Table 2-14 it is also safe to disregard the contribution of flange bolts. Such simplification will obviously result in a greater level of conservatism and less economical design.

Table 2-13 Upper bound analytical versus experimental resistance according to BS 5950-5 (1998b) and Model 1

Test designation	$M_{j,exp}$	$M_{cy,BS}$	$M_{j,exp}/M_{cy,BS}$	$M_{b,BS}/M_{j,exp}$	$M_{BSF,BS}/M_{j,exp}$	$M_{BWC,BS}/M_{j,exp}$
	kNm	kNm				
T2/A/2x1/d	18.39	21.80	0.84	0.95	1.12	0.99
T3/B/2x2/d	20.19	22.43	0.90	1.52	0.95	0.83
T4/B/2x2/u	17.22	22.35	0.77	1.79	1.11	0.98
T5/C1/3x3/d	18.17	21.78	0.83	1.95	0.99	0.81
T6/C1/3x3/u	16.23	21.60	0.75	2.17	1.10	0.90
T7/C2/3x3/d	20.62	21.98	0.94	2.32	0.91	0.82
T8/C3/3x3/d	20.31	22.25	0.91	2.66	0.96	0.89

The second assumption of the joint full-rigidity is also grossly incorrect as highlighted by the experimental moment-rotation relationships for continuous and jointed beams (see Figure 2-31 to Figure 2-35). In fact the normalised stiffness ratio ($K_{j,nor}$) of the tested joints ranged from 0.56 to 1.3 (see Figure 2-38). When such joints are used in portal frame of 6m span (see

Table 2-4) their stiffness ratios (K_j) would range from 3.4 to 6.7 (i.e.0.56x6=3.4) meaning that they should be classified as semi-rigid joints (see Figure 2-21 and Eq. (2-4)).

The neglect of the slip in moment resisting connections is also very problematic as when the free slip rotation occurs in the joint the stiffness of the frame decreases rapidly causing engagement of other components e.g. building envelope in carrying the load. When the critical load is reached then tearing or local buckling of the cladding can cause leakage and other serious serviceability problems. It is therefore recommended that 3D stressed skin analysis is employed twice and both upper and lower bound joint stiffness are modelled as described in Appendix B.1. The upper bound joint stiffness should be modelled in order to establish the maximum load in the internal frame whereas the lower bound joint stiffness should

be modelled to estimate the maximum load acting on the cladding and gable frames. Figure 2-31 to Figure 2-35 highlight the conservatism of the analytical method summarised in Appendixes B.1 and B.2 as every experimental curve falls between the analytical representation lines in terms of rotational stiffness and rotational capacity.

Table 2-14 Lower bound analytical versus experimental resistance according to BS 5950-5 (1998b) and Model 2

Test designation	$M_{j,exp}$	$M_{cy,BS}$	$M_{j,exp}/ M_{cy,BS}$	$M_{b,BS}/ M_{j,exp}$	$M_{BSF,BS}$ / $M_{j,exp}$	$M_{BWC,BS}$ / $M_{j,exp}$
	kNm	kNm				
T2/A/2x1/d	18.39	21.80	0.84	0.75	0.90	0.77
T3/B/2x2/d	20.19	22.43	0.90	1.45	0.88	0.76
T4/B/2x2/u	17.22	22.35	0.77	1.70	1.02	0.89
T5/C1/3x3/d	18.17	21.78	0.83	1.71	0.85	0.69
T6/C1/3x3/u	16.23	21.60	0.75	1.90	0.94	0.76
T7/C2/3x3/d	20.62	21.98	0.94	2.16	0.85	0.75
T8/C3/3x3/d	20.31	22.25	0.91	2.52	0.92	0.84

In order to comment on the effect of bolt-group length on the moment capacity of the bolted joint, the experimental data needs to be normalised against nominal yield strength and nominal dimensions. This was done for tests T5, T7 and T8 by dividing the test results and analytical results by the coefficient (R_s). The coefficient (R_s) was calculated according to the equation:

$$R_s = M_{cy,BS,act} / M_{cy,BS,nom}$$

(2-15)

Where:

$M_{cy,BS,act}$ – bending capacity of the channel section assessed based on actual yield strength and actual dimensions,

$M_{cy,BS,nom}$ – bending capacity of the channel section assessed based on nominal yield strength and nominal dimensions.
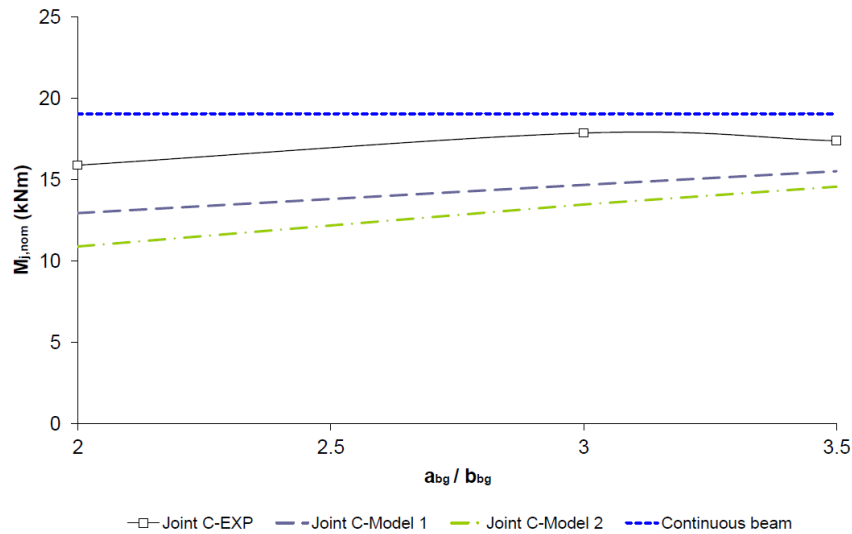
Figure 2-37 Effect of bolt-group length on the capacity of the joint

The comparison of experimental and analytical relationships between bolt-group size (a_{bg}/b_{bg}) and nominal moment capacity (M_{nom}) is presented in Figure 2-37. It can be seen that none of the investigated joints reached the full capacity of the continuous member (highlighted on the graph by the dashed line). As observed from experiments (see Figure 2-37), the capacity of the joint increased linearly with the bolt-group length until the ratio of 3 was reached then a decrease in the capacity was observed. The trends of experimental and analytical relationships diverge when the ratio of bolt-group length-to-width passed the value of 3. The analytical method may not be conservative in designing joints in which the bolt-group length-to-width ratio is greater than 3.5

Analogously, the relationship between the bolt-group length and the joint rotational stiffness was drawn in Figure 2-38, using normalised stiffness ratio K_j. As can be seen in Figure 2-38 the investigated joints are largely flexible falling just above pin classification according to Section 2.1 marked on the plot by the dashed line.
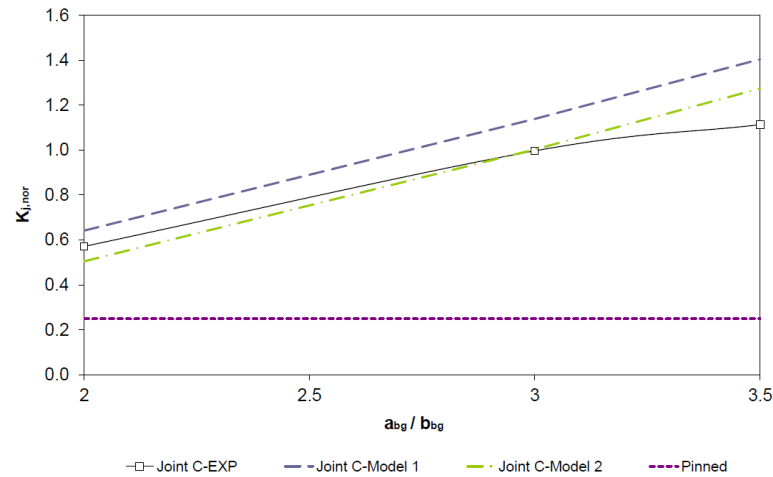
Figure 2-38 Effect of bolt-group length on the rotational stiffness of the joint

As expected the analytical method was also unable to predict the increase of strength when the compressed flange was bolted with the bracket. When comparing the normalised experimental bending capacity, 17% and 11% increases in strength were observed, when the joint was subject to downward load, for 2x2 and 3x3 bolt-arrays respectively.

It is shown in this section that the analytical methods based on the work of Chung and Lau (1999),Yu et al. (2005),Chung and Ho (2005),Dubina et al. (2008), Dubina and Ungureanu (2008) can produce safe predictions of the joint capacity. They are however, not free of inaccuracies and they do not describe 'true' mode of failure. It is believed that buckling failure of the member was actually triggered by the additional compression stress due to warping torsion as it was first described by Baigent and Hancock (1978)(see Figure 2-39b). The authors measured local stress distribution due to the bi-moment as the load applied in the plain of the web was not passing through the shear centre of the single channel cross-section. It was shown that the bi-moment value can be evaluated as moment in plan of the web times the distance from the web to the shear centre of the section. Although one could say that this theory should not apply to back-to-back double symmetric channel beams the evidence of the bi-moment action were visually detected for such arrangement as shown in Figure 2-39a. Theoretically, in the symmetric cross-section under pure bending, the bottom flange should be in tension thus should not show evidence of

compression buckling as presented in Figure 2-39a. The bi-moment stress distribution (see Figure 2-39b) shows the concentration of compression stresses at the exact location where buckling was observed.

a) local buckling of the bottom flange and lip close to outer line of bolts
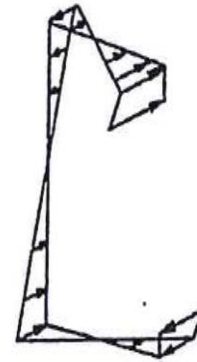
b) Stress distribution due to bi-moment in single channel section

Figure 2-39 Evidence of the additional stress due to bi-moment

As the bi-moment method described by Baigent and Hancock (1978) is not capable of predicting the strength increase due to bolt-group length it was not used as it requires further research.

The greatest accuracy in predicting the ultimate strength of the presented bolted joints can be obtained by Finite Element Analysis (FEA) carefully calibrated against the experimental data which will form a future study. The simple analytical model presented in Appendices B.1 and B.2, with its limitations highlighted here, can offer viable alternative to more complex and time consuming analysis methods.   Due to the fact that the model is based on well-known and well-understood analysis methods, it may be used by practising steel designers to avoid unsafe designs.

3   ROOF SHEETING PANELS ACTING IN SHEAR

3.1   Literature review

Stressed skin action takes into account the inherent resistance and stiffness of the metal cladding in a 3D analysis of the whole building. It has been demonstrated through extensive research that stressed skin action can reduce or eliminate the need for wind bracing. It reduces sway deflections under horizontal forces and also reduces the outward movement of the frame under vertical load. Stressed skin design was originally researched and published by Bryan (1973) and design recommendations were first presented in the 'European recommendations for the stressed skin design of steel structures' ECCS - XVII -77-1E (1977). This document formed the foundation for later publications such as: 'Manual of stressed skin diaphragm design' Davies and Bryan (1982), BS 5950-9 (1994a), ECCS TC7 (1995) and subsequently Eurocode 3 BS EN 1993-1-3 (2006).

The basic idea behind the stressed skin design is to recognize the ability of cladding panel to act as the 'web' of a cantilever beam, as shown in Figure 3-1.
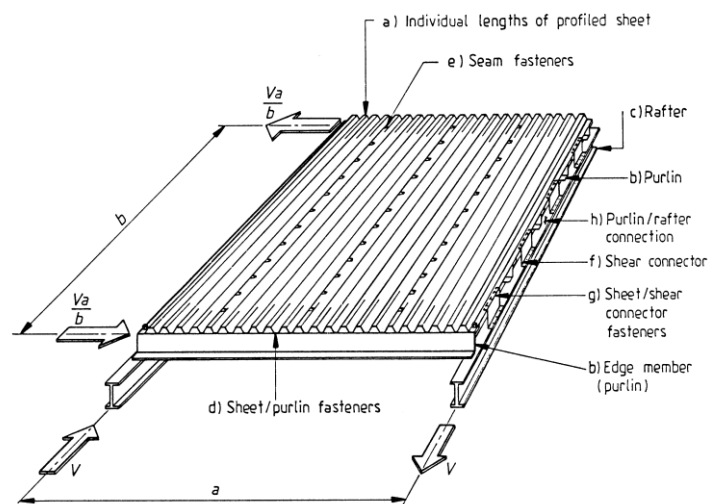
Key
a is the width of the shear panel in a direction perpendicular to the corrugations (in mm);
b is the depth of the shear panel in a direction parallel to the corrugations (in mm);
V is the applied force on the shear diaphragm (in kN).

Figure 3-1 Typical cantilever shear panel as illustrated in BS 5950-9 (1994a), pp.2

A designer can therefore choose to model the roofing and cladding panels acting in shear to offer lighter design of low-rise clad frame. The cladding panels however, due to their inherent stiffness would carry the same loads regardless of whether they are included in analysis or not. By ignoring the stressed skin action, excess force may be transferred to the roof panel and to the gable frame causing rafter or purlin failure.

Codes of practice present the principles of stressed skin design for the following diaphragms configurations, as presented in Figure 3-2.
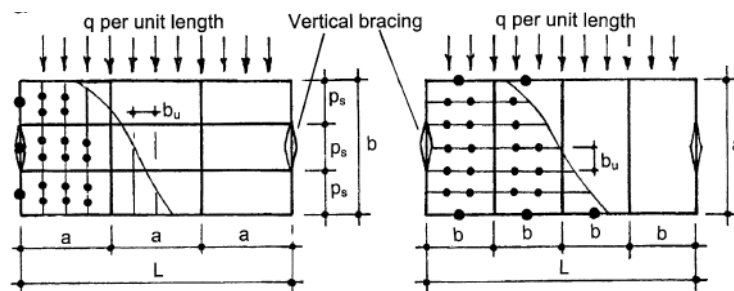
a) beam diaphragm - sheeting perpendicular to span

b) beam diaphragm - sheeting parallel to span
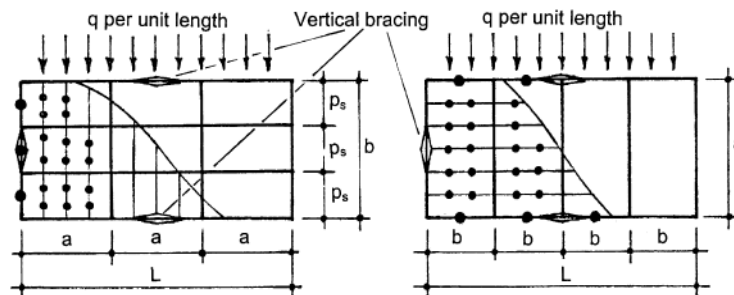
● Seam fixings connecting adjacent sheets

● Shear connector fixings (optional)

c) cantilever diaphragm - sheeting perpendicular to span

d) cantilever diaphragm - sheeting parallel to span

Figure 3-2 Basic diaphragm design orientations (after Davies (2006), pp.1251)

The classification of a shear diaphragm is based on two fixing arrangements:

1) Sheeting fastened on 4 sides (with shear connectors, see Figure 3-1)

2) Sheeting fastened on 2 sides (without shear connectors)

Thus, the shear panel presented in Figure 3-1 may be classified as a cantilever diaphragm with the sheeting spanning perpendicular to the span of the diaphragm and all four sides fastened by using short shear connectors between the rafter and sheeting. The design failure modes and deformations which should be considered when analysing a shear panel are presented in Figure 3-3.
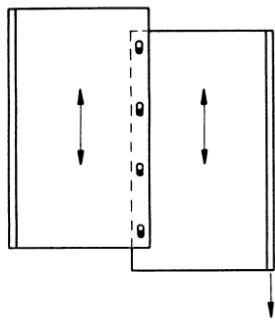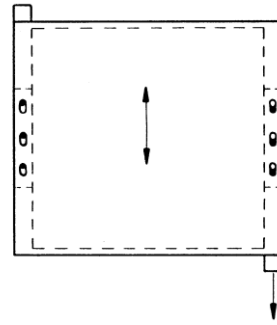
a) Seam fasteners   b) Sheet/shear connector fasteners
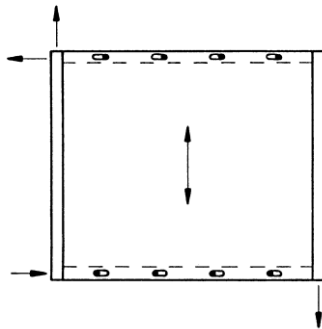
c) Sheet/purlin fasteners (4 sides fastened)   d) Sheet/purlin fasteners (2 sides fastened)
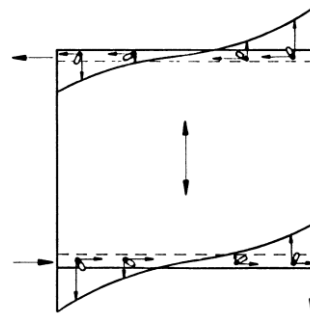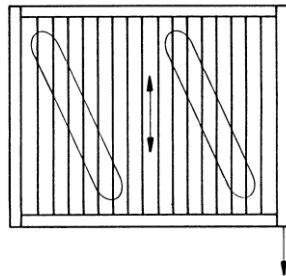
e) Shear buckling   f) Edge member forces

g) End collapse of profile   h) Profile distortion (every   i) Profile distortion (alternate troughs
                                   trough fastened   fastened

j) Shear strain in sheeting   k) purlin/rafter connection
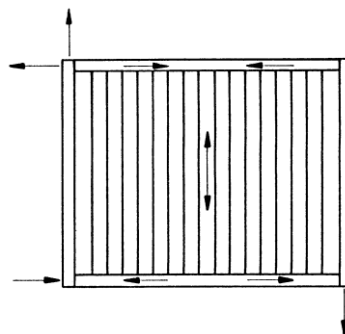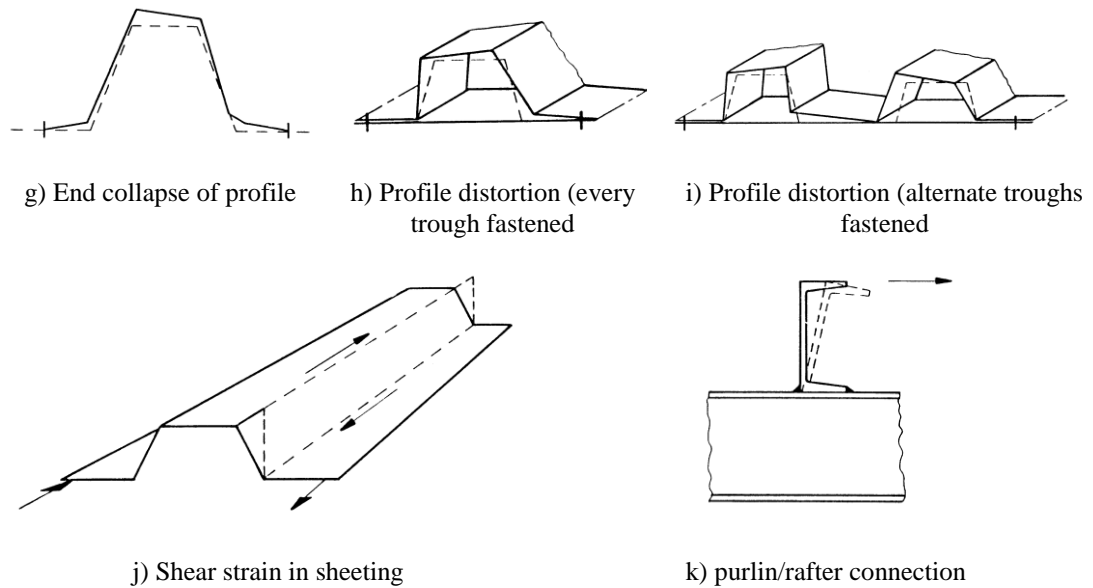
Figure 3-3 Shear resistance and flexibility design issues according to BS 5950-9 (1994a), pp.18

The shear resistance and stiffness of the panel can be significantly improved by fixing the sheeting on all four sides. For this type of diaphragm, the shear connectors transfer forces to the rafters. Shear connectors are usually in the form of purlin offcuts fixed to the rafter and the sheeting, as shown in Figure 3-1. Such detail however is labour-intensive and an alternative option without shear connectors is also available in current design codes. In a two-sided fastened diaphragm, the purlin/rafter connections on the unfastened edge can be designed to transfer shear between the sheeting and rafters. The purlin/rafter connection detail will also influence the panel resistance and flexibility, as shown in Figure 3-3k. Currently BS 5950-9 (1994a) in Table 7 pp. 24 offers guidance on ten different connection details both in terms of design resistance and flexibility. The presented values however, are only applicable, if exact connection detail is used. For other connection details, the design of such connections should be verified by testing.

The shear resistance and flexibility of a steel diaphragm depends on shear resistance and slip flexibility of the single fastener lap joint. In practice, the mechanical characteristic of each joint should be established experimentally. However design shear values for most popular fasteners are presented in Table 5 of

BS 5950-9. A considerably larger database on the subject of resistance and slip of different fasteners can also be found in Davies and Bryan (1982).

A second important factor contributing largely to the shear flexibility of the panel is profile distortion defined by the factor $c_{1.1}$ (see Figure 3-3h). It is given by the formula:

$$c_{1.1} = (\,ad^{2.5}K)/(Et^{2.5}b^2)\ \ (in\ mm/kN)$$

(3-1)

Where:

a – width of the shear panel (in mm)

b – depth of the shear panel in the direction parallel to the profile corrugation (in mm)

d - pitch of the corrugations (in mm)

t - net sheet thickness (in mm)

E – modulus of elasticity of the metal (kN/mm^2)

K – sheeting constant as a function of the profile geometry and fixing arrangement

The development of the analytical method for deriving the sheeting constant (K) presented the biggest challenge. This constant is a function of the sheeting cross-section and should be derived for every cross-section shape. Values of the sheeting constant (K) are widely available for trapezoidal profiles (see Figure 3-4a). The values are presented in tabular form in BS 5950-9 (1994a) for two practical design cases of sheeting being fixed in every trough (see Figure 3-3h) and alternate troughs (see Figure 3-3i). The sheeting constant (K) was also presented in Davies and Bryan (1982) and later modified by Davies (1986b). Davies also developed a robust analytical model which was later used to derive sheeting constant (K) for more complex trapezoidal sheeting cross-section with stiffeners (see Figure 3-4a b). The general conclusion was that stiffeners did not affect the shear flexibility of the sheeting profile to the extent that should be considered in the analysis.

The other contributors in the field of stressed skin research were: Baehre and Ladwein (1994), Fan et al. (1997), Davies and Lawson (1999) and De Matteis and Landolfo (1999). Their contributions are presented later in this chapter.

a) trapezoidal   b) trapezoidal with stiffeners   c) corrugated (sinusoidal)
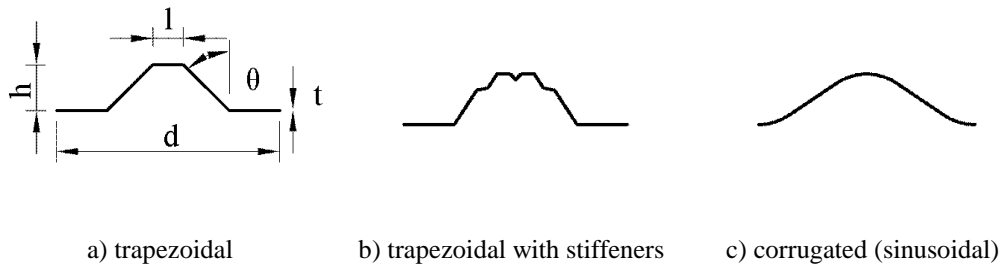
Figure 3-4 Different sheeting profiles investigated by Davies (1986a, Davies (1986b))

Existing codes of practice offer guidance for designing of single-skin diaphragms composed of trapezoidal cladding. Most of the theory presented in these documents although still valid was developed 30 years ago. The current focus should be directed toward updating existing codes to include the effect of modern forms of roof construction incorporating thick insulation.

3.1.1   Baehre and Ladwein

Baehre and Ladwein (1994) conducted extensive experimental investigations on the shear behaviour of composite panels, including 65 shear component tests on fastenings and 25 full-scale test on complete diaphragms. The first stage of testing on fasteners included:

1)   30 tests on single lap joints as described in Figure 3-5a using 6.3mm diameter screws and 3 different combinations of plate thicknesses. Each combination was tested 10 times in order to evaluate the standard deviation of the shear resistance.

2)   30 tests on special lap joint arrangement as shown in Figure 3-5b using three different composite panels of 40mm, 60mm and 80mm thickness. In these tests load was applied to the composite panel through the outer skin and tests were repeated 10 times for each thickness.

3) 5 tests on a special lap joint arrangement as shown in Figure 3-5c with the load only applied through the bottom skin of the 60mm thick composite panel.

The second stage of loading covered tests on full-scale diaphragms of the various sizes and three different types of edge connections as presented in Figure 3-5d to f. A typical cantilever arrangement was tested and is shown in Figure 3-1. The diaphragm tests could be split to 4 groups:

1) Diaphragms with joint Type 1 and without seam fasteners between the panels. Such an arrangement would be the most common practical application in constructing composite walls.

2) Diaphragms with joint Type 2 and without seam fasteners.

3) Diaphragms with joint Type 1 where the composite panel is fixed on all four edges, including seam connectors at the adjacent panels simulating typical composite roof.

4) Diaphragms with special edge joint Type 3 used to obtain ultimate resistance and stiffness of composite panel in shear. For this reason, a timber member was screwed and glued to the composite panel to minimise the effect of fasteners slip.

The general conclusion from these tests was that the stiffness of the diaphragm is highly dependent on the number of fasteners. If a significant increase in resistance and stiffness is required, an edge connection reinforcement method was proposed (see Figure 3-5f).

3.1.2   Fan et al.

Fan et al. (1997) focused on modelling the shear behaviour of single screw lap connections, similar to that presented in Figure 3-5a, using Finite Element Analysis (FEA). The 3-dimensional contact elements including friction and cohesion coefficient were used to simulate 'true' contact between following components: thick to thin plate, thin plate to neoprene washer, screw shaft to thick and thin plate and screw thread to the bottom sheet.
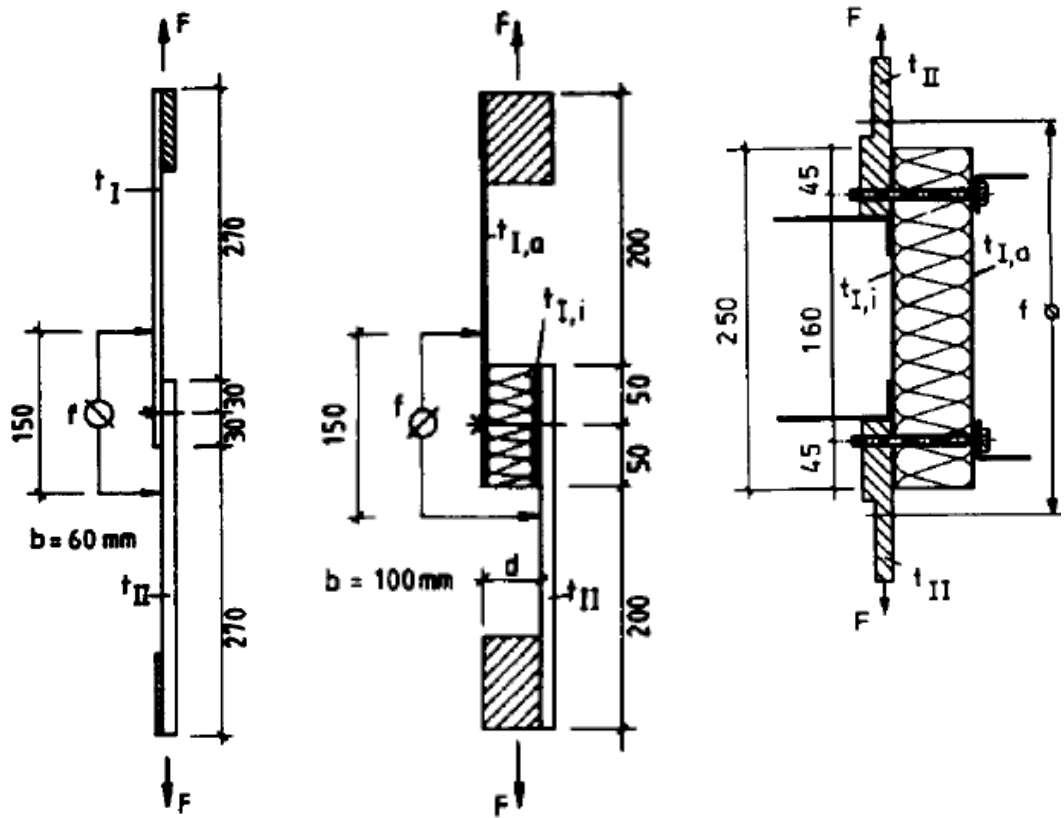
| a) single lap joint pp.308 | b) composite panel joint-load applied to outer skin pp.309 | c) composite panel joint – load applied to inner skin pp.309 |

| d) edge joint Type 1 pp.312 | e) edge joint Type 2 pp.312 | f) edge joint Type 3 pp.312 |
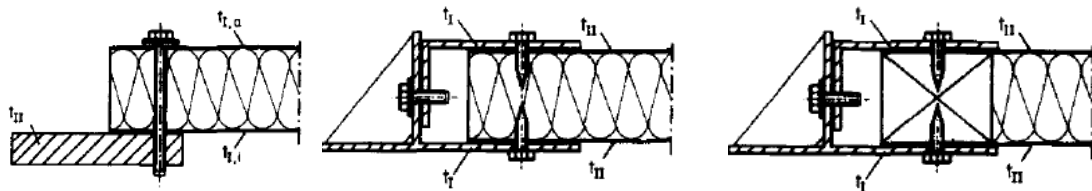
Figure 3-5 Different composite panel connections investigated by Baehre and Ladwein (1994)

The stress-strain curves were obtained for the steel plates through coupon tests and the elasto-plastic material properties were implemented. In order to capture the tearing phenomenon, a crude method, using different stress-strain relationships for tension and compression elements, was employed with sufficient accuracy. The results of 3 simulations were calibrated against 15 test results carried out on three

types of single lap joints. In each case, the thin plate was of 0.63mm thick and the thin-to-thick ratios t_1/t_2 were 4.76, 2.38 and 1.00. As expected, due to the complexity of the problem, there was significant scatter recorded in force-displacement relationship between repeated tests, and thus the FEA results were compared against average values.

Generally good agreement between analytical and experimental results was observed in terms of shear resistance of the connections. The model also captured well the combined screw bearing and screw tilting phenomena and computed shear stiffness was only slightly higher than the mean experimental stiffness. This could be explained by the fact that rigid body movements such as lack-of-fit were not captured by the FEA model.

3.1.3   Davies and Lawson

Davies and Lawson (1999) conducted tests on eight different double skin insulated roof systems in order to establish their performance in stressed skin design. They also used analytical methods described in Section 3.1 in order to analyse resistance and stiffness of each individual skin which were combined and compared against experimental data for the double skin panel system. The investigated roof systems were described as follows:

1) Built-up roof with liner panel. This structural system uses short-spanning trapezoidal liner profiles usually of 0.4mm thickness, supported on the purlins. The liner tray profile serves as a support for the dense or soft insulation. In the case of the dense insulation, the outer watertight profile is supported on the insulation itself. In the case of soft insulation, additional spacers are provided as shown in Figure 3-6a to support the outer skin on the purlin.

2) 'Built-up' roof with structural liner trays (cassette). This roof system replaces short-spanning liner panels by structural liner trays of a deeper C cross-section and much higher spanning capability (see Figure 3-6b). The web of the structural liner tray serves as a support

for the insulation where the flanges act as spacers for installation of the outer skin.

3) Composite (sandwich) panels roof. This roof system uses rigid double skin panels manufactured from inner and outer steel profiles bonded by the insulation core. The inner skin is usually of 0.4mm thickness and the outer skin is usually of 0.5mm thickness. As can be seen in Figure 3-6d, the composite panel could be fixed to the purlins either by self-drilling screws or clip-fix brackets (see Figure 3-6c), also called 'secret fix'.

The tests showed the generally good performance of built-up roof systems with the liner panel and spacer brackets (see Figure 3-6a) in terms of the stressed skin design properties. It was also shown that the analytical methods produce sufficiently close prediction of the behaviour of such diaphragms. The resistance of such roof panels was controlled by the shear buckling phenomenon of the liner profile between its ribs. A significant level of the 'composite' action between the inner and outer skin also developed through the use of spacer members.

The shear buckling failure was also observed in the structural liner tray roof system (see Figure 3-6b). The shear resistance of the liner tray on its own was well predicted by the analytical method. The authors however, observed a large discrepancy (nearly 40%) between the analytical value of the shear flexibility according to BS EN 1993-1-1 and the test results. The complete roof assembly test including liner trays and outer sheeting proved the load transfer between the skins through flanges of the liner trays. Such a built-up roof system led to good characteristics for stressed skin diaphragm design. Due to the geometry of the liner tray, neither purlins nor spacers members are required. The shear buckling resistance of the liner trays could be controlled by rolling additional stiffeners to the web of the cassette.

In the case of built-up roofs with standing seam clipped fixings, little 'composite' action was observed and the authors suggested that such diaphragms should be designed based only on the resistance and stiffness of the liner profile.
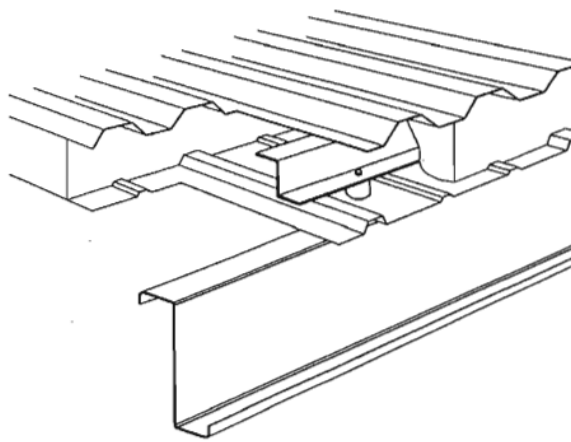
a) Built-up roof with Z spacers (SCI P397 (2012) pp.95
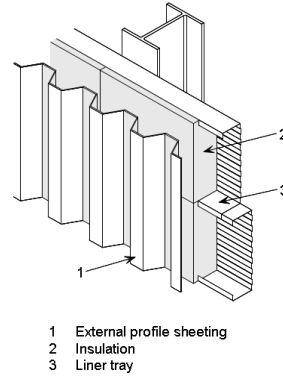
b) Typical cassette wall assembly (SCI (2012c))
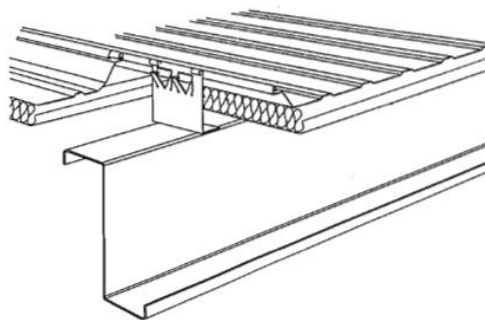
c) Built-up roof with 'standing seam' also called 'secrete fix' (SCI (2012b))
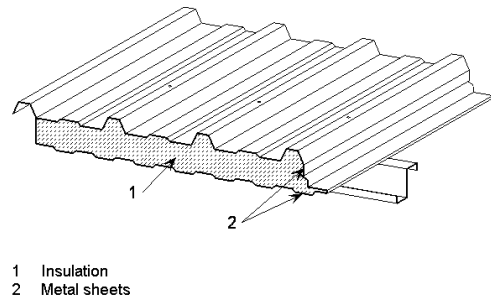
d) Composite panel with through fixings (SCI (2012a))

Figure 3-6 Examples of roof construction systems tested by Davies and Lawson (1999)

In two tests carried out on 60mm and 80mm thick rigid composite panels, their ability to act as a shear diaphragm was found to be limited. As described, the resistance and stiffness of such a roof system relied heavily on the through fixing tilting behaviour under the eccentric shear force. Because of the fact that the inner skin is usually thinner, the point where a fixing passes through the outer skin becomes a pivot point and tearing of the inner skin occurs. Two different fixing arrangements were tested: one with the composite panels only fixed at the ends (see Figure 3-6d) and second with the composite panels fixed along the purlins and the presence of the standing seam (see Figure 3-6c). Both arrangements were not

recommended for stressed skin action without enhancing their shear resistance characteristics.

3.1.4   De Matteis and Landolfo

The authors conducted tests supported by analytical study on the shear behaviour of mechanical fasteners in composite panels. Unlike Baehre and Ladwein (1994) and Davies and Lawson (1999) the researchers focused on investigating the shear characteristic of single fastener connections through component tests rather than a full-scale diaphragm test. The main subject of the investigation was composite panels using 0.6mm steel skin and a 40mm thick polyurethane core. Overall six tests were conducted consisting three different panel-to-panel joints (see Figure 3-7a) and three panel-to-frame joints (see Figure 3-7b) both under monotonic and cyclic load. The main motivation for the research was to develop a mathematical model which can simulate the monotonic behaviour of the connection so it can be used in cyclic load simulation. In order to form a mathematical model, the Ramberg-Osgood relationship was chosen to describe the behaviour of the joint (linear-elastic with nonlinear strain hardening). The exponent was calibrated against experimental data for each joint type and later used to form the analytical relationship based on unfactored ultimate joint resistance according to BS EN 1993-1-3 (2006) and the flexibility relationship after Zadanfarrokh and Bryan (1992)(see Section 2.1.3). The main conclusion was that although the analytical equations were never intended to describe the resistance and stiffness of the examined joints, with small adjustments they offered satisfactory accuracy.
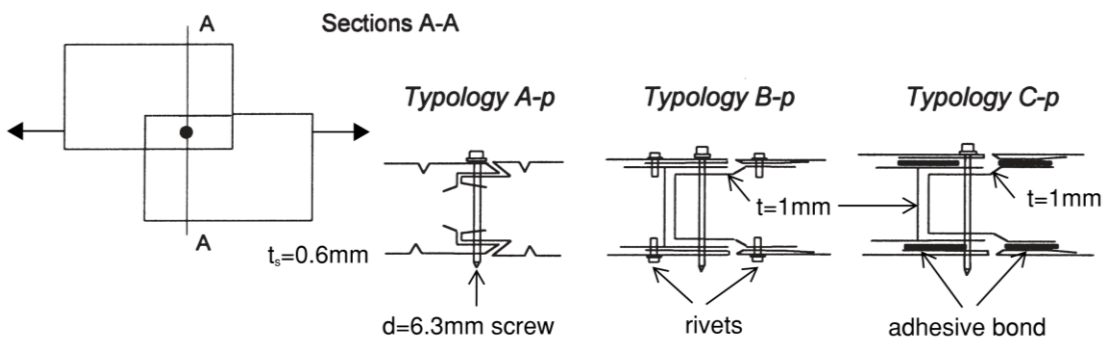
a) Panel-to-panel connection
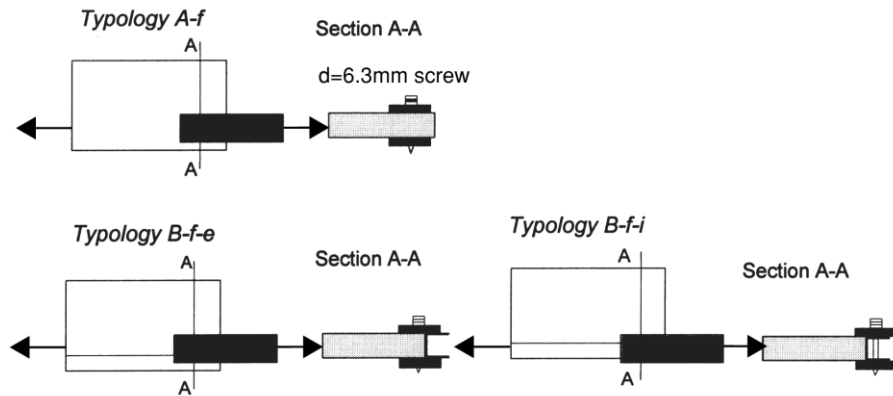
b) Panel-to-frame connection

Figure 3-7 Types of composite panel screw connections investigated by De Matteis and Landolfo (1999) pp.67

3.2 Justification for research

Roof systems are consistently evolving often leaving existing standards out-of-date. To the author's knowledge, since the last tests on the double skin roof systems by Davies and Lawson (1999) little research had been performed on current roof systems in terms of stressed skin performance. The author's objectives were to conduct an experimental study of different roof panels in order to validate the relevance of the existing state of the art analytical methods for predicting shear resistance and stiffness of modern roof panels.

The novel aspects of the experimental research were as follows:

1) The typical connection detail for purlin to rafter connections, recognised by the BS 5950-9 (1994a), includes C or Z purlins connected to the rafters through a web cleat (see Figure 3-8a). Such a detail has relatively low stiffness in shear unless, heavy web cleats are used. However, the use of modern top-hat shaped purlins can simplify the connection detail and improves purlin to rafter connection stiffness (see Figure 3-8b).
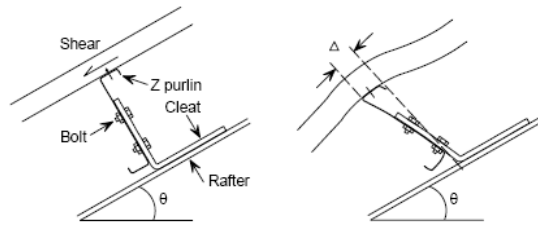
a)   Shear deformation of typical Z purlin connection
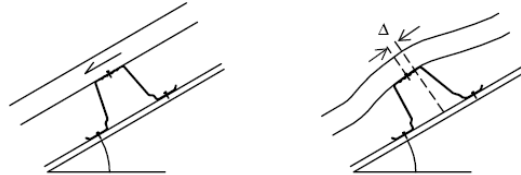
b)   Shear deformation of the top-hat purlin connection

Figure 3-8 Shear deformation of two types of purlin/rafter connection details

2) The theory on shear flexibility of sinusoidal corrugated sheeting fixed in alternate troughs was presented in Davies and Bryan (1982) and Davies (1986b). Such a connection detail is now considered as impractical and rarely used in the industry due to potential leakage problems. Now the fixings are installed on the ridge of the profile, which will significantly reduce the shear resistance of the roof panel. The experimental resistance and stiffness of this type of roof panel was investigated, including the mode of failure.

3) Due to the growing popularity of composite panels, their poor ability to act as a shear diaphragm (as reported in Davies and Lawson (1999)) was investigated further. The main difference between previous studies was that the 'standing seam' was replaced by seam screws which restrain a lateral movement of the composite panels and improve its shear performance.

4) BS 5950-9 (1994a) recommends that the net thickness of the roof or wall sheeting profile should not be less than 0.55mm. Thinner steel however, is often used to manufacture cladding profiles and liner trays and the shear performance of very thin panels was investigated. In fact, the industry standard for the thickness of the wall sheeting is 0.48mm due to the fact that such component is not subject foot traffic during construction.

3.3   Testing methodology

A novel type of purlin connection detail was investigated for a range of cladding types following the recommendations given in clause 11.4 of BS 5950-9 (1994a). Each test was carried out on a cantilever panel of approximately 3m x 3m subject to shear force, as shown in Figure 3-9a. The test set-up consisted of cold-formed steel double lipped channels of 3mm thickness for the rafters, top-hat shaped purlins of 61mm depth x 1mm thickness and top-hat for the shear connectors, as shown in Figure 3-9c. The left hand side rafter was fixed at both ends and the load was only applied through the right hand side free rafter. The free rafter was placed on a galvanized steel plate lined with PTFE sheets (i.e. Teflon) to minimise the friction between the free rafter and the concrete floor.

Using the test recommendations in BS 5950-9 (1994a), each panel was loaded in four stages:

- Bedding down – the panel was loaded continuously up to approximately 80% of the serviceability loading; this load was maintained for 15 min. and then removed.
- Acceptance test - the load was reapplied up to approximately 80% of the calculated shear capacity of the panel; this load was maintained for 15 min and released.
- Strength test – the panel was reloaded until it reached the load equal to the calculated shear capacity of the panel; this load was maintained for 15 min. and released.
- Failure test – the panel was loaded until failure of the specimen (i.e. until no increase in load was recorded).

At each stage of testing, the displacements and shear force were logged. The panel's displacement was measured by linear displacement transducers and overall deflection (δ) was calculated from the formula:

$$\delta = \delta_1 - \delta_2 - [(a/b)(\delta_3 - \delta_4)] \qquad (3\text{-}2)$$

Where:

$\delta_{1...4}$ – defection of the four corners (as shown in Figure 3-9a)

a – width of the shear panel

b – depth of the shear panel in the direction parallel to the corrugations
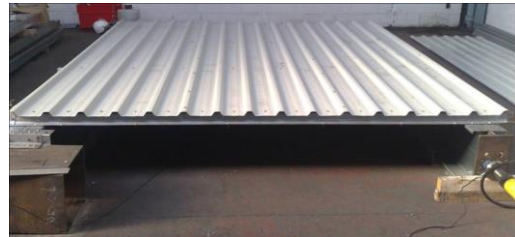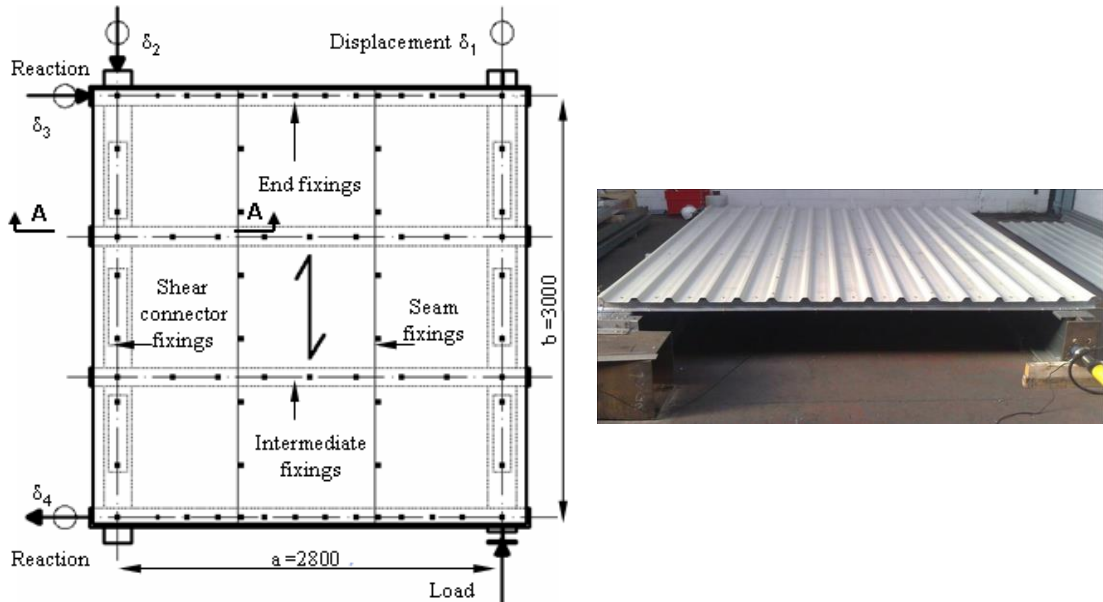
a) Plan view   b) Front view – clad roof panel

c)   Front view – bare roof panel

Figure 3-9 Test arrangement of shear panel test

The complementary information on shear panel test components is presented as follows:

- Members used as rafters and purlins (see Appendix C.1)

- The bending and compressive capacities of top-hat purlins (see Appendix C.2)

- The sheeting profiles used to construct roof shear panels (see Appendix C.3)

- The fasteners used in shear panel tests (see Appendix D.1)

- Types of connection (see Appendix D.2)

- Lap joint testing methodology (see Appendix D.3)

- Lap joint test series (see Appendix D.4)

- Lap joint test results (see Appendix D.5)

- Lap joint experimental results versus analytical prediction (see Appendix D.6)

- Concluding remarks on shear resistance and shear flexibility of screw connection (see Appendix D.6)

3.4   Tests on cladding panels assemblies with shear connectors

For this experimental study, 9 different diaphragms were tested containing 4 types of single skin cladding profiles in 2 different thicknesses and one composite panel comprising rigid polyisocyanurate (PIR) insulation. Shear connectors were used in all tests to connect the diaphragms on all four sides, as shown in Figure 3-10.

3.4.1   Single skin roof panels

The total of eight tests on different roof diaphragms was conducted for the test set-up shown in Figure 3-10. In each test, the purlin/rafter connection detail was kept the same and used four self-drilling, self-tapping screws as shown in Figure 7-11e. The spacing and the number of stitching screws (also known as seam screws see Figure 7-11a) and cladding/shear connector screws was the same in all tests as shown in Figure 3-10. The same fastener of 6.3mm diameter was used for the seam and cladding/shear connector joints (see Figure 7-10b). The remaining variables were the geometry of the cladding profile and the number of screws in the cladding/purlin

connection (see Figure 7-11b). The trapezoidal profiles were fixed in every trough to the end purlin and alternate troughs to the intermediate purlin (Figure 3-10). The sinusoidal cladding profile was fixed in every third crest to both the end and intermediate purlins. In terms of shear performance of the cladding panel, the cladding fixings should be placed in the troughs rather than crest to prevent bending of the fixings. Such a joint detail however, is often problematic in terms of preventing water leakage. The industry standard fixing method was therefore examined (see Figure 7-11c) taking into consideration that by doing so the stiffness of the shear panel will be compromised.

The special longer screws used in crown-fix panels are shown in Figure 7-10d. A description of each test is presented in Table 3-1 with the number of fasteners and geometrical properties of the sheeting profiles, according to BS 5950-9 (1994a).
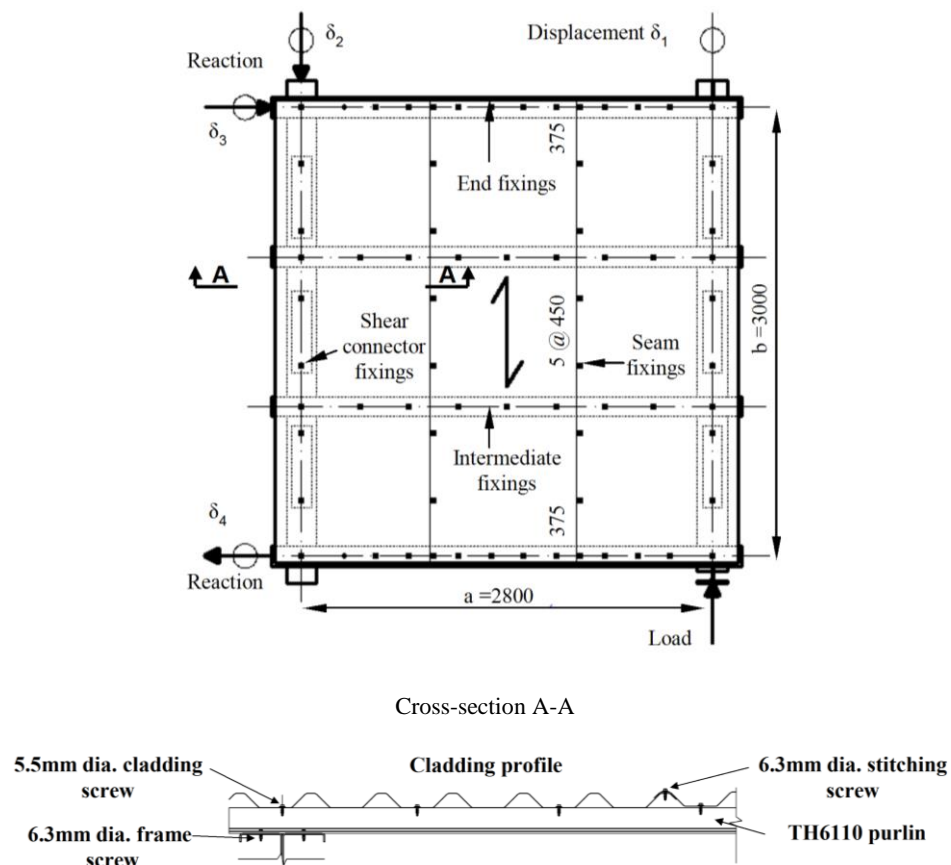
Figure 3-10 Test arrangement for single skin diaphragm fixed on 4 sides

The test designation consists of: test number followed by the sheeting profile name starting from capital letters AS followed by profile height and nominal thickness in millimetres. A description of sheeting geometry is found in Table 7-13 and each sheeting type was tested in two nominal thicknesses of 0.5mm and 0.7mm. The specification of sheeting profiles used in shear panel tests can be found in Appendix C.3. The shear resistances and flexibilities of tested panels were assessed according to APPENDIX F, cross-referenced with Table 3-1.

Table 3-1   Tests description of single skin diaphragm

Test designation	t_{cor}	n_s	n_{sc}	n_p	n_{sh}	n_f	p_{end}	p_{int}	u	I_y	K
							mm	mm	mm	mm^4	
T1 AS34/0.5	0.48	8	6	4	3	6	167	334	194	15959	0.070
T2 AS34/0.7	0.65	8	6	4	3	6	167	334	194	21574	0.070
T3 AS30/0.5	0.48	8	6	4	3	5	200	400	230	14253	0.054
T4 AS30/0.7	0.65	8	6	4	3	5	200	400	230	19285	0.054
T5 AS24/0.5	0.48	8	6	4	3	6	167	334	193	6854	0.047
T6 AS24/0.7	0.65	8	6	4	3	6	167	334	193	9271	0.047
T7 AS18/0.5	0.48	6	6	4	3	5	229	229	87	1572	1.081
T8 AS18/0.7	0.65	6	6	4	3	5	229	229	87	2164	1.081

t_{cor} – sheet thickness excluding coating

n_s – number of seam fasteners excluding those passing through sheet and purlin

n_{sc} – number of shear connectors fasteners along the one side of the sheet

n_p – number of purlins within the diaphragm

n_{sh} – number of sheets within the diaphragm

n_f – number of fasteners per sheet width at the end of the sheet

p_{end} – fasteners spacing at the end purlin

p_{int} – fasteners spacing at the intermediated purlins

u – perimeter length of a complete single corrugation

I_y – second moment of area of single corrugation about its neutral axis

K – sheeting constant: T1 to T6 according to Table 12, BS 5950-9 (1994a), T7 to T8 according to Davies (1986b)

3.4.2   Rigid composite roof panels

A common example of a double skin roof diaphragm was investigated. This consisted of rigid insulated composite panels fixed to the purlins by the long self-drilling, self-tapping screws as shown in Figure 3-11. The seam screws were also

used to join two panels and the same spacing of seam screws were used as in previous tests (see Figure 3-10). The screws used for fixing composite panels with purlins are shown with Figure 7-10e and Figure 7-11d.

As can be seen in Figure 3-11, a composite panel comprises two sheeting profiles bonded together by the insulation foam. The detail geometry of the top and the bottom skin is described in Table 7-13 and Figure 7-9.

The standard analytical method presented in BS 5950-9 (1994a) does not include rigid composite panels thus the effect of bonded insulation is ignored and shear resistances and flexibilities of bottom and top skins are calculated according to APPENDIX F, cross-referenced with Table 3-2.
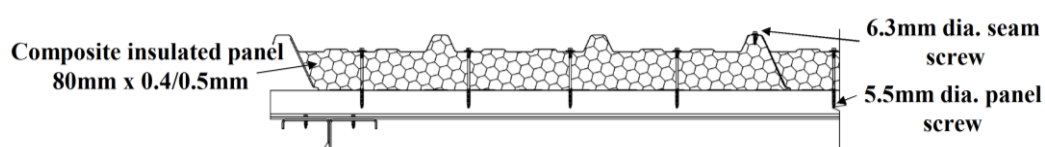
Figure 3-11 End purlin fixings arrangement of the composite diaphragm with shear connectors

Table 3-2   Tests description of composite roof panel

Sheet thickness	t_{cor}	n_s	n_{sc}	n_p	n_{sh}	n_f	p_{end}	p_{int}	u	I_y	K
							mm	mm	mm	mm^4	
T9	0.48	8	6	4	3	4	255	350	384	22837	0.020
AS35/80	0.36	0							98	9	0.008

K – sheeting constant: T9 according to Table 12, BS 5950-9 (1994a)

3.4.3   Test results

In this section, the results of nine shear roof panels tested with shear connectors are presented. The testing procedure is described in Section 3.3 and the load-deflection curves for each test to failure are presented in Figure 3-12, Figure 3-13 and Figure 3-14. Photographs of the failure modes observed within each test and a short comment is also provided in these figures.

The shear connector failure did not occur in tests T1 to T6. In the other tests, the hole elongation around the shear connector screws were always less than those of the seam connection. In fact the shear capacity calculated based on the shear connector design criterion was on average 33% lower than the ultimate test load (see Table 7-20). This design criterion was therefore neglected and the ultimate analytical shear capacity of the panel (V*) was taken as that of the seam fasteners' resistance (V_s) (see Table 7-20) and was marked on the load-deflection plot.

The analytical shear resistances (V) and flexibilities of panels (c) denoted as "Anl." (see Table 7-20) were calculated according to APPENDIX F. As the behaviour of the shear panel is dependent on shear properties of individual single lap joints, several component tests were conducted as described in APPENDIX D. For Test 2, 4, and 6, the shear resistance and flexibilities of panels were also derived based on upper bound (denoted "Max. Exp.") and characteristic values (denoted as "Char. Exp.") obtained from the lap join tests.

In order to measure the ultimate shear deflection of each individual panel, the load was continued until sudden loss of resistance or failure of the edge purlin had occurred. It should be noted that in the case of test T3, the initial test results were not recorded due to equipment malfunction (see Figure 3-12b). The linear load-deflection relationship was used to replace the missing data.

Generally in all the tests, tearing of the sheeting around the seam screws had an important effect on the failure of the panels. However in the case of the diaphragms with 0.5mm thick sheeting, (see Figure 3-12a, b, c) profile distortion was also observed.

As expected in the case of cladding profiles fixed at the crest such as test T7 (see Figure 3-12d), test T8 (see Figure 3-13d) and composite panels test T9 (Figure 3-14), tilting of the fixings determines the behaviour of the shear diaphragm. The tilted screws act not only in shear but also in bending and this can cause unwanted breaking failure of the screw which was observed in test T8 (see Figure 3-13d).

In tests T2, T4 and T6, tearing of the sheeting around the seam screws was observed (see Figure 3-13a, b, c). However, in tests T4 and T6, the panels failed due to the buckling of the end purlin in compression at higher loads (see Figure 3-13b, c). Extensive local shear distortion of the profile in test T4 was observed in the early stage of loading, causing higher flexibility than predicted.
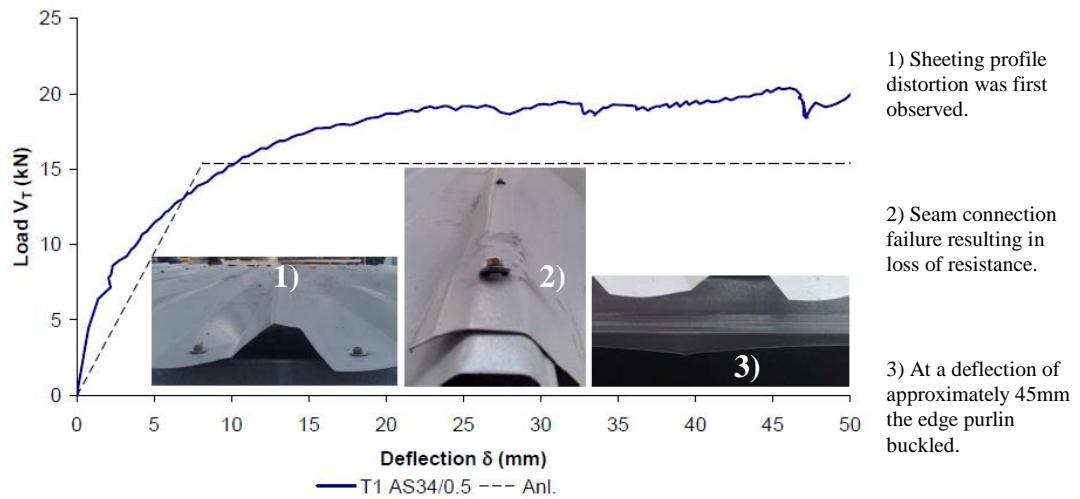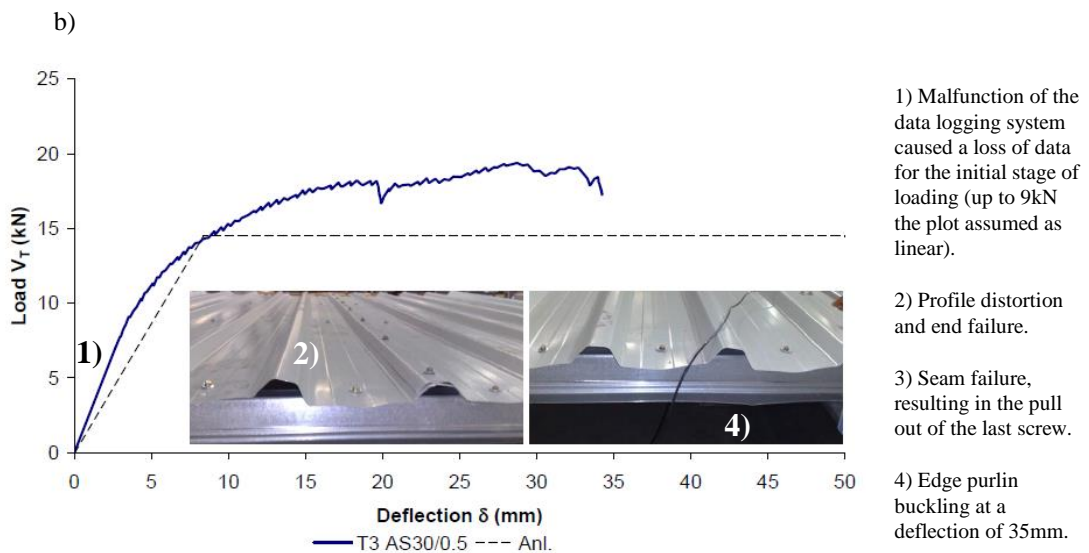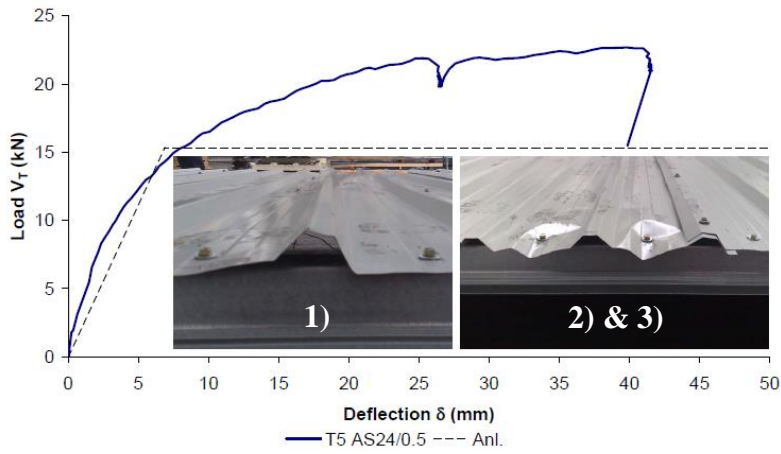
1) Sheeting profile distortion was first observed.

2) Seam connection failure resulting in loss of resistance.

3) At a deflection of approximately 45mm the edge purlin buckled.

a) Test 1

b)

1) Malfunction of the data logging system caused a loss of data for the initial stage of loading (up to 9kN the plot assumed as linear).

2) Profile distortion and end failure.

3) Seam failure, resulting in the pull out of the last screw.

4) Edge purlin buckling at a deflection of 35mm.

c) Test 3

89

1) Profile distortion propagating into the shear buckling in the central section of the panel between alternate trough fasteners.

2) Seam failure.

3) Deformation of the cladding around the end fasteners.

d) Test 5
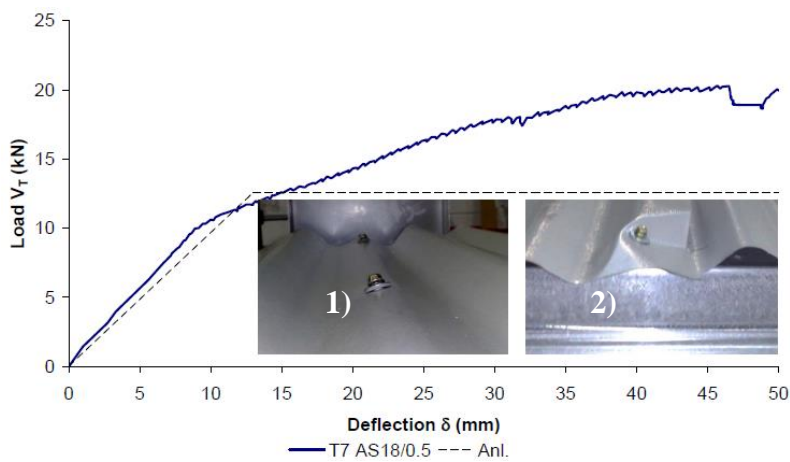
1) Tilting of the screws causing dents in the sheeting profile.

2) Large deformation of the sheeting profile around the end screws.

e) Test 7

Figure 3-12 Load-deflection curves for single skin sheeting of 0.5mm thickness
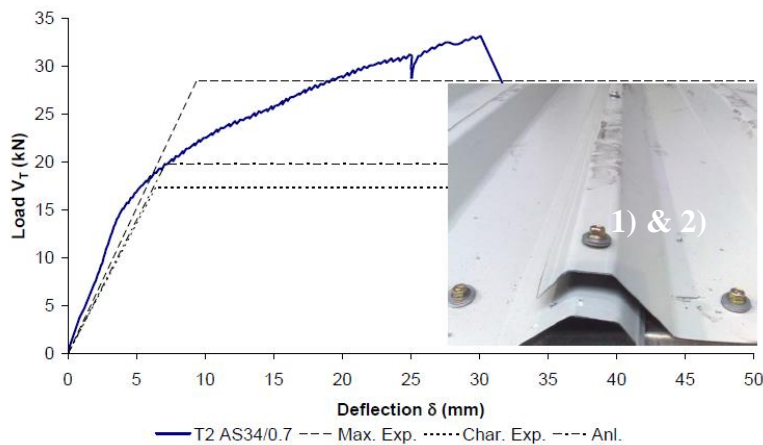
1) Seam failure by tearing the metal around the screws.

2) Sudden loss of resistance by the pull-out of the end seam screw.

a)   Test 2
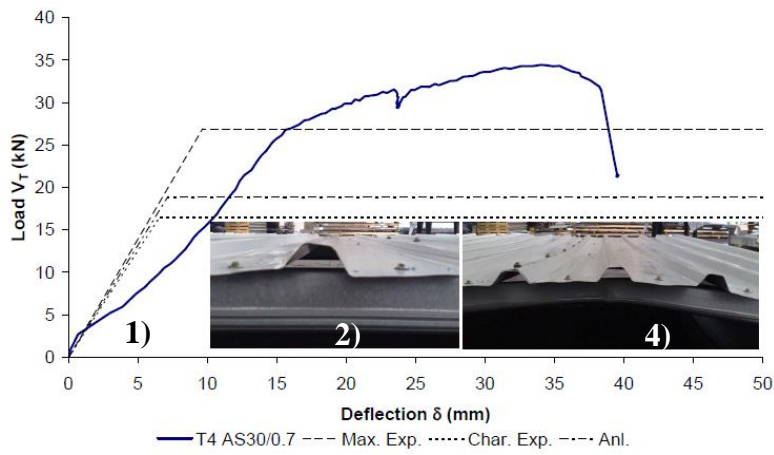
1) Significant loss of stiffness in the initial stage of loading. No observation was made regarding potential cause.

2) Profile distortion.

3) Seam failure.

4) Sudden loss of resistance by flexural buckling of the end purlin.

b) Test 4
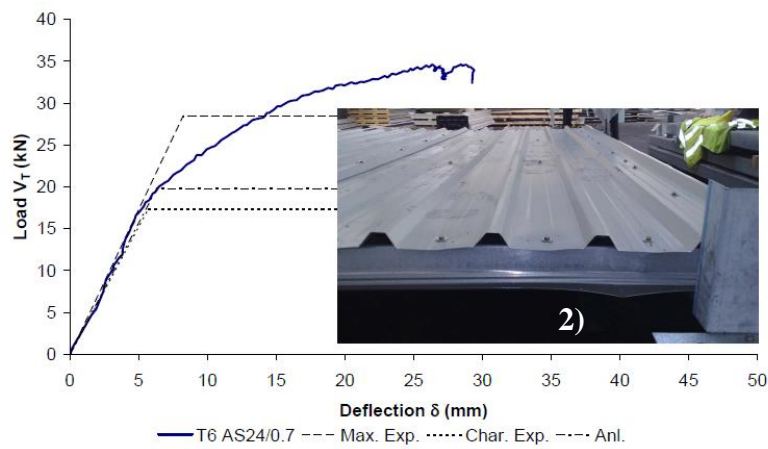
1) Seam failure by tearing the metal around the screws.

2) Edge purlin buckling at the deflection of approximately 30mm.

c) Test 6
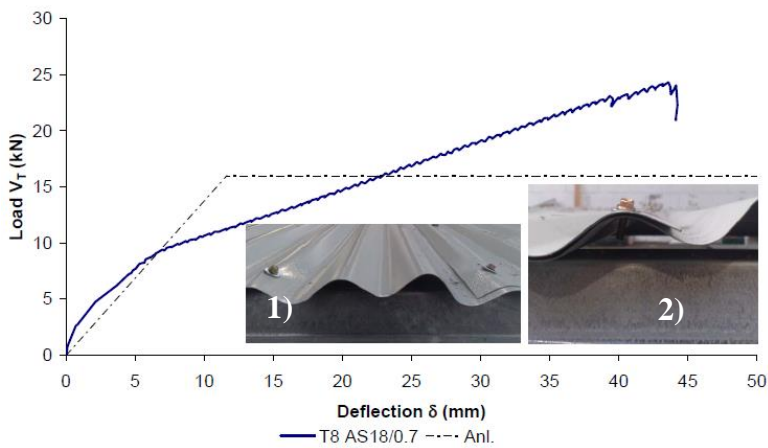
1) Tilting of the screws causing dents in the sheeting profile.

2) Sudden failure due to shear braking of the screw.

d) Test 8

Figure 3-13 Load-deflection curves for single skin sheeting of 0.7mm thickness

1) Seam failure by tearing the metal around the screws.

2) Tilting of the panel to purlin screws and tearing of the metal around these screws at the thinner bottom liner tray.

3) Edge purlin buckling at a deflection of approximately 55mm.
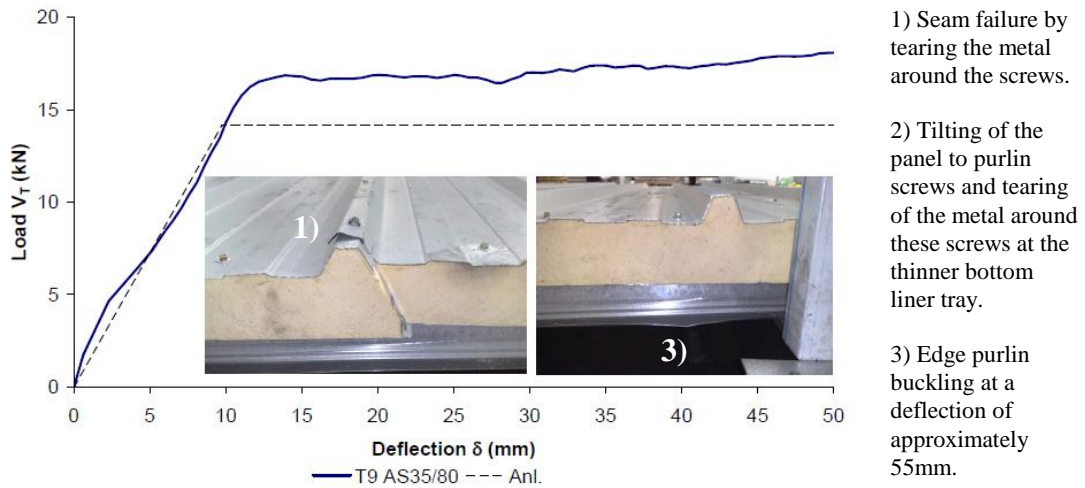
Figure 3-14 Load-deflection curves for single skin sheeting of 0.5mm thickness

3.4.4 Concluding remarks

Despite the complexity of the problem, the calculated methods offered adequate prediction of shear resistance of the investigated panels due to seam failure. In Table 3-3 the analytical shear resistance V* was taken as the shear resistance of the seam connection (V_s) in accordance with APPENDIX F. This assumption was based on the observation that holes elongation was not observed around the shear connector screws, suggesting that the 'true' level of loading was significantly lower than that assumed by standard design methods. It should be noted that the standard design method neglects the contribution of the top-hat purlins in carrying direct shear. As a result realistic shear load transferred via shear connectors may be significantly overestimated adding to the conservatism of the shear resistance prediction. It is suggested that this problem should be investigated further by more details analysis methods such as Finite Element Analysis so that more accurate diaphragm design can be available.

In the case of panel, in which the shear resistances of individual fasteners were established by the use of the analytical equation, Toma et al. (1993)(model "Anl."), predicted shear capacities that had an average 55% safety margin. As expected, the safety margin was reduced to the average of 25% when upper bound experimental values of fastener shear resistance (model "Max. Exp.") were used in

the calculations. This model gave results closest to the values obtained in the full-scale panel tests. The least accuracy was obtained when the shear resistances of individual fasteners were reduced to the characteristic values (model "Char. Exp."), this method offered almost half the resistance as compared with the values obtained from the tests.

In terms of tests shear flexibilities of the panels versus the analytical flexibilities, a good correlation was obtained for 0.7mm thick sheeting (see Table 3-3). It should be noted that the experimental flexibility (c_T) was idealised to a linear behaviour at the point in which the shear panel reached 60% of its ultimate test load according to Sections 11.4.5 and 11.4.6 of BS 5950-9 (1994a). As shown in Table 3-3, in the case of test T4 AS30.0.7, unexpected behaviour was recorded and the initial test flexibility was 69% greater than that predicted by the calculated method (see Figure 3-13b). No explanation can be offered to this unforeseen behaviour.

As can be seen in Table 3-3, the test flexibilities of the 0.5mm thick sheeting panels were not as sensitive to the thickness of the sheeting as indicated by the calculated method. The upper bound shear capacity and fastener slip, presented in APPENDIX D, were not used in calculations due to the lack of experimental data.

It was shown however in tests on shear panels with 0.7mm cladding that the proposed calculated method for predicting the slip of individual fasteners offers sufficient accuracy in assessing the shear flexibility of the panel (lines gradients of "Max. Exp." and "Anl." are very similar in Figure 3-13a, b and c).

The corrugated sheeting profiles fixed in crests (test T7 and T8) require more research before they can be used in stressed skin design. Due to extensive fixing inclination, non-linearity of the load-deflection relationship was observed in the early stage of loading thus their ability to act elastically can be in question. It was demonstrated that such shear panels are still capable of transferring load between the frames and their ultimate shear deflection capacity should be taken into account in portal frame design in order to prevent breaking of the fixings (see Figure 3-13d).

Table 3-3 Comparison of the analytical versus experimental shear capacities and shear flexibilities of the tested panels

Test designation	Model	V^*	c	V_T	c_T	V_T/V^*	c_T/c
		kN	mm/kN	kN	mm/kN		
T1 AS34/0.5	Anl.	14.88	0.55	19.20	0.27	1.29	0.49
	Max. Exp.	27.74	0.34	33.20	0.29	1.20	0.85
T2 AS34/0.7	Char. Exp.	16.88	0.38	33.20	0.29	1.97	0.76
	Anl.	19.38	0.36	33.20	0.29	1.71	0.81
T3 AS30/0.5	Anl.	13.95	0.61	18.20	0.39*	1.30	0.63
	Max. Exp.	26.07	0.37	34.50	0.63*	1.32	1.69
T4 AS30/0.7	Char. Exp.	15.91	0.41	34.50	0.63*	2.17	1.52
	Anl.	18.40	0.39	34.50	0.63*	1.88	1.60
T5 AS24/0.5	Anl.	14.88	0.47	21.90	0.34	1.47	0.72
	Max. Exp.	27.74	0.30	34.30	0.30	1.24	1.01
T6 AS24/0.7	Char. Exp.	16.88	0.34	34.30	0.30	2.03	0.90
	Anl.	19.38	0.33	34.30	0.30	1.77	0.92
T7 AS18/0.5	Anl.	11.79	1.06	20.20	0.90	1.71	0.85
T8 AS18/0.7	Anl.	15.20	0.72	24.30	0.85	1.60	1.18
T9 AS35/80 top	Anl.	13.52	0.72	16.90	0.71	1.25	0.98
	Anl.					1.55	0.91
Average	Max. Exp.					1.25	1.19
	Char. Exp.					2.06	1.06

* Experimental data affected by unexpected behaviour or malfunction of the equipment

3.5 Tests on cladding panels assemblies without shear connectors

As the installation of shear connectors is labour-intensive they are often not needed in practical application. Due to the fact that stressed skin design is also rarely implemented in portal frame design, there is a greater need to investigate the shear behaviour of roof panels without shear connectors (i.e. sheeting fixed on 2-sides). This type of roofing may have sufficient shear stiffness to carry significant load which normally is not considered in the design. According to Davies and Bryan (1982) the design resistance (F_{pr}) and flexibility (s_{pr}) of the purlin/rafter connection can be established by a component test as described in APPENDIX E.

In this research, tests on full-scale panels without shear connectors were also carried out so direct comparison against 4-sided fixed panels can be made. For this reason, panels in tests T11 to T16 were assembled the same way as those in tests T1 to T6 (see Table 3-1) but shear connectors were not present ($n_{sc}=0$). A description of the test set-up is shown in Figure 3-15.

In tests T17 and T18, the number of sheet to end purlin fixings (n_f) was increased to one screw in alternate corrugations ($n_f=7$) to avoid the shear failure of fixings, as observed in tests T8 (see Figure 3-13d). The sheeting constant K=0.494 was used in calculations of the shear flexibility according to Davies (1986b).

In test T18, the number of end fixings in the composite panel (n_f) was increased from 4 to 6 per each panel, as shown in Figure 3-16.

As the flexibilities of panels without shear connectors were expected to be significantly higher, in every test, the end purlins were doubled by nesting and stitching top-hat legs, to prevent buckling failure of the edge purlin before failure of the sheeting (see Figure 3-13b and c).

3.5.1 Test results

The shear capacity of panels in tests T11 to T19 is controlled by the resistance of sheet/end purlin connections for the sheeting fixed on two sides. The

design capacities for each potential mode of failure are presented in Table 7-21 of APPENDIX F.
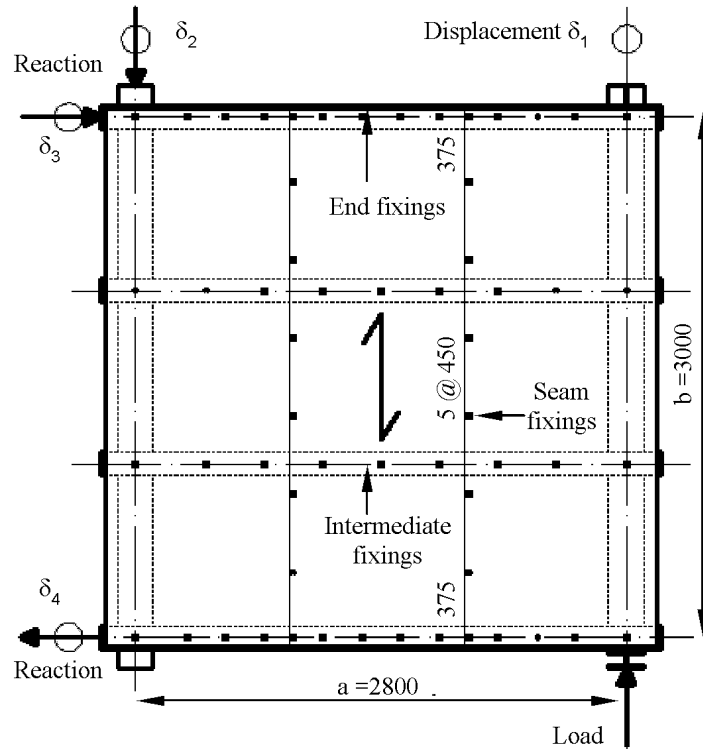
Figure 3-15 The single skin diaphragm fixed on 2 sides - test arrangement
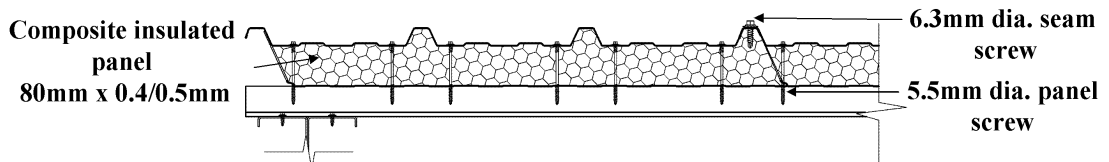
Figure 3-16 End purlin fixing arrangement in composite diaphragm without shear connectors

The ultimate test loads however, proved to be significantly higher than those calculated. A similar observation was made for the tests on 4-side fixed panels, that the design capacity of the seam connection is still conservative when compared against the failure load. This design capacity was therefore included in Figure 3-17, Figure 3-18, Figure 3-19 and Table 3-4. The shear capacities based on calculated values of lap screw connections are denoted "Anl." and whenever experimental and

characteristic values are used for calculations, they are denoted as "Max. Exp." and "Char. Exp." (see Table 3-4).

In the case of test T11, permanent deformation due to hole elongation in the sheet /end purlin connection was observed around a shear force of 13.8kN. The panel failed eventually at the seam connection (see Figure 3-17a) at a shear load of 18kN. The design resistance for this mode of failure was calculated as 14.9kN. Panels in tests T13 and T15 failed due to shear buckling of the sheeting profile initiated by end collapse of the profile (see Figure 3-17b and c). The design capacity of panels due to the end collapse of the sheeting was calculated as 21.2kN and 23.2kN (see Table 7-20).
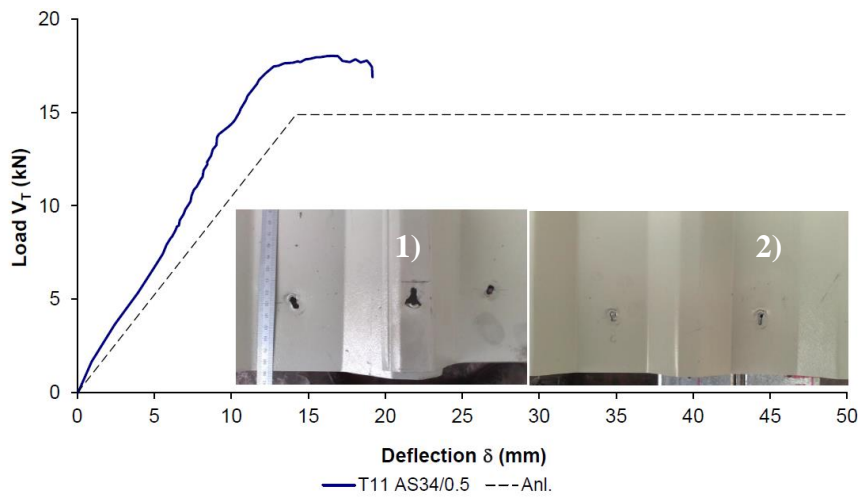
1) Seam connection failure by tearing of the cladding around the seam screws.

2) A similar mode of failure was also observed at the sheet/end purlin connection. The shear panel lost its water-tightness as the holes around the screws were much greater than washer diameter (around 15mm diameter).

a) Test 11
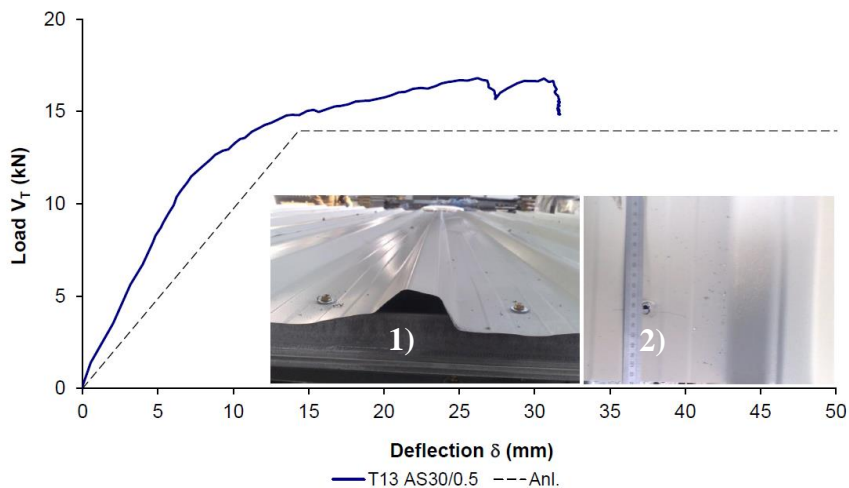
1) Profile distortion propagating into the shear buckling in the central section of the panel between alternate trough fasteners.

2) The shear panel lost its water-tightness as the holes around the seam and sheeting/end purlin screws were much greater than washer diameter.

b) Test 13
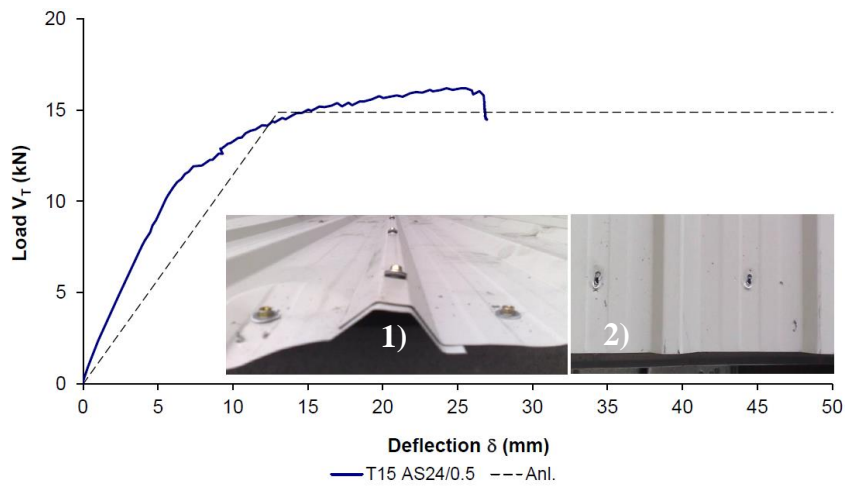
Shear panel followed the behaviour as in Test 13.

c) Test 15
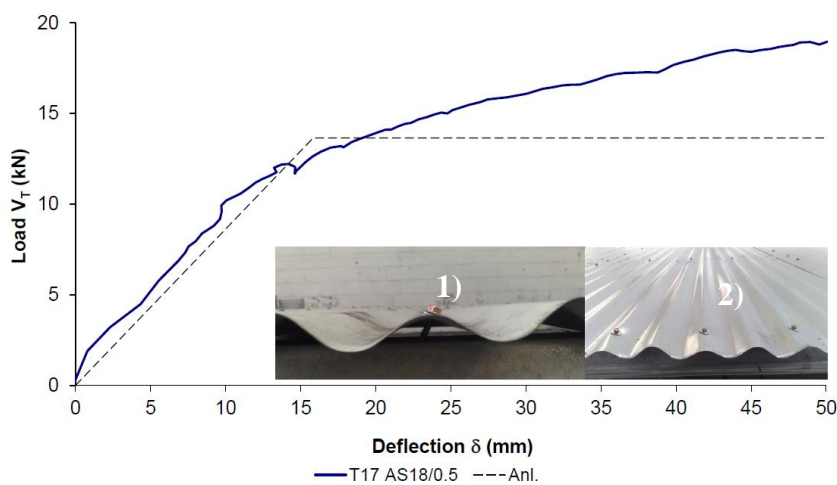
1) Tilting of the screws causing dents in the sheeting profile.

2) Large deformation of the sheeting profile around the end screws. The shear panel lost its water-tightness as the holes around the seam screws were much greater than washer diameter

d) Test 17

Figure 3-17 Load-deflection curves for single skin diaphragm of 0.5mm thickness

Similar behaviour to test T11 was observed in panels of tests T12, T14 and T16. The sheeting profiles tore around seam and end-purlin fixings almost simultaneously (Figure 3-18a, b and c). Again the ultimate test loads were higher than the design resistance of seam connections.

Increasing the number of end fixings in tests T17 and T18 did not offer much improvement in panel behaviour. Although it prevented the sudden shear failure of fixings experienced in test T8, it did not stop extensive screw inclination. As an effect of this phenomenon in tests T17 and T18, non-linearity of the load-deflection relationship was observed in an early stage of loading (around 3kN). Both

panels failed due to a combination of extensive screw inclination and local failures of corrugated profile (see Figure 3-17d and Figure 3-18d).

In test T19, the ultimate resistance of the sheet/end purlin connection for the thinner 0.4mm thickness bottom skin was calculated as 9.2kN. In the test, signs of this mode of failure were observed at slightly above this load. More load was transferred to the top skin, therefore the composite panel failed at the seam connection (see Figure 3-19) at a load slightly higher than that calculated for the top skin seam failure. The shear flexibility calculated for the top skin only proved to be significantly higher than that obtained in the test.
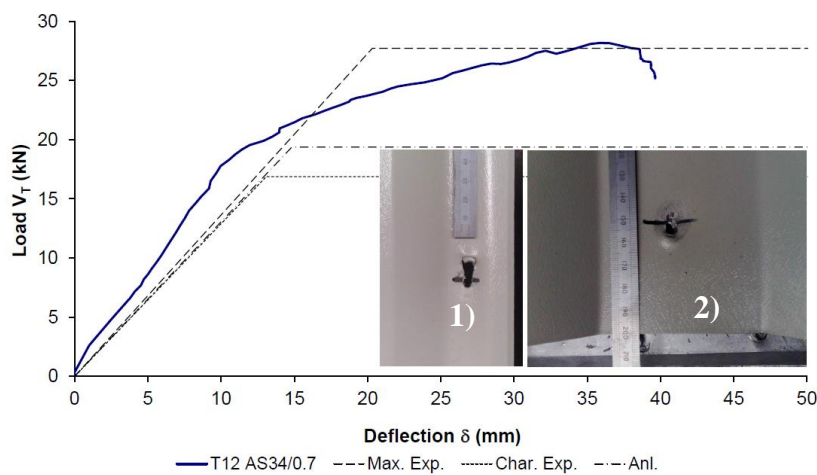
1) Tearing of the sheeting around the seam screws and the end fixings.

2) The shear panel lost its water-tightness as the holes around the sheeting/end purlin screws were much greater than the washer diameter.

a) Test 12
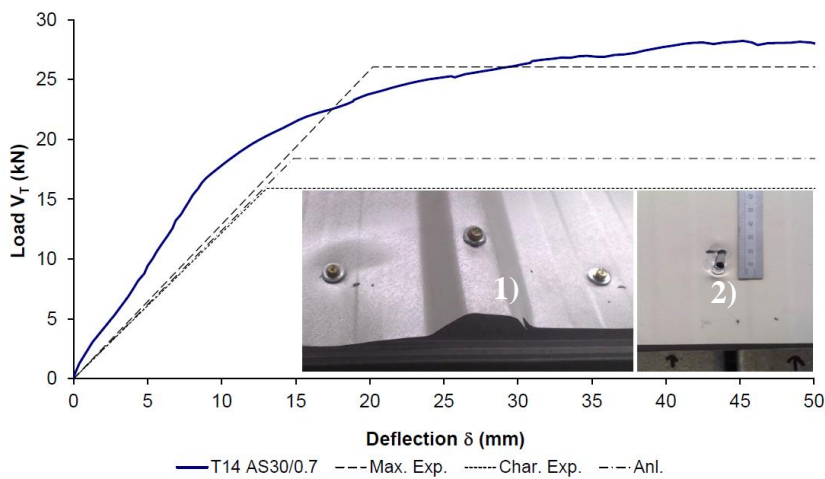
The shear panel followed the behaviour as in Test 12.

b) Test 14
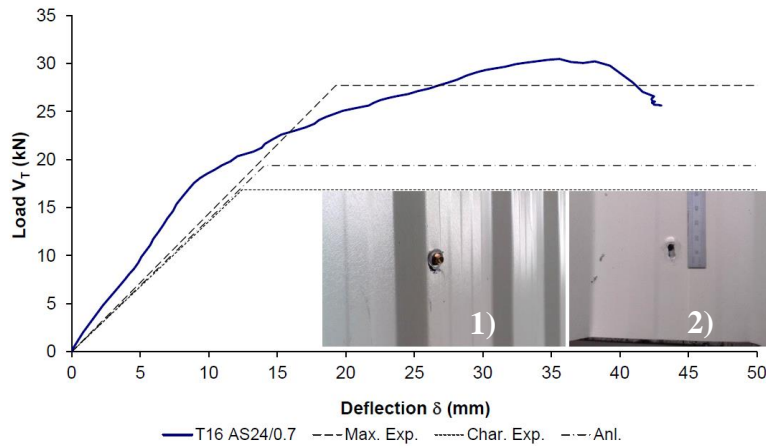
The shear panel followed the behaviour as in Test 12.

c)   Test 16
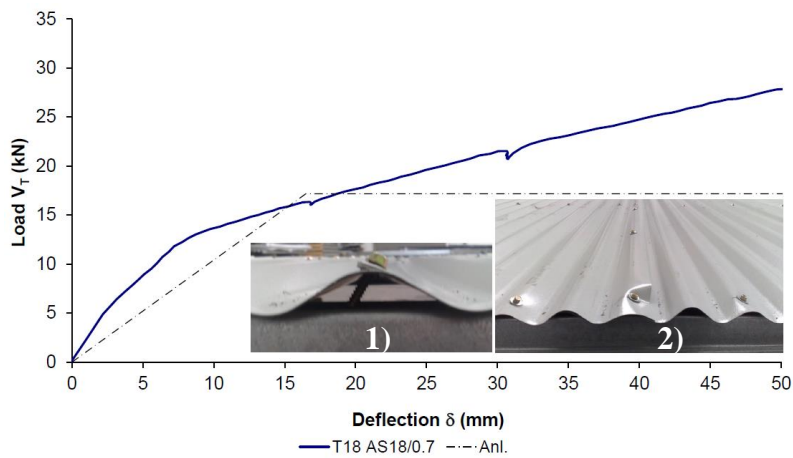
The shear panel followed the behaviour as in Test 17.

d)   Test 18

Figure 3-18 Load-deflection curves for single skin diaphragm of 0.7mm thickness
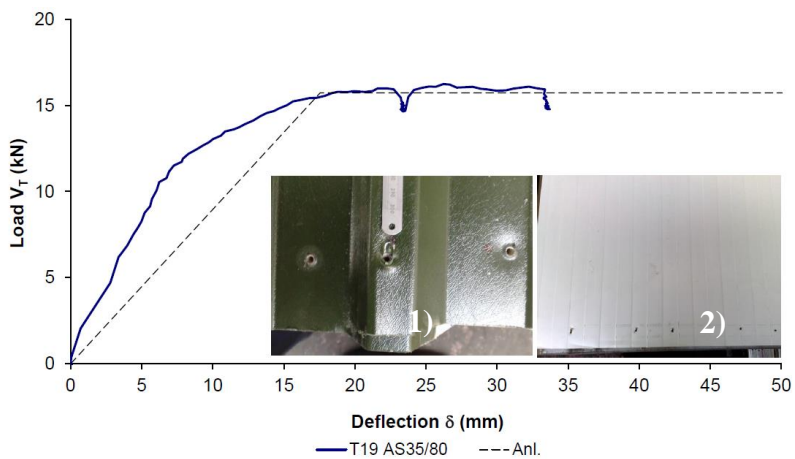
1) Seam failure by tearing of the sheeting around the screws.

2) Tilting of the panel to purlin screws and tearing of the metal around these screws at the thinner bottom liner tray.

Figure 3-19 Load-deflection curves for rigid composite panel of 80mm thickness

3.5.2 Concluding remarks

Calculated shear capacities and flexibilities of 2-side fixed roof panels are presented in Table 3-4. The design shear capacities of each diaphragm (V*) were taken as the seam capacities (V_s). In the calculated method, the seam capacity is the same for shear panels with and without shear connectors and this value was found to be always lower than the ultimate test loads.

In the case of panels, in which the shear resistances of individual fasteners were established by the use of the analytical equation Toma et al. (1993)(model "Anl."), predicted shear capacities of panels were on average 35% lower than ultimate test loads (see Table 3-4). As expected, the safety margin was reduced to the average 7% when upper bound experimental values of fastener shear resistance (model "Max. Exp.") were used in the calculations. This model gave results closest to the values obtained in the full-scale panel tests. The greatest level of conservatism was obtained when the shear resistances of individual fasteners were reduced to the characteristic values (model "Char. Exp.") and this method offered 75% lower resistance then those obtained from the tests.

All investigated panels without shear connectors showed between 37% and 28% lower shear flexibility than from the calculated method, regardless of the slip models of individual fasteners. The shear flexibility of a panel without shear connectors relies largely on purlin/rafter connection flexibility (s_{pr}), which was established through a component test (see APPENDIX E).

When a comparison of deformed shapes of top-hat purlin was made between component test (see Figure 3-20a) and the full-scale test (see Figure 3-20b), differences in behaviour were observed. In the full-scale test, the rotation of the purlin top flange was restrained by the cladding profile resulting in compression of one of the legs. It can be expected that in such a case, the shear flexibility may be significantly reduced compared with that obtained by the component test. The purlin/rafter connection flexibility (s_{pr}) obtained in the component test, when reduced by half and used in calculations, gave good match with the full-scale test results. The

highlighted difference in the behaviour of the purlin/rafter connection flexibility with sheeting attached should be investigated in future by more complex analysis methods such as Finite Element Analysis (FEA). As shown in APPENDIX F the component test flexibility (s_{pr}) was used in calculations and affected the accuracy of the stiffness prediction (see Figure 3-17, Figure 3-18, Figure 3-19). In all cases, the shear stiffness of tested panels were under-estimated.

a)   Component test   b)   Full-scale roof panel test
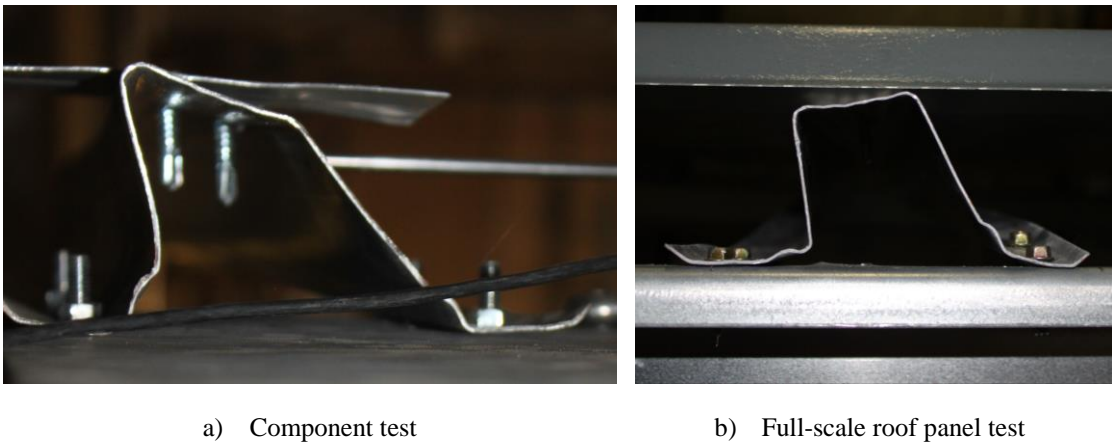
Figure 3-20 Differences in shear deformation of top-hat purlin

By comparing the test shear flexibilities of the same panels with and without shear connectors (see Table 3-5), it can be established that shear connectors increase the stiffness by a factor of two.

Similar to the tests with shear connectors, sinusoidal sheeting profiles fixed in the crests (test T17 and T18) require more research before they could be used in stressed skin action design. It was demonstrated that such panels are still capable of transferring significant load between the frames although this load is often neglected in 2D portal frame analysis. In Figure 3-13d, it was demonstrated that the industry standard for number of fixings used to fix corrugated profiles may not be sufficient as they are usually designed to resist the wind uplift only. By fixing sinusoidal panels in every second crest rather than every third crest, shear breaking of fasteners was prevented.

Table 3-4 Comparison of the analytical versus experimental shear capacities and shear flexibilities of tested panels

Test designation	Model	V^*	c	V_T	c_T	V_T/V^*	c_T/c
		kN	mm/kN	kN	mm/kN		
T11 AS34/0.5	Anl.	14.88	0.95	18.02	0.54	1.21	0.57
T12 AS34/0.7	Max. Exp.	27.74	0.73	28.17	0.56	1.02	0.76
	Char. Exp.	16.88	0.78	28.17	0.56	1.67	0.72
	Anl.	19.38	0.77	28.17	0.56	1.45	0.73
T13 AS30/0.5	Anl.	13.95	1.03	16.80	0.59	1.20	0.57
T14 AS30/0.7	Max. Exp.	26.07	0.78	28.23	0.53	1.08	0.68
	Char. Exp.	15.91	0.82	28.23	0.53	1.77	0.64
	Anl.	18.40	0.81	28.23	0.53	1.53	0.65
T15 AS24/0.5	Anl.	14.88	0.87	16.19	0.52	1.09	0.60
T16 AS24/0.7	Max. Exp.	27.74	0.70	30.49	0.50	1.10	0.72
	Char. Exp.	16.88	0.74	30.49	0.50	1.81	0.68
	Anl.	19.38	0.73	30.49	0.50	1.57	0.69
T17 AS18/0.5	Anl.	13.65	1.34	19.15	1.05	1.40	0.78
T18 AS18/0.7	Anl.	17.17	1.14	29.05	0.61	1.69	0.53
T19 AS35/80 top	Anl.	15.73	1.12	15.99	0.59	1.02	0.53
Average	Anl.					1.35	0.63
	Max. Exp.					1.07	0.72
	Char. Exp.					1.75	0.68

The ability of typical composite panel (test T19) to transfer shear force between frames was much greater than predicted analytically for just the top skin. As shown in Figure 3-19, the roof panel became unserviceable at a shear deflection of approximately

20mm. Unlike shear resistance when using the lower value will offer safe design, in terms of shear flexibility, upper and lower bound flexibilities should be considered. When a higher cladding flexibility is used in 3D analysis, the level of shear loading acting on the roof panel and gable frame will be under-predicted.

Table 3-5   Comparison of the measured shear flexibilities of full-scale panels with and without shear connectors

Test designation	Shear connectors	$c_{T,sc}$ mm/kN	$c_{T,sc}/c_{T,nsc}$	$c_{T,nsc}$ mm/kN	Shear connectors	Test designation
T1 AS34/0.5	Yes	0.27	0.50	0.54	No	T11 AS34/0.5
T5 AS24/0.5	Yes	0.34	0.58	0.59	No	T15 AS24/0.5
Avr.			0.54			
T2 AS34/0.7	Yes	0.29	0.52	0.56	No	T12 AS34/0.7
T6 AS24/0.7	Yes	0.30	0.56	0.50	No	T16 AS24/0.7
Avr.			0.54			

4 RESULTS OF FULL-SCALE FRAME TESTS

4.1 Literature review

The behaviour of pitched, bare portal frames using hot-rolled steel sections is well understood. Two well established analysis methods have been used to design such type of structure:

1) Plastic analysis – frames engineered from relatively thick sections class 1 which are capable of developing plastic hinges so that the bending moments can be redistributed;

2) Elastic analysis – frames engineered from compact sections which do not have ability to develop plastic hinges of sufficient rotational capacity or sections which can be subject to buckling failure.

The research on stressed skin action started at the University of Manchester in late 1960's proved that clad portal frames behave much differently from bare frames due to the stiffening effect of the cladding diaphragm (Bates et al. (1965)), Bryan and Mohsin (1972), Bryan (1973). The main motivation for this research was that, due to the introduction of higher grades of steel, portal frames had become more flexible. Depending on the ratio of the frame to cladding stiffness, the load is redistributed between adjacent frames and in some design cases the failure can occur in the cladding first, rather than in the frame itself.

The shear resistance and stiffness of roof panels was reviewed and investigated experimentally in Chapter 3. The method of including the inherent resistance of the cladding into a frame design was first introduced by Davies (1972) and was called stressed skin analysis. The principles of stressed skin analysis are outlined in Figure 4-1 and Figure 4-2. In this method, a clad 3D structure can be reduced to a two dimensional system of coinciding plane frames coupled through linear springs representing the shear stiffness of the cladding and roofing.

In the early days, Davies (1972) focused on developing a computational method which can be used to design sheeted buildings having complex geometry using limited computational systems. The complexity of the calculations as well as lack of appropriate software was a primary reason why the stressed skin design method, although widely acknowledged, was never widely applied in steel frame design.

a) Stressed skin action in flat roof building

b) Stressed skin action in a pitch roof building
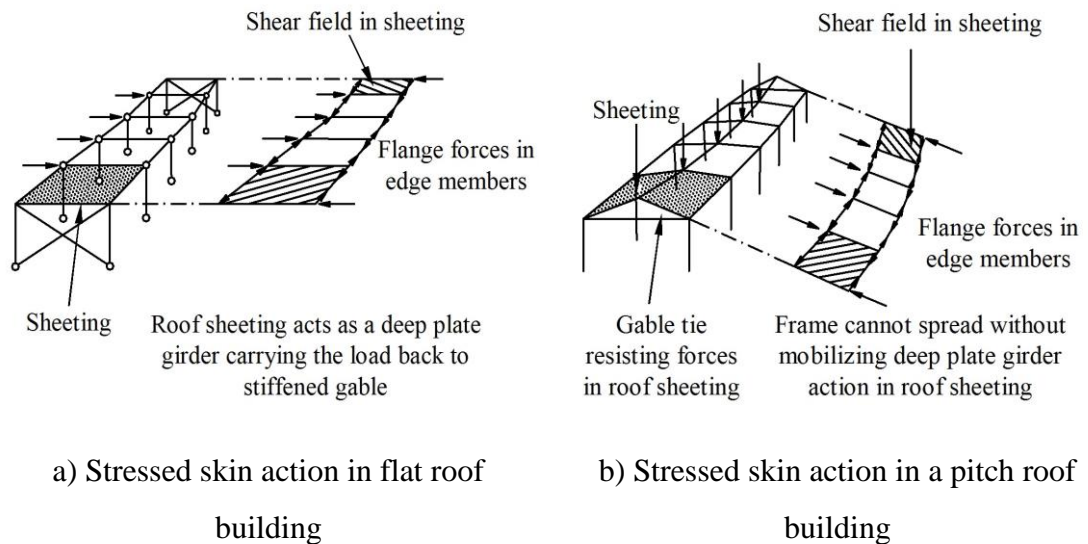
Figure 4-1 Stressed skin action in clad buildings BS 5950-9 (1994a), pp.14

a) Flat roof frame with sheeted gables   b) Pitched roof frame with braced gables
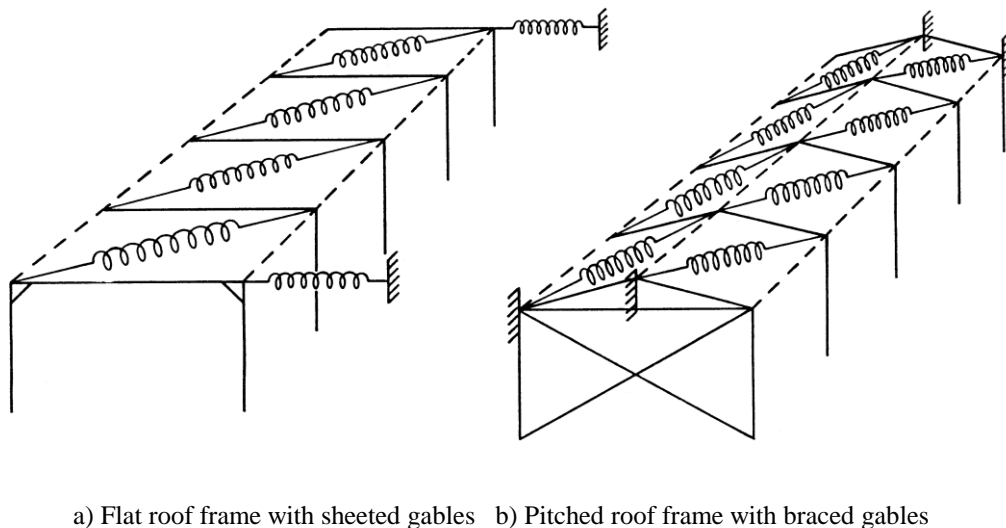
Figure 4-2 Computational models simulating behaviour of sheeted building after BS 5950-9 (1994a), pp.49

106

3D structural analysis has now become a standard tool for designing complex structures as it gives a more accurate representation of the structural behaviour. However, portal frame structures are still predominantly modelled as 2D bare frames in which interaction between the frames is ignored.

Cold-formed steel portal frames have more flexible joints (Zadanfarrokh and Bryan (1992)) and also use relatively stiffer top-hat purlins, which means that greater shear load is transferred between frames and it can lead to roof or gable frame failure at serviceability loads (see Phan et al. (2015) and Wrzesien et al. (2015)).

In his paper Hairsine (2010) presents a few examples of how standard 3D frame analysis software could be used for designing portal frames and compares the results against classic 2D design output. The contribution of the stressed skin effect was however neglected in the analysis. The only significant difference between the 3D and 2D analysis, which was considered unsafe, was the development of extra axial forces in the longitudinal eaves members and roof bracing between gable and penultimate frame which otherwise would be ignored by many designers. The roofing panels can be idealised as a diagonal bracing member and thus can be easily modelled in a 3D analysis. Although in the classic design approach roof bracing is only designed to resist the wind load from the gable, it is also carrying the forces due to relative displacement between frames under the gravity load case. These extra forces have caught the author's attention and they were quantified by 3D analysis. The importance of these extra forces has been questioned due to the flexibility of the joints and the successful history of traditional design practice. In Figure 3-13b, however test data was presented, which showed that the cladding panel in shear can develop axial force in the edge member sufficient to cause buckling failure. In fact, the existing design code BS 5950-9 (1994a) for stressed skin design suggests that the panel edge members/eaves beams should be designed to resist the vertical load plus 1.25 times the axial loads from the diaphragm action. The classical 2D design approach would not consider this requirement unless the stressed skin design procedure was implemented.

These effects will therefore be investigated in this chapter in order to establish if the stressed skin effect may always be conservatively ignored without underestimating loads carried by other parts of the structure.

A review of full-scale portal frame tests reported in the literature is presented in Table 4-1. As can be seen, the research is quite dated and focuses mainly on hot-rolled steel portal frames with sufficiently rigid joints.

4.1.1 Bates et al

A hot-rolled steel portal frame buildings of large span of 46m was tested under gravity load by Bates et al. (1965) (see Table 4-1). A series of non-destructive tests were carried out at the construction site before frame operational use, by use of ballast weights suspended from the apex. This full scale investigation showed that stressed skin action can reduce the vertical deflection of the apex (in the central frame) by as much as 50% as compared with the apex deflection of the bare frame.

The test data was based on a comparison between tests on the bare and on the sheeted structures and was one of the first attempts to validate the stressed skin concept. These tests motivated other researchers to investigate this phenomenon and develop analytical methods of predicting shear strength and stiffness of cladding panels of typical construction and size.

4.1.2 Bryan and Mohsin

Since the first experimental study reported by Bates et al. (1965), significant progress in developing analytical methods for predicting stressed skin behaviour was made and a full-scale test was designed to validate the analytical method by Bryan and Mohsin (1972). The main frame was designed to include stressed skin action and due to its effect a 25% lighter design was produced as compared with traditional 2D frame design. Generally the analytical prediction followed closely the experimental response in the elastic range of the roof panel stiffness.

Table 4-1 Full-scale tests on sheeted buildings

Author	Frame						Main members	Joints		Stressed skin			Load case
	Type	Span	Height	Pitch	No. of bays	Spacing	Section type	Eaves/apex	Base	Sheeting	Shear panel tests	Gable bracing	
		m	m	°		m							
Bates et al. (1965)	PRS	45.72	5.48	12.1	10	10.21	Universal Beam	Rigid	Partial fixed	Roof only	Yes	No	Gravity
Bryan and Mohsin (1972)	PRS	12.00	3.40	13.1	5	6.00	Rectangular Hollow Section	Rigid	Pinned	Roof only	No	Yes	Gravity
Davies (1973)	PRS	4.88	2.44	30	6	2.44	Square Hollow Section	Rigid	Pinned	Roof only	Yes	Yes	Gravity
	FR	6.85	3.05	0	4	4.57	Universal Beam	Rigid	Pinned	Roof and gables	No	No	Horizontal
	FR	6.85	3.05	0	4	4.57	Universal Beam	Rigid	Pinned	Roof only	No	Yes	Horizontal
Strnad and Pirner (1978)	PRS	12	-	-	5	6	2 channels welded to form a box section	Pinned	-	Roof , walls and gables	Yes	No	Horizontal
Davies et al. (1990)	PRS	12	4	-	2	-	Universal Beam /Reinforced Steel Joist	Rigid	Pinned	Spread stiffness of the gable close to 0 to avoid stressed skin action			Gravity

Table 4-1 Continued

Author	Frame						Main members	Joints		Stressed skin			Load case
	Type	Span	Height	Pitch	No. of bays	Spacing	Section type	Eaves/ apex	Base	Sheeting	Shear panel tests	Gable bracing	
		m	m	°		m							
Robertson (1991)	PRS	12	4	10	6	4	Swagebeam	Rigid	Pinned Semi-rigid 'Fixed'	Stressed skin action not investigated			Gravity Horizontal
Heldt and Mahendran (1998) Mahendran and Moor (1999)	PRS	12	4.2	5	4	6	Hollow flange beam	Rigid	Pinned	Roof and side walls	Yes	Yes	Longitudinal wind, Gravity, Cross-wind
Darcy and Mohendran (2008)	PRS	5.4	2.3	10	1	5.4	Frameless	-	-	Roof , side walls and gables	No	No	Cross-wind
Wrzesien et al. (2012b)	PRS	6	3	10	1	3	Back-to-back cold-formed lipped channel	Semi-rigid	Pinned	Roof	Yes	Yes	Gravity Horizontal

The correlation started to diverge when the cladding panel reached its failure point and its stiffness became non-linear. The analytical method predicted a 15% lower failure load than that obtained in the test and a straight comparison of the experimental collapse loads of the bare and the clad frame showed a 28% increase in load carrying capacity due to stressed skin action.

4.1.3   Davies

Experiments on a 4.88m span hot-rolled steel, duo-pitch portal frame with rigid joints and pinned bases (Davies (1973)) showed the following:

- First yield at the sheeting panel was recorded at 71% of the bare frame collapse load;
- The first plastic hinge formed in the central frame at 103% of the bare frame collapse load
- The highest load measured during the clad frame test was 132% of the bare frame collapse load.

The investigated frame was subject to gravity load and had a relatively steep roof of 30 degrees for which it was expected that stressed skin action would have a notable effect. The tests showed that the ultimate collapse load of the clad frame was 32% higher than the bare frame collapse load and that stressed skin design in combination with plastic design of portal frames can be safely used.

Stressed skin action in flat roof portal frames under horizontal load was investigated in a series of tests. In the first test the gable was not braced to allow the gable cladding to act as a shear diaphragm. Typical cladding construction was used consisting steel sheeting and a combination of self-drilling self-tapping screws and aluminium pop rivets. In this test the importance of the stressed skin action was highlighted. The test was terminated at 77% of the theoretical collapse load of the bare frame due to insufficient deformation capacity of the roof cladding. The aluminium pop rivets sheared causing rapid deterioration in strength and stiffness of the structure and severe damage to the cladding panel.

In the second test on the same frame, this mode of failure was avoided by redesigning the roof panel to increase its shear strength and stiffness. The following results were recorded:

- First yield in the sheeting was observed at 71% of the bare frame collapse load
- The first plastic hinge formed in the central frame at 148% of the bare frame collapse load
- The highest load measured during the clad frame test was 166% of the bare frame collapse load.

4.1.4   Strnad and Pirner

The authors investigated the response of a light portal frame under static and dynamic loading by a number of non-destructive tests on the bare frame building with purlins and side rails and on a fully sheeted building (see Table 4-1). Dynamic shear tests on four panels were also conducted in order to investigate the resistance of the building envelope and fixings to fatigue failure under repeated loads. From the plot of horizontal load versus eaves deflection, it was shown that stressed skin action can reduce the horizontal deflection of the central frame by a factor of nearly 20 as compared with the horizontal deflection of a bare frame. The tested frames had a unique construction with pinned jointed eaves and eaves tie bracing; but it was not clear what arrangement was used at the column base connection. The general conclusions were that the dynamic effects of the wind load do not need to be taken into account in the case of the tested frame. The building envelope is capable of sustaining the cyclic wind loading with neither strength nor stiffness degradation.

4.1.5   Robertson

The effect of partial rigidity of the base connection on the behaviour of the Swagebeam portal frame was investigated by Robertson (1991) (see Table 4-1). The test data showed that when modelling partial stiffness of the base as a rotational spring, the base bending moment as a percentage value of the analytical fixed base

moment can depend on the load case. The partial base fixity has a greater effect on the bending moment redistribution under the horizontal load, therefore test data is needed in order to interpret the results from the full-scale tests. In this paper, plans for future tests on cold-formed steel portal frames with cladding are also mentioned; but the reports on such tests were not found.

4.1.6   Mahendran et al.

This research on full-scale portal frames focused on investigating the capacity of bare frame and sheeted building under wind uplift load (see Table 4-1). A complex loading system was developed in order to simulate 'patch wind loading' as a point load applied to the purlin/side rails in the case of bare frames and to the cladding in the case of sheeted frame. A series of non-destructive tests were conducted on the same bare framework under different wind and gravity loads with and without cladding. The novel aspect of this study was the use of a building envelope in which the cladding is crest-fixed to follow the industry practice in Australia. As shown in Sections 3.4.3 and 3.5.1 of Chapter 3, such connections would decrease the shear strength and stiffness of the cladding panel and were not included in the design rules of BS 5950-9 (1994a). In Figure 3-13d of Chapter 3, the shear tests on the crest-fixed panels were reported where undesirable brittle failure of the sheeting screws was observed. The full-scale tests were complemented by full-scale shear panel tests. General conclusions from the test confirmed the theory of stressed skin action as published by Davies and Bryan (1982). Diaphragm action had little effect in load cases inducing eaves spread, such as gravity or longitudinal load cases, but had a large effect on the sway load cases, such as the transverse wind load, even when a flexible roof construction was used. When comparing the test results from bare frame and clad building tests under the transverse wind load case, a 72% reduction in the windward eaves deflection and a 33% reduction in bending moment were recorded.

4.1.7 Darcy and Mohendran

In the Darcy and Mohendran (2008) paper, a novel 'frameless' steel building was investigated. It was constructed entirely from deep corrugated sheeting profiles of 0.42mm thickness rolled from high tensile steel of 550 Grade. The sheeting profiles were overlapped at each rib forming the equivalent of a frame member and were jointed at the eaves and the apex by matching brackets prefabricated to the required roof pitch as shown in Figure 4-3. Similar brackets were used for the base connections and were buried in the concrete slab. An interesting observation was made that the 'frameless' structure showed very similar behaviour in terms of resistance to bending moments as compared with that of a conventional frame structure. The bending moments calculated from the strain gauges matched closely the bending moment calculated based on the simple bending theory, rib cross-section geometry and twice the cladding thickness. Significant diaphragm action was also observed. In the destructive test, non-linear behaviour of the structure was first recorded at 50% of the design load due to local buckling of the cladding panels. The apex deflection in the transverse wind load case reached a ratio of span/80, which is 3 times higher than the recommended span/250. The horizontal eaves deflection however was acceptable reaching the ratio of height/250 due to the beneficial effect of the stressed skin action. The general conclusion was that the structure can only resist 40% of the required ultimate design transverse wind load (wind speed 21 m/s).

a) Full-scale structure

114
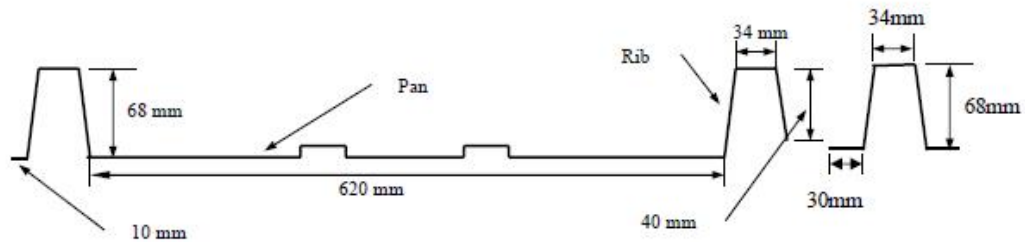
b) Geometry of the cladding profile and matching bracket

Figure 4-3 'Frameless' cold-formed steel portal frame after Darcy and Mohendran (2008) pp.663

4.2 Justification for tests on clad portal frames

As summarised in Table 4-1, stressed skin design was originally investigated for traditional hot-rolled steel portal frames with 'rigid' joints. In the UK, buildings with spans of up to 20 m and composed entirely of cold-formed steel (see Figure 4-4), can be a viable alternative to conventional hot-rolled steel portal frames. In such light-weight steel portal frames, channel-sections are used for the column and rafter members, and top-hat sections may be used for the purlins and side rails. Top-hat sections are considered to be more efficient than zed-purlins for cold-formed steel portal frames where the frame spacings (or purlin spans) are in the range of 3 m to 4.5 m, compared with 6 m for conventional hot-rolled steel frames. They are also much stiffer than zed-purlins in terms of transferring shear load to the roofing as shown in Chapter 3.

For the case of cold-formed steel portal frames that have more flexible joints and use stiffer top-hat purlins, not including the effects of stressed skin action may lead to roof failure at serviceability load, for example by tearing of the fixings and hence water leakage into the building. To the author's knowledge, full-scale tests on cold-formed steel portal frames with semi-rigid bolted moment connections and the inclusion of stressed skin effects have not previously been reported. Due to the growing popularity of such framing system, there is great need to thoroughly investigate the effects of the stressed skin action.

Figure 4-4 Typical cold-formed steel portal framing system (curtesy of Capital Steel Buildings)

Furthermore, for cold-formed steel portal frames, designers often refer to guidance for equivalent hot-rolled steel frames (SCI P397 (2012)) in terms of deflection limits of bare frames, but these are discretionary. As a result, designers sometimes relax these deflection limits to achieve a more economical design under the assumption that the roof panel will reduce the deflections, possibly by as much as 50% as stated in the   guide. However, relaxing deflection limits and reducing the stiffness of the internal frames in a 2D design, can result in an underestimation of the forces in the roofing and hence in the gable end-frames. Figure 4-5 shows the consequences of diaphragm action loads on the gable rafter. Such loads would be ignored in bare frame analysis. This is even more important when the joint rotation adds to frame flexibility.

Welding of galvanized steel is not recommended, and so mechanical fasteners are the only means of connecting the members. Joint rotation in cold-formed steel portal frames is associated with the bearing of the mechanical fasteners acting in shear on relatively thin steel plates (see Chapter 9).

a) Buckling of the edge purlin   b) Failure of purlin connection and deformation
of the gable-frame rafter

Figure 4-5 Failure of purlin connection and deformation of the gable-frame rafter

In this chapter, the results of six full-scale tests on cold-formed steel portal frames are presented. The joints are formed using brackets that are bolted between the webs of the cold-formed steel channel-sections. Two different bolt-group sizes are considered for the joints, with each bolt-group size (and therefore bracket size) having a different rotational stiffness. Firstly, tests on frames without roof sheeting are described. Vertical loading was applied in one set of tests, and horizontal loading was applied in another set. Secondly, for the case of horizontal loading only, the frame tests were repeated with roof sheeting to determine the effect of stressed skin action. For both the roof panels and the joints, small-scale tests are described separately in Sections 3.4, 3.5 and Section 2.5.

The full-scale tests were designed to validate the assumption that the component pure bending tests results can be used to model the behaviour of full-scale structures and also to investigate the difference in the behaviour of the members under 'true' combined states of loading. The geometry of the frame along with other novel structural features are all summarised in the Table 4-1.

4.3   Testing methodology

The full-scale portal frame tests were carried out in the Strathclyde University Heavy Structures Laboratory. The frames used in all buildings have a span

of 6 m, height of 3 m, and pitch of 10˚ and the column bases are pinned, as shown in Figure 4-6. The results of the clad frame tests are intended to represent the behaviour of building of 9m overall length, having two braced gable frames and internal frames, with a frame spacing of 3 m between the frames.

Due to symmetry and also due to laboratory space limitations, only one gable frame and one internal frame were used for each clad frame test. The span and the bay size were intentionally kept similar to the dimensions of the shear panels investigated in Chapter 3 so the test shear strength and stiffness could be easily implemented into the model of the clad structure. For this reason, the construction of the roof was kept the same in the full-scale tests as in shear panel tests.

The schematic views presenting the full-scale test set-up for both vertical and the horizontal load case are presented in Figure 4-7. As shown, the test set-up has a front test frame (internal frame) and a back reaction frame restrained in-plane and out-of-plane (gable frame). Detail drawings of the test frames and the back frames are presented in APPENDIX G. The out-of-plane restraints to the gable frame were provided through a set of ties. The reaction force in each tie was measured through S-type strain gauge load cells.

Linear displacement transducers (LVDTs) were used at positions around the frame according to Figure 4-7. The sensors were connected to the common data logger saving live data every second during the experiment. The load was applied through a number of hand-operated hydraulic jacks in approximately 0.5kN load increments. Each jack was equipped with a strain gauge load cell. After the loads in all jacks had been levelled the load remained constant for approximately one minute then the data was saved. Only the data saved after each load increment is presented.

The test frames were subject to the self-weight loading of the structure plus the test rig components which can be considered as bedding down load. In this work only failure tests were conducted in order to follow joint testing procedure.

The columns were erected first with the eaves brackets attached to them. The bolts were lightly tightened by hand to ensure that low torque was applied to the connection as in the pure bending joint tests. The verticality of the column in both

directions was checked by digital inclinometer of $\pm 0.1°$ accuracy. Then the side rails were fixed by four self-drilling, self-taping screws on each side of the frame. Thereafter the rafter assembled on the ground using the same procedure for tightening bolts, was hoisted into position. The final set of bolts connecting rafter members with the eaves brackets were put in place.

The gable frame served as a reaction frame and remained unchanged throughout the experimental investigations although, depending on the loading case, different bracing systems were introduced (see Figure 4-7).

The out-of-plane stiffness of the gable frame was provided by a set of tension only members composed of M24 threaded rods and turn-buckles fixed either to the strong floor or to the existing rigid steel frame. The side walls and gable frame were not clad in order to follow the load paths and simplify the analysis of the results. Previous research by the Davies (1972) suggested that a clad gable can be idealised as a rigid body both in and out-of-plane. This assumption can be valid in terms of hot-rolled steel frames but the out-of-plane strength and stiffness of a cold-formed steel frame is much less. For this reason, the gable frame apex was restrained in order to prevent out-of-plane buckling failure of the rafter should there be any out-of-plane load acting at the apex. Such load could cause an uncontrolled and dramatic collapse and had to be prevented but it did not occur in the test.

Purlins and side rails were installed in order to provide discrete lateral-torsional restraints to column and rafters. Each purlin/rail was fixed with 4 self-drilling self-tapping screws apart from the tests on bare frames subject to horizontal load case where only one screw was used on the roof to create a pin connection. It was observed in the initial tests that the 4 screw purlin connection carried significant in-plane bending as load transfer between internal and gable frame was measured by load cells R_{6A} and R_{6B} (see Figure 5-4b). By using pinned connections no load transfer between frames was detected therefore behaviour closer to the bare frame analysis model was simulated.

a) Bare frame (vertical load)

b) Clad frame (horizontal load)

Figure 4-6 Front view of the full-scale test frame
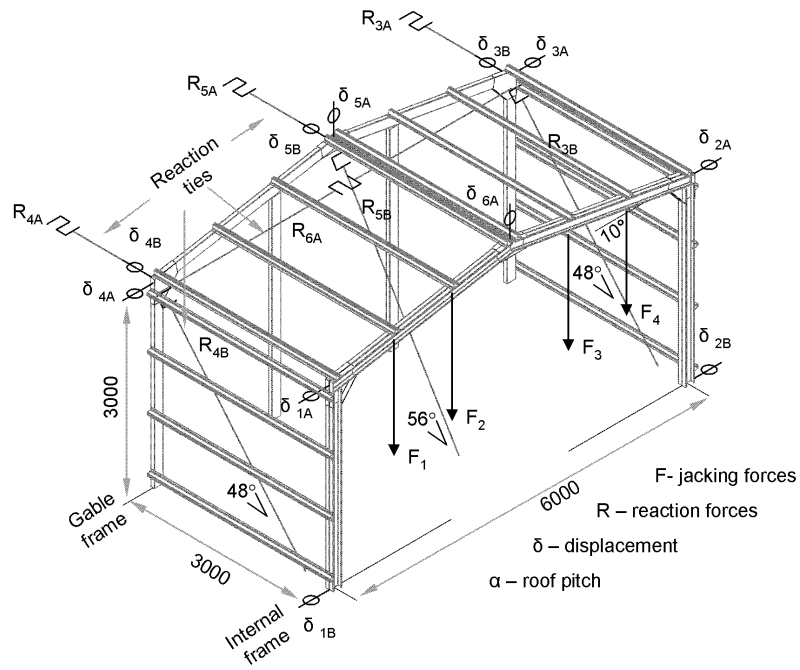
a) Vertical load
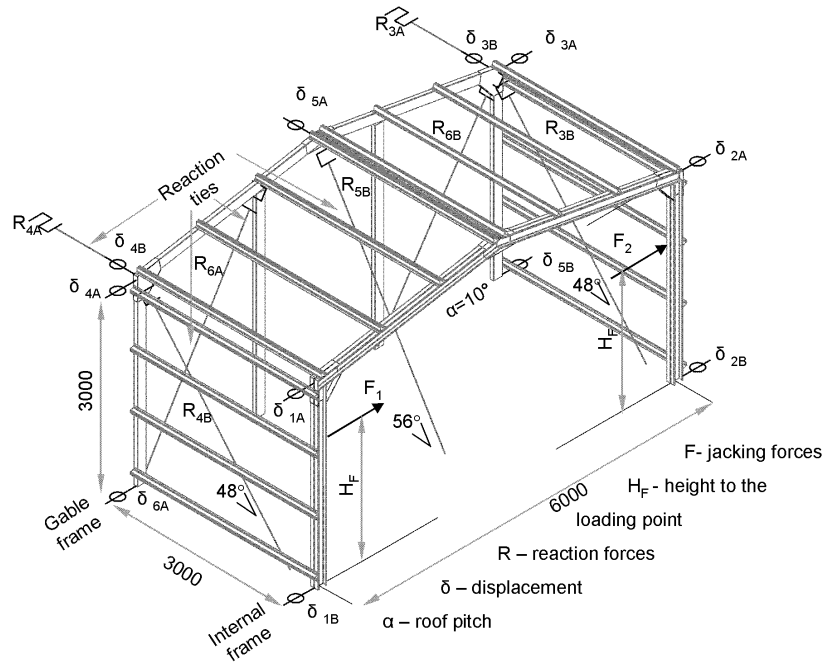
HF=2500 mm and 2400 mm for Frame A and Frame B respectively

b) Horizontal load

Figure 4-7 General arrangement of the full-scale test structure

For both load cases the load was applied through the column/rafter members by means of flat plates passed between channel sections and bolted through the webs. There was no case where the load was applied through eves/apex bracket, so the 'true' load paths were simulated and the brackets had ability to move freely.

Two load cases were considered in the full-scale tests:

a) Vertical load case (see Figure 4-7a)

b) Horizontal load case (see Figure 4-7b)

It should be noted that previous research reported by Bates et al. (1965) and Bryan and Mohsin (1972) shown that stressed skin action can offer saving in the case of vertical loads for steeper and deeper roof diaphragms. In this study a typical roof pitch of 10 degrees was chosen, which minimised the stressed skin effect under vertical loading. The stressed skin analysis also showed that for the investigated frame stressed skin action should have very little effect in the vertical load case; therefore only tests on bare frame were carried out.

4.4   Full-scale test programme

A total of six frames was tested and their test characteristics are summarised in Table 4-2. Frames 1 to 3 used a bolt-group arrangement of 160 mm x 80 mm for the eaves and apex joints, which are referred to as Joints A. Figure 4-8a shows details of Joints A and the size of the brackets suit this bolt-group size. Fully threaded M16 bolts were used in 18 mm diameter bolt-holes. Similarly, Frames 4 to 6 used a bolt-group size of 280 mm x 80 mm for the joints (see Figure 4-8b).The eaves and apex joints of these buildings are referred to as Joints B.

For each frame with Joints A and B, one test was conducted in respect to vertical loading and two tests with horizontal loading. For vertical loaded frames, all tests were conducted without sheeting, as the effect of stressed skin action for this case was calculated to be insignificant. For the case of horizontal loading, one test was conducted with sheeting and one without sheeting.

Table 4-2 Summary of full-scale frame tests

Frame	Eaves/Apex Joint	Bolt-group length x width (mm)	Load case	Sheeting type
1			Vertical	No
2	A	160 x 80	Horizontal	No
3			Horizontal	Yes (AS30/0.7)
4			Vertical	No
5	B	280 x 80	Horizontal	No
6			Horizontal	Yes (AS30/0.7)
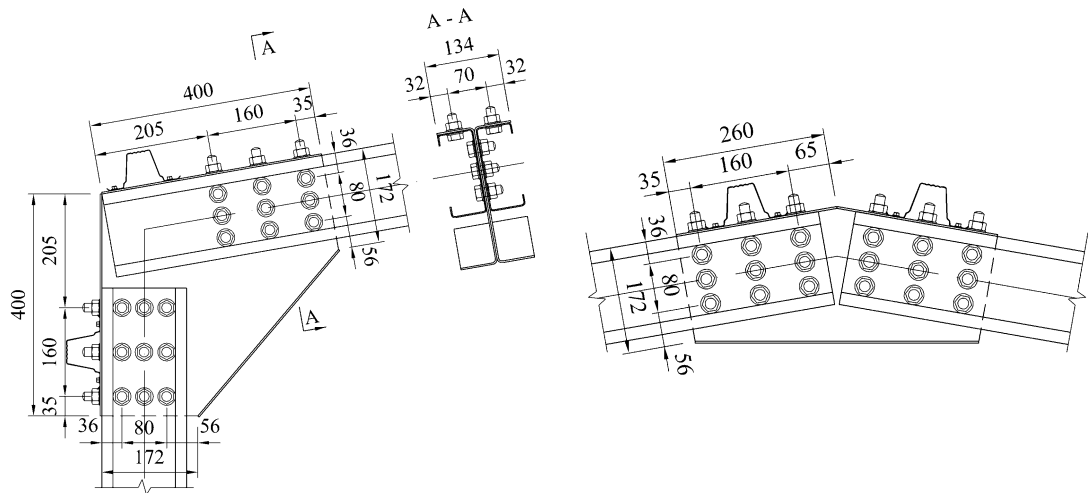
a) Joints A
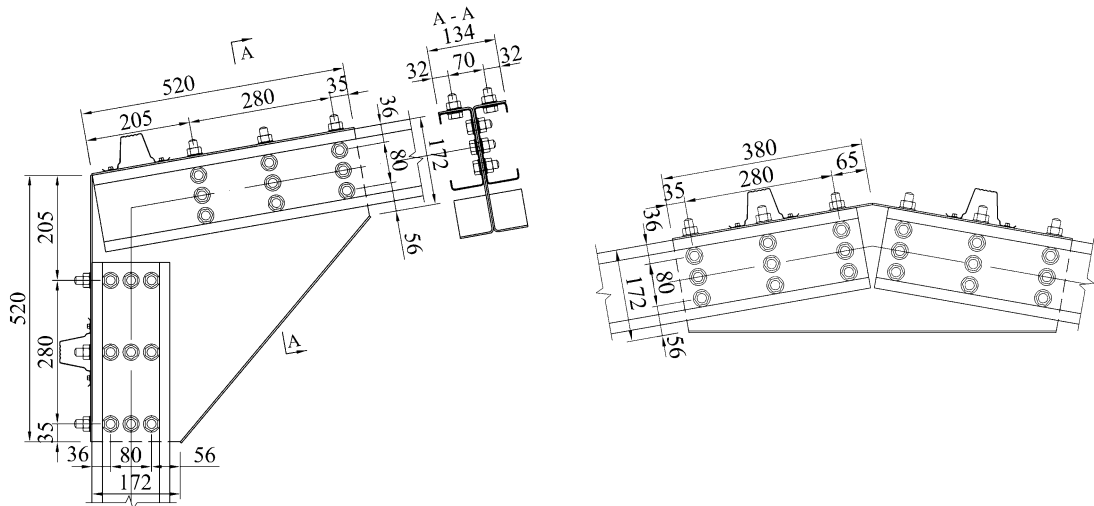
b) Joints B

Figure 4-8 Details of eaves and apex joins

Figure 4-9a shows the nominal dimensions of the channel-sections used for the frames in all six buildings. In the internal frames, the channel-sections were placed back-to-back; in the gable frames (including the gable posts) single channel-sections were used. Figure 4-9b shows the nominal dimensions of the single skin roof sheeting. The roof profile has a depth of 30 mm and a nominal thickness of 0.7 mm. Figure 4-9c shows the nominal dimensions of the top-hat purlins of 1mm thickness. The description of the components used in the full-scale tests can be found in APPENDIX G. Material specification can be found in relevant parts of Chapter 2 and 3 and measured mechanical properties of steel are presented in Table 4-3.

a) Column/rafter   b) Sheeting profile   c) Purlin
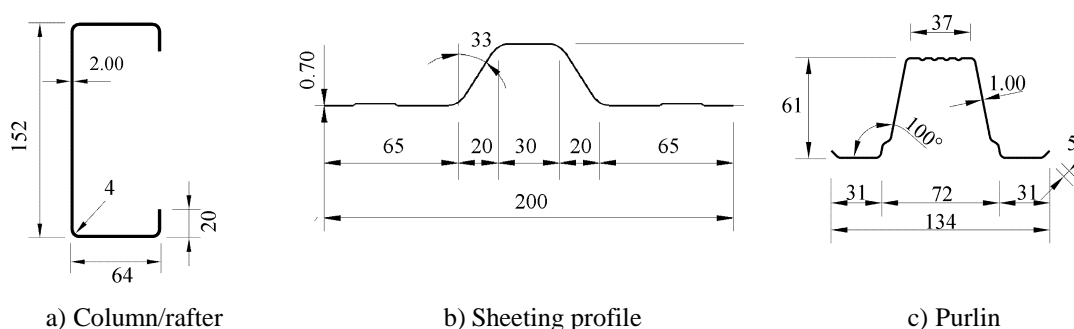
Figure 4-9 Nominal components used for full-scale frame tests

Table 4-3 Steel properties obtained from tensile coupon tests BS EN 10002-1:2001 (2001)

Component	Position	Number of tensile tests	Proof strength	Tensile strength	Non-proportional elongation at maximum stress	Elongation after fracture
			(MPa)	(MPa)	(%)	(%)
Channel section	Flat portion of a flange	3	395	502	15	22
Top-hat purlin	Flat portion of a web	3	590	608	4	5
Sheeting profile	Flat portion of a web	3	301	380	23	44

4.5   Full-scale frame test results

The initial slope of the roof (α_{sw}) and verticality of the columns ($\delta_{6A,sw}$ and $\delta_{2A,sw}$) were measured using a digital inclinometer, and are presented in Table 4-4.

The values of initial sagging of the rafter as well as horizontal displacement of the top of the column under self-weight were calculated based on the difference in angle between perfect and measured geometry. The self-weight of the tested frame along with test rig components is presented in Table 4-4 as the total vertical load ($F_{v,sw}$).

Table 4-4   Initial changes of the geometry under the self-weight

Frame	$F_{v,sw}$	α_{sw}	$\delta_{6A,sw}$	$\delta_{2A,sw}$
	(kN)	(deg)	(mm)	(mm)
1	2.36	9.60	21.0	5.2
2	1.18	9.85	7.9	1.4
3	1.78	9.65	18.3	4.5
4	2.48	10.00	0.0	0.0
5	1.27	10.00	0.0	0.0
6	1.87	9.85	7.9	2.1

The in-plane and out-of-plane interaction forces in clad frames were measured at the eaves level along with respective displacement. Measured values of stiffness (k_j) for each tie restraint are presented as bi-linear springs in Table 4-5.

Table 4-5 Measured stiffness k_j, of bracing members modelled as bi-linear springs

Spring position	Frame 3			Frame 6		
	k_1	D_1	k_2	k_1	D_1	k_2
	kN/mm	mm	kN/mm	kN/mm	mm	kN/mm
δ_{3A}	1.57	3.19	0.69	0.89	5.51	0.66
δ_{4A}	0.64	3.77	0.85	0.96	5.07	0.94
δ_{3B}	1.13	0.84	1.39	0.89	2.37	1.73
δ_{4B}	1.77	1.25	1.93	1.65	2.03	2.00

k_1 – stiffness in the initial phase of loading, D_1 – displacement limiting initial phase of loading, k_2 – stiffness in the second phase of loading

4.5.1 Vertical loads

Figure 4-10 shows the variation of load against apex deflection for the case of vertical loading. As can be seen, the failure load is almost independent of the bolt-group size, as the frame with Joint B failed at a total load of only 4% greater than frame with Joint A. However, in terms of stiffness, the frame with Joints B was approximately 60% stiffer that the frame with Joints A. At the failure load, the eaves joint failed on the column side (see Figure 4-11), with a mode of failure similar to that observed in the joint tests (see Figure 2-36 of Chapter 2).
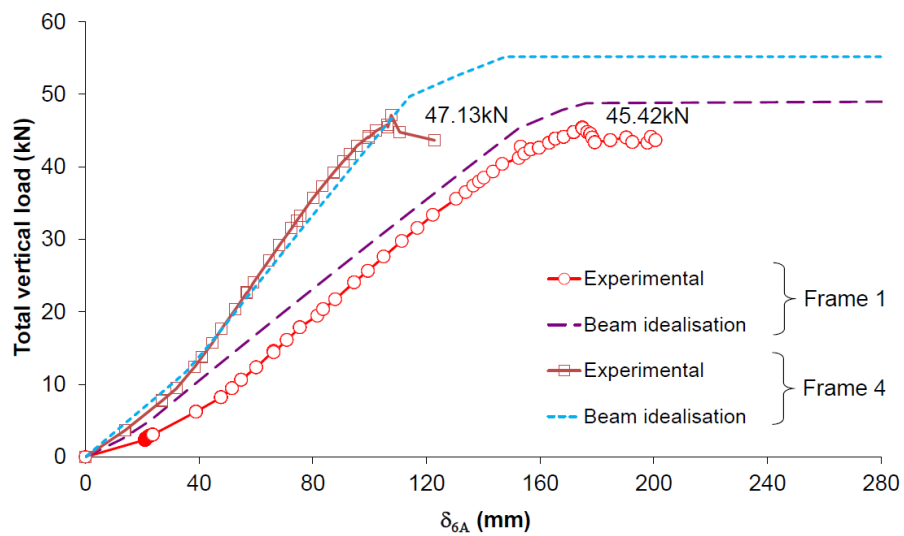
Figure 4-10 Variation of load against apex deflection for frames loaded in vertical direction

| a) Frame 1 (right hand side column) | b) Frame 4 (left hand side column) |
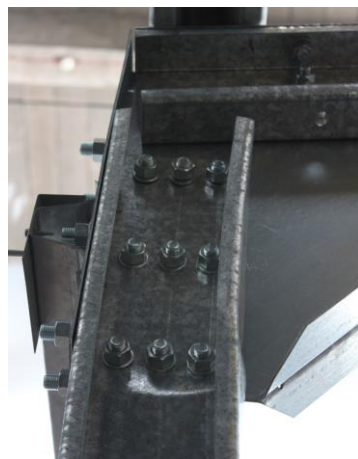
126
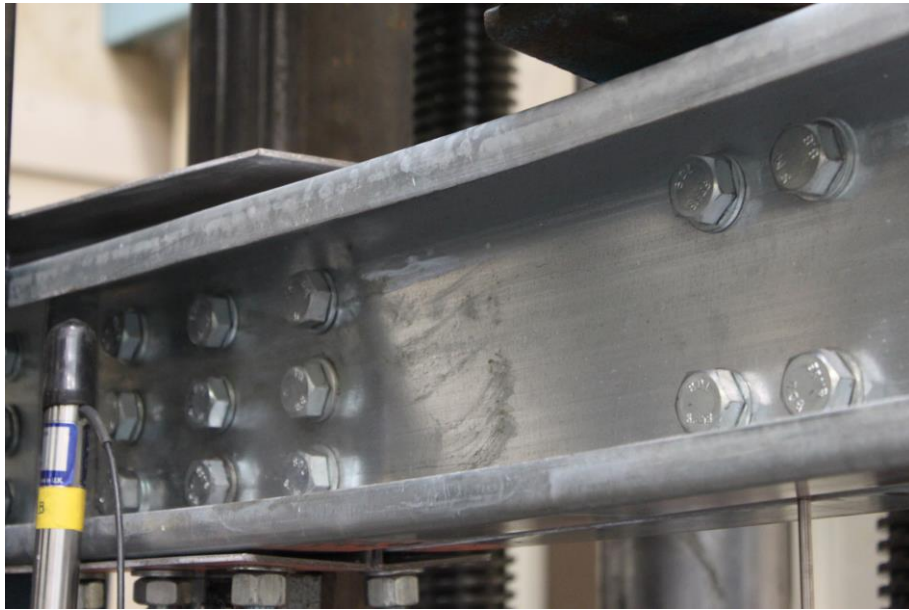
c) Joint test T6/C1/3x3/u (see Section 2.5.7)

Figure 4-11 Modes of failure at the columns versus pure bending test

Buckling of the column occurred in the close vicinity of the connection bracket and the modes of failures were very similar in the shorter (Joint A) and longer (Joint B) bolt-group cases.

4.5.2   Horizontal loads

Figure 4-12a and b show the variation of the total load against horizontal deflection of the bare horizontally loaded frames with Joint A and B. Again there is little difference in the failure load of the bare frames as the building with Joints A failed at a load of 18.0 kN, and the building with Joints B failed at 17.5 kN.

Figure 4-12 also shows the variation of load against horizontal deflection of horizontally loaded frames with roof sheeting. There is again little difference in the failure load of the clad frames; the frame with Joints A failed at a total load of 54.3 kN, while the frame with Joints B failed at 58.8 kN. However, compared with the failure load of the bare frame, the failure load has increased by almost a factor of three. Furthermore, the stiffness of the frame increased by almost a factor of almost

ten. In both tests, failure of the roof panels as well as severe deformations of the purlins and gable rafters were observed (as shown in Figure 4-13).
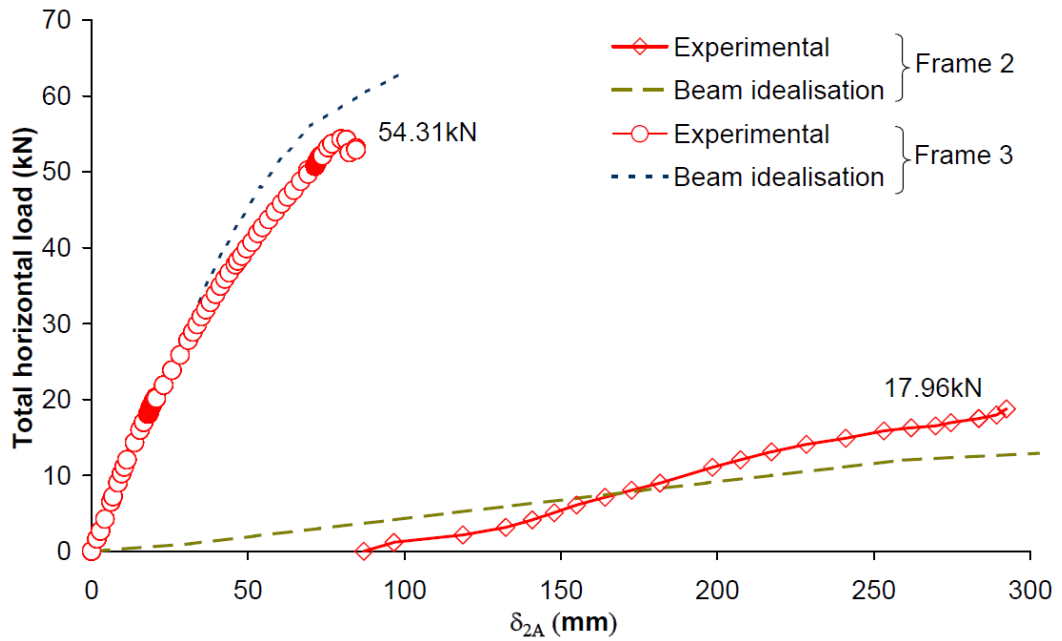
(a) Frames with joints A
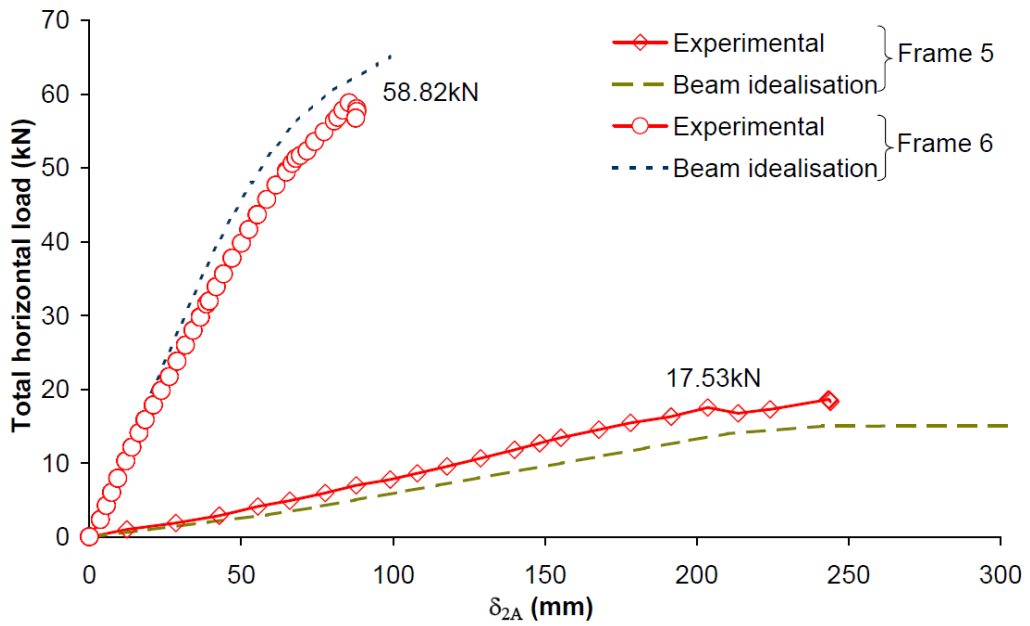
(a) Frames with Joint B

Figure 4-12 Variation of load against horizontal deflection for bare and clad frames

a) Frame 2
b) Frame 3

c) Frame 5
d) Frame 6

Figure 4-13 Modes of failure of bare and clad frames

4.6 Beam idealisation based on joint tests

The elastic frame analysis program Robot Structural Analysis Professional 2010 Autodesk Inc. (2009) was used for the numerical studies. Figure 4-14 shows details of the beam idealization of the full-scale laboratory test. The beam element used had six degrees of freedom per node. For the purposes of graphical plotting, fifteen elements were used for the columns and thirty for the rafters.
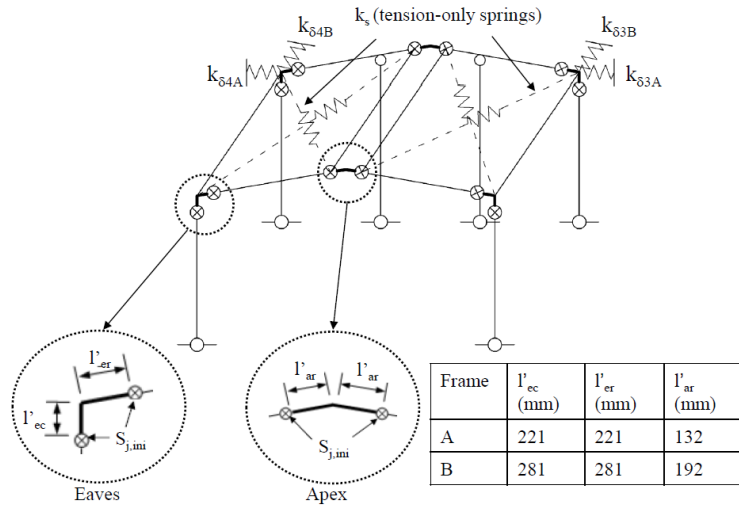
Figure 4-14 Frame idealisation of the full-scale test

In the beam idealization, the rotational stiffness of the joints was modelled using the experimentally determined moment-rotation curve of the joint (see Figure 2-33 for Joint A and Figure 2-35 for Joint B). This was idealised as a bi-linear rotational spring which was placed at the centre of gravity of the bolt-group following an elastic design method. The joint test results used in the beam idealisation are shown in Table 4-6.

Table 4-6 Rotational springs representing the joints

| Spring position | Model | ϕ_{sl} | $S_{j,ini.sl}$ | $S_{j,ini,exp}$ | $M_{j,exp}$ |
	Moment sign	rad	kNm/rad	kNm/rad	kNm
Frame 1, 2 and 3					
Eaves and apex	Positive	0.004	278	596	16.23
Eaves and apex	Negative	0.004	278	596	18.17
Frame 4, 5 and 6					
Eaves and apex	Positive	0.007	547	1229	18.15
Eaves and apex	Negative	0.007	547	1229	20.31

130
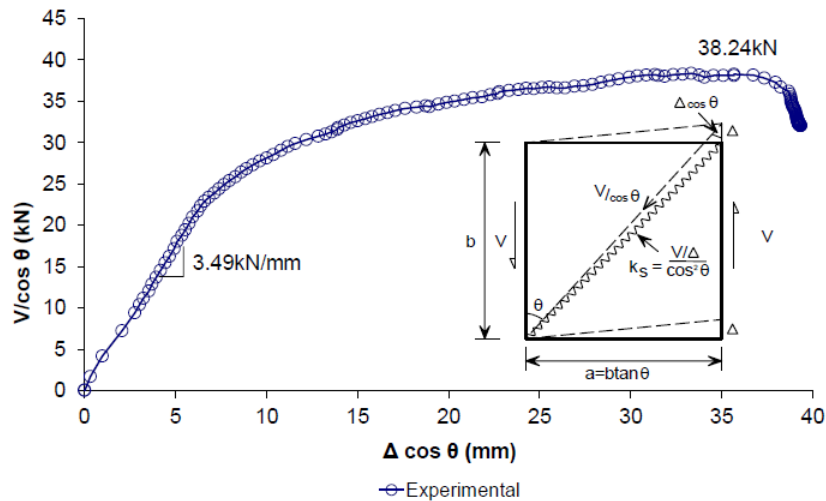
Figure 4-15 Experimental shear stiffness of the roof panel expressed as diagonal spring

The Instantaneous Centre of Rotations of eccentrically loaded bolt-groups Crawford and Kulak (1971) were ignored as they could not be included in the beam idealisation. Stressed skin action was modelled using tension-only bracing members using the experimentally determined load-deflection curve of the roof panel (see Figure 3-18b). The shear flexibility of the panel was converted into equivalent diagonal stiffness (k_s) according to Figure 4-15.

The purlins and side rails were not modelled. The edge beams connecting the gable frame to the internal frames were idealised as having no bending stiffness and so only carried axial load. As the effect of the axial stiffness of the top-hat edge purlin on the roof panel shear stiffness was already included in the test data, a high axial stiffness was used to represent the purlins in the beam idealisation, so this effect was not considered twice. The beam idealisation of the roof panel was calibrated against the results of the roof panel tests in shear.

The frame analysis results for the case of the vertical loading are shown in Figure 4-10. Good agreement with the test results was obtained for the buildings with both Joints A and B. As may be expected, the frame analysis slightly over-predicted the failure load as the effect of axial forces was not considered. The experimentally

131

determined bending capacities of the joints and continuous members were used as limiting factors in the frame analysis. Although the effect of axial load is not significant for the given geometry and lateral restraint conditions, the effect should be considered in a frame design using cold-formed steel members (Stratan et al. (2006)).

Figure 4-12a and b also show the test and frame analysis results for the case of the horizontal loading with no roof sheeting and the frame analysis results under-predicted both the stiffness and strength of the frames. On the other hand, there is good agreement for the stiffness of the internal frame, for the case of the structure with its roof sheeting, (see Figure 4-12).

4.7   Concluding remarks

So far, much stiffer hot-rolled steel portal frames with rigid joints have been investigated in respect to stressed skin design, as shown in Table 4-1. It was demonstrated that for such frames the behaviour of the component (e.g. bare frame) is different from the clad system. The behaviour of the novel flexible cold-formed steel portal frames with non-linear frame stiffness was investigated as even greater effect of stressed skin action was expected.

This chapter describes a series of six full-scale laboratory tests conducted on cold-formed steel portal frames in order to investigate the effects of joint flexibility and stressed skin diaphragm action. The buildings tested were of 6m span, 3m height, 10° pitch and 3 m frame spacing. Two different joints were considered: Joint A and B, and the stiffness of Joint B was approximately twice that of Joint A. Investigated joint are similar to what can be found in the practice and the tests using these connections take account of initial slip of bolts in oversized holes.

From the full-scale tests on the bare frames, it was observed that the failure load was almost independent of whether Joint A or B were used and structure failed at approximately the same load. In terms of stiffness, the bare frame with Joint B was approximately 60% and 30 % stiffer that the same building with Joint A under vertical load and horizontal load, respectively. However, when roof cladding was

introduced in the test, the horizontal resistance of the building was increased by approximately a factor of three. This could be explained by the fact that 70% (Joint A) of the total load applied to the internal frame was transferred to the braced gables by the roof diaphragm as recorded by the reaction load cells. The test frame therefore subject to only 30% of the total horizontal load applied to the structure and the rest was resisted by the gable frame.

The eaves horizontal deflections are also reduced by approximately a factor of ten compared to the bare frame model, as the roof diaphragm acts like bracing system between intermediate frames and its braced gables.

The 2D bare frame analysis model used to design the internal frames can lead to a failure of the cladding or the gable frame. It was also shown that the 3D analysis model incorporating the stiffness of internal and gable frames as well as the roof envelope stiffness is more suitable for the design of clad portal frames with flexible joints.

In comparison, for hot-rolled portal frames with rigid joints, stressed skin action is less important than in more flexible cold-formed frames and can be conservatively ignored when 2D frame analysis can be used. Such frames often span over 15m and their stiffness is much greater than cold-formed steel frames in order to meet vertical deflection requirement. If the design of portal frames is governed by horizontal deflections (e.g. for the design case with rigid joints), then it is shown that stressed skin analysis should be carried out to ensure that 'true' loads transferred to the gable frames are accounted for.

5   PORTAL FRAME DESIGN

5.1   Investigation of building geometry

Using the beam idealization described in the Chapter 4, six buildings having 3 to 8 bays were analysed for both ultimate and serviceability limit state design in accordance with Eurocode 1 loading. The span of 6 m, height to eaves of 3 m, roof pitch of 10 degrees and frame spacing were kept the same and only the length of the building was increased. The building length is expressed as length-to-span ratio ranging from 1.5 (i.e. 3x3 m bays) to 4 (i.e. 8x3 m bays). The size of the sheeting panel was therefore kept similar to the shear panel test so accurate experimental strength and stiffness characteristic can be used.

The design process was repeated for each of joint types A, B and C, in which a new Joint C (see Figure 5-1) was designed to satisfy horizontal deflection requirement in 2D bare frame analysis (SCI P397 (2012)). This design was chosen to highlight consequences of using traditional 2D design method in opposed to 3D stressed skin design (joint types A and B). Frame with Joint C also highlights how much heavier cold-formed steel portal frame design can be if stressed skin action is not considered.

Back-to-back channel sections of 300 mm depth and 2.5 mm thickness were used for columns and rafters of the internal frames. The gable frames were assumed to be constructed from single C sections, the same as those in buildings with Joint B. A bolt-group size of 620 mm x 208 mm was used, comprising five bolts in two rows (see Figure 5-1). The rotational stiffness of such joint was calculated to be 7358 kNm/rad (Zadanfarrokh and Bryan (1992) Johnston et al. (2013)). The joint bending resistances were calculated as 71.4 kNm (see Dubina et al. (2004), Johnston et al. (2013) and Phan et al. (2015). 2D bare frame analyses of the internal and gable frames were also conducted for comparison with the results for the clad frames.

5.2   Load cases and load combinations

Figure 5-2 shows the unfactored actions applied to the frame according to the SCI design guide SCI P397 (2012). The permanent (g_k), snow (s_k) and live loads (q_k) are based on loads of 0.18 kN/m^2, 0.4 kN/m^2 and 0.6 kN/m^2, respectively (see BS EN 1991-1-1:2002 (2002), BS EN 1991-1-3:2003 (2003), NA to BS EN 1991-1-1:2002 (2005), NA to BS EN 1991-1-3:2003 (2005)). The wind action (w_k) is based on a peak pressure of 1.0 kN/m^2 acting in the transverse direction (BS EN 1991-1-4:2005+A1:2010 (2005), NA to BS EN 1991-1-4:2005+A1:2010 (2008)) .

a) Eaves joint

b) Apex joint
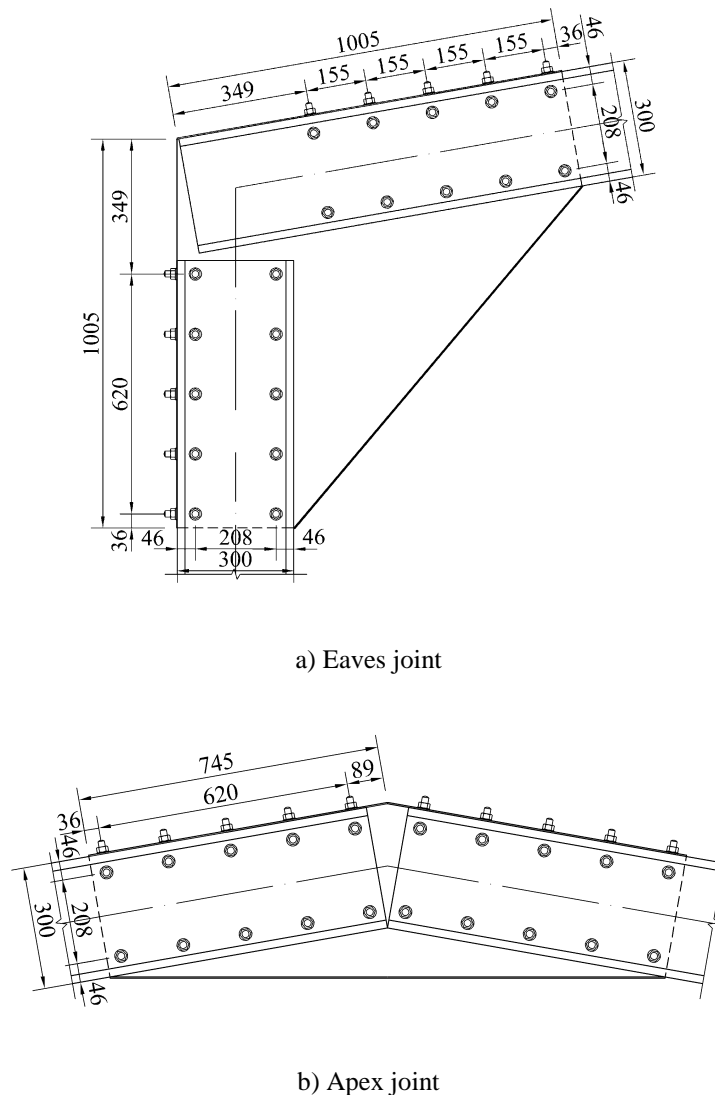
Figure 5-1 Details of Joint C

The internal and gable frames are checked at the ultimate limit state for the following load combinations (ULCs) (see BS EN 1990:2002+A1:2005 (2002), NA to BS EN 1990:2002+A1:2005 (2004)):

$$ULC1 = 1.35g_k + 1.5\,q_k \tag{5-1}$$

$$ULC2 = 1.35g_k + 1.5s_k + 1.5 \text{x} 0.5 w_k \tag{5-2}$$

$$ULC3 = 1.35g_k + 1.5w_k + 1.5 \text{x} 0.5 s_k \tag{5-3}$$

$$ULC4 = 1.0g_k + 1.5w_k \text{ (for wind uplift)} \tag{5-4}$$

The internal frame and cladding are also checked at the serviceability limit state. For the internal frame, the serviceability deflection limits recommended by the Steel Construction Institute (SCI) are:

- Absolute horizontal deflection of column: height/100 (30 mm for this case)
- Differential horizontal deflection relative to adjacent frame of frame: spacing/200 (15 mm for this case)
- Differential ridge deflection relative to adjacent frame: frame spacing /100 (30 mm for this case)

It is assumed that the cladding fails the serviceability limit state when the shear force exceeds 60% of its ultimate strength. This assumption is based on experimental investigations of the cladding panels and prevents permanent deformation of the panel within the working load which is approximately 60% of the factored load (Wrzesien et al. (2009b)). The following serviceability load cases (SLCs) are selected as they are considered to be critical (see BS EN 1990:2002+A1:2005 (2002), NA to BS EN 1990:2002+A1:2005 (2004)):

$$SLC1 = 1.0q_k \tag{5-5}$$

$$SLC2 = 1.0w_k \tag{5-6}$$

136

a) Permanent action	b) Imposed load	c) Wind action
	(Snow load)	
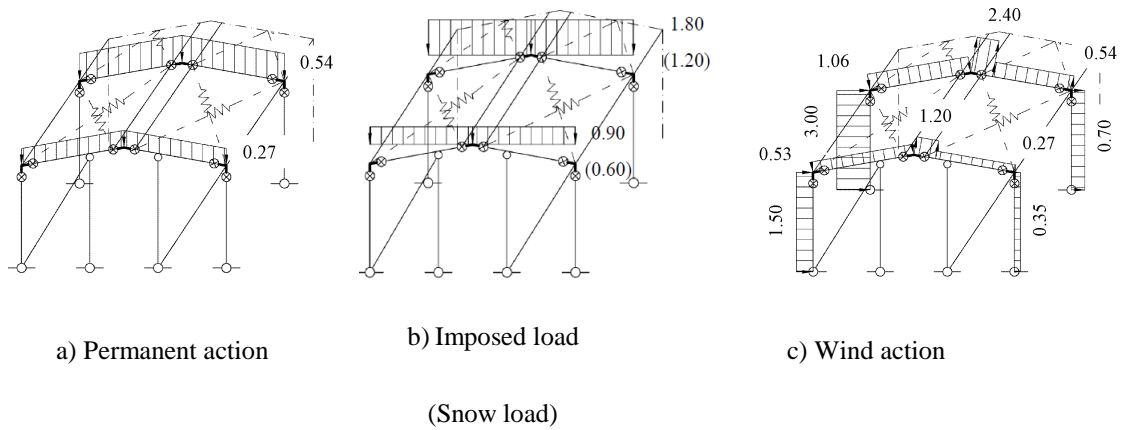
Figure 5-2 Applied actions in kN/m

5.3 Unity factors based on proposed design method

5.3.1 Design assisted by testing

Figure 5-3 and Figure 5-4 summarise the unity factors at the ultimate limit state (ULS) for the internal frame, gable frame and sheeting panel. These are defined as the ratio of the applied load to the resistance for the critical mode of failure as follows:

- Internal frame

$$UF_{3D} = M_{j,Ed,3D} / M_T \tag{5-7}$$

$$UF_{2D} = M_{j,Ed,2D} / M_T \tag{5-8}$$

- Gable frame

$$UF_{3D} = N_{Ed,3D} / N_{t,Rd} \tag{5-9}$$

$$UF_{2D} = N_{Ed,2D} / N_{t,Rd} \tag{5-10}$$

- Sheeting panel

$$UF_{3D} = V_{d,Ed,3D} / V_{d,T} \tag{5-11}$$

where:

$M_{j,Ed,3D}$, $M_{j,Ed,2D}$ – bending moments acting on the bolt-group centre of rotation based on 3D and 2D frame analysis

M_T – connection moment resistance obtained in joint test (see Table 4-6

$N_{Ed,3D}$, $N_{Ed,2D}$ – tension forces acting on the gable bracing based on 3D and 2D frame analysis

$N_{t,Rd}$ – design resistance for uniform tension of the bracing member (26.95kN)

$V_{d,Ed,3D}$ – shear force acting on a roof panel next to gable based on 3D analysis

$V_{d,T}$ – shear resistance of a panel obtained in component test (see Figure 5-6)

The unity factors are calculated based on 3D analysis (UF_{3D}) and the results for different length-to-span ratios of the building are marked by the solid lines on the plots. For comparison, the unity factors based on 2D design (UF_{2D}) are also presented as horizontal dashed lines. The load under prediction can be identified when the solid line representing 'true' redistributed loads lies above a dashed line. The critical load combinations (see section 5.2) to which unity factors are calculated for both 3D and 2D models are also presented. The loads ratios (r) obtained from the 3D models relative to the loads obtained in the 2D models are presented for the extremes of the analysis (see Figure 5-3):

- Internal frame

$$r_I = M_{y,Ed,3D} / M_{y,Ed,2D} \tag{5-12}$$

- Gable frame

$$r_G = N_{Ed,3D} / N_{Ed,2D} \tag{5-13}$$

If the load ratio (r) is greater than 1, the 2D analysis model is unsafe and loads should be increased by the given factor (i.e. from Figure 5-3c r_G=3.38 x 0.5 bay ≈ 1.7 bay). Hence in a 2D analysis of given structure, the gable frame should be designed to resist wind load resulting from approximately two times that acting on a single bay between frames.

An analogous approach was used in Figure 5-5 in order to demonstrate the effect of stressed skin action on building deflections. The serviceability limit state (SLS) unity factors and deflection ratios were calculated as follows:

- Live load

$$UF_{3D}=\delta_{a,3D}/\delta_{a,SCI} \qquad (5\text{-}14)$$

$$UF_{2D}=\delta_{a,2D}/\delta_{a,SCI} \qquad (5\text{-}15)$$

$$r_{LL} = \delta_{a,3D}/\delta_{a,2D} \qquad (5\text{-}16)$$

- Wind load

$$UF_{3D}=\delta_{e,3D}/\delta_{e,SCI} \qquad (5\text{-}17)$$

$$UF_{2D}=\delta_{e,2D}/\delta_{e,SCI} \qquad (5\text{-}18)$$

$$r_{WL}= \delta_{e,3D}/\delta_{e,2D} \qquad (5\text{-}19)$$

where:

$\delta_{a,3D}, \delta_{a,2D}$ – apex vertical deflection under the imposed load based on 3D and 2D frame analysis

$\delta_{a,SCI}, \delta_{e,SCI}$ – apex and eaves deflection limits SCI P397 (2012)

$\delta_{e,3D}, \delta_{e,2D}$ – eaves horizontal deflection under the wind load based on 3D and 2D frame analysis

Figure 5-3 shows that there is little difference between the unity factors for the frames with Joints A and B. For the internal frame, the design of the bare frame is

controlled by a combination of wind and snow load. However, when stressed skin effects are taken into account, the frame is controlled by the strength of the roof cladding next to the gable (see Figure 5-4). The critical load combination for roof cladding design changes from gravity combination (ULC1) to combination of wind and snow load (ULC3) when the overall length-to-span ratio reaches 2.5. As expected, the longer the building, the larger the load in the roof panels. The failure of the roof sheeting can be prevented by the use of stiffer joints, particularly at the eaves. The load in the roof panel is reduced between 21% and 7% when Joints B rather than Joints A are used. In order to meet SCI deflection limits, the rotational stiffness of the joints was increased by approximately a factor of six. By doing so, the shear force in the roof panel is reduced (see Figure 5-4).

For the gable frame, it can be seen from Figure 5-3 that the design of the frame is controlled by the strength of the gable bracing irrespective of the joint stiffness. In all cases, a 2D analysis under-estimates the load in the gable frame by a factor of 3 for a three bay building and by a factor of 7 for an eight bay building (see Figure 5-3a and b). If the stiffness of the internal frames is increased to satisfy SCI serviceability requirements, the load transferred to the gable through the roof panels is reduced by a factor of approximately 2.5. In the 3D analysis, the gable frame loading is still 3 times higher than in a 2D analysis (see Figure 5-3c), so if diaphragm action is ignored, the stiffness of the internal frames should be increased further.

a) Buildings with Joint A
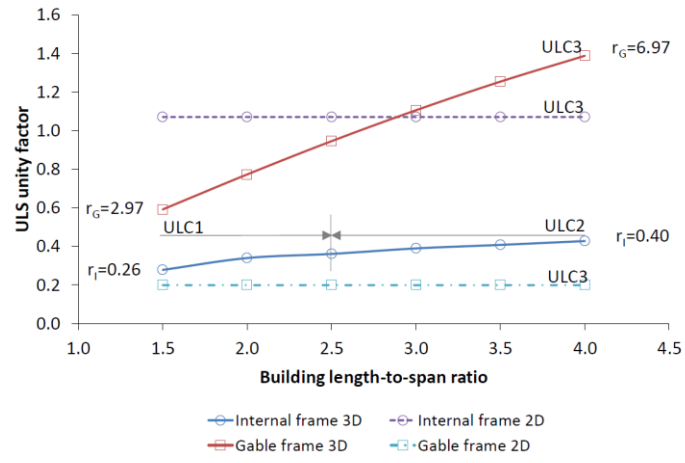
140

b) Buildings with Joint B

c) Buildings with two 300 mm x2.5 mm C sections as intermediate columns, rafters and Joint C

Figure 5-3 Ultimate limit state unity factors for frames
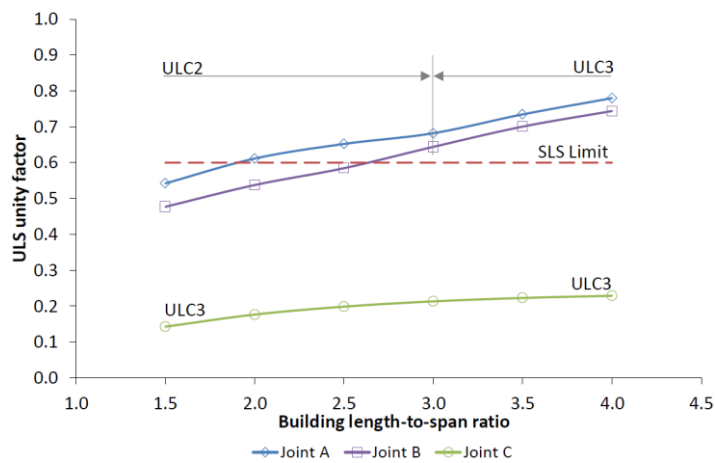
Figure 5-4 Ultimate limit state unity factors for roof panel
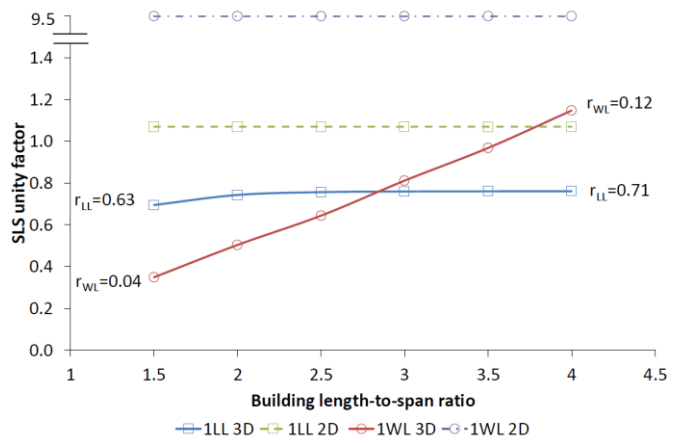
141

a) Buildings with Joint A

b) Buildings with Joint B
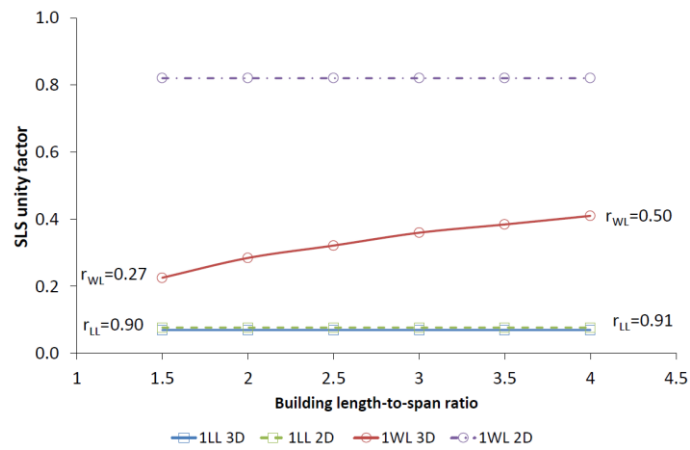
c) Buildings with two 300 mm x2.5 mm C sections as intermediate columns, rafters and Joint C

Figure 5-5 Serviceability limit state unity factor according to SCI P397 (2012)

Alternatively the gable frame should be designed for horizontal load resulting from the wind loading on an estimated one and a half bays regardless of length-to-span ratio. This also means that the in–plane bracing and the foundations to the bracing have to be designed for these higher loads. From Figure 5-4, it can be concluded that serviceability failure of the roof cladding can be prevented for buildings with Joints A and B if their overall length-to-span ratio is less than 2.5.

Figure 5-5 shows the unity factors at the serviceability limit state. As can be seen from Figure 5-5a and b, diaphragm action reduces the vertical deflection of a three bay building by 32% compared to that obtained for a bare frame. In the case of horizontal deflections, diaphragm action reduces deflections of a bare frame with Joints C by 50%. In the case of three bay building with the flexible joints (e.g. Joint A), the horizontal deflection is only 3% of that calculated for a bare frame.

5.3.2 Proposed analytical methods

It has been demonstrated in previous chapters that load redistribution in a 3D clad structure depends on the horizontal stiffness of internal frames. The gable frame stiffness and a shear stiffness of the sheeting panels are also expected to have significant effect on the behaviour of clad structure. These parameters need be established accurately otherwise design load in structural components can be falsely estimated. The analytical model based on the experimental data and presented in Section 4.6 was used. The curves representing behaviour of frames with joints B (see Figure 5-7b, Figure 5-8, Figure 5-9b) based on joint tests were used as a benchmark to the proposed analysis models. As presented in Section 2.5.6 slip of bolts in oversized holes contributes largely to the joint flexibility. The rotational stiffness at the slip stage cannot be conclusively established without testing hence, a rotation stiffness envelope analysis was proposed for untested joints. Two joint rotational stiffness models were presented in Table 5-1. Model 1 which provides an upper bound to the joint rotational stiffness represents the design case in which slip is excluded from the analysis as it often takes place in practical design. Model 1 would represent 'true-fit' bolted connection, screwed connection or friction grip bolted

connection. The joint rotational stiffness is therefore associated with bearing of the bolts on relatively thin steel plates. Model 2 represents a more realistic case in which slip due to hole tolerance and the bolt bearing are modelled by bi-linear rotational springs. It was assumed, based on the experimental investigation presented in Chapters 2 and 4, that the rotational stiffness at the slip stage can be taken as 5% of that calculated for a bearing stage.

In terms of strength and rotational stiffness, Model 1 allows a contribution from the additional flange bolts whereas Model 2 neglects their contribution and considers only web bolts. The numerical values presented in Table 5-1 had been calculated in the APPENDIX H for Joint B. The shear stiffness and strength of a sheeting panel was also derived analytically as shown in Chapter 3 and is compared against experimental data in Figure 5-6 .

Table 5-1 Rotational springs representing analytical upper and lower bound joint characteristic

Spring position	Moment sign	ϕ_{sl}	$S_{j,ini,sl}$	$S_{j,ini,anl}$	$M_{j,anl}$
		rad	kNm/rad	kNm/rad	kNm
Model 1 (upper bound stiffness model excluding slip)					
Internal frame joints	Symmetry	-	-	1771	17.43
Gable frame joints	Symmetry	-	-	885	8.71
Model 2 (lower bound stiffness model including slip)					
Internal frame joints	Symmetry	0.007	80	1607	16.36
Gable frame joints	Symmetry	0.007	40	803	8.18

The ULS unity factor for frame designs with joint Model 1 and 2 were calculated according to equations (5-7) to (5-11). A comparison of the ULS unity factors for building designs supported by testing and designs using the proposed analytical methods is presented in Figure 5-7 and Figure 5-8. Whenever the dotted (Model 1) or the dashed (Model 2) curve falls below a solid line the unsafe design

can be made as the design unity factors are smaller than unity factors calculated from full-scale tests. It is shown that the proposed analytical method is conservative across the range of analysed structures if lower bound rotational stiffness of joints is used in the design (Model 2). For the internal and gable frame designs the difference in unity factors range from 14% to 16% and 0% to 6% respectively (see Figure 5-7). Much greater conservatism with the proposed method had been observed in terms of sheeting panel design reaching 64% (see Figure 5-8). This can be explained by the fact that analytical method under-predicts both shear strength and stiffness of a sheeting panel (Figure 5-6). If however the rotational stiffness of joints is over-predicted (e.g. Model 1) the loads acting on the gable frames can be under-predicted by 9% (see Figure 5-7).
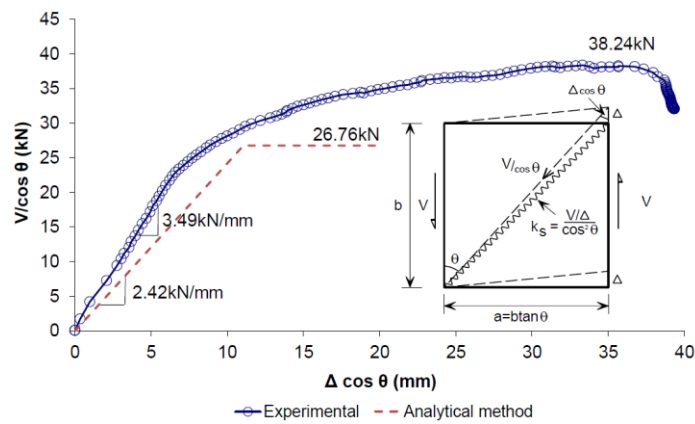
Figure 5-6 Comparison of shear panel characteristics
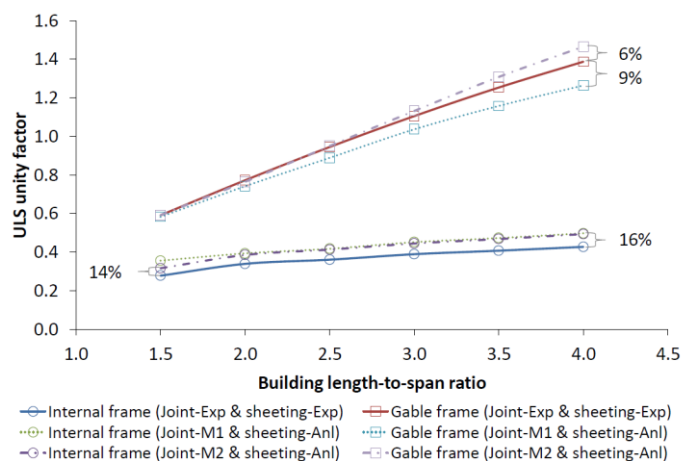
Figure 5-7 Comparison of ultimate limit state unity factors for frames

The very conservative joint rotational stiffness model also contributes greatly to conservatism of the proposed method in predicting 'true' deflections of frames. The joints are considered as pinned in a slip stage hence frame stability is provided by the sheeting. As expected, such a model over-estimates frames deflections (see Figure 5-9 and Figure 5-12) by as much 80% and 34% for vertical and horizontal deflections respectively. If however the slip is ignored, the vertical apex deflections can be under-estimated by as much as 34%. It is recommended that the lower bound strength and stiffness of the sheeting and joints should be used in the analysis model if experimental characteristics of those components are not available.
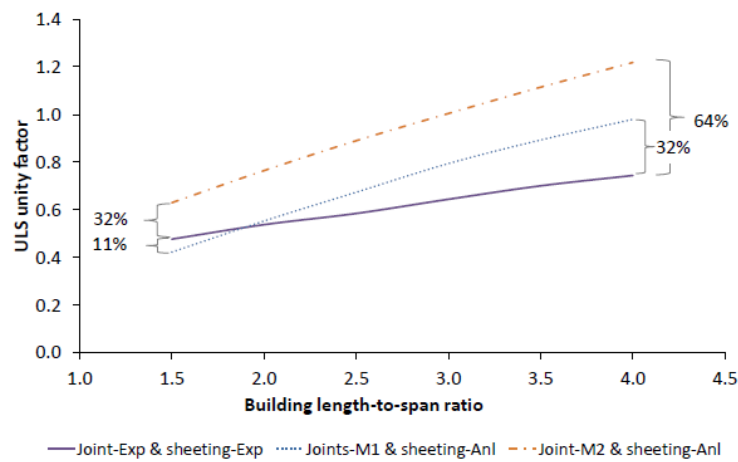
Figure 5-8 Comparison ultimate limit state unity factors for roof panel
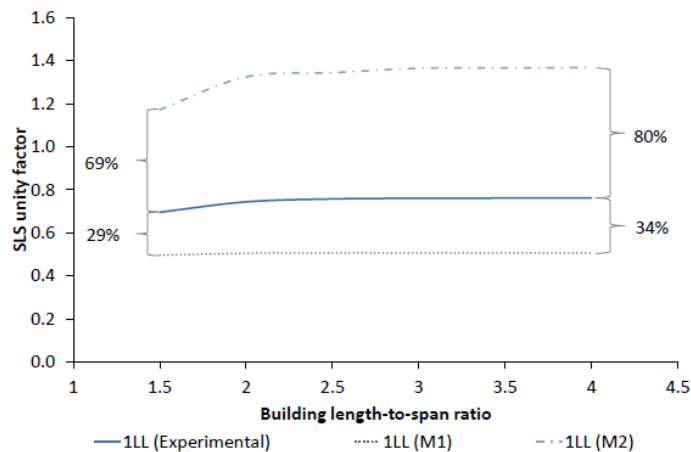
Figure 5-9 Comparison of serviceability limit state unity factor for vertical loading according to SCI P397 (2012)

146
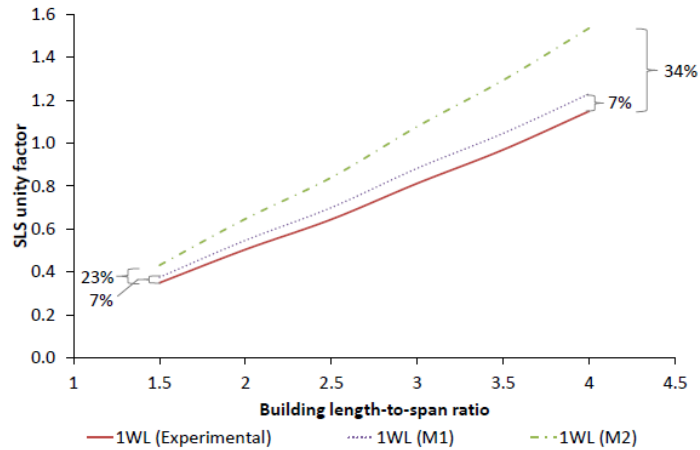
Figure 5-10 Comparison of serviceability limit state unity factor for horizontal loading according to SCI P397 (2012)

5.4   Implication for design

In comparison, for hot-rolled portal frames with rigid joints, stressed skin action is less important than in more flexible cold-formed frames and can be conservatively ignored when 2D frame analysis can be used. If the design of portal frames is generally governed by horizontal deflections (e.g. for the design case with Joint C), then it is shown that stressed skin analysis must be carried out.

c) Buckling of the edge purlin

d) Failure of purlin connection and deformation of the gable-frame rafter

Figure 5-11 Mode of failures observed in clad frame tests

147

As the roof construction is constantly evolving, it is also shown that existing design methods (BS 5950-9 (1994a), ECCS TC7 (1995)) need be updated for modern roof systems, such as those with top-hat purlins and composite panels, so that relative flexibility ratio of the frame to the roof system can be accurately assessed (see Figure 5-6). Although the design methods   BS 5950-9 (1994a) were developed in the past, these were re-examined in this thesis in the context of cold-formed steel frames with flexible joints and it is recommended that a 3D non-linear analysis model (FEA) is used for cold-formed steel portal frames for the following reasons:

- Figure 4-10 and Figure 4-12 show that the sway and spread flexibilities of bare frames are non-linear relationships due to slip.
- The reduction factors on sway bending moments (see Table 16 of BS 5950-9 (1994b)) are only suitable on the assumption that the gable frame are rigid both in and out-of-plane. The flexibility of a gable frame was measured in the tests (see Table 4-5) and should not be ignored.
- The assumption in the design methods that wind forces act as point loads at the eaves level, is a simplification, as when the wind load is modelled as a distributed load (see Figure 5-2c), the maximum bending moment may occur at mid-column height rather than eaves.

A 3D analysis allows the designer to follow 'true' load paths and produce a design which is often more economical. In such designs however, the roof sheeting may become a key structural component responsible for the building's stability and so it follows that the stability of the structure can be compromised if the roof sheeting is removed or the stiffness of the roof panel is changed (e.g. by adding openings or replacing sheeting profiles).

5.5   Concluding remarks

The end gable frames are often designed as braced frames as better economy can be obtained by avoiding expensive moment-resisting joints. It was shown that in such design cases the bare gable frame analysis model is unsafe and will lead to under-estimation of forces even if SCI deflection limits are adopted. The additional

load due to roof diaphragm action may lead to less dangerous tearing of the roof sheeting or failure of purlin-to-rafter connections at the gable frame (see Figure 5-12) but it should be included in the design of gable rafters, connections, gable bracing and gable foundations so that structural failure of the end gable frame is prevented. From Figure 5-3c it can be concluded that for buildings of 6 m span and height to the eaves of 3 m it is appropriate to design end gable frames for wind loading resulting from one to two depending on the building length. The common misconception that stressed skin action can be conservatively ignored in bare frame design is therefore false for some design cases. It was also shown that the horizontal deflection limits in bare frame design must be satisfied as relaxing these limits will lead to even further under-estimation of loads in gable end frames.

It is therefore recommended that stressed skin analysis is employed in the design of cold-formed steel portal frames with flexible joints. It had been demonstrated that the stiffness of individual components of cold-formed steel portal buildings has an important effect on the realistic assessment of the distribution of the loading. All the factors which may affect the stiffness of frames (i.e. slip due to holes tolerance and bolt bearing) should be considered in the analysis models so that the design checks are done for realistic frame loading. The 3D non-linear beam idealisation of the clad building produces conservative results if the lower bound joint rotational stiffness and sheeting shear stiffness are used.
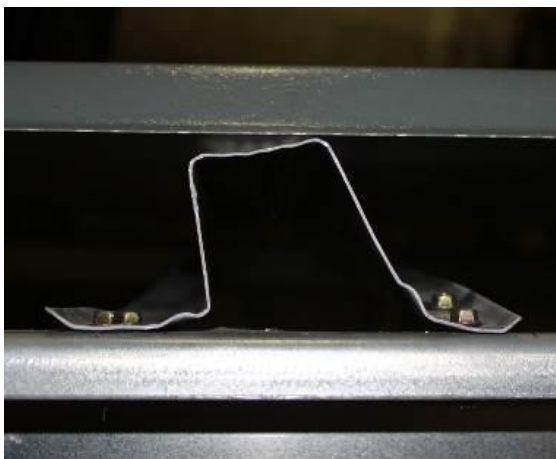
a) Shear deformation due to diphragm action

b) Failure of purlin-to- end-rafter connection

Figure 5-12 Behaviour of top-hat sections acting as purlins in a clad frame

6   CONCLUSIONS

6.1   Resistance of bolted joints

As expected, there is no clear correlation between the results from minimum weight and minimum cost analysis of cold-formed steel portal frames as cost may be dictated by pricing strategy of individual business. It is however important that realistic prices of framing systems are presented especially when cold-formed and hot-rolled components are used in one system. It was shown in Section 2.4 that for typical cold-formed joints the cost does not exceed 30% of the frame overall cost. This proportion increases up to 60% if the hot-rolled welded connection brackets are used. In order to choose the most economic framing system, factors such as loading conditions, building geometry and joint cost should be taken into account. For example, as can be seen from Section 2.4, the best performing joints in terms of steel usage and cost are those without brackets but they are only suitable for short span applications and relatively small loading. The least expensive frame design is offered by the Swagebeam system (Kirk (1986) which offers much greater spans (up to 18m in the UK); however the same system is the heaviest in terms of steel usage. The extra steel used for swages in columns, rafters and brackets exceeds the savings from stiff and full-strength joints which can be modelled as rigid. As such, taking joint effects explicitly into the design process provides an opportunity to devise an appropriate balance between joints and member properties and thus reduce material use.

The highest cost is expected for frames with hot-rolled steel connection brackets (Dubina et al. (2004), Rhodes and Burns (2006). Frames with such joints are approximately 1.5 times more expensive than these built entirely from CFS components.

It is recommended that the design of cold-formed steel moment resisting joints is validated by testing as the current design codes do not offer sufficient guidance. The experimental data in Section 2.5.7 shows that all tested joints should

be classified as partial-strength with the strength reduction factor ranging from 0.77 to 0.94. Whenever light-gauge channels are bolted through the web, local web buckling governs the joint design. As this mode of failure was not highlighted in early design recommendations (i.e. Rhodes (1991), SCI P125 (1993)), designers often only consider a bearing capacity check. It was also demonstrated in Section 2.5.8 that following this approach may result in overestimation of the joint capacity by a factor of 3.

In practice, cold-formed steel joints are not considered as torque controlled joints, due to the low friction coefficient. While it is expected that friction will reduce a bearing load of the bolt shank onto a steel plate, for 'pure' bearing resistance joints with little torque were tested. It was found that the current design practice of increasing EC3 calculated bearing resistance by a factor of 2 for bolted joint in double shear may not produce safe designs. In Appendix A.4 it is shown that maximum test load was 9% smaller than the EC3 calculated resistance. The difference increases up to 50% when a characteristic bearing resistance based on 3mm displacement limit (ECCS TC7 TWG recommendation) was compared against the EC3 calculated bearing resistance. It is therefore recommended that test bolt bearing capacity of double lap joints is used in the design.

Baigent and Hancock (1978) observed that in a single channel frame, the web buckling failure is actually triggered by the additional compressive stress due to the bi-moment as the load applied in the plane of the web was not passing through the shear centre of the single channel section. It was proposed that the bi-moment can be simply evaluated as moment in plan of the web times the distance from the web to the shear centre of the section. Although one could say that this theory should not apply to back-to-back double symmetric channel beams the evidence of the bi-moment action were highlighted recently by Lim et al. (2016a). This simplified method of including the effect of bi-moment into the joint design offers conservative moment-resistance for most of the design cases, it fails however to include a beneficial effect of bolt-group length on the joint moment-resistance demonstrated in joint test.

In this document different analytical models to estimate joint moment capacity were presented, based on work of Chung and Lau (1999),Yu et al. (2005),Chung and Ho (2005),Dubina et al. (2008),Dubina and Ungureanu (2008). The resultant transverse load due to bolt forces is calculated following a typical bolt bearing check and is examined for combined bending and shear and bending and web crippling (see Appendix B.2). It is the combined bending and web crippling design criterion which governed the design in 6 out of 7 design cases and only this design criterion produced conservative results. It was shown that it can produce safe predictions of the joint capacity albeit only if bolt-group length-to-width ratio is less than 3.5. Both methods although widely published, are not free of inaccuracies and they do not describe the 'true' mode of failure. The authors failed to recognise evidence presented by Baigent and Hancock (1978) who actually measured the strains due to bi-moment.

As the conclusive method of calculating a capacity of channels loaded via their webs is not yet presented, it is recommended that for best accuracy such joints are analysed by more advanced Finite Element Analysis (FEA) calibrated against test results.

6.2   Stiffness of the bolt joints

Because galvanized members cannot be welded, the use of fasteners and their bearing into the steel plate make joints semi-rigid. In tests on single and double lap joints (see Appendix A.3) the shear stiffness was measured and compared against analytical methods. In two sets of test results it was shown that the shear stiffness of the double lap joints was almost twice of the stiffness of the single lap joint. For predicting the stiffness of a lap joint, the analytical method proposed by Zadanfarrokh and Bryan (1992) proved to be acceptable. It was also shown that incorporating the EC3 joint resistance in the design will result in non-linear shear stiffness, which should be considered in the analysis of the structural system, as it can lead to force redistribution. It was demonstrated that rotational stiffness of the bolted joint can be calculated based on the elastic method and the shear stiffness of the lap joint. The stiffness ratios K_j of the tested joints (see Eq. (2-4) and L_b=1m) ranged

from 0.56 to 1.3 where this ratio needs to be at least 8 so that the joint can be classified as rigid. It was found that the contribution of the additional flange bolts should be ignored for lower bound rotational stiffness values.

The effect of joint rotational stiffness on the design economy of bare CSF portal frames was presented in Section 2.4. In the case of joint Type A, the joint rotational stiffness was reduced in size to follow industry practice. In terms of typical 2D design such joint will produced the heaviest portal frame amongst all reviewed portal frame systems. It was concluded that stiffer joint Type B, although larger, offered average 32% improvement on the weight and cost of portal frame design. Joint Type B offered the second best average efficiency rating amongst all reviewed portal frame systems.

The second important problem which was demonstrated in lap joint tests is a slip of the bolt in the oversized hole. Estimating and incorporating the slip in the beam model is very problematic but it should be done. When the free slip rotation occurs in the joint, the stiffness of the frame decreases rapidly causing engagement of other components e.g. building envelope in carrying the load. If the critical load is reached then local failure of the cladding can cause leakage and other serious serviceability problems.

6.3   Roof sheeting panels with shear connectors

As roof construction is constantly evolving, existing design methods need to be updated for modern roof systems, such as those with top-hat purlins and composite panels, so their strength and stiffness can be calculated. A total of 18 full-scale tests were conducted on panels with and without shear connectors.

Despite the complexity of the problem, the calculated methods offered adequate prediction of shear resistance of the investigated panels due to seam failure. Holes elongation was not observed around the shear connector screws, suggesting that the 'true' level of loading was significantly lower than that assumed by standard design methods. It should be noted that the standard design method neglects the

contribution of the top-hat purlins in carrying direct shear and this simplification adds to the level of conservatism in predicting the shear resistance of the panel. It is suggested that this problem should be investigated further by more detailed analysis methods such as Finite Element Analysis so that more accurate diaphragm design can be available.

In the case of a panel, in which the shear resistances of individual fasteners were established by the use of the analytical equations (Toma et al. (1993)), shear capacities with an average 55% safety margin were predicted. As expected, the safety margin was reduced to an average of 25% when the upper bound experimental values of fastener shear resistance were used in the calculations. This model gave results closest to the values obtained in the full-scale panel tests.

In terms of test shear flexibilities versus the analytical shear flexibilities, a good correlation was obtained for 0.7mm thick sheeting. The test flexibilities of the 0.5mm thick sheeting panels were not as sensitive to the thickness of the sheeting as indicated by the calculated method. It was shown, however, in tests on shear panels with 0.7mm cladding that the calculated method for predicting the shear flexibility of an individual bolts offers sufficient accuracy in assessing the shear flexibility of a screw connection.

The sinusoidal sheeting profiles fixed in crests (Test 7 and 8) require more research before they can be used in stressed skin design. Due to extensive fixing inclination, non-linearity of the load-deflection relationship was observed in the early stages of loading, thus their ability to act elastically can be questioned. It was demonstrated that such shear panels are still capable of transferring load between the frames and their ultimate shear deflection capacity should be taken into account in portal frame design in order to prevent breaking of the fixings which was observed in one of the test.

Composite panels can be used in stressed skin design as long as fixing inclination is taken into account and a sufficient number of end fixings is provided. It was shown that the shear capacity of a composite panel is significantly less than that

of single-skin trapezoidal panels. The increase of resistance and stiffness due to the interaction of the top and bottom skins should not be relied on.

6.4 Roof sheeting panels without shear connectors

The design shear capacities of each diaphragm without shear connectors (2-side fixed) were taken as the seam capacities as they were found to be always lower than the ultimate test loads.

In the case of panels, in which the shear resistances of individual fasteners were established by the use of the analytical equation by Toma et al. (1993), the predicted shear capacities for the panels were on average 35% lower than ultimate test values. As expected, the safety margin was reduced to the average 7% when upper bound experimental values of fastener shear resistance were used in the calculations. This model gave results closest to the values obtained in the full-scale panel tests.

All investigated panels without shear connectors showed between 37% and 28% lower shear flexibility than from the calculated method, regardless of the slip models of individual fasteners. The shear flexibility of panels without shear connectors relied largely on purlin/rafter connection flexibility (s_{pr}), which was established through a component test as such detail is not considered by the design code.

In the full-scale frame test, the rotation of the purlin top flange was restrained by the cladding profile resulting in compression of one of the legs. It can be expected that in such a case, the shear flexibility may be significantly reduced compared with that obtained in the component test. The purlin/rafter connection flexibility (s_{pr}) obtained in the component test, when reduced by half and used in calculations, gave good match with the full-scale test results. The highlighted difference in the behaviour of the purlin/rafter connection flexibility with sheeting attached should be investigated in future by more complex analysis methods such as Finite Element Analysis (FEA).

By comparing the test shear flexibilities of the same panels with and without shear connectors (see Table 3-5), it was shown that shear connectors increase the stiffness by a factor of two.

Similar to the tests with shear connectors, sinusoidal sheeting profiles fixed in the crests require more research before they should be used in stressed skin action design. It was demonstrated that such panels are still capable of transferring significant load between the frames although this load is often neglected in 2D portal frame analysis. It was demonstrated that the industry standard for the number of fixings used to fix corrugated profiles may not be sufficient as they are usually designed to resist wind uplift only. By fixing sinusoidal panels in every second crest rather than every third crest, shear breaking of fasteners was prevented.

The ability of typical composite panels to transfer shear force between frames was much greater than predicted analytically for just the top skin. It was shown that the roof panel became unserviceable at a shear deflection of approximately 20 mm and this limit should be respected in term of relative horizontal displacement between adjacent frames.

6.5   Behaviour of bare and clad frames based on full-scale tests

It has been demonstrated by others that for much stiffer hot-rolled steel portal frames with rigid joints, the behaviour of the component (e.g. bare frame) is different when considered as part of a clad system. The behaviour of novel flexible cold-formed steel portal frames with non-linear frame stiffness was investigated as even greater effect of stressed skin action was expected.

A series of six full-scale laboratory tests were conducted on cold-formed steel portal frames in order to investigate the effects of joint flexibility and stressed skin diaphragm action. The buildings tested were of 6m span, 3m height, 10° pitch and 3 m frame spacing. Two different joints were considered: Joint A and B, and the stiffness of Joint B was approximately twice that of Joint A. The investigated joints

are similar to what can be found in the practice and the tests using these connections take account of initial slip of bolts in oversized holes.

From the full-scale tests on bare frames, it was observed that the failure load was almost independent of whether Joint Type A or B were used and the structures failed at approximately the same load. In terms of stiffness, the bare frame with Joint B was approximately 60% and 30% stiffer that the same building with Joint A under vertical load and horizontal load, respectively. However, when roof cladding was introduced in the test, the horizontal resistance of the building was increased by approximately a factor of three. This may be explained by the fact that 70% (Joint A) of the total load applied to the internal frame was transferred to the braced gables by the roof diaphragm as recorded by the reaction load cells. The test frame was therefore subject to only 30% of the total horizontal load applied to the structure and the rest was resisted by the gable frame.

The eaves horizontal deflections are also reduced by approximately a factor of ten compared to the bare frame model, as the roof diaphragm acts like bracing system between intermediate frames and its braced gables.

6.6   General conclusions for structural design

For cold-formed steel portal frames, steel designers often use generic guidance for equivalent hot-rolled steel frames SCI P397 (2012) for deflection limits of bare frames, but these are discretionary. In fact, UK NA to BS EN 1993-1-1 (2005) specifies that the horizontal deflection limit for portal frames should 'suit the characteristic of the particular cladding'.

It was shown that the 2D bare frame analysis model used to design the internal frames can lead to a failure of the cladding or the gable frame. It was also shown that the 3D analysis model incorporating the stiffness of internal and gable frames as well as the roof envelope stiffness is more suitable for the design of clad portal frames with flexible joints.

The end gable frames are often designed as braced frames as better economy can be obtained by avoiding expensive moment-resisting joints. It was shown that in such design cases the bare gable frame analysis model is unsafe and will lead to under-estimation of forces even if SCI deflection limits are adopted. The additional load due to roof diaphragm action may lead to less dangerous tearing of the roof sheeting or failure of purlin-to-rafter connections at the gable frame but it should be included in the design of gable rafters, connections, gable bracing and gable foundations so that structural failure of the end gable frame is prevented. It can be also concluded that for buildings of 6 m span and height to the eves of 3 m it is appropriate to design end gable frames for wind loading resulting from one to two bay widths depending on the building length. The common misconception that stressed skin action can be conservatively ignored in bare frame design is therefore false for some design cases. It was also shown that the horizontal deflection limits in bare frame design must be satisfied as relaxing these limits will lead to even further under-estimation of loads in gable end frames.

When the experimentally derived data was used to design the building in accordance with the relevant Eurocodes, it was shown that the cladding stiffness cannot be ignored in practice as the loading attracted to the gables may be under-estimated by as much as factor of seven. This has an important effect on the gable frames which are usually designed for a wind load acting on half a bay based on a bare frame model. In order for 2D design to be used safely, horizontal deflection limits more stringent than those recommended by SCI should be adopted or alternatively, the forces acting on the gables should be increased.

It is shown that a lighter internal frame can be designed by including diaphragm action in the 3D analysis. For a typical building of 6m span and 12m length consisting of three internal frames and two end gables, 2D design requires 981kg of steel in the framework and when stressed skin action is considered, the overall weight of the steel framework can be reduced by 42%. In such designs, the roof cladding becomes an important structural component in providing lateral stability.

The following general conclusions can be drawn:

- The bare frame model identifies a wind load combination as being critical; including diaphragm action shows that the critical load combination depends on the length-to-span ratio of the building
- The bare frame design model may not be safe for designing clad structures as it ignores the additional force in the edge purlins, end cladding and gables
- The effect of the stiffness of the joints on the horizontal deflection of the system when sheeting action is taken into account is less than with a bare frame model that predicts the joint stiffness to be a dominant factor in lateral stiffness. Increasing the rotational stiffness of the joints has a larger effect on vertical deflections e.g. increasing their stiffness by the factor of two (Joints A to B) resulted in an approximately 40% reduction in apex deflections.

As presented in Section 2.5.6 slip of bolts in oversized holes contributes largely to the joint flexibility. The rotational stiffness at the slip stage cannot be conclusively established without testing hence, a rotation stiffness envelope analysis is proposed for untested joints.

When the slip rotation of the joints was ignored in the analysis as it is often done in practical design (upper bound rotational stiffness model) the 'true' horizontal load transferred to gable frame via sheeting was under-predicted by 9% hence such assumption may result in under-conservative design of gable frame or sheeting panels. Such model would also under-estimate the 'true' vertical deflection of the intermediate frame between 29% and 34% depends on the length-to-span ratio.

A more conservative bi-linear joint rotational stiffness model was proposed where joints are considered as pinned in a slip stage hence frame stability is provided by the sheeting. It is shown that the proposed analytical method is conservative across the range of analysed structures. For the internal and gable frame designs the difference in unity factors range from 14% to 16% and 0% to 6% respectively.

As expected, such a model over-estimated shear forces in the sheeting panel by 32% and 64% for the range of analysed buildings. The frames deflections were

also over-predicted by as much 80% and 34% for vertical and horizontal deflections respectively.

It is also recommended that until state-of-the-art research in the field of cold-formed steel portal frame systems is fully implemented into design codes, a calibration of the analysis method against existing research should be considered.

It was demonstrated that in the absence of test results, the 3D non-linear beam idealisation of the clad building produces conservative results if the lower bound joint rotational stiffness and sheeting shear stiffness are calculated and used in the analysis model.

6.7   Statement of achievements

During the project following goals have been achieved:

1. Previously untested and economically efficient cold-formed steel joints have been investigated. An analytical model was developed in order to represent the behaviour of such joints. A modelling method using beam elements was also investigated. The joint design method is currently used by industrial sponsor, which supplies the UK market with approximately 1000 cold-formed steel frames each year.

2. The common misconception that the failure mode of the moment-resisting bolted joints occurs by bolt bearing failure was shown to result in an overestimation of the joint capacity by as much as factor of 3. Light gauge steel members often fail in web bucking under the localised compression stresses before the bolt bearing capacity is reached. It was found that the current design practise of increasing EC3 calculated bearing resistance by a factor of 2 for bolted joint in double shear may not produce safe designs (test load was 9% smaller than the EC3 calculated resistance).

3. It was shown that simple analytical equations for predicting the rotational stiffness of a lap bolted joint could be successfully developed. It is important that joints stiffness is modelled (including slip of bolts in

160

oversized holes) in order to capture force redistribution not only in primary members but also in the building envelope.

4. An extensive experimental study was conducted in order to validate the assumption that cold-formed steel portal frame systems could be modelled and designed following a typical 2D design procedure. The general conclusion was that current design codes do not offer enough guidance on designing cold-formed steel frames. In the absence of test results, the method presented in this document produces conservative results if the lower bound joint rotational stiffness and sheeting shear stiffness are used in the analysis model.

5. The shear resistances and stiffness of nearly 20 different roof diaphragms containing novel hat-shaped purlins were investigated. Existing analytical methods were updated to take account of the shear stiffness of such purlins. It was demonstrated that the industry standard for number of fixings used to fix sinusoidal profiles may not be sufficient to prevent shear breaking of fasteners as they are usually designed to resist the wind uplift only.

6. It was demonstrated through full-scale tests on 6m span portal frame buildings that the resistance and stiffness values obtained through component tests can be successfully applied to model the behaviour of the full structure. The analytical method of simulating the behaviour of a full-scale frame using beam elements and springs has been demonstrated.

7. The importance of modelling the resistance and stiffness of the frame sheeting has been highlighted. The typical 2D design method, based on the analysis of intermediate and gable frames separately, misrepresents the 'true' behaviour of the clad building. It was found that accounting for the sheeting can result in a saving of as much as 40% in the steelwork used for main members. It was shown that the cladding stiffness cannot be ignored in practice as the loading attracted to the gables may be under-estimated by over three times. This has an important effect on the gable frames which are usually designed for a wind load acting on half a bay according to bare

frame model. In order for a 2D design to be used safely, horizontal deflection limits more stringent than those recommended by the Steel Construction Institute (SCI) should be adopted or alternatively, the horizontal forces acting on the gables should be increased by a factor of four.

8. A simple analytical method for predicting the behaviour of clad portal frame buildings was successfully developed. This method should now be implemented in the industry in order to provide lighter and better structures. It was also shown that generic serviceability deflection limits for horizontal deflections do not always protect light-gauge frames from local failure. The presented analysis method, including diaphragm action, can be implemented in design software for portal frames of 'typical' geometry, whilst 3D beam idealisation is recommended for bespoke designs. The findings from the research are currently being implemented into the industrial partner design software, so the effect of the stressed skin-action combined with semi-rigid joints can offer lighter and fit-for-purpose cold-formed steel portal buildings.

9. The work presented here contributed to following journal publications:

- WRZESIEN, A. M., LIM, J. B. P. & NETHERCOT, D. A. 2012a. Optimum joint detail for a general cold-formed steel portal frame. *Advances in Structural Engineering,* 15**,** 1623-1639.

- JOHNSTON, R. P., WRZESIEN, A. M., LIM, J. B. P., SONEBI, M. & ARMSTRONG, C. G. 2013. The effect of semi-rigid joints on the design of cold-formed steel portal frame structures. *Civil and Environmental Research,* 5**,** 1-5.

- JOHNSTON, R. P. D., SONEBI, M., LIM, J. B. P., ARMSTRONG, C. G., WRZESIEN, A. M., ABDELAL, G. & HU, Y. 2015. The Collapse Behaviour of Cold-formed Steel Portal Frames at Elevated Temperatures. *Journal of Structural Fire Engineering,* 6**,** 77-101.

- PHAN, D. T., LIM, J. B. P., TANYIMBOH, T. T., WRZESIEN, A. M., SHA, W. & LAWSON, R. M. 2015. Optimal design of cold-formed steel portal frames for stressed-skin action using genetic algorithm. *Engineering Structures,* 93**,** 36-49.

162

- WRZESIEN, A. M., LIM, J. B. P., XU, Y., MACLEOD, I. A. & LAWSON, R. M. 2015. Effect of stressed skin action on the behaviour of cold-formed steel portal frames. *Engineering Structures,* 105**,** 123-136.

- WRZESIEN, A. M., PHAN, D. T., LIM, J. B. P., LAU, H.-H., HAJIRASOULIHA, I. & TAN, C. S. 2016. Effect of stressed-skin action on optimal design of cold-formed steel square and rectangular-shaped portal frame buildings. *International Journal of Steel Structures,* 16**,** 299-307.

- LIM, J. B. P., WRZESIEN, A. M. & NETHERCOT, D. A. 2016b. Sustainable applications of cold-formed steel structures: Portal frames. *In:* YU, C. (ed.) *Recent Trends in Cold-Formed Steel Construction.* 1st ed. Sawston, UK: Woodhead Publishing.

- UZZAMAN, A., WRZESIEN, A. M., LIM, J. B. P., HAMILTON, R. & NASH, D. 2016. Design of Top-hat Purlins for Cold-formed Steel Portal Frames. *Structures,* 7**,** 113-125.

6.8   Future work

Further work could focus on developing a simple method which allows estimating a 'true' tributary area for gable frame design based on number of bays, horizontal stiffness of internal frame, gable frame and roof sheeting. This method will allow designers to conservatively ignore the inherent strength and stiffness of metal cladding in 2D design. It would also estimate additional axial load in the edge purlin/beam due to stressed skin action which is currently ignored in bare frame design.

As grades of steel higher than typical S 280 are widely available now, steel structures will continue losing their inherent stiffness as thinner steel plates offer similar strengths. Although the effect of joint rotational stiffness on the structural modelling was acknowledged by BS EN 1993-1-8 (2005) these rules should be extended to other applications such as design of axially loaded bolted members (i.e. truss members). The joint stiffness should be included in modelling of the structural systems so load redistribution is not overlooked when joint stiffness is less than member stiffness. Future work could therefore focus on popularising existing methods for estimation of the joint stiffness due to bearing of the fastener and validating them against large library of test data published to date. With almost 20 different researches on CFS moment-resisting joint it is time that conclusive design

method is developed and implemented into design guides. Most recent CFS design manual by Dubina et al. (2012) although presents work example on the design of structural members in portal frame, offers no guidance on the joint design.

Component tests show that axial stiffness of lapped bolted joint is not very linear which raises question is the behaviour 'truly' elastic or should stiffness degradation be expected under cyclic loading. The method of quantifying the effect of friction between galvanized plates should be also developed so initial slip stiffness can be calculated and incorporated into analysis models to prevent load redistribution.

Further work could lead to replacing the existing generic deflection limits by more advanced stressed skin analysis in which the behaviour of sheeting panel is accurately predicted. The existing design code for stressed skin design need to be updated to modern roof construction so shear characteristic of the sheeting panel can be calculated more accurately. This will give a designer a tool to calculate relative horizontal deflection to 'suit the characteristic of the particular cladding' (NA to BS EN 1993-1-1 (2005). The focus will therefore be placed on improving existing design methods to modern top-hat purlins, thinner sheeting profiles (0.5mm or less) and composite panels.

7   APPENDICES

APPENDIX A.   Lap bolted joints

A.1   Introductory remarks

The previous research by Zadanfarrokh and Bryan (1992) and Dubina and Zaharia (2006) highlighted the importance of considering the stiffness of the bolted joints in light gauge steel design. This important factor however is not highlighted by existing design codes which put emphasis on the strength of light gauge steel bolted joints rather than their stiffness. As an effect of such approach when designing cold-formed steel systems such as frames or trusses the force redistribution will not be captured if the stiffness of the member only rather than equivalent stiffness is modelled. The equivalent stiffness can be demonstrated based on the axially loaded member bolted at the end. Such arrangement should be modelled by two springs in series as and the equivalent stiffness should be calculated from Equation (7-1):

$$k_{eq} = \frac{k_{b,j} k_m}{k_{b,j} + k_m} \qquad (7\text{-}1)$$

where:

$k_{b,j}$ – axial stiffness of the bolted connection due to bolt bearing (kN/mm)

k_m – axial stiffness of the member (kN/mm)

The approach adopted by previous authors focused on tests on two steel pieces connected by a single bolt (single lap joint). As a result of these studies both authors proposed analytical formulas Eq.   (2-1) and Eq. (2-2) predicting the stiffness of the single lap bolted joint. These formulas however have their limitation due to the complexity of the problem and the range of validity for both is summarised in Table 7-1. The lap joints tested under this study are similar to these investigated by the Zadanfarrokh and Bryan (1992) with two main differences:

1) The torque is not applied in order to obtain lower bound values of the bearing resistance. As the effect of friction is very problematic in terms of FEA modelling the 'frictionless' joint were tested instead so 'pure bearing' resistance can be investigated in the future.

2) Double lap joints (composed of four plates) as well as single lap joints (composed of two plates) were tested, so the difference in the behaviour can be investigated.

Knowing the force-displacement relationship will not only allow the validation of the analytical equations but the research methodology previously described can be employed in developing the stiffness model for the proposed moment resisting joint that has bolts in the web and the flange of the channel section.

Table 7-1 Range of validity of the existing design equation

Investigated features	Range of validity		Proposed features
	Zadanfarrokh and Bryan (1992)	Dubina and Zaharia (2006)	
Single lap joint	Yes	Yes	Yes
Double lap joint	No	No	Yes
Plates thicknesses	$t_1 \leq 8mm$; $t_2 \leq 8mm$	$2 \leq t_1$; $t_2 \leq 4mm$	$t_1=2mm$, $t_2=3mm$
Bolt diameter	M16	M8 to M16	M16
Bolt hole tolerance	2mm	1mm	2mm
Torque	T= 65Nm	Hand tightened using typical spanner	Finger tightened T≈ 0 Nm
Position of the shear plane on the bolts	Threaded portion	Threaded portion	Threaded portion
Joint in tension	Yes	Yes	Yes

A.2   Test arrangements

The test arrangement used was similar to this proposed by Zadanfarrokh and Bryan (1992) and is shown in Figure 7-1 for both single and double lap joint. The Denison universal tensile machine was used to apply the load at an approximate rate of 1kN/min. The displacement was measured by two displacement transducers located on both sides of the bolt connected with the data logger, saving the displacement at 0.5kN load increments. The loading was stopped when the value of

the tension force reached 40kN for the single lap and 70kN for the double lap joint respectively. These values are approximately equal to the bearing resistance of investigated joints calculated to BS EN 1993-1-3 (2006). Only two thicknesses of the plates were considered to emulate the joint between the 2mm thick section and the 3mm thick bracket in both single and double lap joint arrangement. For this reason the plates were also provided with stiffeners to prevent the end of the flat plate from curling. Such behaviour would not be expected in a full-scale joint. Standard ISO Metric Black M16 bolts Grade 8.8 to BS 4190:2014 (2014) with coarse thread pitch of 2mm were used. The washers top and bottom were also used following the industry standard for cold-formed steel joint assembly. A summary of the tested components is presented in Table 7-2. Coupon tests were not conducted since emphasis was placed on the joint stiffness. The test specimens however, were manufactured from the same batch of steel as the components of the joint and full-scale tests; thus the average measured yield and ultimate tensile strength obtained for this batch of steel was used.

a) single lap joint   b) double lap joint   c) transducers arrangement
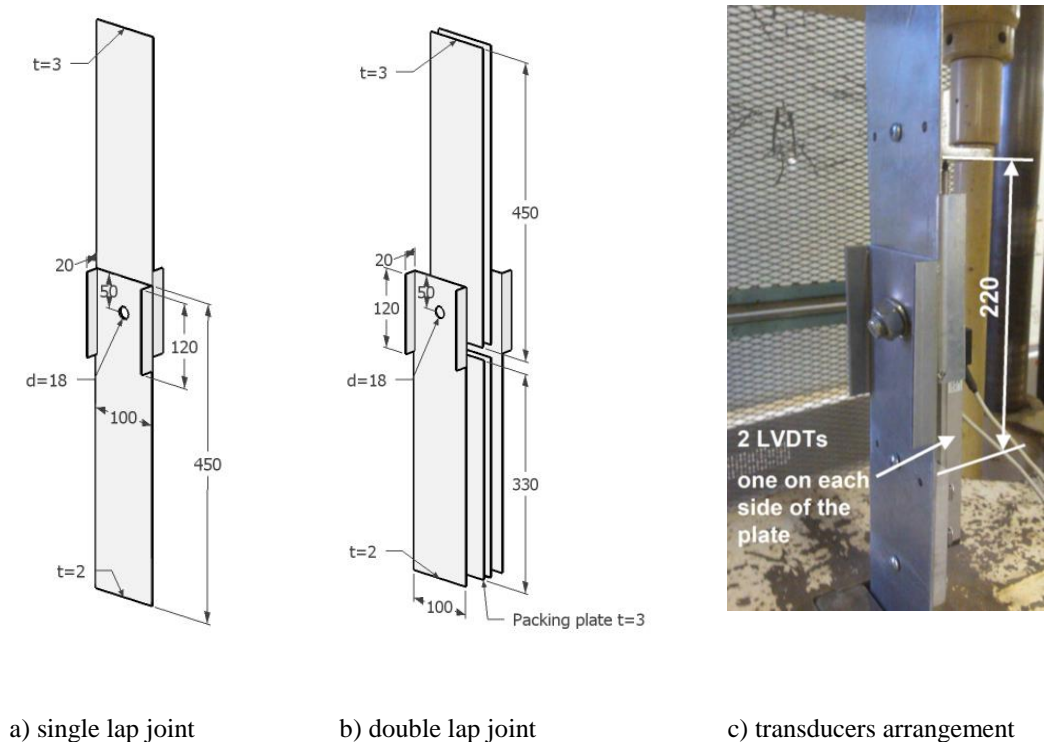
Figure 7-1 Test arrangement for single and double lap joint

Table 7-2 Summary of tested components

Test series	No. of tests	Steel pieces					Fastener		
		Grade of steel – thicker piece	t_2	Grade of steel – thinner piece	t_1		Type	d_w	t_w
			mm		mm			mm	mm
S1/3.0/2.0	3	S350GD +Z275	3.0	S350GD +Z275	2.0		M16	30	2.7
D2/3.0/2.0	3	S350GD +Z275	3.0	S350GD +Z275	2.0		M16	30	2.7

d_w – diameter of the washer, t_w – thickness of the washer

A.3   Test results

In case of bolted joints with oversized holes Zadanfarrokh and Bryan (1992) highlighted the importance of separating the initial slip due rigid body movement of the bolt in the oversized hole from the working extension due the bearing of the bolt into the steel plate. The serviceability requirement of the maximum working extension of 3mm was also included according to ECCS TC7 TWG 7.10 No.124 (2009). The experimental bearing resistance of the joint was taken as a maximum test load (F_T) within 3mm working extension according to Figure 7-2. In this figure one of the experimental load-extension relationships of the single lap joint is presented. The relationship is non-linear thus for simplification each experimental curve is converted into a bi-linear model as shown in the Figure 7-2. The characteristic bearing resistance of the joint was calculated according to the equation:

$$F_k = F_m - kSD \qquad (7\text{-}2)$$

Where:

F_m – mean value of the experimental bearing resistance $F_{max,1}…F_{max,i}$

$k = 3.15$ - coefficient based on three tests BS 5950-9 (1994a) pp. 60

SD – standard deviation
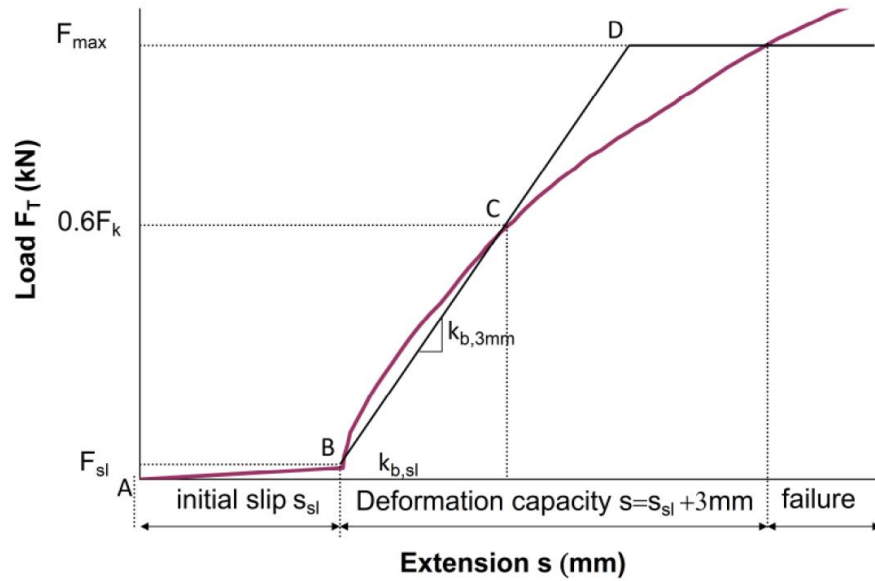
Figure 7-2 Evaluation of test results into bi-linear stiffness model including ECCS failure criterion

Table 7-3 Bearing resistance experimental versus current design code

Test series	Sheet thicknesses excluding coating		Average mechanical properties of steel		Experimental Bearing resistance (3mm extension limit)	Analytical Bearing resistance	Ratio $F_{b,EC3}/F_k$
	$t_{2,cor}$	$t_{1.cor}$	f_y	f_u	F_k	$F_{b,EC3}$	
	mm	mm	N/mm^2	N/mm^2	kN	kN	
S1/3.0/2.0	2.96	1.96	395	502	22.00	39.36	1.79
D2/3.0/2.0	2.96	1.96	395	502	52.57	78.72	1.50

The test results evaluated to ECCS TC7 No. 21 (1990) have been listed for each test series in Table 7-3. In the same table the analytical predictions of bearing resistances according to BS EN 1993-1-3 (2006) with partial safety factor γ_{M2} equal to 1 (characteristic value) are also presented. As can be seen in Table 7-3, the ultimate resistance of the connection with the inclusion of the deformation limit of 3mm is significantly lower than the capacity estimated from the design code. This is because

the EC3 equation predicts ultimate bearing resistance and places different deformation limits, if any, in comparison with the ECCS approach. The shear flexibility of the joint (s_h) is derived at the point of the maximum service load according to ECCS TC7 No. 21 (1990):

$$s_h = \text{mean } (s_1/0.6F_k, \dots s_i/0.6F_k) \tag{7-3}$$

Where:

F_k - characteristic tearing resistance of a fastener

$s_{1\dots i}$ – the extension measure at $0.6F_k$ for each individual test

As shown in Figure 7-2 the shear stiffness value depends on the data evaluation approach as the load-extension relationship is non-linear. The experimental shear stiffness ($k_{b,exp}$) values for both single and double lap joints are presented in Table 7-4 (cross-referenced with Figure 7-2) and are compared against analytical methods described in section A.1 and Eq. (2-1) and (2-2). The experimental stiffness ($k_{b,exp}$) was calculated as the gradient of the load-extension relationship ($k_{b,3mm}$) shown in Figure 7-2 divided by 2. The average displacement due to slip (s_{sl}) was recorded in Table 7-4 and the equivalent stiffness of the joint in the slip stage ($k_{b,sl}$) was also evaluated and presented in the same table.

Since the analytical methods provide guidance only for a single lap joint, in the case of the double lap joint the full symmetry assumption was considered thus the resistance and stiffness of the single lap joint was multiplied by 2.

Figure 7-3 present the typical modes of failure observed during the tests for the single and double lap joints. Due to the eccentricity of the load in the single lap joint, elongation of the holes along with bolt tilting was observed as shown in Figure 7-3a. Unlike in single lap joint, the double lap joint failed in pure bearing of the bolt on the steel plate (see Figure 7-3b)

Table 7-4 Shear stiffness of the joint - experimental versus analytical approach

Test series	Experimental			Analytical			
	s_{sl}	$k_{b,sl}$	$k_{b,exp}$	$k_{b,Zad}$	$k_{b,Zad}$ / $k_{b,exp}$	$k_{b,Zah}$	$k_{b,Zah}$ / $k_{b,exp}$
	mm	kN/mm	kN/mm	kN/mm		kN/mm	
S1/3.0/2.0	2.70	0.19	5.58	6.32	1.13	8.59	1.54
D2/3.0/2.0	1.61	3.10	11.06	12.64	1.14	17.18	1.55
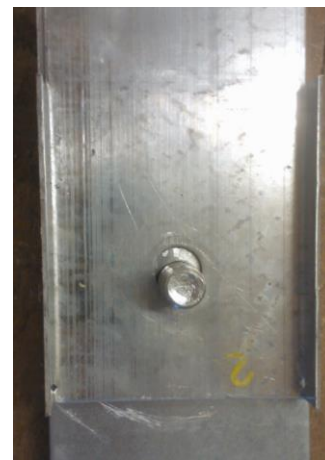
a) Single lap joint   b) Double lap joint

Figure 7-3 Bearing modes of failures

A.4 Concluding remarks

The fundamental difference between the behaviour of the single lap joint and double lap joint is that the first is influenced by two phenomena: bolt bearing and bolt tilting. In two set of test results however there was no significant difference in terms of shear stiffness as the stiffness of the double lap was almost twice of the stiffness of the single lap. The Figure 7-4 presents test results for both single and double lap joint test series, each series containing 3 tests. For predicting the stiffness of a lap joint, both in terms of range of validity and the accuracy, the analytical

method proposed by Zadanfarrokh and Bryan (1992) proved to be acceptable (see Eq. (2-1) and n=5) and was plotted on the experimental load-extension curve in Figure 7-3, denoted as ANL(Zad). The ultimate joint resistance was also estimated according to BS EN 1993-1-3 (2006) and was plotted in the Figure 7-4 for comparison against the experimental data (denoted as ANL(EC3)). As can be seen in Figure 7-4, incorporating the EC3 joint resistance in the design will allow very large non-linear extension, which should be considered in the force analysis of the structural system, as it can lead to force redistribution. For this reason the ECCS method to limit the working extension of such joints was considered and the joint resistance based on 3mm extension was also marked in Figure 7-4, denoted EXP (ECCS).

As presented in Figure 7-4a the test results shows that the EC3 design equation offers safe prediction of the ultimate bearing resistance of the investigated single lap joint. In the case of the double lap joint however the common design practice is to increase the capacity by 2 since design codes do not differentiate these two cases. The test results show (see Figure 7-4b) that such assumption is incorrect as the double lap joint failed to reach twice the capacity of the single lap joint. It is therefore recommended that test bolt bearing capacity of double lap joints is used in the design.
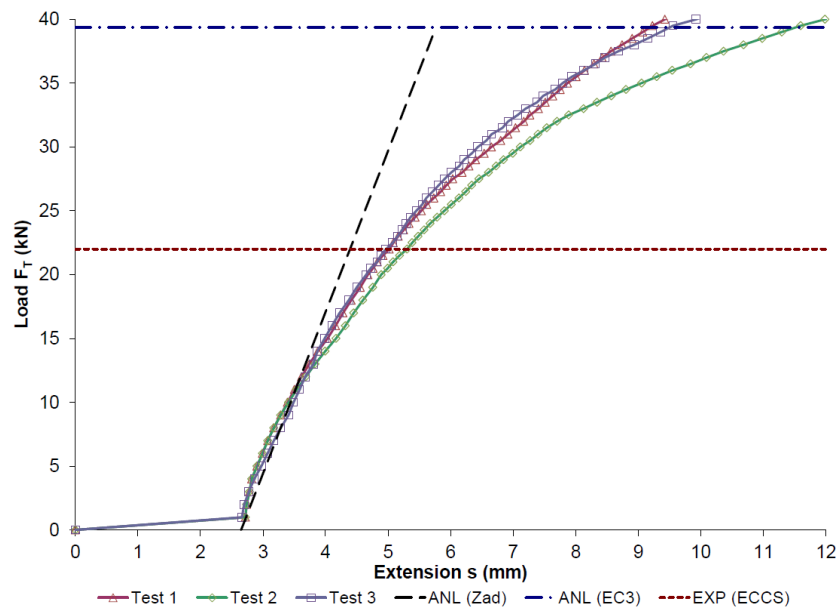
a) Single lap joint
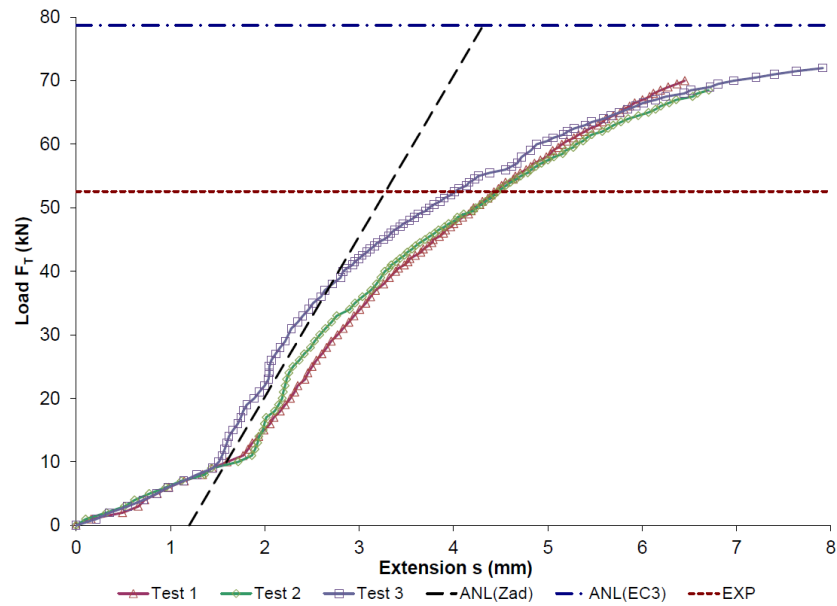
b) Double lap joint

Figure 7-4 Load - extension relationship

In order to ensure that the effect of friction, on the shear resistance of the joints, was minimised, very little torque was applied to the joint. In practice, cold-formed steel joints are not classified as torque controlled joints, due to the very low friction coefficient.   As can be seen in Figure 7-4, the slip load F_{sl} was almost reduced to 0 in the single lap finger tight joint but in the double lap joint composed of four plies the average slip load recorded was around 10kN.

In terms of predicting stiffness of such joints two distinctive behaviours are observed:

1) Slip due to rigid body movement of the bolt shank into the oversized hole (see Figure 7-4),

2) Bearing of the bolt shank into the steel plate.

Slip is a very complex phenomenon which can be treated as a stochastic problem. Theoretically the maximum slip extension in the lap joint is twice the bolt hole clearance. It was observed during the experiments that the slip extension never reached the maximum of 4mm and in the case of the double lap joint was significantly lower than the single lap joint (see Table 7-4). Based on the

experimental data use of a slip extension equal to hole tolerance is therefore recommended.

The test results have also shown that, when past the slip stage of loading (see Table 7-4), the stiffness of the double lap joint is twice that of the stiffness of the single lap. As shown in Figure 7-4 the ECCS recommendations not only allow safe prediction of lap joints but also limit the working extension to the region in which the stiffness is much more linear. It is therefore recommended that this recommendation is used in lap joint design assisted by testing.

APPENDIX B. Analysis models for practical design

B.1   Analytical methods of predicting the rotational stiffness of the joints

For joints types A, B and C, the elastic bolt-group design method was used in order to establish the centre of the rotation. The fundamental assumption of the method is that the level of force in the bolt is proportional to the distance between the bolt and the centre of the rotation. The centre of the rotation is therefore established based on this assumption and static equilibrium of bending moment, longitudinal forces (F_x) and transverse forces (F_y) (see Eq. (7-4)).

In order to develop an analytical model representing the behaviour of a joint with bolts in the web and bolts in the flange, the following assumptions were made:

1) The linear stiffness of the springs representing the web bolt ($k_{b,w}$) are equal in longitudinal and transverse directions,

2) Once the bolt is in contact with the steel plate, the linear stiffness of the spring representing the flange bolt (single lap joint) is assumed to be half of that representing a web bolt (double lap joint) according to Section A.3; thus if a single channel is considered the $k_{b,f} = k_{b,w} = k_b$,

3) The bracket stiffener is in contact with the flange of the member. This prevents free rotation at the joint therefore the linear slip allowed was assumed as 1mm (half of the hole tolerance)

4) In Model 1 the flange bolts are engaged in carrying the loads and the transverse stiffness of the sections flange of 2mm thickness is neglected in the analysis thus flange bolts are only able to carry longitudinal forces (see Figure 7-5); this model represents an upper bound of joint stiffness

5) In Model 2 the flange bolts are not included in carrying the loads as it was shown in Section A.3 that single lap joints may have greater initial slip; this model represents a lower bound of joint stiffness,

6) The value of linear stiffness (k_b) was assumed as 11.06 kN/mm according to Table 7-4

7) The symmetry of the joint about the y axis was considered thus the x coordinate of the centre of the rotation (cor) was assumed as half of the bolt-group length (a_{bg})

Based on these assumptions, the analytical models including the contribution of the flange bolts (Model 1) are shown in Figure 7-5. When the flange bolts are not engaged in carrying the load (Model 2, F_f=0), the centre of the rotation is shifted down and the centre of rotation coincides with the centre of gravity of the bolt-group.
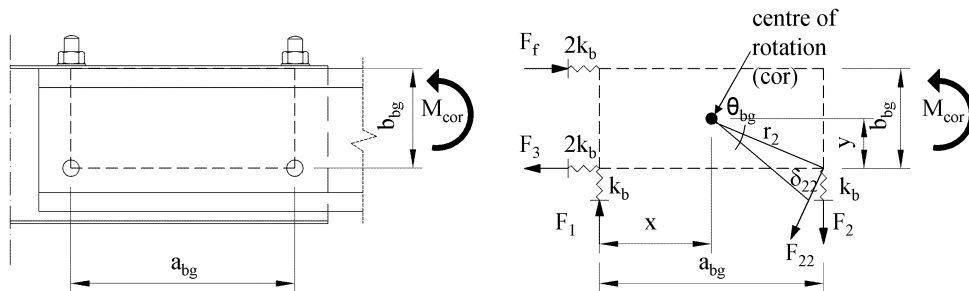
a) Joint type A -2x1 bolt array
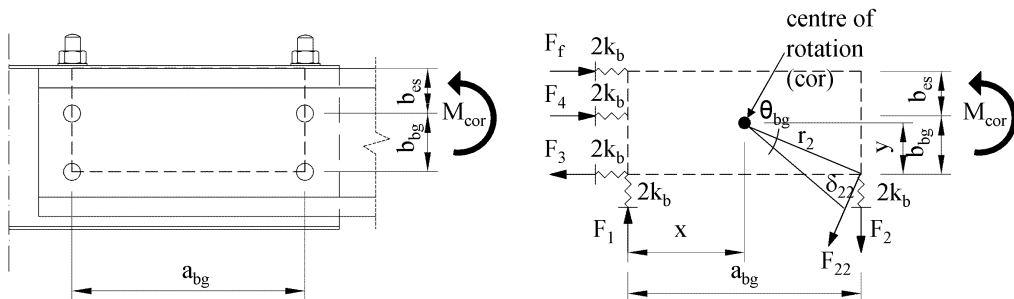
b) Joint type B – 2x2 bolt array

175
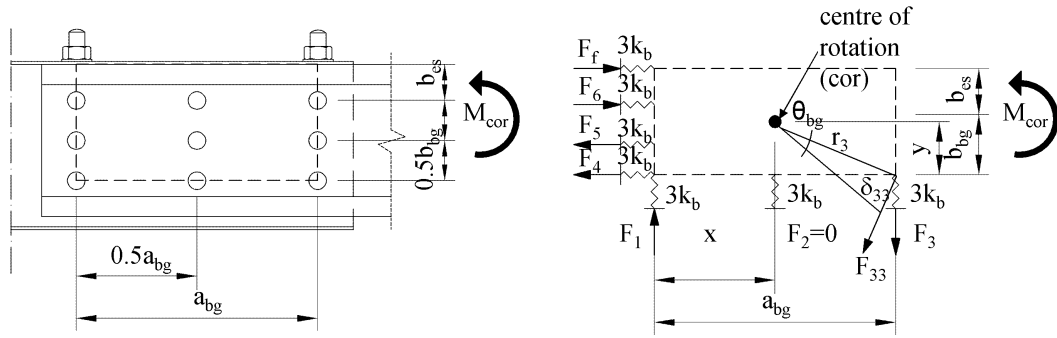
b) Joint type C – 3x3 bolt array

Figure 7-5 Joints behaviour analytical models including contribution of the flange bolts

In order to work out the location of the centre of rotation (cor) and forces in each row of bolts a set of equations was assembled according to Figure 7-5a:

$$\left[F_1 x + F_2 \left(x - a_{bg}\right)\right] + \left[F_3 y + F_f \left(y - b_{bg}\right)\right] = M_{cor} \tag{7-4}$$

$$F_1 + F_2 = 0$$

$$F_3 + F_f = 0$$

$$\frac{F_1}{x} = \frac{F_2}{(x - a_{bg})}$$

$$\frac{F_3}{y} = \frac{2F_2}{(x - a_{bg})}$$

$$\frac{F_3}{y} = \frac{F_f}{(y - b_{bg})}$$

where:

$F_{1...1}$, F_f – forces in the relevant lines of bolts according to Figure 7-5, Table 7-6 and Table 7-7

x,y – distances to the centre of the rotation bolts according to Figure 7-5

176

a_{bg}, b_{bg} – length and width of the bolt-group according to Figure 7-5

b_{es} – distance between flange a web line of bolts according to Figure 7-5

k_b – linear bearing stiffness of the single bolt in shear

Analogically similar set of equations were assembled for the 2x2 and 3x3 bolt array (see Figure 7-5b and Figure 7-5c respectively). The solutions including locations of centres of rotations (cor) and forces in each line of bolts are presented in Table 7-8 and Table 7-9 respectively for the upper and lower bound models. The rotational stiffness formulas were also worked out for each bolt array according to Equation (7-5) and are presented in Table 7-5.

$$S_{j,ini} = M_{cor}/\theta_{bg} \tag{7-5}$$

Where:

M_{cor} – bending moment about the centre of the rotation

$\theta_{bg} = \delta_i/r_i$ – angle of the rotation according to Figure 7-5

For each stiffness model these formulas are presented in Table 7-5

Table 7-5 Model 1 and Model 2 – rotational stiffness formulas for joints type A, B and C

Joint configuration	Rotational stiffness according to Model 1 $S_{j,ini,1}$	Rotational stiffness according to Model 2 $S_{j,ini,2}$
2x1 bolt array	$\dfrac{\left(a_{bg}^2 + 2b_{bg}^2\right)k_b}{2}$	$\dfrac{a_{bg}^2 k_b}{2}$
2x2 bolt array	$\dfrac{\left(3a_{bg}^2 + 4b_{bg}^2 + 4b_{bg}b_{es} + 4b_{es}^2\right)k_b}{3}$	$\left(a_{bg}^2 + b_{bg}^2\right)k_b$
3x3 bolt array	$\dfrac{3\left(8a_{bg}^2 + 11b_{bg}^2 + 12b_{bg}b_{es} + 12b_{es}^2\right)k_b}{16}$	$\dfrac{3\left(a_{bg}^2 + b_{bg}^2\right)}{2}k_b$

Table 7-6 Joints types A,B and C with flange bolts contribution (Model 1) – design formulas

Notation (Figure 7-5)	2x1 bolt array	2x2 bolt array	3x3 bolt array
x	$\dfrac{a_{bg}}{2}$	$\dfrac{a_{bg}}{2}$	$\dfrac{a_{bg}}{2}$
y	$\dfrac{b_{bg}}{2}$	$\dfrac{2b_{bg}}{3}+\dfrac{b_{es}}{3}$	$\dfrac{5b_{bg}}{8}+\dfrac{b_{es}}{4}$
F_1	$\dfrac{M_{cor}a_{bg}}{a_{bg}^{2}+2b_{bg}^{2}}$	$\dfrac{3M_{cor}a_{bg}}{3a_{bg}^{2}+4\left(b_{bg}^{2}+b_{bg}b_{es}+b_{es}^{2}\right)}$	$\dfrac{8M_{cor}a_{bg}}{8a_{bg}^{2}+11b_{bg}^{2}+12\left(b_{bg}b_{es}+b_{es}^{2}\right)}$
F_2	$\dfrac{M_{cor}a_{bg}}{a_{bg}^{2}+2b_{bg}^{2}}$	$\dfrac{3M_{cor}a_{bg}}{3a_{bg}^{2}+4\left(b_{bg}^{2}+b_{bg}b_{es}+b_{es}^{2}\right)}$	0
F_3	$\dfrac{2M_{cor}b_{bg}}{a_{bg}^{2}+2b_{bg}^{2}}$	$\dfrac{2M_{cor}\left(2b_{bg}+b_{es}\right)}{3a_{bg}^{2}+4\left(b_{bg}^{2}+b_{bg}b_{es}+b_{es}^{2}\right)}$	$\dfrac{8M_{cor}a_{bg}}{8a_{bg}^{2}+11b_{bg}^{2}+12\left(b_{bg}b_{es}+b_{es}^{2}\right)}$
F_4	$\dfrac{2M_{cor}b_{bg}}{a_{bg}^{2}+2b_{bg}^{2}}$	$\dfrac{2M_{cor}\left(b_{bg}-b_{es}\right)}{3a_{bg}^{2}+4\left(b_{bg}^{2}+b_{bg}b_{es}+b_{es}^{2}\right)}$	$\dfrac{10M_{cor}\left(b_{bg}+0.4b_{es}\right)}{8a_{bg}^{2}+11b_{bg}^{2}+12\left(b_{bg}b_{es}+b_{es}^{2}\right)}$
F_5	-	-	$\dfrac{2M_{cor}\left(b_{bg}+2b_{es}\right)}{8a_{bg}^{2}+11b_{bg}^{2}+12\left(b_{bg}b_{es}+b_{es}^{2}\right)}$
F_6	-	-	$\dfrac{2M_{cor}\left(3b_{bg}-2b_{es}\right)}{8a_{bg}^{2}+11b_{bg}^{2}+12\left(b_{bg}b_{es}+b_{es}^{2}\right)}$
F_f	$\dfrac{2M_{cor}b_{bg}}{a_{bg}^{2}+2b_{bg}^{2}}$	$\dfrac{2M_{cor}\left(b_{bg}+2b_{es}\right)}{3a_{bg}^{2}+4\left(b_{bg}^{2}+b_{bg}b_{es}+b_{es}^{2}\right)}$	$\dfrac{6M_{cor}\left(b_{bg}+2b_{es}\right)}{8a_{bg}^{2}+11b_{bg}^{2}+12\left(b_{bg}b_{es}+b_{es}^{2}\right)}$

Table 7-7 Joints type A,B and C without flange bolts contribution (Model 2) – design formulas

Notation (Figure 7-5)	2x1 bolt array	2x2 bolt array	3x3 bolt array
x	$\dfrac{a_{bg}}{2}$	$\dfrac{a_{bg}}{2}$	$\dfrac{a_{bg}}{2}$
y	$\dfrac{b_{bg}}{2}$	$\dfrac{b_{bg}}{2}$	$\dfrac{b_{bg}}{2}$
F_1	$\dfrac{M_{cor}}{a_{bg}}$	$\dfrac{M_{cor}a_{bg}}{a_{bg}^2 + b_{bg}^2}$	$\dfrac{M_{cor}a_{bg}}{a_{bg}^2 + b_{bg}^2}$
F_2	$\dfrac{M_{cor}}{a_{bg}}$	$\dfrac{M_{cor}a_{bg}}{a_{bg}^2 + b_{bg}^2}$	0
F_3	-	$\dfrac{M_{cor}b_{bg}}{a_{bg}^2 + b_{bg}^2}$	$\dfrac{M_{cor}a_{bg}}{a_{bg}^2 + b_{bg}^2}$
F_4	-	$\dfrac{M_{cor}b_{bg}}{a_{bg}^2 + b_{bg}^2}$	$\dfrac{M_{cor}b_{bg}}{a_{bg}^2 + b_{bg}^2}$
F_5	-	-	0
F_6	-	-	$\dfrac{M_{cor}b_{bg}}{a_{bg}^2 + b_{bg}^2}$
F_f	0	0	0

B.2   Analytical methods for predicting ultimate strength of the joints

Two main criteria have to be considered when designing cold-formed steel joints. First of all, bearing capacity of the thin plate cannot be reached and local buckling of the plate under concentrated forces from bolts must be prevented.

The design equations for predicting the bearing capacity of the plate $F_{b,Rd}$ could be found either in BS 5950-5 (1998b) or in BS EN 1993-1-3 (2006) and the maximum force $F_{i,max}$ in the farthest bolt must be less than the calculated bearing capacity of the plate to satisfy Equation (7-6):

$$F_{i,max} / F_{b,Rd} \leq 1 \qquad (7-6)$$

In Section 2.5.8 it is shown that this design criterion rarely governs the design since reaching the bearing capacity of the plate would result in unacceptable joint rotation.

The design codes also offer little guidance regarding an analysis method for preventing local web buckling mode of failure. The following analytical methods were reported in the literature:

1) Lim and Nethercot (2003b) conducted extensive parametric study based on finite element shell model, which was calibrated against four tests on 3x3 bolt array of the same width and different lengths of the bolt-group. Investigated joints consisted web bolt only. As a result following design equation was proposed:

$$M_{j,Lim}/M_{cy,BS} = \alpha \ln(a_{bg}/D) + \beta \qquad (7-7)$$

Where:

$M_{j,Lim}$ – ultimate bending capacity of joint type A,

$M_{cy,BS}$ – bending resistance of double channel section according to BS 5950-5 (1998b),

a_{bg} – bolt-group length

D – depth of the channel section

α, β - parameters

2) Yu et al. (2005) proposed a design method based on using a quadratic interaction equation for combination of shear and bending. The Effective Width Method was used for predicting bending capacity of the channel

section $M_{cy,BS}$ according to BS 5950-5 (1998b) and a modified equation for critical shear buckling stress was proposed:

$$(M_{Ed}/M_{cy,BS})^2 + (V_{Ed}/V_{c,Rd,})^2 \leq 1 \tag{7-8}$$

Where:

$$V_{c,Rd} = q_{cr,Chung} A_V \tag{7-9}$$

$$q_{cr,Chung} = \left(\frac{\pi^2 E}{12(1-\nu^2)}\right) 6.9 \left(\frac{t}{D-t}\right)^2 \tag{7-10}$$

$$A_V = (D - n_v d_o)t \tag{7-11}$$

The force distribution was assumed to be based on a beam idealisation and elastic joint design as presented in Figure 7-6. The critical cross-section lies on the right hand side of the first line of bolts (cross-section 4). The effective cross-section area of the web in shear A_V was reduced by the bolt holes at the critical cross-section;

3) Dubina et al. (2008) proposed an analytical method of predicting the ultimate strength of the bolted joint based on an interaction equation for combination of bending and web crippling (BS EN 1993-1-3 (2006):

$$(M_{Ed}/M_{cy,Rd}) + (F_{Ed}/V_{w,Rd}) \leq 1.25 \tag{7-12}$$

The interaction equation describing the same phenomenon was previously presented in slightly modified form in BS 5950-5 (1998b):

$$(M_{Ed}/M_{cy,BS}) + 1.1(F_{Ed}/V_{w,BS}) \leq 1.50 \tag{7-13}$$

The D/t≈77 ratio of the investigated channel sections lies outside the range of validity for Method 1) (Lim and Nethercot (2003b)) thus it will not be used for the estimation of the bending resistance. In methods 2 and 3 the critical cross-section coincided with the line of bolts closest to the end of the bracket. The maximum bending moment and the maximum transverse force acting on the member in the critical cross-section can be calculated from (e.g. Joint type C and Model 1):

$$M_{Ed} = M_{cor} - \left[\frac{F_4 y + F_5(-0.5b_{bg} + y) + F_6(b_{bg} - y) + F_f(b_{bg} + b_{es} - y)}{3} \right] \qquad (7\text{-}14)$$

Where:

M_{cor} – bending moment about the centre of the rotation (see Figure 7-5c)

$F_4...F_f$ - force in the respective line of bolts according to Figure 7-5c and Table 7-6

$$V_{Ed} = F_{Ed} = F_1 \qquad (7\text{-}15)$$

Where:

F_1 - force in the first line of bolts according to Figure 7-5c and Table 7-6
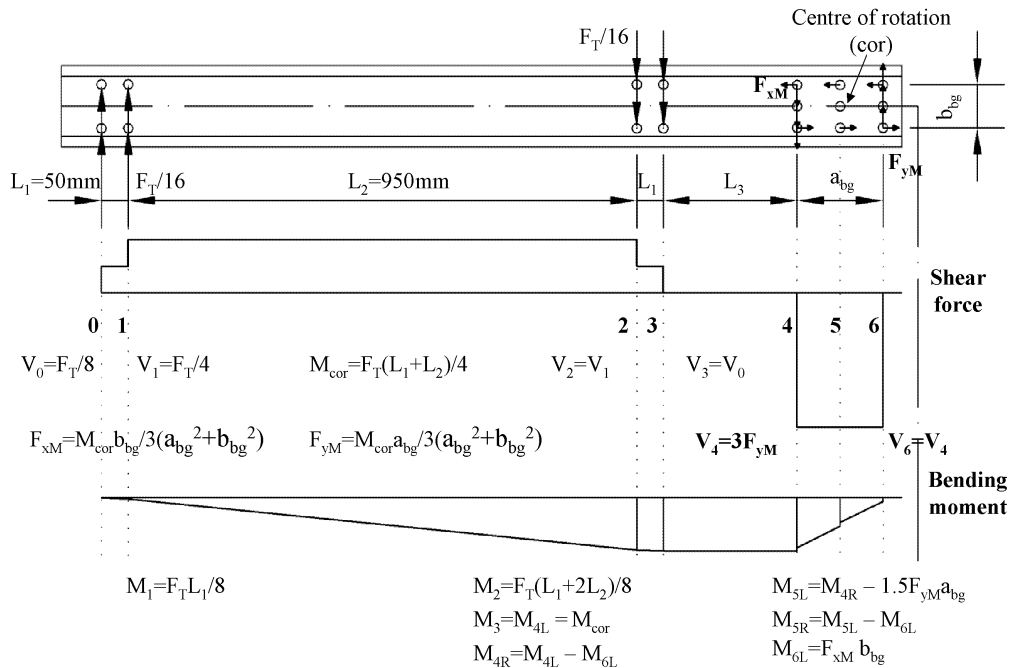
Figure 7-6 Force distribution within the half of the jointed beam considering single channel section (Model 2)

The analytical joint capacities were computed using limit state criteria and design rules according to British Standard (BS) and Eurocode 3 (EC). The relevant limit state design equations are quoted in Table 7-8 and Table 7-9. The ultimate

bending capacity of the continuous member (M_{cy}) is also computed for comparison. The ultimate bending capacity of the tested joint was taken as a minimum of three moment capacities representing the bearing capacity of plate (M_b), combined bending and shear force (M_{BSF}) and combined bending and web crippling (M_{BWC}). The ultimate bending capacity according to Yu et al. (2005) has been also computed ($M_{BSF,Chung}$) and presented in Table 7-8 as it contains a slight modification of the critical shear buckling stress as compared with that adopted by the British Standard.

Tensile coupon tests were carried out to determine the material properties of the channel sections. The tensile coupons were taken from the centre of the flange plate in the longitudinal direction of the untested specimens. The tensile coupons were prepared and tested according to the BS EN 10002-1:2001 (2001). Table 7-8 summarises the yield strength (f_y) taken as the measured static 0.2% proof stress and the ultimate static tensile strength (f_u) for the channel section which first showed signs of failure.

In all tests the combined bending and web crippling design criterion governed the capacity and the values computed to EC3 were significantly lower than those computed to BS.

Table 7-8 Upper bound analytical resistances according to BS 5950-5 (1998b) ultimate limit state design criterions

Test designation	f_y	f_u	$M_{cy,BS}$	$M_{b,BS}$	$M_{BSF,BS}$	$M_{BSF,Chung}$	$M_{BWC,BS}$
				Eq. (7-6)	Eq. (7-8)	Eq. (7-8), (7-9)	Eq.(7-13)
	N/mm^2	N/mm^2	kNm	kNm	kNm	kNm	kNm
T2/A/2x1/d	386	502	21.80	17.50	20.62	20.40	18.26
T3/B/2x2/d	395	501	22.43	30.74	19.20	18.64	16.84
T4/B/2x2/u	398	504	22.35	30.79	19.06	18.56	16.80
T5/C1/3x3/d	397	508	21.78	35.51	17.94	16.67	14.81
T6/C1/3x3/u	393	499	21.60	35.17	17.84	16.60	14.67
T7/C2/3x3/d	403	506	21.98	47.92	18.76	17.71	16.94
T8/C3/3x3/d	395	501	22.25	54.04	19.60	18.70	18.12

Table 7-9 Upper bound analytical resistances according to BS EN 1993-1-3 (2006) ultimate limit state design criterions

Test designation	f_y	f_u	$M_{cy,EC}$	$M_{b,EC}$ Eq. (7-6)	$M_{BSF,EC}$ Eq. (7-8)	$M_{BWC,EC}$ Eq. (7-12)
	N/mm^2	N/mm^2	kNm	kNm	kNm	kNm
T2/A/2x1/d	386	502	21.17	17.96	20.00	16.39
T3/B/2x2/d	395	501	21.71	30.79	19.00	15.16
T4/B/2x2/u	398	504	21.65	30.79	18.86	15.14
T5/C1/3x3/d	397	508	21.22	36.02	17.63	12.90
T6/C1/3x3/u	393	499	21.07	35.34	17.53	12.80
T7/C2/3x3/d	403	506	21.44	47.61	18.46	15.23
T8/C3/3x3/d	395	501	21.56	54.23	19.05	16.15

APPENDIX C. Shear panel test components

C.1   Rafters and purlins

All the primary and secondary structural members used in the experimental study were manufactured in cold-formed processes from hot-dipped galvanized steel sheets. The back-to-back lipped channel section beam of 400mm depth and 3mm thickness was used as a rafter member as presented in Figure 7-7a. The designated name for such beam contains the number of channel sections (i.e. 2C), followed by the depth in millimetres (i.e. 400) and the nominal thickness with one decimal point accuracy (i.e. 30 = 3.0mm thickness). In the case of purlin members, cold-rolled galvanized steel top-hat section of the geometry shown in Figure 7-7b, were used. The designated name of such purlin contains letter TH denoting top-hat sections, followed by the depth in millimetres (i.e. 61) and the nominal thickness with one decimal point accuracy (i.e. 10 = 1.0mm thickness).

Due to the large number of components, coupon tests were not carried out but the Mills Test Certificates were provided by the manufacturer for the particular batch of steel used for rolling the tested components.
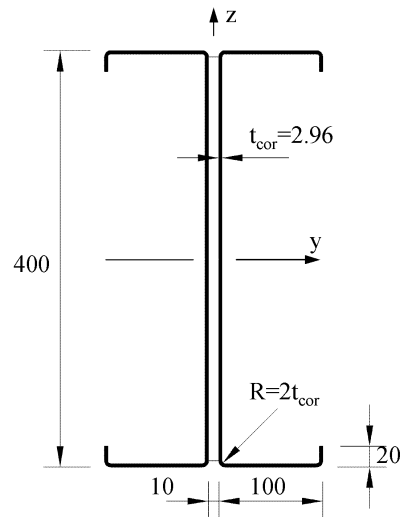
A=36.72cm², Iy=8216.46cm⁴, Iz=657.48cm⁴   A=2.21cm², Iy =12.16cm⁴, I$_z$=26.85cm⁴
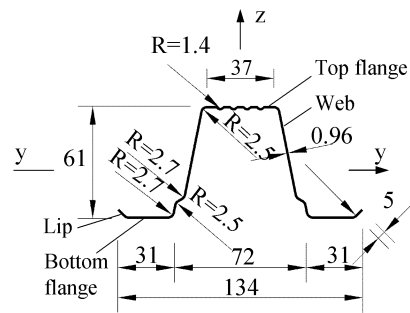
a) Rafter – 2C 40030   b) Top-hat purlin – TH 6110

Figure 7-7 Dimensions of the component cross-sections (mm)

Based on this data, average values of the yield strength ($f_{y,a}$) and the ultimate tensile strength ($f_{u,a}$) were established and are presented in Table 7-10. The grade of steel along with the standard which the steel complies to is also listed in that table. Both the nominal thickness (t) and the thickness excluding the coating (t_{cor}) as well as the nominal yield strength ($f_{y,nom}$) and the nominal ultimate strength ($f_{u,nom}$) are listed in Table 7-10.

Table 7-10 Steel characteristics of the components

Section name	Steel Grade	Specification	t	t_{cor}	$f_{y,nom}$	$f_{u,nom}$	$f_{y,a}$	$f_{u,a}$
			mm	mm	N/mm²	N/mm²	N/mm²	N/mm²
C 40030	S350GD +Z275	BS EN 10326:2004 (2004)	3.0	2.96	350	420	392	496
TH 6110	S550GD +AZ150	BS EN 10326:2004 (2004)	1.0	0.96	550	560	648	655

C.2 Calculated capacity of the top-hat purlin

The capacities of the top-hat purlins used in diaphragm tests were established using the DSM method and free software CUFSM according to Li and Schafer (2010). The elastic critical stresses for local and distortional buckling modes for each type of loading are presented in Table 7-11.

The nominal geometry was used as shown in Figure 7-7b and the appropriate mechanical properties as given in Table 7-10 were also included in the analysis. The results from the buckling analysis carried out using the CUFSM software are summarised in Table 7-11. It was assessed that the elastic critical buckling stresses predicted by the semi-analytical finite strip method (CUFSM) were more accurate that those calculated from Section 5.5.3 of BS EN 1993-1-3 (2006). The effects of local and distortional buckling were considered by calculating effective cross-section properties based on the elastic critical stresses presented in Table 7-11. This analysis was carried out using the Scia Engineer 2012.0 software and the results are presented in Table 7-12 in the form of effective section properties. The nominal cross-section (see Figure 7-7b) was divided into 59 segments, the round corners were idealised by 2 segments, and the swages at the top flange were divided into 6 segments. For the purpose of the standard analysis, the foot and the toe of the top-hat were considered to act as double edge stiffener of the web and the fold in the web was considered as a web intermediate stiffener (see Figure 7-8a).

a) Gross cross-section   b) Effective cross-section
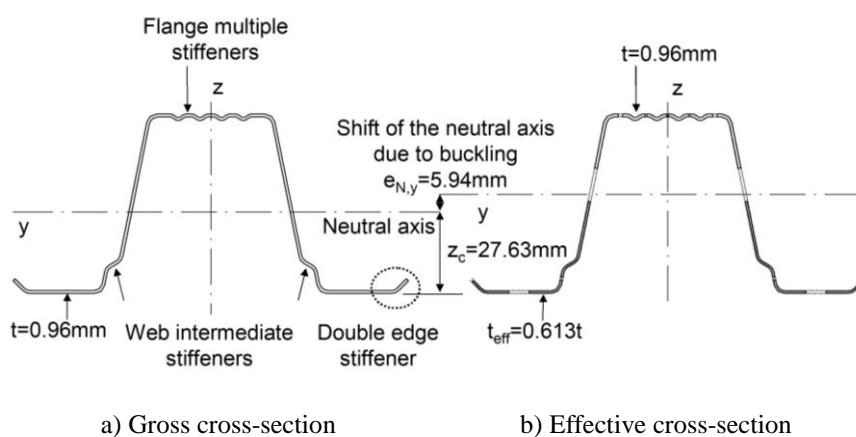
Figure 7-8   Gross and Effective cross-section of TH6110 under the uniformed compression according to EC3

The effective widths of individual segment as well as the effective thickness were calculated by the software in an iterative process. The calculated effective section properties for axial compression (A_{eff}) and effective section modulus (W_{eff}) for bending about the y and z axis, are shown in Table 7-12. The calibration of the analytical method against experimental results and the FEA analysis was published in Uzzaman et al. (2014). According to the EC3 recommendation the effect of the neutral axis shift ($e_{N,y}$) was also considered as shown in Figure 7-8b).

Table 7-11 Elastic critical buckling stresses for TH6110 purlin (after Li and Schafer (2010))

Load case	Local buckling	Distortional buckling
	N/mm^2	N/mm^2
Axial compression	392	397
Moment about the y-y axis top flange in compression (+)	695	2415
Moment about the y-y axis bottom flange in compression (-)	1423	485
Moment about the z-z axis	1055	491

Table 7-12 Gross and effective section properties of TH6110

Section	A	I_y	I_z	I_w	I_t	A_{eff}	$W_{eff,y,+}$	$W_{eff,y,-}$	$W_{eff,z}$
	cm^2	cm^4	cm^4	cm^6	x10^{-4}cm^4	cm^2	cm^3	cm^3	cm^3
TH 6110 (1.69kg/m)	2.21	12.16	26.85	55.88	67.88	1.37	3.48	3.34	3.47

C.3   Sheeting profiles

The test roof panels were chosen to cover the wide range of sheeting profiles offered by the industry. Three different types of sheeting profiles were considered, shown in Figure 7-9. Type 1 is the typical trapezoidal sheeting profile, Type 2 is the trapezoidal sheeting with additional stiffeners of 1mm height rolled into the every trough and Type 3 is the standard sinusoidal corrugated profile. The dimensions of

each profile are presented in Table 7-13. Each sheeting panel was considered in two thicknesses of 0.5 and 0.7mm.
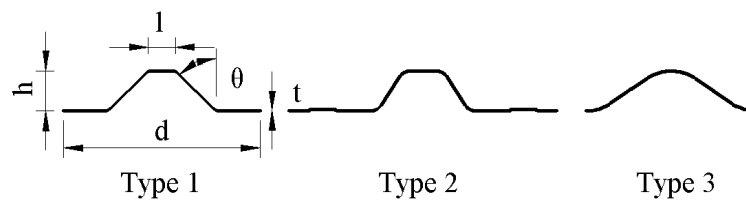
Figure 7-9 Different sheeting profiles

Table 7-13 Sheeting profile dimensions

Profile name	Type (see Figure 7-9)	Height h (mm)	Thickness t (mm)	Pitch d (mm)	Width l (mm)	Angle θ (°)
AS34	1	34	0.5&0.7	167	23	45
AS30	2	30	0.5&0.7	200	30	33
AS24	2	24	0.5&0.7	167	20	34
AS18	3	18	0.5&0.7	76	-	-
AS35/80	Weather skin 2	35	0.5	333	30	25
	Liner skin 1	1	0.4	100	48	45

A rigid composite panel (AS35/80) of the overall thickness of 80mm was also included in the investigation. The composite panel consists of two coated steel profiles, as described in Table 7-13, bonded with the PIR (Polyisocyanurate) insulation core.

Generally three different steel sheets of 0.4, 0.5 and 0.7mm thickness were used to manufacture the investigated sheeting profiles. The 0.4mm thick coil finished with white lining enamel was only used for liner sheets, where 0.5 and 0.7mm thick coil finished with leather-grain embossed PVC (Plastisol), were used for all on the weather sheets. The description of the steel used is presented in Table 7-14 including net thickness of the steel core and mechanical properties of the steel based on the average values obtained from Mills Test Certificates.

Table 7-14 Steel characteristic for the investigated profiles

Steel coil type	Steel Grade	Specification	t	t_{cor}	$f_{y,nom}$	$f_{u,nom}$	f_y	f_u
			mm	mm	N/mm^2	N/mm^2	N/mm^2	N/mm^2
0.4 Lining enamel	S250GD +AS150	BS EN 10154:1996 (1996)	0.4	0.36	250	330	323	397
0.5 Plastisol	S250GD +AZ150	BS EN 10326:2004 (2004)	0.5	0.48	250	330	334	405
0.7 Plastisol	S250GD +AZ150	BS EN 10326:2004 (2004)	0.7	0.65	250	330	301	380

APPENDIX D. Single lap screw connections

Considering that the shear resistance and stiffness of the roof panel is dependent on the ultimate resistance and flexibility of individual connections, this section presents the component tests on connections used in full panel assemblies. All the connections can be classified as single lap screw connections. Parameters such as: thickness of the connected parts, grade of steel, screw diameter, size and type of the washer, are expected to contribute to the performance of such joints. For this reason the analytical study is carried out parallel with the experimental investigation to allow comparisons. In terms of establishing the slip in individual fixings BS 5950-9 (1994a) advises that this parameter should be obtained experimentally for each particular connection.

D.1   Fasteners

The self-drilling, self-tapping screws were used in order to form a variety of joints in the investigated shear roof panels. The screws are classified based on the different joints they are used for and their dimensions are presented in Figure 3-10. Two different diameters are considered: 5.5mm and 6.3mm following the industry standards. All the screws passing through the weather sheets contain metal washers with EPDM rubber seals. The diameter of the washer was 16mm for the single skin sheeting and 19mm for the composite panel. The mechanical characteristics of each

screw including ultimate shear strength ($F_{v,Rd}$) and ultimate tensile strength ($F_{v,Rd}$), as provided by the manufacturer, are presented in Figure 7-10.
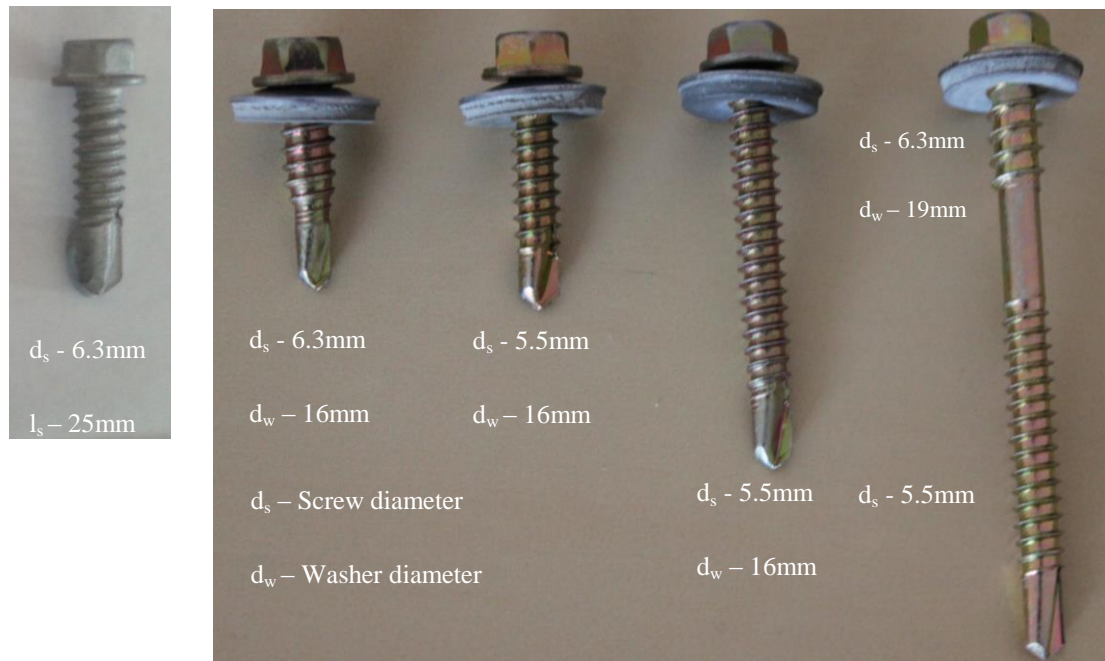
Fv,Rd =8.36kN   Fv,Rd = 12.70kN   Fv,Rd = 8.36kN   Fv,Rd = 8.36kN   Fv,Rd = 8.96kN

Ft,Rd = 14.10kN   Ft,Rd = 17.20kN   Ft,Rd =12.50 kN   Ft,Rd =12.50kN   Ft,Rd = 12.90kN

a)Frame screw   b) Stitching screw   c) Cladding screw   d) Cladding screw – crown fix   e) Composite panel screw

Figure 7-10   Dimensions and mechanical properties of screws

D.2   Different types of connections

In order to use the calculation method to predict the shear flexibility and the shear resistance of the full-scale panel assembly, the shear characteristic of each individual joint was analysed. The investigated panels contain the following single lap connections:

a) Seam connection joining two adjacent sheets through the use of 6.3mm stitching screws (see Figure 7-11a);

b) Cladding/purlin connection joining cladding profile and usually thicker purlin member through the use of 5.5mm diameter screws (see Figure 7-11b);

c) Cladding/purlin – the crown fix connection; the main difference between this joint and the one before is that the eccentricity of the shear force cause extensive tilting of the screw as shown in Figure 7-11c. As a result of this eccentricity, the screw is a cantilever loaded in combined shear and bending. Such a joint was excluded from the lap joint tests due to the difficulties in replicating the real loading conditions using the standard testing apparatus.

d) Composite panel/purlin connection; the same way to the joint described in c), in this case the shear force is also applied eccentrically causing not only shearing but also bending of the usually quite long screw. The typical modes of failure of such connection are described in ECCS TC7 TWG 7.4 No.66 (1991) and are presented in Figure 7-11d. These modes of failure are likely to occur when the thickness of the purlin is substantial and a significant bending moment can develop. In the case of thin purlins, it is more likely that tearing of the linear tray occurs rather than breaking of the fastener. Due to the complexity of the test set-up, such joints were not investigated using single lap test.

e) The purlin/rafter connections shown in Figure 7-11e were made using four screws. This connection is complex in its behaviour as top-hat purlin transfers shear between the sheeting and the rafter contributing to the overall shear flexibility of the panel. The tests on such connection are described in APPENDIX E

| a) Seam connection | b) Cladding/purlin connection | c) Cladding/purlin – crown fix connection |

d) Composite panel/purlin connection   e) Purlin/rafter connection
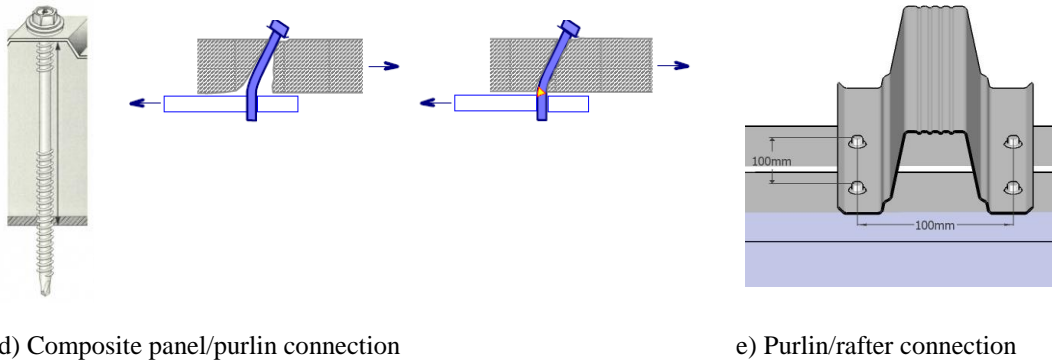
Figure 7-11 Different types of connections

D.3   Lap joint testing methodology

In order to establish shear characteristic of different lap joints the testing procedure described in Section 11 of BS 5950-9 (1994a), using two fasteners per lap joint, was adopted. The details of the test arrangement are presented in Figure 7-12. For these tests the standard Zwick Roell tensile machine was used. The displacement between two points outside the jointed part was measured by a set of LVDTs. The load was applied to the specimen continuously at a rate of 0.01mm/s to meet standard requirements. The load and corresponding slip of the joints were logged during the experiment. The relationship between total load (F_T) and average slip (s) was then plotted. Each type of joint was tested 5 times in order to carry out a statistical analysis.

The test tearing resistance of the joint (F) was established as the maximum test load (F_T) for a slip value less or equal to 3mm. By following this procedure the serviceability requirement proposed in ECCS TC7 TWG 7.10 No.124 (2009) is also incorporated. The characteristic tearing resistance of the joint was calculated according to the equation:

$$F_k = F_m - kSD \tag{7-16}$$

Where:

F_m – mean value of the experimental tearing resistance $F_1 \ldots F_i$

k – coefficient based on the number of tests

SD – standard deviation according to BS 5950-9 (1994a) pp. 59
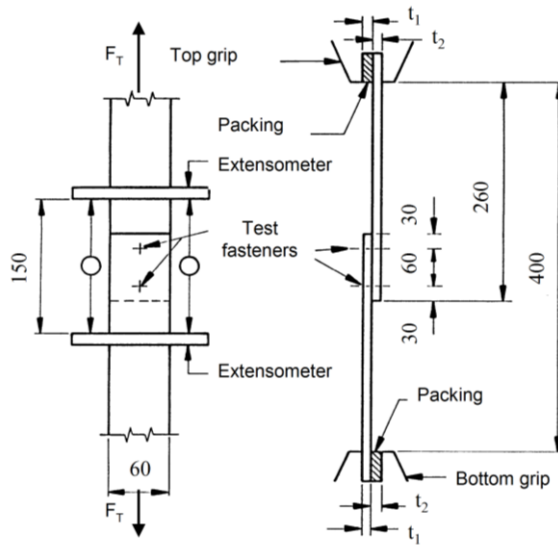
d) Test arrangement after BS 5950-9 (1994a) pp. 59   e) Photograph of the test in progress

Figure 7-12   Single lap screw joint – test arrangement

The design tearing resistance of the joint was calculated from:

$$F_d = F_k/1.11 \qquad\qquad (7\text{-}17)$$

Where:

F_k – characteristic tearing resistance

1.11 – partial factor of safety according to BS 5950-9 (1994a)

The joint flexibility was taken from the experimental plot as a mean value of the displacement at the serviceability load, which is approximately 60% of the characteristic tearing resistance according to the equation:

$$s = \text{mean } (s_1/0.6F_k, \ldots \, s_i/0.6F_k) \qquad\qquad (7\text{-}18)$$

Where:

$s_{1\ldots i}$ – the displacement measured at $0.6F_k$ for each individual test

It should be noted that two fastener joints were tested therefore the characteristic tearing resistance (F_k) obtained from test was divided by two for a single fastener joint.

D.4   Test series

Generally, three different lap joints were investigated each one of them in two thicknesses of steel. The steel pieces for a lap joint tests were cut out from the same batch of steel as full-scale panel tests (Sections 3.4 and 3.5). This provided an accurate shear characteristic of different connections later used in the full-scale shear panel tests. Overall, six series of tests were conducted, as described in Table 7-15, along with the characteristic of each component. The thickness t_1 is the thickness of steel piece in contact with the head of the screw.

Table 7-15 Summary of tested components

Test series	No. of tests	Grade of steel – bottom piece	t_2	Grade of steel – top piece	t_1	Type	d_s	d_w
		Steel pieces				Fastener		
			mm		mm		mm	mm
S1/0.5/0.5	5	S250GD +AZ150	0.5	S250GD +AZ150	0.5	SS	6.3	16
S2/0.7/0.7	5	S250GD +AZ150	0.7	S250GD +AZ150	0.7	SS	6.3	16
S3/1.0/0.7	4*	S550GD +AZ150	1.0	S250GD +AZ150	0.7	CS	5.5	16
S4/2.0/0.7	5	S350GD +Z275	2.0	S250GD +AZ150	0.7	CS	5.5	16
S5/2.0/1.0	5	S350GD +Z275	2.0	S550GD +AZ150	1.0	FS	6.3	-
S6/3.0/1.0	4*	S350GD +Z275	3.0	S550GD +AZ150	1.0	FS	6.3	-

* – data logger malfunction the slip data not available, SS – seam screw, CS – cladding screw, FS – frame screw

The tests provided experimental values of tearing resistance and joint flexibility of seam connections, cladding/purlin connections and purlin/rafter connections.

D.5   Test results

Each series contained 5 tests on the same type of joint however on two occasions malfunctions of the data logging system occurred thus the experimental values in series 3 and 6 were derived based on 4 tests. Generally the same mode of failure was observed in every joint named by ECCS TC7 TWG 7.10 No.124 (2009) as bearing and tilting (B+T). The failure mechanism is shown in Figure 7-13

Typical load-slip relationships obtained from 5 tests of series S1/0.5/0.5 are presented in Figure 7-14. The mean, characteristic and design values of tearing resistance along with slip flexibility value were calculated using Eq. (7-16) and Eq. (7-17). The joint contained two steel plates of 0.48mm thickness and two screws of 6.3mm diameter. Similar to the test results presented by Fan et al. (1997) significant scatter of test results from the same joints were reported, both in terms of resistance and flexibility. The test results from the remaining 5 series were post-processed in the same way and are summarised in Table 7-16. In the case of series 4 and series 5, one out of 5 tests showed greater slip within the serviceability range of deflections which influenced the mean value.

 a) Tearing of material and the hole elongation   b) Screw tilting

Figure 7-13 Single lap screw joint – shear mode of failure
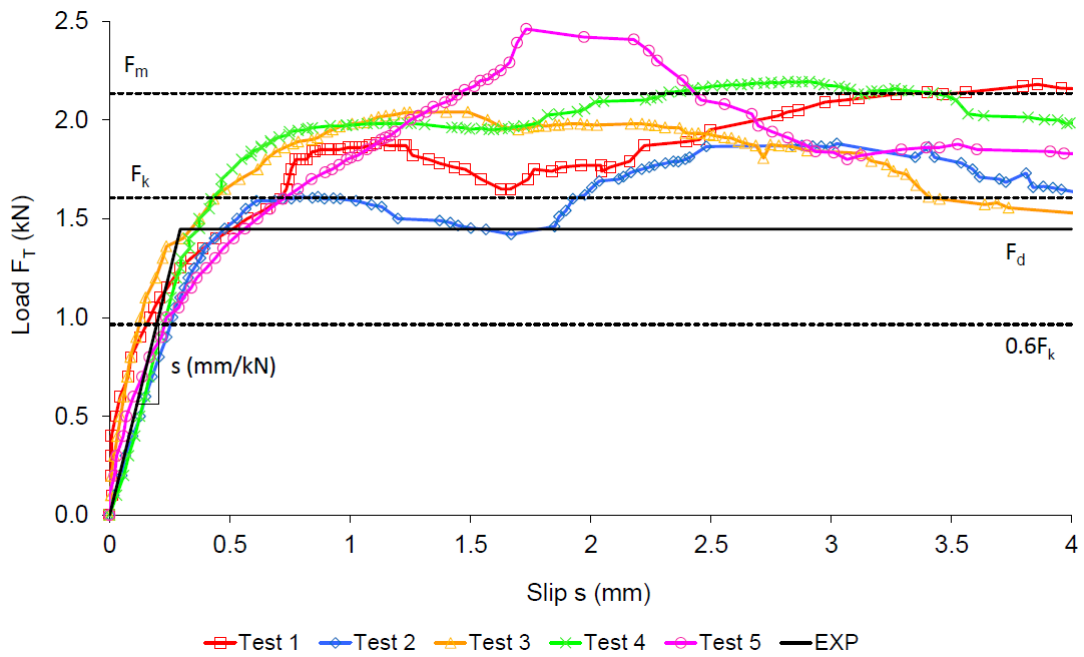
Figure 7-14 Test series S1/0.5/0.5

Table 7-16 Experimental shear resistance of single fastener

Test series	Sheet remote from the screw head			Sheet in contact with the screw head			Resistance		
	$t_{2,cor}$	f_y	f_u	$t_{1.cor}$	f_y	f_u	F_{min}	F_k	F_{max}
	mm	N/mm^2	N/mm^2	mm	N/mm^2	N/mm^2	kN	kN	kN
S1/0.5/0.5	0.48	334	405	0.48	334	405	0.94	0.81	1.23
S2/0.7/0.7	0.65	301	380	0.65	301	380	1.56	1.30	2.07
S3/1.0/0.7	0.96	648	655	0.65	301	380	2.56	1.90	3.28
S4/2.0/0.7	1.96	491	525	0.65	301	380	2.64	2.16	3.42
S5/2.0/1.0	1.96	491	525	0.96	648	655	5.36	4.67	6.90
S6/3.0/1.0	2.96	496	580	0.96	648	655	8.02	7.07	9.07

D.6   Experimental results versus analytical methods

Many semi-empirical formulas for predicting the shear resistance of screw joints have been presented i.e. Baehre and Berggren (1973), ECCS TC7 No. 21 (1990), Peköz (1990), Toma et al. (1993), BS 5950-5 (1998b) and BS EN 1993-1-3 (2006). In this section, only three of those formulas will be considered:

1) Baehre and Berggren (1973)

196

$$P_{v,Baehre} = K_1(d+10)(t_1{}^2+0.22)f_u \qquad (7\text{-}19)$$

Where:

$K_1=0.156[(t_2/t_1)-1]^2 + 0.35$ if $t_2/t_1 < 2.5$

$K_1=0.7$ \qquad if $t_2/t_1 \geq 2.5$

d – screw diameter (mm)

t_1 - thickness of the thinner sheet in contact with the screw head (mm)

t_2 – thickness of the thicker sheet remote from the screw head (mm)

f_u – ultimate tensile strength of the thinner sheet

2) ECCS TC7 No. 21 (1990) and BS 5950-5 (1998b)

$$P_{v,BS} = K_1 f_y \qquad (7\text{-}20)$$

Where:

$K_1=\min(3.2(t_1{}^3 d)^{0.5}, 2.1t_1 d)$ \qquad if $t_2/t_1=1$

$K_1=2.1t_1 d$ \qquad if $t_2/t_1 \geq 2.5$

$K_1=$ from linear interpolation if $1< t_2/t_1 < 2.5$

f_y – design yield stress of the thinner sheet

3) Toma et al. (1993) and BS EN 1993-1-3 (2006)

$$P_{v,EC} = K_1 t_1 d f_u \qquad (7\text{-}21)$$

Where:

$K_1=\min(3.2(t_1/d)^{0.5}, 2.1)$ \qquad if $t_2/t_1=1$

$K_1=\min(3.2(t_1/d)^{0.5}, 2.1)$ if $t_2/t_1 \geq 2.5$ and $t_1<1$mm

$K_1=2.1$ if $t_2/t_1 \geq 2.5$ and $t_1 \geq 1$mm

$K_1=$ from linear interpolation if $1< t_2/t_1<2.5$

The shear resistance equations are based on the factor (K_1) derived experimentally for different thick/thin ratios. In fact the K_1 factors in Eq. (7-20) and (7-21) have the same numerical values. The other fundamental difference between the equations is that Eq. (7-19) and (7-21) uses the ultimate tensile strength where Eq. (7-20) uses design yield strength of the steel. In addition, in the latest Eurocode 3 design equation (Eq. (7-21)), a further condition is added in which a lower bound value of strength is assumed if the thinner sheet thickness is less than 1mm. This condition was not included by Toma et al. (1993) whose research formed the base to the Eurocode 3 equation. For the tested lap joints, the analytical shear resistance was computed and is presented in the Table 7-17 along with the mean and characteristic values obtained in the experimental study.

Table 7-17 Experimental shear resistance versus analytical prediction

Test series	$t_{2,cor}/t_{1,cor}$	d	Experimental values		Analytical values			
			F_k	F_m	Baehre	BS	Toma	EC3
		mm	kN	kN	kN	kN	kN	kN
S1/0.5/0.5	1.0	6.3	0.81	1.07	1.04	0.89	1.08	1.08
S2/0.7/0.7	1.0	6.3	1.30	1.87	1.39	1.27	1.60	1.60
S3/1.0/0.7	1.5	5.5	1.90	2.79	1.46	1.53	1.93	1.93
S4/2.0/0.7	3.0	5.5	2.16	3.00	2.65	2.26	2.85	1.49
S5/2.0/1.0	2.0	6.3	4.67	6.21	6.33	7.21	7.29	7.29
S6/3.0/1.0	3.1	6.3	7.07	8.36	8.53	8.23	8.32	4.95

The geometrical and material characteristics were presented in Table 7-16. As can be seen, the design equation presented by Toma et al. (1993) and that published in BS EN 1993-1-3 (2006) gives the same numerical values apart from joints with a thickness ratio around 3. In this case, the shear resistance predicted by

the Eurocode is significantly reduced and this reduction is not confirmed by experimental data.

There is no codified method to predicted flexibility of the lapped joint connection, but De Matteis and Landolfo (1999) suggested that Eq. (2-1) developed by Zadanfarrokh and Bryan (1992) can be used with sufficient accuracy. The equation used to calculate the flexibility of the joint was originally developed for bolted lap joints with slip due to tolerance of the holes. Thus an additional flexibility reduction factor is considered following the findings of Zadanfarrokh (1991). The self-drilling, self-tapping screw lap joint is an example of perfect fit fastener joint. Two equations presented in the previous chapter are used to calculate the joint flexibility:

1) Eq. (2-1) by Zadanfarrokh and Bryan (1992) with flexibility factor n=5
2) Eq. (2-2) by Zaharia and Dubina (2006)

Table 7-18 Experimental slip flexibility versus analytical prediction

Test series	$t_{2,cor}/t_{1,cor}$	d	Experimental values	Analytical values			
			s	Zadanfarrokh	Scatter	Zaharia	Scatter
			(s_{min}, s_{max})				
		mm	mm/kN	mm/kN	%	mm/kN	%
S1/0.5/0.5	1.0	6.3	0.41 (0.25,0.52)	0.40	3.3	0.46	-13.4
S2/0.7/0.7	1.0	6.3	0.29 (0.15,0.45)	0.29	0.8	0.34	-16.2
S3/1.0/0.7	1.5	5.5	0.34 (0.31,0.37)	0.24	30.0	0.30	12.2
S4/2.0/0.7	3.0	5.5	0.33 (0.28,0.37)	0.18	44.0	0.23	29.7
S5/2.0/1.0	2.0	6.3	0.18 (0.09,0.2)	0.14	24.9	0.16	12.0
S6/3.0/1.0	3.1	6.3	0.09 (0.07,0.13)	0.12	-31.1	0.14	-53.6
				12.0	Average		-4.9

In both equations, a flexibility reduction factor $n_{pf}=0.4$ due to perfect fit fasteners is considered and a comparison of the mean experimental flexibility versus analytical flexibility is presented in Table 7-18.

D.7   Concluding remarks on shear resistance and shear flexibility of screw connections

A general conclusion drawn from the test programme on screw lap joints was that despite all the calculation methods used, due to the complexity of the problem, it is still recommended to measure the shear resistance of the screw joint by testing. When comparing the mean resistance (F_m) obtained from the 6 series of tests against the unfactored resistance from three calculation methods, the following results were obtained:

- Baehre and Berggren (1973) – average error of 13.9%, and 2 of 6 results were unsafe,
- BS 5950-5 (1998b) – average error of 17.4%, and 1 of 6 results was unsafe,
- Toma et al. (1993) – average error of 5.4%, and 2 of 6 results were unsafe.

Based on test results, it can be concluded that the design equation presented by Toma et al. (1993), without the additional condition included in Eurocode 3, offers the closest prediction in terms of joint shear resistance. It was demonstrated in the tests that the repeatability of the results was not very consistent and thus it is important to include the standard deviation in the analysis. When the calculated resistances are compared against characteristic test resistances (F_k) the following results are obtained:

- Baehre and Berggren (1973) – average error of -15.2%, and 5 of 6 results were unsafe,
- BS 5950-5 (1998b) – average error of -10.6%, and 4 of 6 results were unsafe,
- Toma et al. (1993) – average error of -27.3%, and all results were unsafe.

In terms of joint flexibility prediction, both calculated methods were considered to be satisfactory with an average scatter of 12.0% and -4.9% respectively for the Zadanfarrokh and Bryan (1992) and Dubina and Zaharia (2006) formulas. In most of

test series, the calculated flexibilities from both methods fitted within or just outside the flexibility envelope marked by 5 test results of the same series. The most significant difference was observed in series S4/3.0/1.0. In this test series, the calculated flexibility fell outside the flexibility envelope where the tested joints proved to be significantly stiffer than calculation methods predicted.

APPENDIX E. Resistance and flexibility of purlin/rafter connection

E.1   Testing methodology

The recommend test method presented by Davies and Bryan (1982) was modified so that the Tinius Olsen Testing Machine could be used (see Figure 7-15).

a) Front view   b) Side view
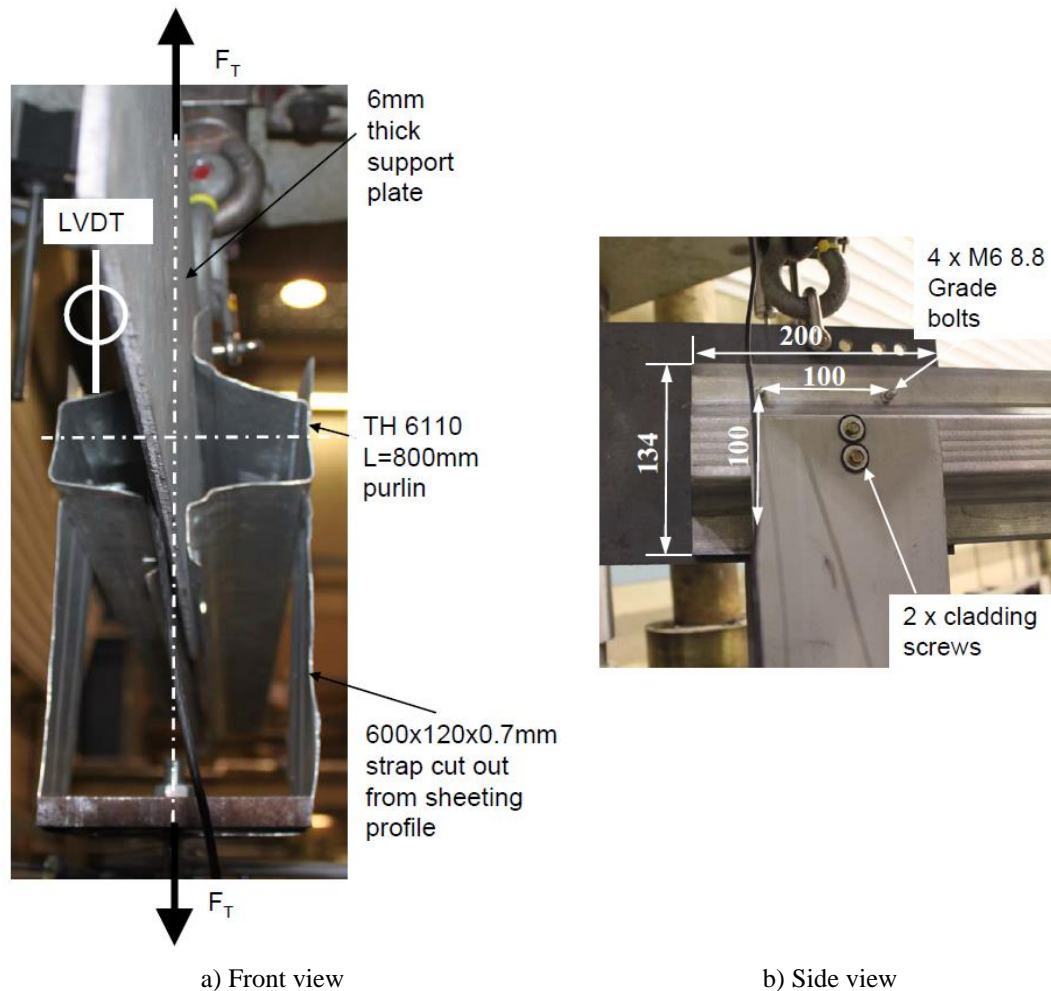
Figure 7-15 Purlin/rafter connection test set-up

Two top-hat TH6110 purlins were fixed to a 6mm thick support plate and the support length was kept consistent with that of the full-scale shear panel tests (see Section 3.5). Standard 6mm diameter bolts without washers were used instead of 6.3mm diameter self-drilling, self-tapping screws in order to emulate the 'true' connection detail in which top-hat legs are in contact with fastener heads. The geometry of the bolt-group was kept consistent with the screwed connection detail used in the full-scale tests as shown in Figure 7-15. The load was applied to the top flanges of the top-hat purlins through a 0.7mm thick strip of cladding. Two cladding screws were used per top flange connection (Figure 7-15) so the connection is reinforced and the purlin section buckles under the load. Due to space limitation, a LVDT was only located on the one side of the test specimen, in-line with the applied load (see Figure 7-15a). The mechanical properties of the steel used for top-hat purlins were established based on the average from three tensile coupons cut out from a flat portion of the web. The average yield strength and ultimate tensile strength were 590N/mm^2 and 608N/mm^2 respectively.

E.2   Test results

Two tests were conducted on the purlin/rafter connection of the top-hat TH611 purlin and the load-displacement relationship per one purlin is presented in Figure 7-16. The overall flexibility of the purlin/rafter connection incorporating bearing of the screws and purlin shear deformation was calculated as 1.21mm/kN based on initial gradients of the load-displacement curves as. It was observed during the test that at a load of approximately 3kN buckling of one of the top-hat legs was initiated (see Figure 7-16). This load was therefore considered as a working limit (0.6 of the ultimate design load) so the elastic buckling of the purlin is prevented under the unfactored load following BS 5950-9 (1994a) analogy. The experiments were stopped when the failure of the sheeting-to-purlin connection occurred. At this point, the purlin member was permanently deformed as shown in Figure 7-16.
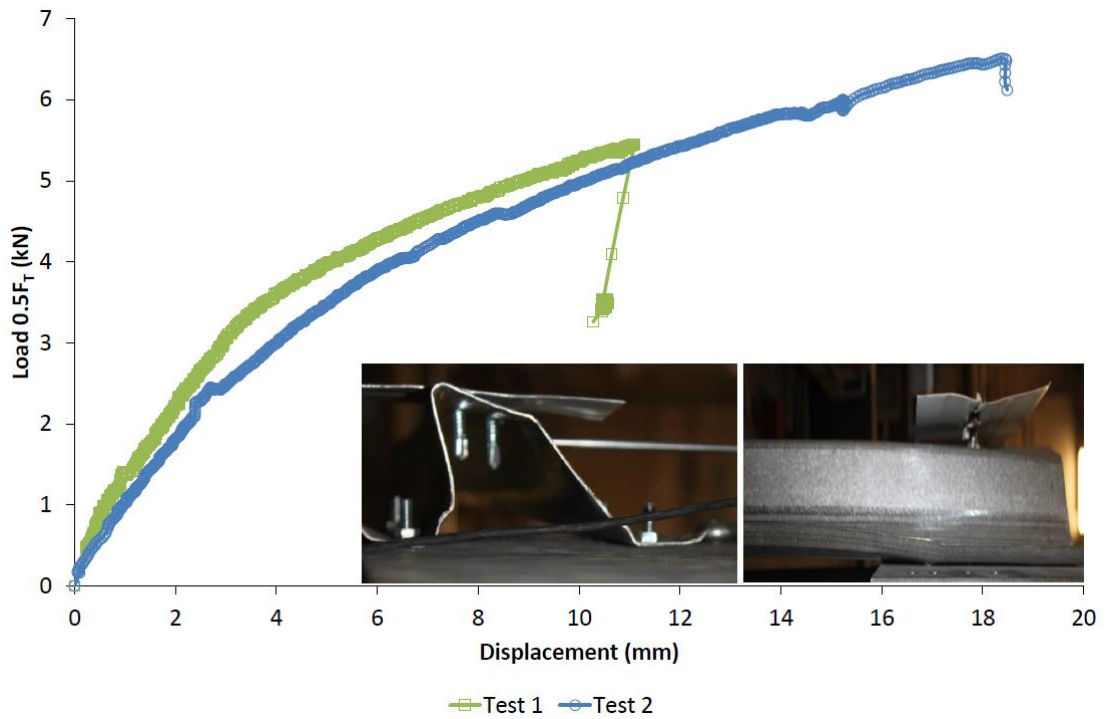
Figure 7-16 Load-displacement relationship

APPENDIX F. Analytical method for predicting shear behaviour of roof diaphragms

The analytical method presented in the BS 5950-9 (1994a) and adopted by BS EN 1993-1-3 (2006) was used in order to establish the shear resistance and the shear flexibility of the investigated roof diaphragms. The sheeting profiles were fixed on four and two sides. The data required to evaluate the shear behaviour of the diaphragm for each design criterion is presented in Table 3-1, Table 3-2 and Section 3.5. The shear resistance and flexibilities of individual fasteners are summarised in Table 7-19. The resistance and flexibility of tested diaphragms were evaluated for an upper bound tests set of values for shear resistance and shear stiffness of each individual lap joint and are denoted in Table 7-20 and Table 7-21 as 'Max. Exp.'

Table 7-19 Resistances and flexibilities of the individual joints used for shear diaphragm calculations

Test designation	Source	F_s	F_{sc}	F_p	$F_{pr,s}$	F_{pr}	Source	s_s	s_{sc}	s_p	$s_{pr,s}$	s_{pr}
		kN	kN	kN	kN	kN		mm/kN	mm/kN	mm/kN	mm/kN	mm/kN
T1, 3, 5,11,13,15	Toma (Eq. 7)	1.08	2.08	1.83	8.32	4.2 (6.3)	Zaharia	0.46	0.34	0.37	0.14	1.21 (0.81)
T7,17	Toma (Eq. 7)	1.08	2.08	1.83	8.32	4.2 (6.3)	Zaharia + flexure of the screw shank	0.46	0.73	0.73	0.14	1.21 (0.81)
T2, 4, 6,12,14,16	Max. exp.	2.07	3.28*	3.28	9.07	4.2 (6.3)	Max. exp.	0.15	0.31*	0.31	0.07	1.21 (0.81)
	Characteristic exp.	1.30	1.90*	1.90	7.07	-	Characteristic exp.	0.29	0.34*	0.34	0.09	-
	Toma (Eq. 7)	1.60	2.13	1.93	8.32	-	Zaharia	0.34	0.28	0.30	0.14	1.21 (0.81)
T8, 18	Toma (Eq. 7)	1.60	2.13	1.93	8.32	4.2 (6.3)	Zaharia + flexure of the screw shank	0.34	0.66	0.66	0.14	1.21 (0.81)
T9,19 top	Toma (Eq. 7)	1.08	2.08	2.08	8.32	4.2 (6.3)	Zaharia	0.46	0.34	0.37	0.14	1.21 (0.81)
T9,19 bot.		0.69	1.65	1.65	8.32	4.2 (6.3)		-	0.45	0.45	0.14	1.21 (0.81)

* experimental data was not available thus values assumed based on the experimental data of test series S3/1.0/0.7 (see Table 7-16 and Table 7-18)

( ) equivalent value used in BS 5950-9 (1994a) calculations for the design case in which edge top-hat purlins were doubled

The set of characteristic test values was also used to evaluate resistances and flexibilities of investigated diaphragms which are presented in Table 7-20 and Table 7-21 (denoted 'Chr. Exp.').The last set of values denoted as 'Anl.' in Table 7-20 and Table 7-21 were evaluated based on the shear resistance and the shear stiffness of each individual lap joint according to Toma et al. (1993) and Zaharia and Dubina (2006). The following notations were used in Table 7-20 and Table 7-21 in order to describe the shear resistance of panels with respect to the modes of failure recognised as follows:

V_s – seam capacity (see Table 7-20a),

V_{sc} – shear connector fasteners capacity (see Table 7-20a),

V_p – sheet/purlin fasteners capacity (see Table 7-20c and d),

V_{sb} – shear buckling capacity of the sheeting profile see (Table 7-20e),

V_{ec} – end collapse of the sheeting profile (Table 7-20g)

V_{epj} – edge purlin joint capacity under axial force (Table 7-20f)

V_{pr} – purlin/rafter joint capacity under shear force (Table 7-20k)

c – overall flexibility of the shear panel

It should be recognized that tests T7 and T8 represent a special cases in which sheeting/purlin fasteners and sheeting/shear connector fasteners are subject to shear force applied on a lever arm equal to the height of the sheeting profile equal to 18mm. The analytical values of slip calculated by the Zaharia and Dubina (2006) equation and presented in Table 7-19 were therefore increased by the flexibility of the single screw acting as cantilever. This flexibility was calculated as 0.36mm/kN for a screw diameter of 4.8mm which represented the sheeting/purlin screw of 5.5mm nominal diameter.

In the case of tests T9 and T19 in which diaphragms were constructed from 80mm thick composite panels, the resistances and flexibilities were evaluated for the

top and bottom skins separately and the results are presented in Table 7-20 and Table 7-21. In the case of shear panels fixed on 2 sides (Tests 1 to 19), the input data for the BS 5950-9 (1994a) analytical method and key differences in construction of shear panels with and without shear connectors are discussed in Section 3.5.

Table 7-20 Analytical shear capacities and shear flexibility of shear panels with shear connectors

Test designation	Model	V_s	V_{sc}	V_p	V_{sb}	V_{ec}	V_{epj}	c
		kN	kN	kN	kN	kN	kN	mm/kN
T1 AS34/0.5	Anl.	14.88	12.48	21.97	84.83	23.23	28.53	0.55
T2 AS34/0.7	Max. Exp.	27.74	19.68	39.38	133.50	33.00	31.1	0.34
	Char. Exp.	16.88	11.40	22.81	133.50	33.00	24.24	0.38
	Anl.	19.38	12.78	23.17	133.50	33.00	28.53	0.36
T3 AS30/0.5	Anl.	13.95	12.48	18.30	68.16	21.21	28.53	0.61
T4 AS30/0.7	Max. Exp.	26.07	19.68	32.8	107.35	30.12	31.1	0.37
	Char. Exp.	15.91	11.40	19.00	107.35	30.12	24.24	0.41
	Anl.	18.40	12.78	19.30	107.35	30.12	28.53	0.39
T5 AS24/0.5	Anl.	14.88	12.48	21.97	45.06	23.23	28.53	0.47
T6 AS24/0.7	Max. Exp.	27.74	19.68	39.38	70.95	33.00	31.1	0.3
	Char. Exp.	16.88	11.40	22.81	70.95	33.00	24.24	0.34
	Anl.	19.38	12.78	23.17	70.95	33.00	28.53	0.33
T7 AS18/0.5	Anl.	11.79	12.48	15.98	26.99	*	28.53	1.06
T8 AS18/0.7	Anl.	15.20	12.78	16.86	43.05	*	28.53	0.72
T9 AS35/80 top	Anl.	13.52	12.48	14.38	*	*	28.53	0.72
T9 AS35/80 bot.		6.86	9.90	12.97	*	*	28.53	0.74

Table 7-21   Analytical shear capacities and shear flexibility of shear panels without shear connectors

Test designation	Model	V_s	V_p	V_{pr}	c
		kN	kN	kN	mm/kN
T11 AS34/0.5	Anl.	14.88	10.25	25.2	0.95
	Max. Exp.	27.74	18.37	25.2	0.73
T12 AS34/0.7	Char. Exp.	16.88	10.64	-	0.78
	Anl.	19.38	10.81	-	0.77
T13 AS30/0.5	Anl.	13.95	9.15	25.2	1.03
	Max. Exp.	26.07	16.4	25.2	0.78
T14 AS30/0.7	Char. Exp.	15.91	9.5	-	0.82
	Anl.	18.4	9.65	-	0.81
T15 AS24/0.5	Anl.	14.88	10.25	25.2	0.87
	Max. Exp.	27.74	18.37	25.2	0.70
T16 AS24/0.7	Char. Exp.	16.88	10.64	-	0.74
	Anl.	19.38	10.81	-	0.73
T17 AS18/0.5	Anl.	13.65	11.42	25.2	1.34
T18 AS18/0.7	Anl.	17.17	12.04	25.2	1.14
T19 AS35/80 top	Anl.	15.73	11.65	25.2	1.12
T19 AS35/80 bot.		8.05	9.24	25.2	1.07

Due to the fact that for panels fixed on 2 sides, the edge purlin members had to be doubled, the test shear flexibility (s_{pr}) of the purlin-to-rafter joint (see section E.2 and Table 7-19) was replaced by equivalent shear flexibility of 0.81 mm/kN to take account of the fact that edge purlins are twice stiffer than the intermediate

purlins. The shear capacity due to purlin/rafter connection, calculated to standard equation for 4 purlins was also increased to the equivalent value of 6.3 kN. The axial stiffness of the single top-hat edge purlins was also doubled in the calculations.

APPENDIX G. Structural details of full-scale frames

G.1 Test frame with Joints A

As presented in Figure 7-17, the frame with Joint A was constructed from back-to-back cold-formed steel sections of C152x64x20x2. The back-to-back C sections were interconnected according to the rules published in BS 5950-5 (1998b) so an integral I section can be assumed for analysis purpose. The lateral stability of the column and rafter members was provided by the purlins / side rails members fixed by four self-drilling self-tapping screws at each end.
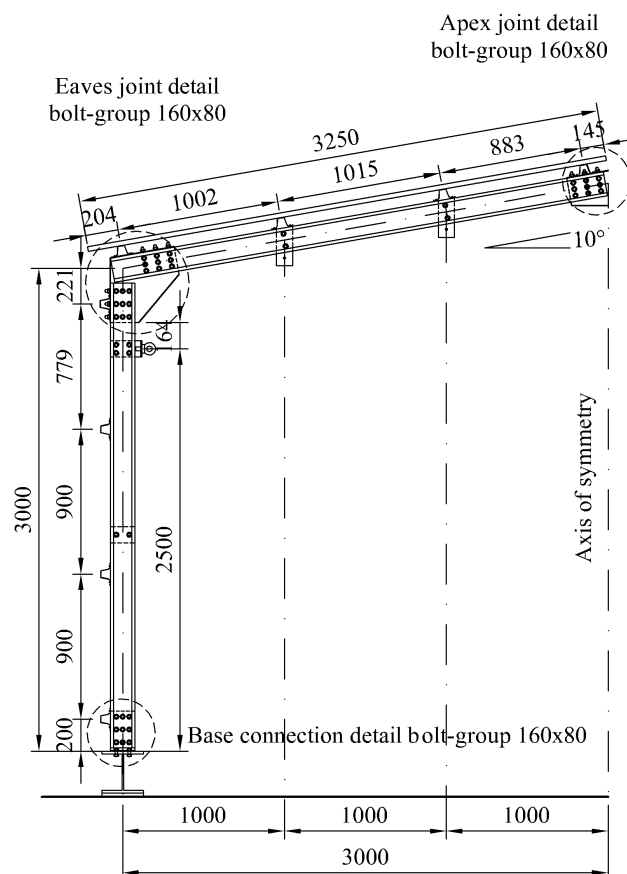
Figure 7-17 Front view of the test frame with Joint A

These only restrained the outer side of the column/rafter member as no stays were used. It should be mentioned however that in the vertical load, the way the load was applied to the underside of the rafter had a stabilising effect against lateral-torsional buckling. The eaves/apex joints were formed by back-to-back cold-formed steel brackets of 3 mm thickness. A 3x3 bolts array of 160mmx80mm was used in the web together with an additional 6 bolts in the flange to connect the bracket with the end of each structural member.

G.2   Test frame with Joint B

In case of the frame with Joint B, all the structural components were identical to the frame with Joint A apart from the length of the bolt-group, which was increased to 280mm in order to increase the stiffness of the eaves and apex joint (see Figure 7-18). The location of the top side rails as well as the ridge purlins was also adjusted so that the members are always located above the bolt-group centre of rotation as shown in Figure 7-18.
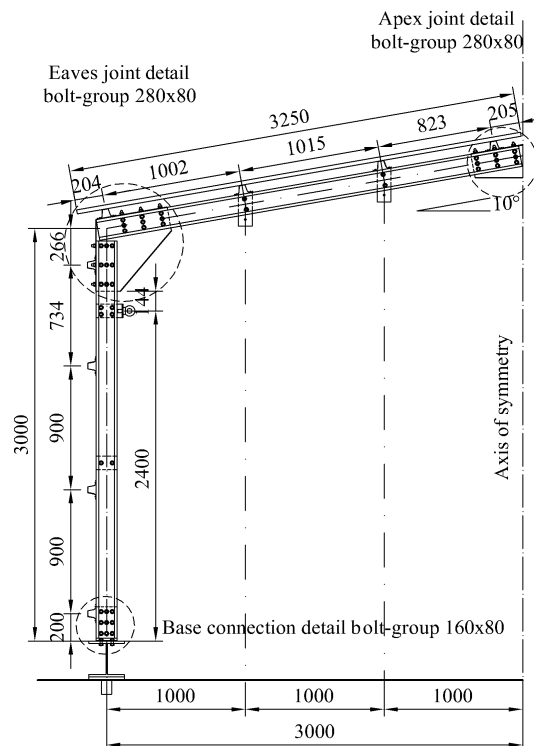
Figure 7-18 Front view of the test frame with Joint B

G.3   Base connection

The research presented in Section 5.1 highlights the influence of the partial fixity of the base connection on the sway stiffness of the bare frame. In order to minimise this effect, the details of the joint was designed to act as 'perfect pin' so that clear interpretation of the test results was possible. The base connection was also subject to a pure bending test and this test proved the negligible stiffness of the base connection. Back-to-back L shape base cleats were used, fixed by 3x3 bolts array 160mmx80mm as presented in Figure 7-19. Standard M16 8.8 Grade bolts were used in the connection detail.
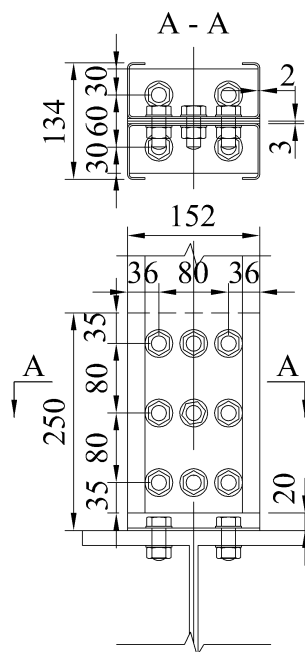
Figure 7-19 Pinned base connection detail

The base cleats were bolted to a reaction beam made out of Universal Column (section designation 254x254x89) fixed to the laboratory strong floor. The base connection remained the same throughout the entire test investigation.

G.4   Gable frame – vertical load

To agree with industry practice, single double lipped channels were used for the main framework as shown in Figure 7-20. The frame was bolted to the heavy

reaction beams fixed to the laboratory floor. Top-hat purlins (see Figure 4-9c) were used as purlins/side rails members connected through four self-drilling frame screws. As can be seen in Figure 4-7, the gable frame was heavily instrumented in order to determine any load sharing between the adjacent frames. The in-plane and out-of-plane stability of the eaves and apex key point was provided by the set of six tension only bracing members each equipped with a load cell. An additional bracing member equipped with a load cell was also introduced across the eaves so that any spread action in the gable frame could be determined. Such a bracing arrangement was developed to simplify the modelling of the full-scale tests where the key nodes can be modelled as supported on linear springs. The gable frame was not loaded during the test and served as a reaction. The load was applied to the internal frame as shown in Figure 7-17 and Figure 7-18 at four points under the purlin members through M12 Grade 8.8 threaded rods equipped with through-hole load cells. The level of load at each point was controlled by hand operated jacks and data was manually logged when the forces at each loading point reached the required values.
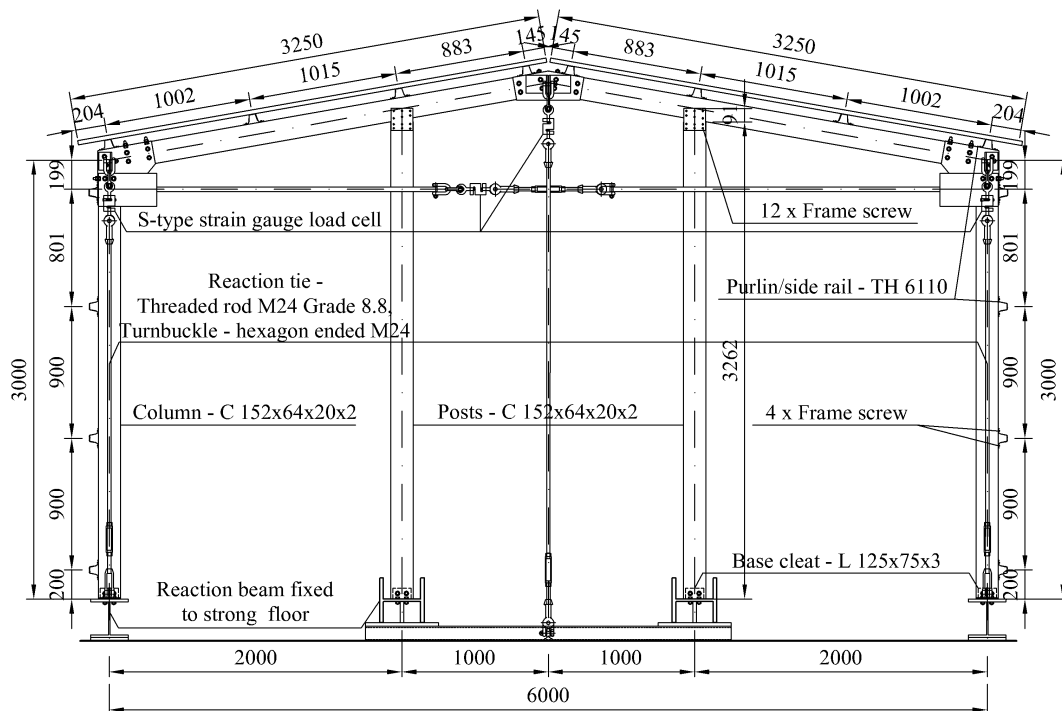
Figure 7-20 Vertical load test set-up – gable frame

G.5　Gable frame – horizontal load

Considering different load paths, the gable frame in all horizontal cases was modified in order to measure the load transfer due to the roof diaphragm action between the loaded test frame and the unloaded gable frame. For this reason, two diagonal bracing rods were used to brace the gable frame in-plane as shown in Figure 7-21. Each bracing rod, equipped with S-type strain gauges, was connected to the gable frame through 10mmn thick S275 steel plates. It was recognized that top-hat roof purlins are able to carry a transverse bending moment when they are fixed with 4 screws. In the horizontal tests on bare frames only, one screw connection was used at the test frame end of each roof purlin, so that the horizontal load is not transferred between frames.
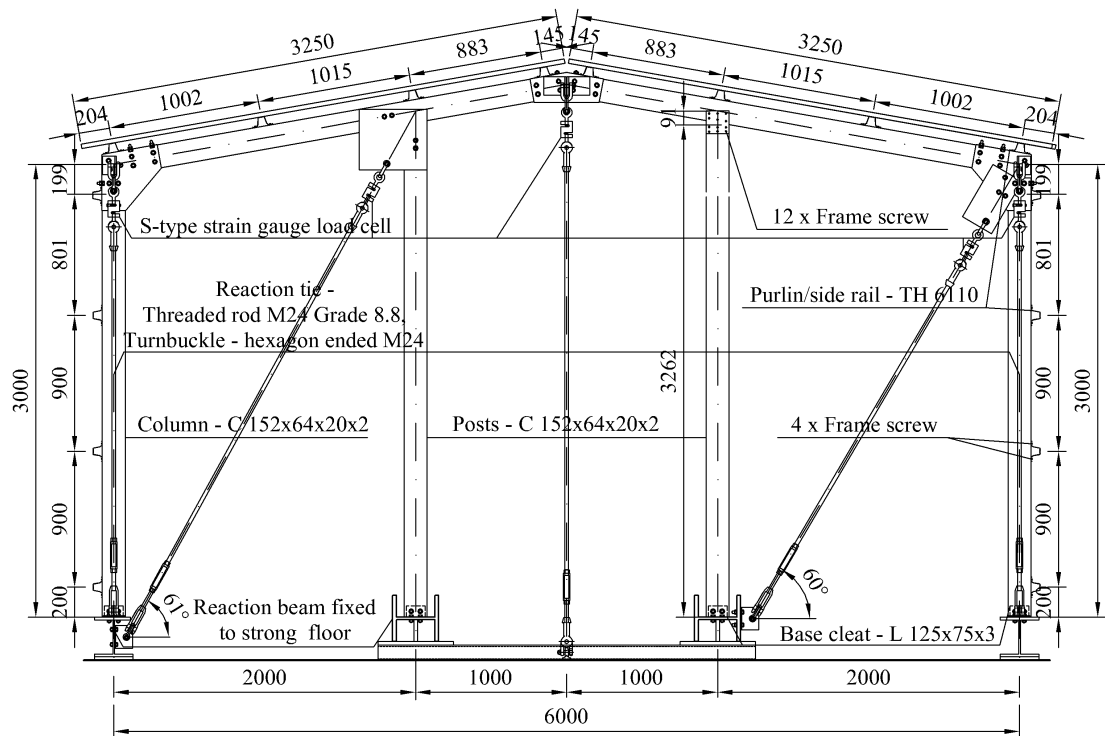
Figure 7-21 Horizontal load test set-up – gable frame

APPENDIX H. Worked example

H.1 Joints rotational stiffness and moment capacity for Model 1 and Model 2

<u>Joint geometry according to</u> Figure 4-8b

t_1=1.96mm - section thickness excluding coating

t_2=2.96mm – bracket thickness excluding coating

a_{bg}=280mm – bolt-group length

b_{bg}=80mm - bolt-group width

b_{es}=36mm- edge distance

<u>Double lap joint linear stiffness</u>

$$c_{Zad} = 5 \cdot 5 \cdot \left[\frac{\left(10 \frac{mm^2}{kN}\right)}{t_1 + 0.04mm} + \frac{\left(10 \frac{mm^2}{kN}\right)}{t_2 + 0.04mm} + -2 \frac{mm}{kN} \right] \cdot 10^{-3} = 0.158 \cdot \frac{mm}{kN}$$	Eq. (2-1)
$$k_b = \frac{2}{c_{Zad}} = 12.63 \cdot \frac{kN}{mm}$$	Stiffness for back-to-back joint

<u>Joint rotational stiffness models based of pure bending</u> (see Figure 2-30)

<u>Model 1 (upper bound)</u>

$\phi_{sl,anl,1}$=0rad

$$S_{j.ini.1} = 3 \left(\frac{8a_{bg}^2 + 11 \cdot b_{bg}^2 + 12b_{bg} \cdot b_{es} + 12 \cdot b_{es}^2}{16} \right) \cdot k_b = 1771 \cdot kN \cdot \frac{m}{rad}$$	Table 7-5

<u>Model 2 (lower bound)</u>

$\delta_{i.th} = 1mm$	Recommended slip displacement 0.5 of hole tolerance
$r_{i.2} = 0.5 \cdot \sqrt{a_{bg}^2 + b_{bg}^2} = 145.602 \cdot mm$	
$\phi_{sl.anl.2} = \dfrac{\delta_{i.th}}{r_{i.2}} = 0.0069$	Eq. (2-13)
$S_{j.ini.2} = 3 \left(\dfrac{a_{bg}^2 + b_{bg}^2}{2} \right) \cdot k_b = 1607 \cdot kN \cdot \dfrac{m}{rad}$	Table 7-5
$S_{j.ini.sl} = 0.05 \cdot S_{j.ini.2} = 80 \cdot kN \cdot \dfrac{m}{rad}$	Joint rotational stiffness at a slip stage assumed as 5% of a stiffness at a bearing stage

<u>Critical moment at the Centre of a Rotation of a bolt-group</u>

E=210GPa

f_y=397MPa

Nominal geometry of a channel according to Table 2-8

$M_{cy,BS}$=21.32kNm - Moment capacity to BS 5950-5 (1998a)

$V_{w,BS}=P_w$=79.08kN - Concentrated transverse load resistance to BS 5950-5 (1998a)

<u>Forces in bolts – Model 1 (see Figure 7-5c)</u>

Try moment at the Centre of the rotation M_1=17.43kNm

$y_1 = \dfrac{5 \cdot b_{bg}}{8} + \dfrac{b_{es}}{4} = 59 \cdot mm$	Table 7-7

$$F_{1.1} = \frac{8 \cdot M_1 \cdot a_{bg}}{8 \cdot a_{bg}^2 + 11 \cdot b_{bg}^2 + 12 \cdot b_{bg} \cdot b_{es} + 12 \cdot b_{es}^2} = 52.217 \cdot kN$$

$$F_{2.1} = 0 = 0 \cdot kN$$

$$F_{3.1} = \frac{8 \cdot M_1 \cdot a_{bg}}{8 \cdot a_{bg}^2 + 11 \cdot b_{bg}^2 + 12 \cdot b_{bg} \cdot b_{es} + 12 \cdot b_{es}^2} = 52.217 \cdot kN$$

$$F_{4.1} = \frac{10 \cdot M_1 \cdot b_{bg} + 4 \cdot M_1 \cdot b_{es}}{8 \cdot a_{bg}^2 + 11 \cdot b_{bg}^2 + 12 \cdot b_{bg} \cdot b_{es} + 12 \cdot b_{es}^2} = 22.006 \cdot kN$$

$$F_{5.1} = \frac{2 \cdot M_1 \cdot b_{bg} + 4 \cdot M_1 \cdot b_{es}}{8 \cdot a_{bg}^2 + 11 \cdot b_{bg}^2 + 12 \cdot b_{bg} \cdot b_{es} + 12 \cdot b_{es}^2} = 7.087 \cdot kN$$

$$F_{6.1} = \frac{6 \cdot M_1 \cdot b_{bg} - 4 \cdot M_1 \cdot b_{es}}{8 \cdot a_{bg}^2 + 11 \cdot b_{bg}^2 + 12 \cdot b_{bg} \cdot b_{es} + 12 \cdot b_{es}^2} = 7.833 \cdot kN$$

$$F_{f.1} = \frac{6 \cdot M_1 \cdot b_{bg} + 12 \cdot M_1 \cdot b_{es}}{8 \cdot a_{bg}^2 + 11 \cdot b_{bg}^2 + 12 \cdot b_{bg} \cdot b_{es} + 12 \cdot b_{es}^2} = 21.26 \cdot kN$$

$$M_{Ed.1} = M_1 - \left[\frac{F_{4.1} \cdot y_1 + F_{5.1} \cdot (y_1 - 0.5 \cdot b_{bg}) + F_{6.1} \cdot (-y_1 + b_{bg}) + F_{f.1} \cdot [-y_1 + (b_{bg} + b_{es})]}{3} \right]$$

Eq. (7-13)

$$M_{Ed.1} = 16.49 \, kN \cdot m$$

$$F_{Ed.1} = F_{1.1} = 52.22 \cdot kN$$

Eq. (7-15)

$$1.1 \left(\frac{F_{Ed.1}}{V_{w.BS}} \right) + \left(\frac{M_{Ed.1}}{M_{cy.BS}} \right) = 1.5$$

Eq. (7-13)

OK

Forces in bolts – Model 2

Try moment at the Centre of the rotation M$_2$=16.36kNm

$$y_2 = \frac{b_{bg}}{2} = 40 \cdot mm$$

$$F_{1.2} = \frac{M_2 \cdot a_{bg}}{a_{bg}^2 + b_{bg}^2} = 54.019 \cdot kN$$

$$F_{3.2} = \frac{M_2 \cdot a_{bg}}{a_{bg}^2 + b_{bg}^2} = 54.019 \cdot kN$$

$$F_{4.2} = \frac{M_2 \cdot b_{bg}}{a_{bg}^2 + b_{bg}^2} = 15.434 \cdot kN$$

$$F_{5.2} = 0 = 0 \cdot kN$$

$$F_{6.2} = \frac{M_2 \cdot b_{bg}}{a_{bg}^2 + b_{bg}^2} = 15.434 \cdot kN$$

$$F_{f.2} = 0 = 0 \cdot kN$$

$$M_{Ed.2} = M_2 - \left[\frac{F_{4.2} \cdot y_2 + F_{5.2} \cdot (y_2 - 0.5 \cdot b_{bg}) - F_{6.2} \cdot (y_2 - b_{bg}) - F_{f.2} \cdot \left[y_2 - (b_{bg} + b_{es}) \right]}{3} \right]$$

$$M_{Ed.2} = 15.95 \, kN \cdot m$$

$$F_{Ed.2} = F_{1.2} = 54.02 \cdot kN$$

$$1.1 \left(\frac{F_{Ed.2}}{V_{w.BS}} \right) + \left(\frac{M_{Ed.2}}{M_{cy.BS}} \right) = 1.5$$

H.2 Strength and flexibility of a sheeting panel

<u>Input data:</u>

Diaphragm type – sheeting

Fasteners positions – every corrugation at both sheet ends and alternate corrugation at the intermediate purlins

a=3000mm – width of the shear panel equal to a frame spacing

b=2840mm – depth of the shear panel equal to distance between edge purlins (see Figure 7-18)

Mechanical properties of steel

Sheeting - E=210GPa, f_{ys}=301MPa (see Table 7-14)

Purlins - E=210GPa, f_{ys}=590MPa (see Table 7-10)

Sheeting profiles AS30 - geometry (see Figure 7-9 and Table 7-13)

h=30mm, t=0.65 (excluding coating), d=200mm, l=30mm, θ=33˚

Sheeting panel characteristic (see Table 3-1)

n_s=8, n_{sc}=0, n_p=4, n_{sh}=3, n_f=5, p_{end}=200mm, p_{int}=400mm, u=230mm, I_y=19285mm^4, K=0.054, A_p=221mm^2 (see Table 7-12)

Screws characteristic (see Figure 7-10)

d_s=6.3mm – diameter of stitching screw

d_p=5.5mm – diameter of cladding screw

d_{pr}=6.3mm – diameter of purlin to rafter screw (frame screw)

F_s=1.60kN – design strength of individual seam fastener (Table 7-19)

F_p=1.93kN - design strength of individual sheeting to purlin fastener (Table 7-19)

F_{pr}=6.30kN - design strength of purlin to rafter connection (Table 7-19)

s_s=0.34mm/kN – slip per seam fastener (Table 7-19)

s_p=0.30mm/kN – slip per sheeting to purlin fastener (Table 7-19)

F_{pr}=0.81mm/kN – slip per purlin to rafter connection (Table 7-19)

β_1=0.58	
β_2=1.25	
β_3=1.25	
α_1=1	
α_2=0.75	
α_3=0.9	
α_4=1	
Diphragm shear strength	
$V_{ulta} = n_s \cdot F_s + \left(\dfrac{\beta_1}{\beta_3}\right) \cdot n_p \cdot F_p = 18.4 \cdot kN$	
$V_{ultb} = \beta_2 \cdot n_p \cdot F_p = 9.65 \cdot kN$ $V_{ultc} = n_p \cdot F_{pr} = 25.2 \cdot kN$	
V*=18.4kN	The seam capacity was considered as a design strength Section 3.5.2

$V_{critc} = \dfrac{\left(0.9 \cdot t^{1.5} \cdot b \cdot p_{ys}\right)}{d^{0.5}} = 28.509 \cdot kN$ $V_{critc} \geq V*$	ok

Diphragm shear flexibility	
$$c_{11} = \frac{a \cdot d^{2.5} \cdot \alpha_1 \cdot \alpha_4 \cdot K_1}{E \cdot t^{2.5} \cdot b^2} = 0.159 \cdot \frac{mm}{kN}$$	
$$c_{12} = \frac{2 \cdot a \cdot (1 + \nu) \cdot \left[1 + \left(2 \cdot \frac{h}{d}\right)\right]}{E \cdot t \cdot b} = 0.026 \cdot \frac{mm}{kN}$$	
$$c_{21} = \frac{\left(2 \cdot a \cdot s_p \cdot p\right)}{b^2} = 0.045 \cdot \frac{mm}{kN}$$	
$$c_{22} = \frac{\left[2 \cdot s_s \cdot s_p \cdot \left(n_{sh} - 1\right)\right]}{\left(2 \cdot n_s \cdot s_p\right) + \left(\beta_1 \cdot n_p \cdot s_s\right)} = 0.073 \cdot \frac{mm}{kN}$$	
$$c_{23} = \frac{2}{n_p} \cdot \left(s_{pr} + \frac{s_p}{\beta_2}\right) = 0.523 \cdot \frac{mm}{kN}$$	
$$c_3 = \frac{2 \cdot a^3}{3 \cdot E \cdot A_p \cdot b^2} = 0.0481 \cdot \frac{mm}{kN}$$	
$$C_d = c_{11} + c_{12} + c_{21} + c_{22} + c_{23} + c_3 = 0.874 \cdot \frac{mm}{kN}$$ $$\theta = 46.57°$$ $$k_{s\_d} = \frac{\frac{1}{C_d}}{(\cos(\theta))^2} = 2.42 \cdot \frac{kN}{mm}$$	
$$V_d = \frac{V_{ulta}}{\cos(\theta)} = 26.76 \cdot kN$$	

219

REFERENCES

AISI 2004. Appendix 1: Design of cold-formed steel structural members using the Direct Strength Method. *2004 supplement to the north American specification for the design of coldformed steel structures.* Washington (DC): American Iron and Steel Institute.

AS/NZS 4600:2005 2005. Cold-formed steeel structures. Sydney / Wellington: Standards Australia / Standards New Zealand.

AUTODESK INC. 2009. Autodesk Robot Structural Analysis Professional 2010 Training Manual - Metric Version. Available: http://images.autodesk.com/adsk/files/robot_2010_training_manual_metric.pdf [Accessed 1 February 2010].

BAEHRE, R. & BERGGREN, L. 1973. Joints in sheet metal panels. Stockholm: National Swedish Building Research.

BAEHRE, R. & LADWEIN, T. 1994. Diaphragm action of sandwich panels. *Journal of Constructional Steel Research,* 31**,** 305-316.

BAIGENT, A. H. & HANCOCK, G. J. 1978. The behaviour of portal frames composed of cold-formed members. Sydney: University of Sydney, School of Civil Engineering.

BAIGENT, A. H. & HANCOCK, G. J. 1982a. The strength of cold-formed portal frames. *6th International Specialty Conference in Cold-Formed Steel Structures.* St Louis, Missouri, USA.

BAIGENT, A. H. & HANCOCK, G. J. 1982b. Structural analysis of assemblages of thin-walled members. *Engineering Structures* 4**,** 207–216.

BATES, W., BRYAN, E. R. & EL-DAKHAKHNI, W. M. 1965. Full-scale tests on a portal frame shed. *The Structural Engineer,* 43**,** 199-208.

BRYAN, E. R. 1973. *The stressed skin design of steel buildings, Constrado monographs,* London, Crosby Lockwood Staples.

BRYAN, E. R. 1993. The design of bolted joints in cold-formed steel sections. *Thin-Walled Structures,* 16**,** 239-262.

BRYAN, E. R. & MOHSIN, M. E. 1972. The design and testing of a steel building taking account of the sheeting. *The International Association of Bridge and Structural Engineering, 9th Congress, Preliminary Report.* Amsterdam: 305-314.

BS 4190:2014 2014. ISO metric black hexagon bolts, screws and nuts – Specification. London: British Standards Institution.

BS 5950-5 1998a. Structural use of steelwork in building *Part 5: Code of practice for design of cold formed thin gauge sections.* London: British Standards Institution.

BS 5950-5 1998b. Structural use of steelwork in building *Part 5: Code of practice for design of cold formed thin gauge sections.* London: British Standards Institution.

BS 5950-9 1994a. Structural use of steelwork in building. *Part 9: Code of practice for stressed skin design.* London: British Standards Institution.

BS 5950-9 1994b. Structural use of steelwork in building. *Part 9: Code of practice for stressed skin design.* London: British Standards Institution.

BS EN 1990:2002+A1:2005 2002. Eurocode - Basis of structural design (Incorporating corrigenda December 2008 and April 2010). London: British Standard Institution.

BS EN 1991-1-1:2002 2002. Eurocode 1: Actions on structures — Part 1-1: General actions — Densities, self-weight, imposed loads for buildings (Incorporating corrigenda December 2004 and March 2009). London: British Standard Institution.

BS EN 1991-1-3:2003 2003. Eurocode 1 — Actions on structures — Part 1-3: General actions — Snow loads (Incorporating corrigenda December 2004 and March 2009) London: British Standard Institution.

BS EN 1991-1-4:2005+A1:2010 2005. Eurocode 1: Actions on structures — Part 1-4: General actions — Wind actions (Incorporating corrigenda July 2009 and January 2010). London: British Standard Institution.

BS EN 1993-1-3 2006. Eurocode 3 - Design of steel structures. *Part 1-3: General rules - Supplementary rules for cold-formed members and sheeting.* Brussels: European Committee for Standardization.

BS EN 1993-1-8 2005. Eurocode 3 - Design of steel structures. *Part 1-8: Design of joints.* Brussels: European Committee for Standardization.

BS EN 10002-1:2001 2001. Metallic materials - Tensile testing. *Part 1: Method of test at ambient temperature.* Brussels: European Committee for Standardization.

BS EN 10154:1996 1996. Continuously hot-dip aluminium-silicon (AS) coated steel strip and sheet - Technical delivery conditions. Brussels: European Committee for Standardization.

BS EN 10326:2004 2004. Continuously hot-dip coated strip and sheet of structural steels - Technical delivery conditions. Brussels: European Committee for Standardization.

CHUNG, K. F. & HO, H. C. 2005. Analysis and design of lapped connections between cold-formed steel Z sections. *Thin-Walled Structures,* 43**,** 1071-1090.

CHUNG, K. F. & LAU, L. 1999. Experimental investigation on bolted moment connections among cold formed steel members. *Engineering Structures* 21**,** 898-911.

CHUNG, K. F., YU, W. K., HO, H. C. & WANG, A. J. 2005. Advances in analysis and design of cold-formed steel structures. *Joint Structural Division Annual Seminar 2005.*

CRAWFORD, S. F. & KULAK , G. L. 1971. Eccentrically Loaded Bolted Connections. *Journal of the Structural Division, ASCE,* 97**,** 765–783.

DARCY, G. & MOHENDRAN, M. 2008. Development of a new cold-formed steel building systems. *Advances in Structural Engineering,* 11**,** 661-677.

DAVIES, J. M. 1972. Computer analysis of stressed skin buildings. *Civil Engineering and Public Works Review,* 67**,** 1154 -1157.

DAVIES, J. M. 1973. The plastic collapse of framed structures clad with corrugated steel sheeting. *ICE Proceedings,* 55**,** 23-42.

DAVIES, J. M. 1986a. A general solution for the shear flexibility of profiled sheets. I: Development and verification of the method. *Thin-Walled Structures,* 4**,** 41–68.

DAVIES, J. M. 1986b. A general solution for the shear flexibility of profiled sheets. II: Applications of the method. *Thin-Walled Structures,* 4**,** 151–161.

DAVIES, J. M. 2006. Development in stressed skin design. *Thin-Walled Structures,* 44**,** 1250-1260.

DAVIES, J. M. & BRYAN, E. R. 1982. *Manual of stressed skin diaphragm design,* London, Granada.

DAVIES, J. M., ENGEL, P., LIU, T. T. C. & MORRIS, L. J. 1990. Realistic modelling of steel portal frame behaviour. *The Structural Engineer,* 68.

DAVIES, J. M. & LAWSON, R. M. 1999. Stressed skin action of modern steel roof systems. *The Structural Engineer,* 77**,** 30-35.

DE MATTEIS, G. & LANDOLFO, R. 1999. Mechanical fasteners for cladding sandwich panels: Interpretative models for shear behaviour. *Thin-Walled Structures,* 35**,** 61-79.

DOBOSI, J. n.d. VINAGRO a.s., Macov (15m x 54m) [image online]. Available: http://www.ironex.sk/images/vinagro/tn_vinagro2.jpg [Accessed 22 February 2016].

DUBINA, D., STRATAN, A., CIUTINA, A., FULOP, L. & ZSOLT, N. 2004. Monotonic and cyclic performance of joints of cold formed steel portal frames. *In:* LOUGHLAN, J. (ed.) *4th International Conference on Thin-walled structures.* Loughborough, UK.

DUBINA, D. & UNGUREANU, V. 2008. Behaviour of multi-span purlins of bolted lapped cold-formed Z-sections. *In:* RASMUSSEN, K. & WILKINSON, T. (eds.) *5th International Conference on Coupled Instabilities in Metal Structures.* Sydney, Australia.

DUBINA, D., UNGUREANU, V. & LANDOLFO, R. 2012. *Design of Cold-formed Steel Structures: Eurocode 3: Design of Steel Structures. Part 1-3 Design of cold-formed Steel Structures*, Wiley.

DUBINA, D., UNGUREANU, V. & STRATAN, A. 2008. Ultimate design capacity of pitch-roof portal frames made by thin-walled cold-formed members. *In:* M., M. (ed.) *Fifth International Conference on Thin-Walled Structures. Recent Innovations and Developments.* Brisbane, Australia.

DUBINA, D. & ZAHARIA, R. 2006. Stiffness of joints in bolted connected cold-formed steel trusses. *Journal of Constructional Steel Research,* 62**,** 240-249.

DUNDU, M. & KEMP, A. R. 2006. Plastic and lateral-torsional buckling behaviour of single cold-formed channels connected back-to-back. *Journal of Structural Engineering,* 132**,** 1223-1233.

ECCS - XVII -77-1E 1977. *European recommendations for the stressed skin design of steel structures*, European Convention for Constructional Steelwork, ECCS - XVII -77-1E.

ECCS 1995. *European recommendations for the application of metal sheeting acting as a diaphragm,* Brussels, European Convention for Constructional Steelwork.

ECCS TC7 1995. *European recommendations for the application of metal sheeting acting as a diaphragm - stressed skin design*, European Convention for Constructional Steelwork, ECCS No. 40.

ECCS TC7 NO. 21 1990. *The design and testing of connections in steel sheeting and sections*, European Convention for Constructional Steelwork.

ECCS TC7 TWG 7.4 NO.66 1991. *Preliminary European Recommendation for sandwich panels: Part I design*, European Convention for Constructional Steelwork.

ECCS TC7 TWG 7.10 NO.124 2009. *The testing of connections with mechanical fasteners in steel sheeting and sections*, European Convention for Constructional Steelwork,.

ELKERSH, I. 2010. Experimental investigation of bolted cold formed steel frame apex connections under pure moment. *Ain Shams Engineering Journal,* 1**,** 11-20.

FAN, L., RONDAL, J. & CESCOTTO, S. 1997. Finite element modelling of single lap screw connections in steel sheeting under static shear. *Thin-Walled Structures,* 27**,** 165-185.

HAIRSINE, R. C. 2010. Simplified 3D analaysis of portal structures-observations, problems and solutions. *The Structural Engineer,* 88**,** 25-33.

HAMMOND, G. & JONES, C. 2011. Inventory of Carbon & Energy (ICE) Version 2.0 [accessed online]. January 2011 ed. Bath, UK: University of Bath.

HAZLAN, A. H., TAHIR, M. M. & SULAIMAN, A. 2010. Bolted beam-column moment connections between cold-formed steel members. *In:* UNIVERSITY, V. (ed.) *21st Australasian Conference on the Mechanics of Structures and Materials (ACMSM 21).* Melbourne.

HELDT, T. J. & MAHENDRAN, M. 1998. Full scale experiments of a steel portal frame building. *Journal of the Australian Steel Institute, Steel Construction,* 32**,** 3-21.

ISTRUCTE 2014. Building for a sustainable future: An engineer's guide. *In:* HOPE, T. E. J. & KIRK, L. (eds.). London, UK,: The Institution of Structural Engineers.

JOHNSTON, R. P., WRZESIEN, A. M., LIM, J. B. P., SONEBI, M. & ARMSTRONG, C. G. 2013. The effect of semi-rigid joints on the design of cold-formed steel portal frame structures. *Civil and Environmental Research,* 5**,** 1-5.

KIRK, P. 1986. Design of a cold formed section portal frame building system. *8th International Specialty Conference on Cold-Formed Steel Structures.* St. Louis, Missouri, USA.

KWON, Y. B., CHUNG, H. S. & KIM, G. D. 2006. Experiments of cold-formed steel connections and portal frames. *Journal of Structural Engineering,* 132**,** 600-607.

LI, Z. & SCHAFER, B. W. 2010. Buckling analysis of cold-formed steel members with general boundary conditions using CUFSM: conventional and constrained finite strip methods. *Proceedings of the 20th International Specialty Conference in Cold-Formed Steel Structures.* St Louis, Missouri, USA.

LIM, J. B. P., HANCOCK, G. J., CHARLES CLIFTON, G., PHAM, C. H. & DAS, R. 2016a. DSM for ultimate strength of bolted moment-connections between cold-formed steel channel members. *Journal of Constructional Steel Research,* 117**,** 196-203.

LIM, J. B. P. & NETHERCOT, D. A. 2002. F. E.-assisted design of the eaves bracket of a cold-formed steel portal frame. *Steel & Composite Structures,* 2**,** 411-428.

LIM, J. B. P. & NETHERCOT, D. A. 2003a. Serviceability design of a cold-formed steel portal frame having semi-rigid joints. *Steel & Composite Structures,* 3**,** 451-474.

LIM, J. B. P. & NETHERCOT, D. A. 2003b. Ultimate strength of bolted moment-connections between cold-formed steel members. *Thin-Walled Structures,* 41**,** 1019-1039.

LIM, J. B. P. & NETHERCOT, D. A. 2004. Stiffness prediction for bolted moment-connections between cold-formed steel members. *Journal of Constructional Steel Research,* 60**,** 85-107.

LIM, J. B. P., WRZESIEN, A. M. & NETHERCOT, D. A. 2016b. Sustainable applications of cold-formed steel structures: Portal frames. *In:* YU, C. (ed.) *Recent Trends in Cold-Formed Steel Construction.* 1st ed. Sawston, UK: Woodhead Publishing.

MAHENDRAN, M. & MOOR, C. 1999. Three-dimensional modeling of steel portal frame buildings. *Journal of Structural Engineering,* 125 870-878.

MÄKELÄINEN, P. & KANKAANPÄÄ, J. 1996. Structural design study on a light-gauge steel portal frame with cold-formed sigma sections. *13th International Specialty Conference on Cold-Formed Steel Structures.* St. Louis, Missouri, USA.

MCALINDEN, B. 2015. Energy Briefing Sheet: Embodied Energy and Carbon [accessed online]. [Accessed 6 July 2016].

MILLS, J. & LABOUBE, R. 2004. Self-drilling screw joints for cold-formed channel portal frames. *Journal of Structural Engineering,* 130**,** 1799-1806.

MIRACLE SPAN STEEL BUILDINGS. n.d. Steel Portal Frame Buildings - Miracle Portal[imageonline].Available: https://www.google.co.uk/imgres?imgurl=http%3A%2F%2Fmiraclespan.co.uk%2Fwp-content%2Fuploads%2F2014%2F01%2FMiracle-Portal-Frame-840x400.jpg&imgrefurl=http%3A%2F%2Fmiraclespan.co.uk%2Fproducts%2Fsteel-framed-buildings%2Fmiracle-portal-frame%2F&docid=6akJ41wJxmR7JM&tbnid=ANa76XEN-X0yTM%3A&w=840&h=400&bih=979&biw=1920&ved=0ahUKEwjf3N-00dzNAhVGK8AKHVAlCIIQMwhoKD0wPQ&iact=mrc&uact=8 [Accessed 5 July 2016].

NA TO BS EN 1990:2002+A1:2005 2004. UK National Annex for Eurocode - Basis of structural design (Incorporating National Amendment No. 1). London: British Standard Institution.

NA TO BS EN 1991-1-1:2002 2005. UK National Annex to Eurocode 1: Actions on structures — Part 1-1: General actions — Densities, self-weight, imposed loads for buildings. London: British Standard Institution.

NA TO BS EN 1991-1-3:2003 2005. UK National Annex to Eurocode 1: Actions on structures — Part 1-3: General actions — Snow loads (Incorporating corrigendum no. 1). London: British Standard Institution.

NA TO BS EN 1991-1-4:2005+A1:2010 2008. UK National Annex to Eurocode 1 – Actions on structures Part 1-4: General actions – Wind actions (Incorporating National Amendment No. 1). London: British Standard Institution.

NA TO BS EN 1993-1-1 2005. UK National Annex to Eurocode 3: Design of steel structures. *Part 1-1: General rules and rules for buildings.* Brussels: European Committee for Standardization.

PEKÖZ, T. 1990. Design of screw connections. *Proceedings of the 10th International Specialty Conference in Cold-Formed Steel Structures.* St Louis, Missouri, USA.

PHAN, D. T., LIM, J. B. P., TANYIMBOH, T. T., WRZESIEN, A. M., SHA, W. & LAWSON, R. M. 2015. Optimal design of cold-formed steel portal frames for stressed-skin action using genetic algorithm. *Engineering Structures,* 93**,** 36-49.

RENSBURG, B. W. J. & DE VOS, G. P. 1996. Lower cost lightweight cold-formed portal frames. *13th International Specialty Conference in Cold-Formed Steel Structures.* St Louis, Missouri, USA.

RHODES, J. 1991. *Design of cold formed steel members* London, Elsevier Applied Science.

RHODES, J. & BURNS, R. 2006. Development of a portal frame system on the basis of component testing. *18th International Specialty Conference in Cold-Formed Steel Structures.* Orlando, Florida, USA.

ROBERTSON, A. P. 1991. A study of base fixity effects on portal frame behaviour. *The Structural Engineer,* 69**,** 17-24.

SANTOS, S. & SIMOES DA SILVA, L. 2011. Connections of cold formed profiles in industrial buildings. *6th International Conference on Thin Walled Structures.* Timisoara, Romania.

SCI. 2012a. Insulated panel [image online]. Available: http://www.steelconstruction.info/File:L1_Fig7.png [Accessed 22 February 2016].

SCI. 2012b. Standing seam roof cladding [image online]. Available: http://www.steelconstruction.info/File:L1_Fig9.png [Accessed 22 February 2016].

SCI. 2012c. Structural liner tray cladding systems [image online]. Available: http://www.steelconstruction.info/File:L1_Fig10.png [Accessed 22 February 2016].

SCI ADVISORY DESK NOTES 1991. AD 090: deflection limits for pitched roof portal farmes. Ascot, UK,: The Steel Construction Institute.

SCI P125 1993. Building Design using Cold Formed Steel Sections: Worked Examples to BS 5950: Part 5: 1987. Ascot, UK,: The Steel Construction Institute.

SCI P252 2004. Design of single-span steel portal frames to BS 5950-1:2000. Ascot, UK,: The Steel Construction Institute.

SCI P397 2012. Elastic Design of Single-Span Steel Portal Frame Buildings To Eurocode 3. *In:* KOSCHMIDDER, D. M. & BROWN, D. G. (eds.). Ascot, UK, : The Steel Construction Institute.

STRATAN, A., NAGY, Z. & DUBINA, D. 2006. Cold-formed steel pitched-roof portal frames of back-to-back plain channel sections and bolted joints. *Eighteenth International Specialty Conference on Cold-Formed Steel Structures.* Orlando, Florida, U.S.A.

STRNAD, M. & PIRNER, M. 1978. Static and dynamic full-scale tests on a portal frame structure. *The Structural Engineer,* 56**,** 45-52.

SWIERCZYNA, S. & WUWER, W. 2011. Journal friction in bolted lap joints in complex state of load. *6th International Conference on Thin Walled Structures.* Timisoara, Romania.

TAHIR, M. M. & SIANG, T. C. 2008. Experimental tests on partial strength connection for cold-formed steel double lipped channel sections. *In:* MOHENDRAN, M. (ed.) *5th International Conference on Thin-Walled Structures.* Brisbane, Australia.

TARGET ZERO 2011. Guidance on the design and construction of sustainable, low carbon warehouse buildings. Tata Steel and the British Constructional Steelwork Association.

TOMA, A., SEDLACEK, G. & WEYNAND, K. 1993. Connections in cold-formed steel. *Thin-Walled Structures,* 16**,** 219-237.

UZZAMAN, A., WRZESIEN, A. M., HAMILTON, R., LIM, J. B. P. & NASH, D. 2014. FE-Assisted Design of Cold-Formed Steel Top-Hat Purlins. *In:* TOPPING, B. H. V. (ed.) *Proceedings of the 22nd International Specialty Conference in Cold-Formed Steel Structures 2014.* St. Louis, Missouri.

UZZAMAN, A., WRZESIEN, A. M., LIM, J. B. P., HAMILTON, R. & NASH, D. 2016. Design of Top-hat Purlins for Cold-formed Steel Portal Frames. *Structures,* 7**,** 113-125.

WALENTYŃSKI, R. & WUWER, W. 2010. Analysis of a lap-joint in the thin-walled structure under combain bending and shearing load. *Architecure Civil Engineering Environment (ACCC),* 3**,** 71-82.

WOOLCOCK, S. T. & KITIPORNCHAI, S. 1987. Survey of deflection limits for portal frames in Australia. *Journal of Constructional Steel Research,* 7**,** 399–417.

WRZESIEN, A. M. 2012. Executive Summary of KTP between Capital Steel Ltd and Queen's University Belfast. Glasgow, UK.

WRZESIEN, A. M., LIM, J. B. P. & LAWSON, R. M. 2009a. Stressed skin action in cold-formed steel portal frames. *In:* KOWAL-MICHALSKA, K. & MANIA, R. J. (eds.) *Stability of Structures 12th Symposium* Zakopane, Poland.

WRZESIEN, A. M., LIM, J. B. P. & LAWSON, R. M. 2009b. The ultimate strength and stiffness of modern roof systems with hat-shaped purlins. *In:* CHAN, S. L. (ed.) *Sixth International Conference on Advances in Steel Structures* Hong Kong, China.

WRZESIEN, A. M., LIM, J. B. P. & NETHERCOT, D. A. 2012a. Optimum joint detail for a general cold-formed steel portal frame. *Advances in Structural Engineering,* 15**,** 1623-1639.

WRZESIEN, A. M., LIM, J. B. P., XU, Y., DUNDU, M., MACLEOD, I. & LAWSON, R. M. 2012b. Stressed skin effects on cold-formed steel portal frames with semi-rigid joints - experimental study. *The 6th International Conference on Coupled Instabilities in Metal Structures.* Glasgow, UK.

WRZESIEN, A. M., LIM, J. B. P., XU, Y., MACLEOD, I. A. & LAWSON, R. M. 2015. Effect of stressed skin action on the behaviour of cold-formed steel portal frames. *Engineering Structures,* 105**,** 123-136.

WRZESIEN, A. M., PHAN, D. T., LIM, J. B. P., LAU, H.-H., HAJIRASOULIHA, I. & TAN, C. S. 2016. Effect of stressed-skin action on optimal design of cold-formed steel square and rectangular-shaped portal frame buildings. *International Journal of Steel Structures,* 16**,** 299-307.

WUWER, W., ZAMOROWSKI, J. & SWIERCZYNA, S. 2012. Lap joints stiffness according to Eurocode EC3 and experimental investigations results. *Archives of Civil and Mechanical Engineering,* 12**,** 95-104.

YANG, J. & LIU, Q. 2011. An experimental study of cold-formed steel sigma purlins with sleeve connections. *6th International Conference on Thin Walled Structures.* Timisoara, Romania.

YU, W. K., CHUNG, K. F. & F., W. M. 2005. Analysis of bolted moment connections in cold-formed steel beam–column sub-frames. *Journal of Constructional Steel Research,* 61**,** 1332-1352.

ZADANFARROKH, F. 1991. *Analysis and design of bolted connections in cold formed steel memebers.* PhD, University of Salford.

ZADANFARROKH, F. & BRYAN, E. R. Testing and design of bolted connections in cold-formed steel sections. 11th International Specialty Conference on Cold-Formed Steel Structures, 1992 St. Louis, Missouri, USA. 625-662.

ZAHARIA, R. & DUBINA, D. 2006. Stiffness of joints in bolted connected cold-formed steel trusses. *Journal of Constructional Steel Research.,* 62**,** 240-249.